Precision Measurement of the η Mass

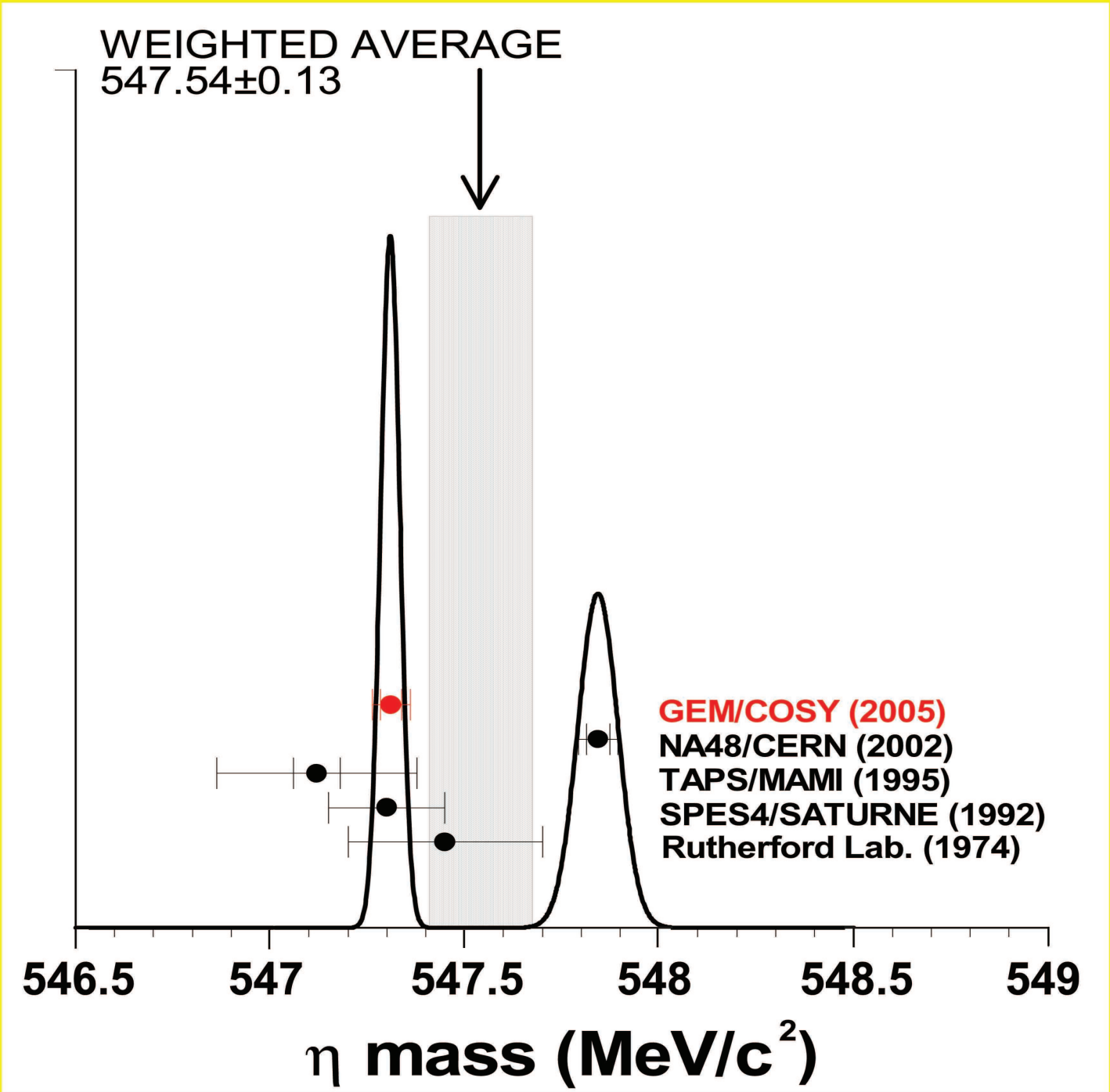

Annual Report 2005

Institut für Kernphysik / COSY

Cover picture:
Ideogram of the η-mass based on the compilation of the Particle Data Group and the recently published value of the GEM collaboration. The disagreement of the NA48 result with all other data triggered the precision measurement of the GEM collaboration making use of the high brilliance COSY beam matched with the high resolution magnetic spectrograph BIG KARL. The present GEM result defines the width of the lower mass branch while the upper one is given by the NA48 result.

Preface

The year 2005 has been a challenging one for the institute: as a consequence of the "mixed results" of the first review in February 2004 within the Research Programme "Physics of Hadrons and Nuclei" in the Research Field "Structure of Matter" of the Helmholtz Centres, IKP was faced with substantial cuts in resources for 2005. An even more serious threat ensued with possible further reductions for the years 2006 – 2009, depending, however, on the outcome of an "in-depth" evaluation of the IKP activities.

The review on "COSY and FZJ contributions to FAIR", conducted by an international committee, and headed by Peter Paul (BNL, USA), took place on two days in April 2005. IKP presented its strategy for the further use of COSY and, in close collaboration with GSI (Darmstadt), the cooperation towards the construction of the FAIR facility. In its report, issued later last year, the committee almost fully supported our plans, and as a result and the financial agreements, which have been negotiated in the meantime, we now have a solid basis for the remainder of the first funding period (2006 – 2009). — I would like to take this opportunity to thank all who contributed to this great success in one way or the other.

One of the explicit recommendations of the committee was to give green light for the relocation of the WASA detector from CELSIUS (Uppsala, Sweden) to COSY. The detector dismount at TSL and transfer to FZJ was completed in 2005, and we are now in the process of installing WASA at an internal target station of COSY — more details are given in the main text. Commissioning of WASA is scheduled to begin in the second half of 2006 and first experiments are expected to start in 2007.

In connection with the WASA-at-COSY project, the IKP had decided to reduce the amount of COSY beamtime for users in 2005 by about 2000 hours. The increased down-time is needed to install WASA in the COSY ring, but also has the positive side-effect that the cost-savings will be used to finance necessary maintenance and upgrades of WASA detector components and electronics. This was part of the financing concept which has been worked out between the IKP directorate and the FZJ board of management.

On the scientific frontier, IKP has made a number of important contributions (details can again be found in the main text):

- The ANKE collaboration has found indications for a heavy hyperon state $Y^{0*}(1480)$ in the analysis of $pp \to pK^+\pi X$ at a beam momentum of 3.65 GeV/c.
- The GEM collaboration has determined the mass of the η meson with unprecedented accuracy, exploiting the reaction $pd \to {}^3\mathrm{He}\eta$ and simultaneously $pd \to t\pi^+$ at the BIG KARL magnetic spectrometer (see cover picture and corresponding article).
- At COSY the efficiency for flipping the proton spin by means of a small rf dipole has been pushed to more than 99.9%.
- The intensity of the polarized ion source for H^- was raised to $50\,\mu$A, thus doubling its original specification.

The involvement of the IKP in the FAIR project to be realized at the GSI was fully honored by the committee. Our efforts are focused on the design and construction of the High Energy Storage Ring (HESR) and significant contributions to the PANDA detector. We are dedicated to make this endeavor a success being aware of its great potential to advance hadron physics and connected fields during the next decades.

We have been able to meet the challenges of 2005 not only due to our own efforts, but because we could rely on the support and advice of many people. I like to express our gratitude to all of them, the colleagues from the infrastructure of our Research Center (FZJ) in particular ZAM, ZAT, and ZEL, the people from the universities and research centers from Germany and all over the world and, last but not least, the CANU community.

Jülich, February 2006 Hans Ströher

Contents

1 Experimental Hadron Physics

1.1 Experiments at COSY

Evidence for an Excited Hyperon $Y^{0*}(1480)$

I.Zychor[a] for the ANKE Collaboration

The reaction $pp \to pK^+Y$ has been studied with the ANKE spectrometer to investigate hyperon production. The final results have been published in Phys. Rev. Lett. [1]. The measurements were performed at a proton beam momentum of 3.65 GeV/c incident on a hydrogen cluster-jet target.

A final state comprising a proton, a positively charged kaon, a pion of either charge together with an unidentified residue X was investigated in the reaction $pp \to pK^+Y \to pK^+\pi^\pm X^\mp$. As an example, in Fig.1 the missing-mass distribution $MM(pK^+\pi^+)$ vs $MM(pK^+)$ is shown for the reaction channels $pp \to pK^+\pi^+X^-$. The triangular shape of the distributions is due to a combination of kinematics and the ANKE acceptance.

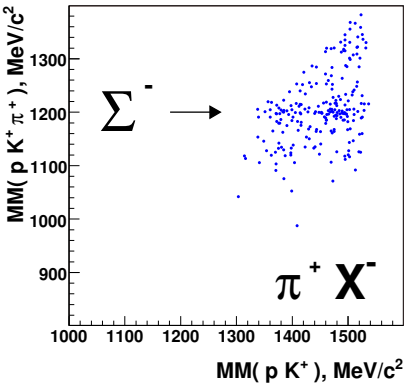

Fig. 1: The missing-mass $MM(pK^+\pi^+)$ vs $MM(pK^+)$ distribution obtained in the reaction 3.65 GeV/c^2 $pp \to pK^+\pi^+X^-$.

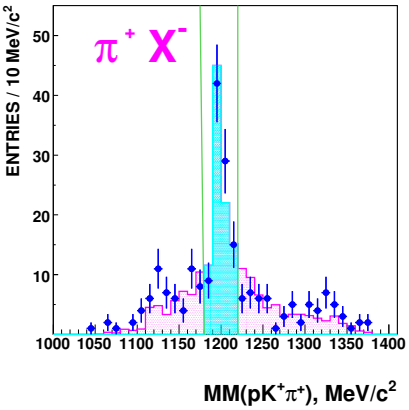

Fig. 2: Projections of Fig.1 onto the three-particle missing mass $MM(pK^+\pi^+)$. Vertical lines show the Σ^- band used for event selection. The results of simulations for $MM(pK^+\pi^+)$ >1050 MeV/c^2 are shown as a filled histogram.

The missing-mass $MM(pK^+\pi^+)$ spectrum in the reaction $pp \to pK^+\pi^+X^-$ shows a flat plateau with a peak at approximately 1195 MeV/c^2, see Fig.2. The peak corresponds to the decay $Y \to \pi^+\Sigma^-(1197)$. In the charge-mirrored $pp \to pK^+\pi^-X^+$ case, the π^- may originate from different sources and the missing-mass distribution for the (π^-X^+)-final state is more complicated.

The missing-mass spectra $MM(pK^+)$ have been analyzed and compared with extensive Monte Carlo simulations.

In the first step we have assumed that measured missing-mass $MM(pK^+)$ spectra can be explained by the production of hyperon resonances and non-resonant contributions. Monte Carlo simulations have been performed including the production of well established excited hyperons $(\Sigma^0(1385), \Lambda(1405)$ and $\Lambda(1520))$ and non-resonant contributions like $pp \to pK^+\pi X$ and $pp \to pK^+\pi\pi X$, X denotes any hyperon which could be produced in the experiment. The comparison of measured and simulated missing-mass distributions shows a necessity to include an additional excited hyperon Y^{0*} with a mass $M(Y^{0*}) = (1480 \pm 15)$ MeV/c^2 and a width $\Gamma(Y^{0*}) = (60 \pm 15)$ MeV/c^2.

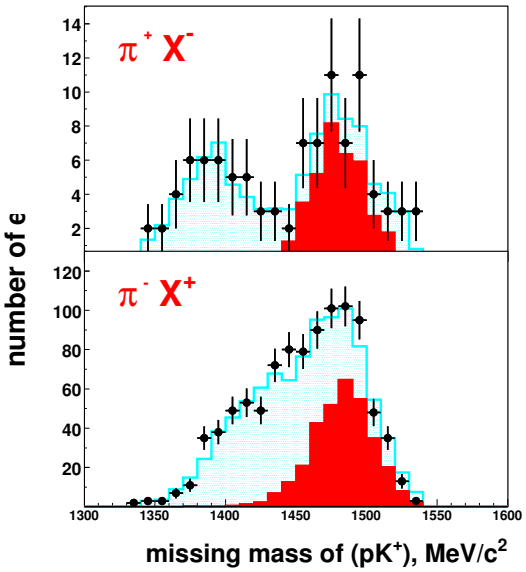

Fig. 3: Missing-mass $MM(pK^+)$ spectra for the reaction $pp \to pK^+\pi^+X^-$(upper) and $pp \to pK^+\pi^-X^+$(lower). Experimental points with statistical errors are compared to the fitted overall Monte Carlo simulations (shaded histogram, blue). The contribution form the Y^{0*} resonance with mass of $M(Y^{0*}) = (1480 \pm 15)$ MeV/c^2 and a width $\Gamma(Y^{0*}) = (60 \pm 15)$ MeV/c^2 is shown as a solid (red) histogram.

In summary, we have found indications for a neutral hyperon resonance Y^{0*} decaying into π^+X^- and π^-X^+ final states in proton-proton collisions at 3.65 GeV/c. Since it is neutral, it can be either a Λ or Σ^0 hyperon. The production cross section is of the order of few hundred nanobarns.

On the basis of available data we cannot decide whether it is a 3-quark baryon or an exotic state. However, it seems to be difficult to validate that a $Y^{0*}(1480)$ hyperon is a 3q-baryon.

References:

[1] I.Zychor et al., Phys. Rev. Lett. **96**, 0123002 (2006)

[a]The Andrzej Sołtan Institute for Nuclear Studies, Świerk, Poland

Analysis of $pp \to pK^0\pi^+\Lambda$ at ANKE

M. Nekipelov, V. Koptev*, H. Ströher

The reaction $pp \to pK^0\pi^+\Lambda$, measured at ANKE at a beam momentum of $p_p = 3.65\,\mathrm{GeV/c}$, allows for the production of a pentaquark $\Theta^+(1540)$. Recent negative results on the Θ^+, mostly obtained at higher energies, have put the existence of the pentaquark under scrutiny. It has been shown, however, that the production of Θ^+ is strongly suppressed compared to the $\Lambda(1520)$ at higher energies [1], therefore hadronic experiments at lower energies become crucial to reveal fate of the pentaquark. The search of the Θ^+ decaying into the pK^0 system in the reaction $pp \to \Theta^+\pi^+\Lambda$ was the main motivation of the analysis made.

The reaction at ANKE has been identified by detecting four particles simultaneously, the π^+ coming from the reaction vertex, the proton from vertex/Θ^+ decay, and the products of the Λ decay: proton and π^-. Besides individual particle iden-

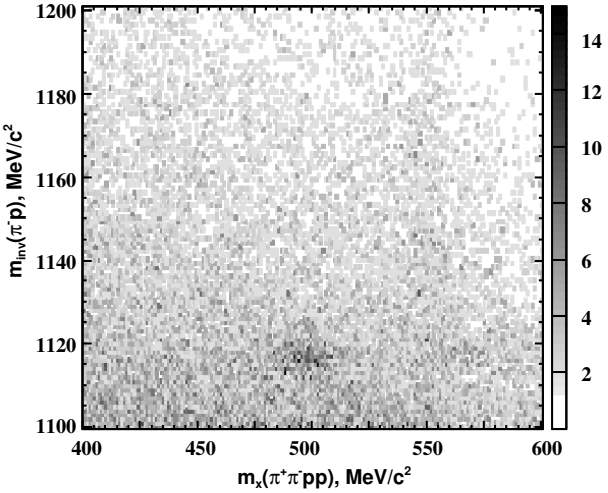

Fig. 1: Mass scatter plot: invariant mass of $\pi^- p$ versus missing mass of $\pi^+\pi^- pp$.

tification, the final state is fixed by the missing mass technique. As it is seen in Fig. 1, a clear enhancement in the scatter plot corresponds to the masses of K^0 and Λ in the missing mass of four detected particles and the missing mass of $\pi^- p$, respectively. Unfortunately, a sizable background remains after cuts on masses are made, and this background is removed by the side band subtraction method.

For normalisation of the data the reaction $pp \to pK^+\Lambda$ has been used. This reaction was measured simultaneously during the experiment. Again all four particles in the final state have been detected. Such normalisation procedure, when the reaction with known cross section [2, 3] and nearly the same final state is measured allows to get rid of most of the systematic uncertainties connected with particle identification and detector efficiencies.

The missing mass distribution $m(\pi^+\Lambda)$, presented in Fig. 2, is the one where the signal from the pentaquark is expected to appear. A combined fit with the sum of resonant and non-resonant channels obtained from the Monte Carlo simulations has been performed (the solid line in Fig. 2), and the hatched area shows a signal produced by the Θ^+. As one can see, there is only a moderate agreement between experimental data and the simulations. While at the high mass part of

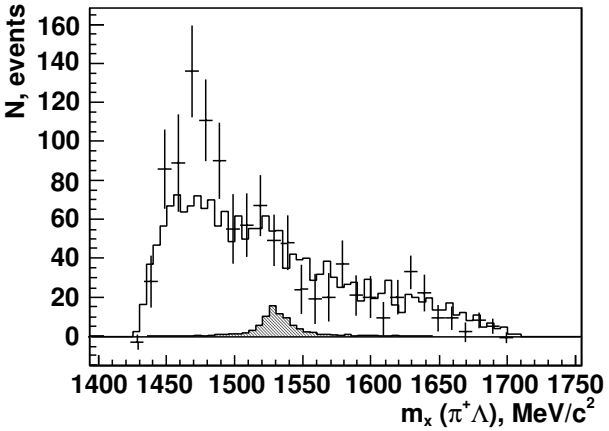

Fig. 2: Missing mass spectrum of $\pi^+\Lambda$ system. The hatched area shows the result of Monte Carlo simulations corresponding to the production of Θ^+. The solid line is the sum of resonant and non resonant contributions.

the spectrum the agreement is nice, an obvious excess of experimental events is observed around $1.47\,\mathrm{GeV/c^2}$. Such an enhancement may be connected with the production of some resonance at an intermediate stage of the reaction. Candidates for this are e.g. $K^*(892)$, Δ^{++}, $N^*(1650)$ or $N^*(1710)$, and $\Sigma(1385)$. Analysis of these possibilities is ongoing.

The number of events in the missing mass of $\pi^+\Lambda$ amounts to 50 ± 30 events, which can be treated as an upper limit for possible Θ^+ production and corresponds to the cross section of

$$\sigma_{\Theta^+\pi^+\Lambda} = 0.17 \pm 0.10 \mu b,$$

which is close to the theoretical expectations of less than $1\,\mu$b at this energy [4]. The total cross section for the reaction $pp \to pK^0\pi^+\Lambda$ including resonant and non-resonant channels is

$$\sigma_{pK^0\pi^+\Lambda} = 1.33 \pm 0.14 \mu b.$$

The errors given are statistical only. The value for the total cross section agrees nicely with the calculations made in Ref. [3]. Although both resonant and non-resonant production cross sections are supported by theory, the discrepancy in the low $\pi^+\Lambda$ missing mass region has yet to be understood.

References:

[1] A. I. Titov et al., Phys. Rev. C70 (2004) 042202.
[2] R. I. Louttit et al., Phys. Rev. 123 (1961) 1465-1471.
[3] K. Tsushima et al., Phys. Rev. C 59 (1999) 369-387.
[4] W. Liu and C. M. Ko., Phys. Rev. C68 (2003) 045203.

* Saint-Petersburg Nuclear Physics Institute, 188300 Gatchina, Russia

K^+ production on proton and deuteron targets

Y. Valdau[a,b] for the ANKE collaboration

The ratio between strangeness production on proton and neutron targets is very poorly known. However, it is an important input parameter for theoretical models of K^+ production in *pA* and *AA* interactions. Using a deuterium cluster-jet target at the magnetic spectrometer ANKE the first experimental data for strangeness production on the deuterium target have been collected. The analysis of the experimental data using naive phase space approach shows a significant difference between strangeness production on the proton and neutron [1]. Several theoretical investigations of the difference have been initiated Ref. [2, 3], but due to the lack of the experimental data collected on the neutron targets all the conclusions are rather model dependent.

In order to extract information about K^+ production on the neutron from the deuterium target one needs either to fully identify particles in the final state or to use the spectator detection technique. Due to the limited acceptance of the ANKE spectator detector prototype [4] it was impossible to perform such a measurement. Another approach requires a very significant amount of the experimental data. Therefore, a simple experiment measuring the ratio between K^+ production on the proton and deuteron targets at the same beam energy has been done.

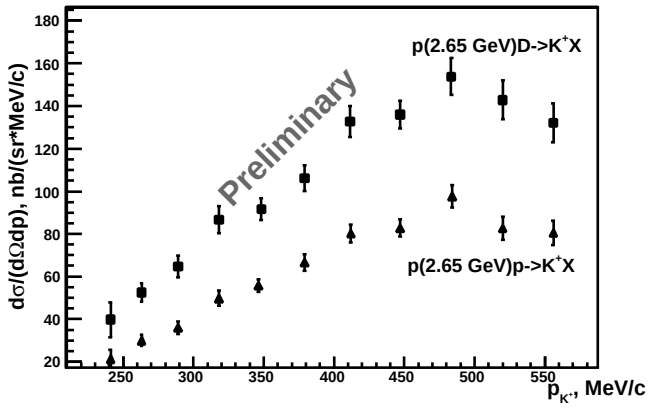

Fig. 1: Double differential cross sections for the K^+ production on the proton and deuteron targets at a proton beam energy of 2.65 GeV

In Fig. 1 two double differential cross sections measured at a proton beam energy of 2.65 GeV on deuterium and proton targets are presented. The deduced ratio between K^+ production on the proton and deuterium targets is of the order of two. Using this value one can conclude that there is no difference between K^+ production on the proton and neutron at 2.65 GeV proton beam energy like it was suggested earlier in Ref. [5].

The error bars of the points in Fig. 1 are mostly due to the systematic uncertainty of the telescope efficiency determination. Since this two experimental data sets have been collected at the same beam energy with the same acceptance and other parameters of the detection system the ratio between K^+ production on the proton and deuteron targets does not depend on the telescope efficiency and can therefore be estimated with relatively small error. The systematic uncertainty of the ratio $\sigma_D^{K^+}/\sigma_p^{K^+}$ mostly depends on the error of the two luminosity determination methods and are in the order of 20%.

In Fig. 2 double differential K^+ production cross sections on the deuterium target at 2.02 GeV [1] and at 2.06 GeV at the proton target are presented. The difference between these

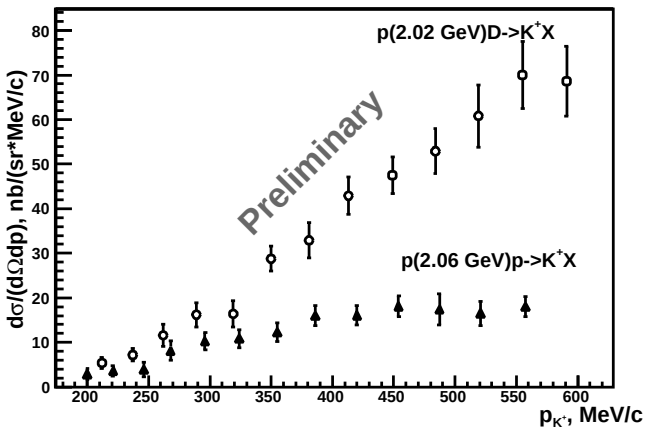

Fig. 2: Double differential cross sections for the K^+ on the proton at 2.06 GeV and on deuterium target at 2.02 GeV

two double differential cross sections is roughly a factor of 2.6. Taking into account that K^+ production double differential cross sections on the proton target at 2.02 and 2.06 GeV should differ by $\sim 15-20\%$ one ends up with a ratio of $\sigma_D^{K^+}/\sigma_p^{K^+} \sim 3$. This value leads to a two times difference between total K^+ production cross section on the neutron and proton, which is in agreement with the number suggested by model in Ref.[6].

The data shown in Fig. 1 suggest a ratio $\sigma_D^{K^+}/\sigma_p^{K^+} \sim 2$ at 2.65 GeV, which leads to the conclusion that there is no difference between K^+ production on the proton and neutron at this energy. On the other hand the analysis of the *pD* inclusive data in Ref. [1] using naive phase space approach gives the $\sigma_n^{K^+}/\sigma_p^{K^+} \sim 3$ at 2.02 GeV. The comparison of the *pD* experimental data at 2.02 GeV with *pp* at 2.06 GeV in Fig. 2 indicates that a $\sigma_D^{K^+}/\sigma_p^{K^+}$ ratio at 2.06 GeV higher than one, but does not allow to make a qualitative conclusion about difference between strangeness production on the proton and deuteron at this energy and possible energy dependence of the $\sigma_n^{K^+}/\sigma_p^{K^+}$ ratio.

Further conclusions about $\sigma_n^{K^+}/\sigma_p^{K^+}$ ratio have to wait for the results of the analysis of the *pp* and *pD* data collected at 2.16 GeV.

References:

[1] M. Büscher *et al.*, *Eur. Phys. J. A* **22**, 301 (2004).
[2] G. Fäldt and C. Wilkin, *Eur. Phys. J. A* **24**, 431 (2005).
[3] A. N. Ivanov *et al.*, nucl-th/0509055.
[4] I. Lehman *et al.*, *NIM A* **530**, 275 (2004).
[5] P.A. Piroué and A. J. S. Smith, *Phys. Rev.* **148**, 1315 (1966).
[6] K. Tsushima *et al.*, *Phys. Rev. C*, **59**, 369 (1999).

[a] IKP FZJ, Germany
[b] PNPI Gatchina, Russia

Investigation of the $a_0^+(980)$ Resonance in the Reaction $pp \to dK^+\bar{K}^0$ with ANKE*

A.Dzyuba[a], M.Büscher, C.Hanhart, V.Kleber[b], V.Koptev[a], M.Nekipelov, A.Sibirtsev

The production of the light scalar resonances $a_0(980)$ and $f_0(980)$ in hadronic interactions is under investigation at the ANKE spectrometer, where their strange decays into $K\bar{K}$ can be observed. Final goal of these studies, which will be later supplemented by measurements of the non-strange decays with the WASA detector, is to learn about the nature of these states, about isospin violating processes in the a_0/f_0 system and FSI effects between antikaons and light nuclei.

The first two experiments on $a_0^+(980)$ production (where contributions of the $f_0(980)$ must be absent) have been performed in pp collisions at $T_p = 2.65$ GeV (2001) [1] and $T_p = 2.83$ GeV (2002). Events of the type $pp \to dK^+X$ have been measured at ANKE, identifying the $\bar{K}^0$ by a missing-mass criterion. Contaminations from misidentified events are smaller than 10%.

Due to a large number of zero elements in the acceptance matrices [2] for the higher beam energy, it is impossible to follow the model independent acceptance correction procedure which has been used for the $T_p = 2.65$ GeV data [1].

However, in the close-to-threshold regime only a limited number of final states can contribute. Thus, for the data analysis we have restricted ourselves to the lowest allowed partial waves, *i.e.* s-wave in the $K\bar{K}$ system accompanied by a p-wave of the deuteron with respect to the meson pair ($a_0^+(980)$-channel) and p-wave $K\bar{K}$ production with an s-wave deuteron (non-resonant prod.) [1]. With this assumption the data at $T_p = 2.65$ GeV are well explained. The square of the transition matrix element can then be written as

$$|\bar{\mathcal{M}}|^2 = C_0^q q^2 + C_0^k k^2 + C_1(\hat{p}\cdot\vec{k})^2 + C_2(\hat{p}\cdot\vec{q})^2 + \\ + C_3(\vec{k}\cdot\vec{q}) + C_4(\hat{p}\cdot\vec{k})(\hat{p}\cdot\vec{q}) \; . \qquad (1)$$

Here $\vec{k}$ is deuteron momentum in the overall CMS, $\vec{q}$ denotes the momentum of the K^+ in the $K\bar{K}$ system, and $\hat{p}$ is the unit vector parallel to the beam direction. Only $K\bar{K}$ p-waves contribute to C_0^q and C_2, only $K\bar{K}$ s-waves contribute to C_0^k and C_1, and only $s \cdot p$ interference terms to C_3 and C_4. In order to determine the coefficients C_i, fits of the uncorrected (to acceptance) distributions have been made using GEANT simulated data samples, varying C_i. The best fit results are displayed in Fig. 1 for two measured invariant-mass and four angular distributions. The fit reveals dominance of $K\bar{K}$ s-wave production (*i.e.* the $a_0^+(980)$-channel) for both beam energies, see Table 1.

Table 1: Quality and results of the fit.

T_p	2.65 GeV	2.83 GeV
χ^2/ndf	1.4	1.1
$K\bar{K}$ s-wave	95%	88%
$K\bar{K}$ p-wave	5%	12%

The results for the data at $T_p = 2.65$ GeV are consistent with the published data where a different method of acceptance correction has been applied.

Having determined the coefficients C_i one can simulate differential distributions at the target, track the events through the ANKE setup and, thus, determine the differential acceptances as a function of the kinematical variables displayed in Fig. 1. Knowing these acceptances, differential cross sections can be extracted from the data which are shown in Fig. 2.

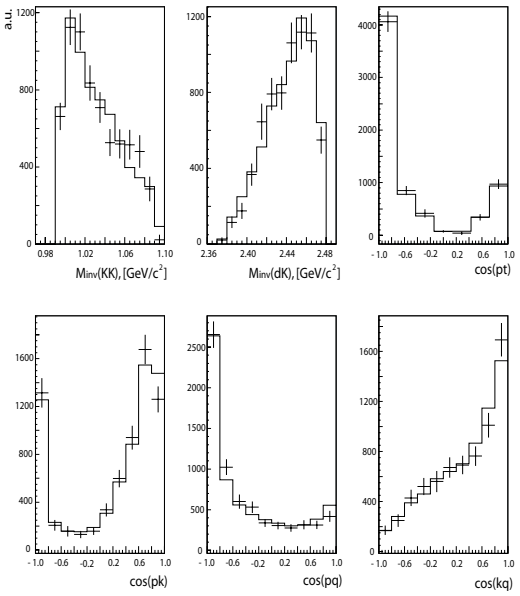

Fig. 1: Best fit of acceptance uncorrected data at $T_p = 2.83$ GeV. Cos(pt) is the angle between the K^+ momentum, measured in the CMS, and the beam proton; all other angles are described in the text.

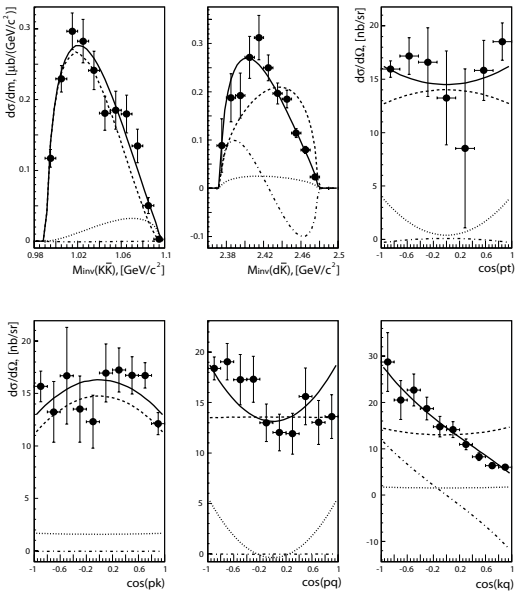

Fig. 2: Angular and invariant mass distributions for $T_p = 2.83$ GeV. The dashed (dotted) line corresponds to $K\bar{K}$ production in a relative s- (p-)wave, the dash-dotted to the interference term and solid line is the sum of them.

References:

[1] V.Kleber et al., Phys. Rev. Lett., **91**, 172304 (2003)
[2] M.Büscher et al., IKP Annual Report 2004.

[a] PNPI, Gatchina, Russia, [b] PI, Universität Bonn

* supported by DFG, RFFI, COSY-FFE program

ANKE Acceptance for the Reaction $pp \to dK^+\bar{K}^{0*}$

V.Kleber[b], M.Büscher, A.Dzyuba[a], C.Hanhart, V.Koptev[a], M.Nekipelov, A.Sibirtsev

In 2001 and 2002 experiments to study the reaction $pp \to da_0^+ \to dK^+\bar{K}^0$ at $T_p = 2.65$ GeV and $T_p = 2.83$ GeV have been carried out at ANKE (see Ref. [1]). In principle, the analysis of the second data set at higher beam energy could be done in the same way as the lower data set (see Ref. [2]). However, it turned out that the acceptance correction method applied before caused problems due to the larger available phase space for the final-state particles.

The 2.65 GeV data have been acceptance corrected with a four dimensional matrix which was built from four independent variables. The binning has been chosen such that in total 500 cells were obtained, fine enough to reconstruct the target distribution model-independently and large enough that there were few acceptance holes. However, the accessible Q range at T_p =2.83 GeV is about twice as large and it is not possible any more to construct a suitable matrix. Thus, it was necessary to develop a new method.

This new method is based on the findings for the older data, namely that the data are well described by the assumption that only s- and p- wave contribute while larger partial waves are suppressed due to the nearness of the threshold. Under this assumption the initial target distribution is "known"; only the corresponding 6 coefficients in the amplitude need to be determined (see Ref. [1]). Since the acceptance strongly depends on the initial distribution, the assumed target distribution has been described with the above ansatz with six coefficients and has then been tracked through the ANKE acceptance with the help of GEANT. In order to safe CPU time, the acceptance of ANKE has been projected in two three-dimensional grids, each containing the momentum components p_x, p_y and p_z. The first grid is for the side detection system where the K^+ mesons are identified, the second is used for the faster deuterons which are detected in the forward system. The grid cell size of each component has been chosen such that it roughly reflects the resolution in this observable. The acceptance for any cell has been determined from 40–50 initial events and is the ratio of detected to started events. For the K^+ mesons the decay probability of each cell has been calculated and multiplied with the corresponding acceptance. The deviation of simulations and generated events weighted with the acceptance determined event-by-event from the grid is below one percent.

In order to fit the partial wave coefficients, a high statistics sample of phase space events has been generated, the acceptance was determined from the grid for each event as a weight, and the amplitude was calculated also event-wise as a weight. The coefficients were then varied such that the χ^2 of the obtained distribution and the experimental distribution (which was corrected for detector efficiencies) became minimal. The distributions with the minimal χ^2 are displayed in Fig. 1. The corresponding target distribution is shown in Fig. 2. The clear advantage of the fit method is that a sixth distribution ($\cos(pt)$) can be reconstructed and that the angles do not have to be mirrored as it was necessary with the matrix method to avoid acceptance holes. In addition, the data have been fitted kinematically before the acceptance correction, thus there are no longer events outside the kinematical limit, as it was the case, *e.g.* at low masses in $m(K\bar{K})$.

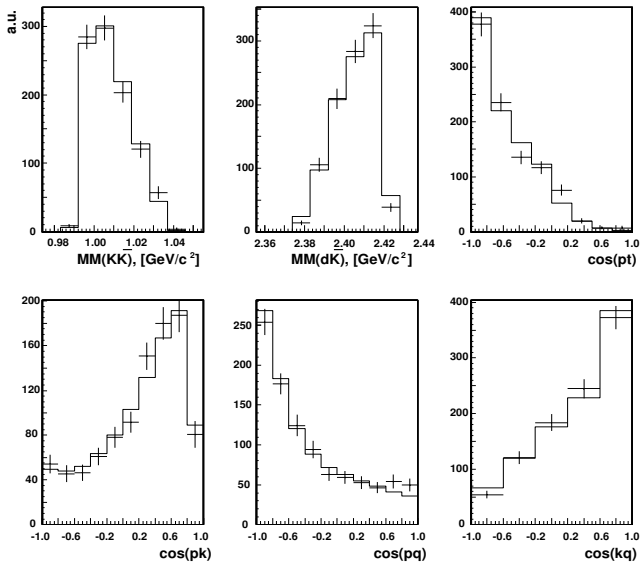

Fig. 1: Best fit of acceptance uncorrected data at $T_p = 2.65$ GeV. For the meaning of the observables, see Ref. [1].

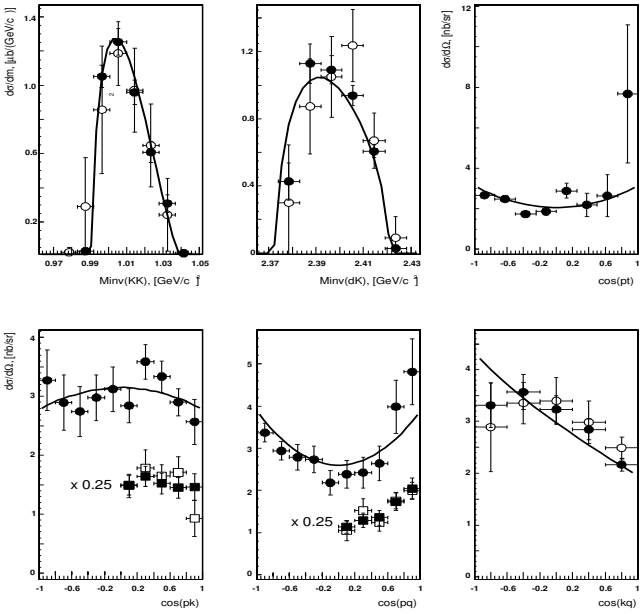

Fig. 2: Angular and invariant mass distributions for $T_p = 2.65$ GeV. The black dots with statistical error bars correspond to the data which are corrected with the fit method, the open dots with statistical and systematic error bars correspond to the data with matrix acceptance corrections. The uncertainty for the matrix method is larger due to the larger matrix cell sizes. Two angles are scaled and mirrored to compare with the published representation ([2]).

References:

[1] A.Dzyuba et al., contribution to this Annual Report.
[2] V.Kleber et al., Phys. Rev. Lett., **91**, 172304 (2003)

[a] PNPI, Gatchina, Russia, [b] PI, Universität Bonn
* supported by DFG, RFFI, COSY-FFE program

The $K^-\,{}^3$He scattering length and the reaction $pd \to {}^3\mathrm{He}\,K^+K^-$ near threshold

V. Yu. Grishina [a], M. Büscher, L.A. Kondratyuk [b] and C. Wilkin [c]

In a recent paper [1], we presented an estimation of the s-wave $K^-\alpha$ scattering length $A(K^-\alpha)$ obtained within the Multiple Scattering Approach. We further discussed the possibility of determining $A(K^-\alpha)$ from the $K^-\alpha$ invariant mass distribution measured in the reaction $dd\to\alpha K^+K^-$ near threshold. Here we show the results of similar calculations for $A(K^-{}^3\mathrm{He})$ (see also Ref. [2].)

In Table 1 the predictions of $A(K^-{}^3\mathrm{He})$ are given for different $\bar{K}N$ inputs. These are taken from a K-matrix fit (Set 1) [3], a constant scattering-length fit (Set 2) [4], and a chiral unitary approach (Set 3) [5].

Table 1: The $K^-\,{}^3$He scattering length for different $\bar{K}N$ scattering lengths $a_I(\bar{K}N)$ $(I = 0, 1)$.

Ref.	$a_0(\bar{K}N)$[fm]	$a_1(\bar{K}N)$[fm]	$A(K^-{}^3\mathrm{He})$[fm]
[3]	$-1.59 + i0.76$	$0.26 + i0.57$	$-1.50 + i0.83$
[4]	$-1.03 + i0.95$	$0.94 + i0.72$	$-1.52 + i1.80$
[5]	$-1.31 + i1.24$	$0.26 + i0.66$	$-1.66 + i1.10$
[6]	$2.88 + i1.12$	$0.43 + i0.30$	$-3.93 + i4.03$

We note that the $\bar{K}N$ scattering lengths described by Sets 1-3 correspond to their vacuum values. In order to demonstrate the sensitivity of our results to possible modifications of the $\bar{K}N$ scattering amplitudes in the presence of nuclear matter, we consider as Set 4 the strongly attractive in-medium solution found in Ref. [6] and given by

$$a_0^{\mathrm{eff}} = (2.9 + i1.1)\,\mathrm{fm}\,, \quad a_1^{\mathrm{eff}} = (0.43 + i0.30)\,\mathrm{fm}\,.$$

The results of our calculations are listed in the last column of Table 1. The values are very similar for Sets 1 and 3, being in the range $A(K^-{}^3\mathrm{He}) = -(1.5 \div 1.7) + i(0.83 \div 1.1)$ fm. Set 2 gives a much larger imaginary part, with $A(K^-{}^3\mathrm{He}) = -1.52 + i1.80$ fm. The "exotic" Set 4 leads to a very large $K^-\,{}^3$He scattering length, with a real part of -4 fm.

We now consider the $K^-\,{}^3$He FSI effect in the reaction $pd \to K^+K^-\,{}^3$He near threshold. In Fig. 1 we present calculations of the $K\,{}^3$He relative energy spectrum at an excess energy of 40 MeV. The solid line shows the calculations for pure phase space, *i.e.* for a constant production amplitude and neglecting FSI. All other lines in the figure represent the results obtained using the different sets of K^-N parameters given in Table 1. The predictions are normalized to the total $pd \to K^+K^-\,{}^3$He cross section of 9.3 nb. It is clear that the FSI can change significantly the $K\,{}^3$He mass spectrum. The blue line corresponding to Set 4, which demonstrates a very pronounced deformation of the K^3He invariant mass spectrum in the region of small invariant masses, is in clear contradiction to the data.

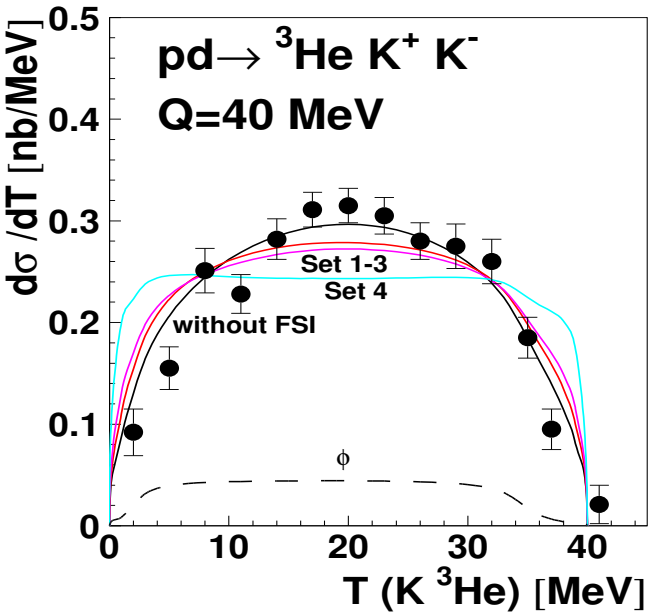

Fig. 1: Distribution of K^3He relative energies from the $pd \to {}^3\mathrm{He}\,K^+K^-$ reaction at 40 MeV. The MOMO experimental data are taken from Refs. [7, 8]. The model predictions (lines) are symmetric around $T = 20$ MeV since the MOMO experiment was insensitive to the signs of the kaon charges. The $\phi(1020)$ resonance, whose effects are shown by the dashed line, contributes about 15% to the total rate.

References:

[1] V.Yu. Grishina *et al.*, Eur. Phys. J. A **25** (2005) 159.
[2] L. Kondratyuk, V. Grishina and M. Büscher, Proc. of STORI2005, Schriften des Forschungszentrums Jülich, **30** (2005) 165 [arXiv:nucl-th/0507021].
[3] R. C. Barrett and A. Deloff, Phys. Rev. C **60** (1999) 025201.
[4] J.E. Conboy, Rutherford-Appleton Lab. Report, RAL-85-091 (1985).
[5] J.A. Oller and U.-G. Meißner, Phys. Lett. B **500** (2001) 263.
[6] Y. Akaishi and T. Yamazaki, Phys. Rev. C **65** (2002) 044005.
[7] H.A. Schitker, *"Zwei-Kaonen-Produktion nahe der Schwelle in der Reaktion $pd \to {}^3He\,K^+K^-$ mit dem Experiment MOMO an COSY"*, Dissertation Univ. Bonn (2002).
[8] F. Bellemann *et al.*, IKP Annual Report 2000, p. 63.

[a] INR, Moscow, Russia
[b] ITEP, Moscow, Russia
[c] Physics & Astronomy Dept., UCL, London, UK
*Supported by DFG and RFFI. V.Yu.G. acknowledges the financial support from the FZJ (FFE grant 41520739(COSY-071)).

Investigation of the ^{3}He η Final State in dp-Reactions at ANKE*

T. Mersmann[1], V. Hejny[2], A. Khoukaz[1], M. Mielke[1], M. Papenbrock[1], and T. Rausmann[1] for the ANKE-Collaboration

The existence of η-mesic nuclei is still an open issue of research. To investigate the possibility of the formation of such bound systems, production measurements with one η meson and one light nucleus in the final state are of great interest. By studying the final state interaction at low excess energies, information about the scattering length of the η-nucleus system can be gained. The latter one is closely related to the properties of such a possible bound state and has to be determined with high precision. The available data sets in the close vicinity of the threshold expose discrepancies, which currently forbid the extraction of scattering length information with sufficient precision [1].

Therefore, the reaction d+p→^{3}He+η has been investigated at the ANKE spectrometer using a continuously ramped accelerator beam at excess energies ranging from below threshold at Q = -4 MeV up to Q = +12 MeV. Additionally, data at excess energies of Q = 20, 40 and 60 MeV have been recorded in order to determine total cross sections and to investigate contributions from higher partial waves [2].

For the analysis of the continuous ramp all data was sorted by the time information in the ramp. A twelve seconds wide interval with an average excess energy Q = 11.35 MeV was picked out to be presented in this report. The resulting width of the excess energy interval is 0.70 MeV.

To search for the events of the reaction channel of interest the ^{3}He nuclei are selected using the ANKE forward detector. The production of η-mesons is identified via the missing mass technique. For the reconstruction of the momenta via the magnetic spectrometer the information of the three drift- and multi-wire proportional chambers are used.

The particle identification is achieved by an energy loss versus momentum plot (ΔE/p) for three segmented scintillation walls, two of the forward system and an additional side wall frame of the positive detector placed behind the forward system. A simultaneous cut on the expected region for ^{3}He nuclei in the (ΔE/p) plot in the three scintillation walls allows for a clear identification of the ^{3}He band. In figure 1b) and c) this plot including the cut is presented for the first and second forward scintillation wall. In the region of 2.6 GeV/c events of the ^{3}He η-production are visible, at 3.2 GeV/c a maximum resulting from events of the two pion production and at 3.4 GeV/c from ^{3}He π^0 can be observed.

The reactions can be identified by plotting the transversal versus the longitudinal reconstructed center of mass (CMS) momenta as shown in figure 1a). For a reaction with two particles in the exit channel one expects a momentum ellipse with a fixed radius. The calculated momentum ellipses of the channels ^{3}He η and ^{3}He π^0 and the kinematical limit for the two pion production are sketched in the plot. Due to the fact that the density of events on an ellipse for events distributed according to phase space is proportional to the transversal momentum, the plot was filled with the reciprocal value of the transversal momentum as an event weight.

In the near threshold region the CMS-momenta of the ^{3}He nuclei are small. Due to this fact the scattering angles ϑ^{LS} for the ^{3}He nuclei after the Lorentz transformation into the laboratory system are small and all ^{3}He nuclei of the reaction channel of interest are in the geometrical acceptance of the

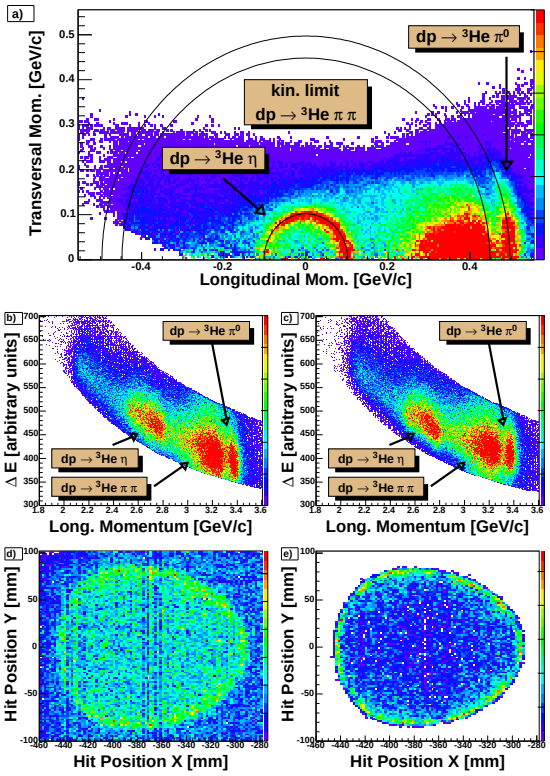

Fig. 1: Preliminary results of the analysis at an average excess energy of Q = 11.35 MeV (timing interval 265 s to 277 s of the continuous ramp)
a) ^{3}He momentum plot to identify CMS momentum ellipses (filled with the reciprocal value of the transversal momentum as event weight).
b), c) (ΔE/p) plot for the first and second scintillation walls (pre-cut on both walls).
d), e) Hit Position of ^{3}He nuclei in the drift chamber system for data (left hand side) and simulations (right hand side) of the reaction d+p→^{3}He+η.

wire chambers of the forward system. For this reason the dp kinematic was used for the beamtime, leading to a full geometrical acceptance in the wire chambers up to an excess energy of 20 MeV. The result is a characteristic image of the hit position in all chambers. In figure 1d) and e) a plot of the hit position of ^{3}He nuclei in ANKE coordinates for the measured data and for Geant4 simulations is shown.

The identification of the η events is done using the missing mass distribution shown in figure 2a). The challenge of the extraction of the η peak from the background near the kinematical limit can impressively be met by using subthreshold data as it was done in [3]. The background reactions, namely the multi pion production and misidentified protons from breakup reactions, have a high excess energy and vary only slowly with the excess energy for the η-production. Subthreshold data of the continuous ramp analysed with the same kinematical conditions as the analysed data are expected to

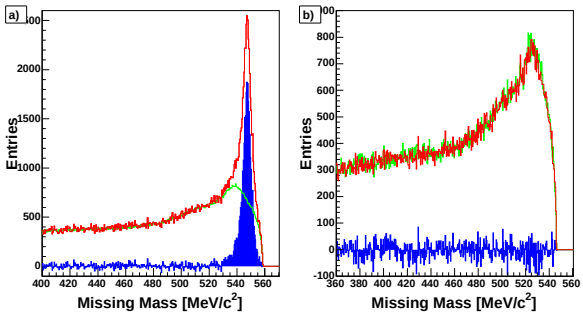

Fig. 2: a) Preliminary missing mass distribution (red line) at an excess energy of Q = 11.35 MeV, the scaled background description (green line) using subthreshold data of the first eighty seconds of the ramp and the background subtracted distribution resulting in a clean η peak (filled histogram).
b) Comparison of the data of the time interval 0 s < t < 10 s of the continuous ramp (Q = -4.4 MeV, green line) with the one of 70 s < t < 80 s (Q = -0.3 MeV, red line) and the difference (blue filled histogram). All events were analysed assuming the same beam momentum.

give a good description of the background behaviour.
The data of the choosen excess energy interval and the subthreshold data were analysed with an expected fixed beam momentum of 3.1865 GeV/c corresponding to the average excess energy Q = 11.35 MeV. The reconstructed ^{3}He momenta were scaled to the same conditions. In figure 2a) the red line shows the resulting missing mass distribution of the data at Q = 11.35 MeV and the green one of the subthreshold data scaled to the red line. The difference, plotted as the filled histogram, corresponds to pure η production.
A check of the method to describe the background is possible by the comparison of the data of the time interval 0 s < t < 10 s corresponding to an average excess energy Q = -4.4 MeV (green line) with the one of 70 s < t < 80 s near threshold at Q = -0.3 MeV (red line) in figure 2b). The difference of the scaled curves (blue filled histogram) vanish, therefore the shape of the background does not vary within the first eighty seconds of the ramp. Thus it can be assumed that this behaviour does not change for the following 180 seconds.
To get angular distributions for the emitted ^{3}He nuclei in the CMS, the missing mass technique is used for different $\cos(\vartheta)^{CMS}$ bins. The background description method is similar and preliminary results are plotted in figure 3.
The resolution of the momentum reconstruction for the ^{3}He nuclei limits the possible binning for angular spectra. A $\cos(\vartheta)^{CMS}$ dependent analysis of the width of the CMS momentum peak for the η-production can be used to determine the transversal and longitudinal resolution.
The current results of the analysis show that the goals of the proposal [2], the investigation of the near threshold region up to intermediate excess energys and extraction of angular distributions, can be realised with complete satisfaction. A data sample with low statistical and systematical errors will help to extract information about the scattering length with high precision and will contibute to the open question about the existence of η-mesic ^{3}He nuclei.

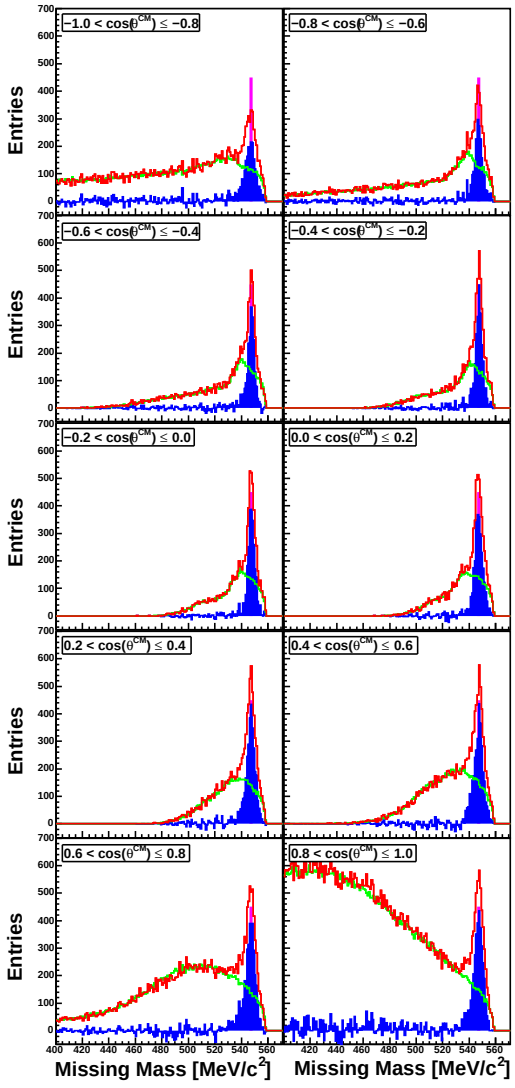

Fig. 3: Preliminary missing mass plots (red line) in $\cos(\vartheta)$ dependence to extract an angular distribution at an excess energy of Q = 11.35 MeV. The background description (green line) and the subtracted η signal (blue filled histogram) are added.

References:

[1] A. Sibirtsev, J. Haidenbauer, C. Hanhart and J. A. Niskanen, *The η^{3}He scattering length revisited*, Eur. Phys. J. A 22, 495-502 (2004)

[2] A. Khoukaz, T. Mersmann, *Investigation of the ^{3}He η final state in the reaction d+p→^{3}He+η at ANKE*, COSY-Proposal, 2004

[3] A. Wronska, *Near threshold eta meson production in the d+d→^{4}He+η reaction*, doctoral thesis, Jagiellonian University, Cracow, 2005

[1] Institut für Kernphysik Westfälische Wilhelms-Universität, 48149 Münster, Germany
[2] Institut für Kernphysik Forschungszentrum Jülich, 52428 Jülich, Germany

*Supported by FZ-Jülich FFE

Study of the multi pion production d+p→^{3}He+N·π close to the η-production threshold at ANKE*

M. Mielke[1], A. Khoukaz[1], T. Mersmann[1], M. Papenbrock[1], and T. Rausmann[1] for the ANKE-Collaboration

In January 05 the reaction d+p → ^{3}He+η was studied at ANKE [1]. Due to the fact that the reaction of interest was measured by detection of the ^{3}He nuclei and reconstruction of the η meson via the missing mass technique, data on the multi pion production near the η threshold was additionally obtained with the same trigger.

The multi pion production causes background in the missing mass spectrum. For the separation of the η signal from this background a systematic study of the multi pion production near the η threshold is required. This can be done by investigating ^{3}He events with a coincidental detected π^- meson.

Additionally to the forward detector used for the ^{3}He detection, the negative system of the ANKE experimental setup was used to detect π^- mesons. The data presented here was obtained at an excess energy of Q = 20 MeV relative to the η threshold and a fixed beam momentum of 3.223 GeV/c.

In the following analysis only events with a coincidental hit of a ^{3}He nucleus in the forward detector and a π^- meson in the negative system are used. The ^{3}He nuclei were identified as described in [2]. T At the used beam energy, particles detected by the negative system in coincidence with a ^{3}He nucleus hit in the forward system can only be pions or leptonic background.

η mesons which decay into pions can be reconstructed via the missing mass of ^{3}He nuclei (figure 1a). The analysed data (filled histogram) is compared to ANKE Root simulations of the specified reactions distributed according to phase space. The expected peak resulting from d+p →^{3}He + η [π^+ π^- π^0] can not yet be explicitly separated here from the multi pion background. However it is expected that a better description of the background as explained in [2] will make this possible.

Multi pion production can be identified in the missing mass distribution of the ^{3}He π^- system (figure 1b). The two charged pion production leads to the left peak at the mass of the π^+ meson which agrees well to the expected distributon. Furthermore, the simulations indicate that the structure on the right hand side of the spectrum results mainly from the reactions d+p → ^{3}He + η [π^+ π^- π^0] and d+p → ^{3}He + π^+ π^- π^0.

The relative contribution of the reaction ^{3}He + η [π^+ π^- π^0] can be quantified as described in [2]. By this the contribution of the direct production of three pions can be determined.

Although there is only a limited angular acceptance for π^- mesons in the negative detector system as visible in figure 1c, the data can help to understand the behaviour of the background in the η analysis. A comparison with the results of other experimental setups with a better angular acceptance for these reactions [3] can be done.

Furthermore, events with two π^- mesons detected in the negative system can be selected to study the four pion production which can cause a background below the η missing mass peak. Due to the fact that the threshold of this reaction is above the η threshold, a study using η subthreshold data is not possible. Even in case that the four pion production is suppressed as expected, an extracted upper limit for the cross section of the four pion production is of high value for the background determination of the η data.

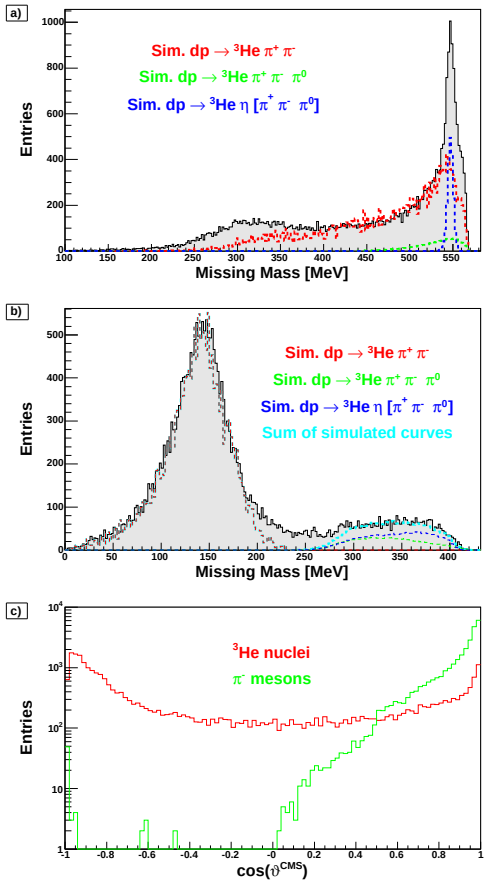

Fig. 1: Spectra for events with a coincident detection of a ^{3}He nucleus and a π^-

a) Missing Mass distribution of detected ^{3}He nuclei compared with ANKE Root simulatons of the given reactions.

b) Missing Mass distribution of the ^{3}He π^- system compared with ANKE Root simulations of the given reactions.

c) Reconstructed scattering angle in the center of mass system for the measured ^{3}He nuclei and π^- mesons.

References:

[1] A. Khoukaz, T. Mersmann *Investigation of the ^{3}He η final state in the reaction d+p→^{3}He+η at ANKE*, COSY-Proposal, 2004

[2] T. Mersmann et al., ibidem, *Investigation of the ^{3}He η Final State in dp-Reaction d+p→^{3}He+η at ANKE*

[3] M. Bashkanov et al., *Exclusive Measurements of pd →^{3}Heππ: the ABC Effect Revisited*, arXiv: nucl-ex/0508011, 2005

[1] Institut für Kernphysik Westfälische Wilhelms-Universität, 48149 Münster, Germany

* Supported by FZ-Jülich FFE

The reaction d+p→^{3}He+π^0 close to the η production threshold at ANKE*

M. Papenbrock[1], A. Khoukaz[1], T. Mersmann[1], M. Mielke[1], and T. Rausmann[1] for the ANKE-Collaboration

In January 05 the reaction d+p→^{3}He+η was studied at the ANKE experimental setup [1]. Due to the fact that the reaction of interest was measured by detection of the ^{3}He nuclei and reconstruction of the η meson via the missing mass technique, data on the π^0 production near the η threshold was additionally obtained with the same trigger. Here we present data obtained at an excess energy of Q = 20 MeV relative to the η threshold, corresponding to Q = 427 MeV with respect to the π^0 threshold.

The ^{3}He nuclei were identified as described in [2]. The extracted transversal versus longitudinal momentum plot in the center of mass system exhibits momentum ellipses for both the exit channels ^{3}He+η and ^{3}He+π^0 [2]. As can be seen in figure 1a), acceptance for the latter reaction is given only for forward and backward scattered ^{3}He nuclei in the center of mass system. Therefore, figures 1b) and c) are restricted to momenta, where the events of the exit channel ^{3}He+π^0 are expected. The plots were filled with the reciprocal value of the transversal momentum as an event weight, as explained in [2]. For forward scattered ^{3}He nuclei, a distribution of events of this reaction is visible on the momentum ellipse (fig. 1b). Since the differential cross section of this channel for backward scattered ^{3}He nuclei is at least one order of magnitude smaller than the one for forward scattered nuclei [3], no entries are visible in the corresponding plot (fig. 1c).

Figure 2 shows the center of mass momentum of the ^{3}He nuclei for different $\cos(\vartheta^{CMS}_{^3He})$ intervalls. For $\cos(\vartheta^{CMS}_{^3He}) < 0$, no clear peak of the π^0 production is visible. In contrast, for $\cos(\vartheta^{CMS}_{^3He}) > 0$, clear π^0 signals on top of background distributions, arising from multi pion production and misidentified protons from breakup reactions are visible.

To describe and to subtract this background, the CMS momenta for simulations of two background reactions as well as of the π^0 production is plotted in figure 1d). The generated events are distributed according to phase space. However, in experiment the angular distribution for the ^{3}He nuclei in the reaction channel d+p→^{3}He+π+π is not isotropic, but increases with $\cos(\vartheta^{CMS}_{^3He})$.

After a careful background subtraction it will be possible to extract differential cross section information for the reaction d+p→^{3}He+π^0.

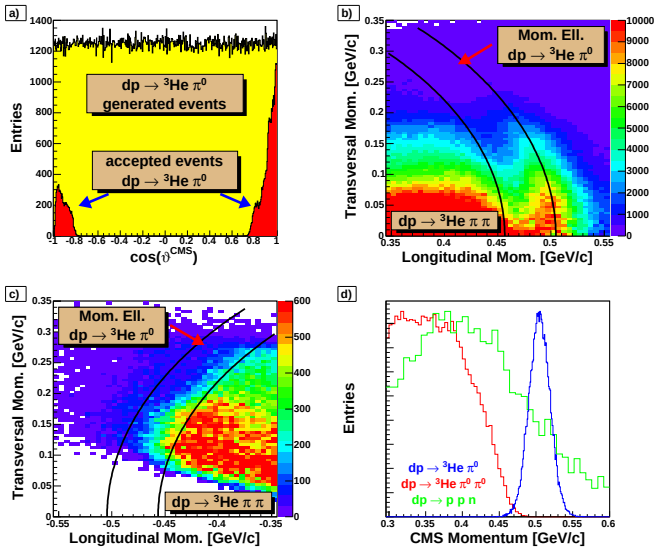

Fig. 1: a) Acceptance of the ANKE detector for the reaction d+p→^{3}He+π^0 (Monte-Carlo simulations).
b) c) Preliminary ^{3}He momentum plots to identify the momentum ellipse of the exit channel ^{3}He+π^0.
d) Center of mass momenta for the named reactions, accepted by the ANKE detector (Monte-Carlo simulations, scaled arbitrarily).

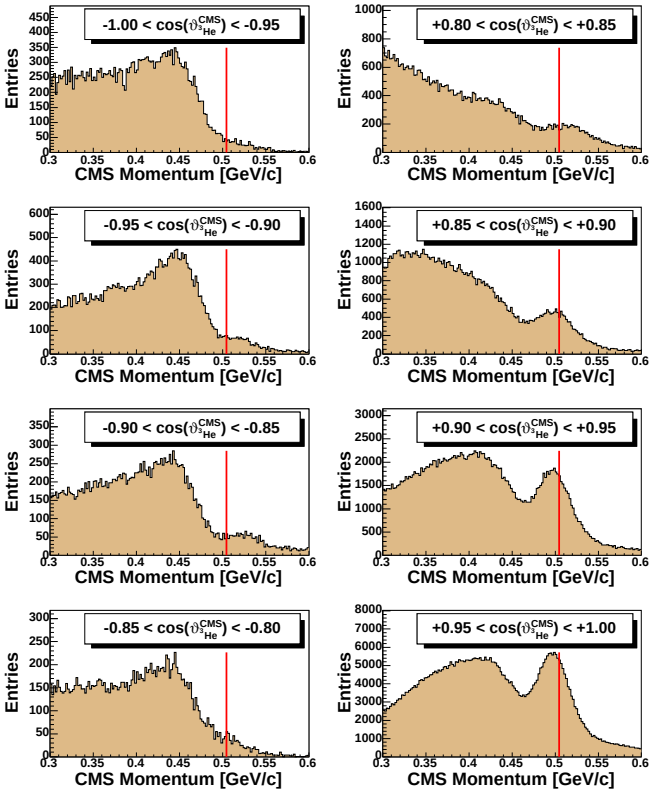

Fig. 2: Center of mass momentum distribution of detected ^{3}He nuclei for different $\cos(\vartheta^{CMS}_{^3He})$ intervals.
The vertical lines indicate the expected position of signals from the π^0 production.

References:

[1] A. Khoukaz, T. Mersmann, *Investigation of the ^{3}He η final state in the reaction d+p→^{3}He+η at ANKE*, COSY-Proposal, 2004

[2] T. Mersmann et al., ibidem, *Investigation of the ^{3}He η Final State in dp-Reaction d+p→^{3}He+η at ANKE*

[3] C. Kerboul *et al.*, Phys. Lett. B **181** (1986) 28.

[1] Institut für Kernphysik Westfälische Wilhelms-Universität, 48149 Münster, Germany

* Supported by FZ-Jüelich FFE

Investigation of the reaction $\vec{d}+p\rightarrow{}^3He+\eta$ at ANKE*

T. Rausmann[1], D. Chiladze[2], A. Kacharava[3], A. Khoukaz[1], T. Mersmann[1], C. Wilkin [4] and the ANKE collaboration

The reaction $\vec{d}+p\rightarrow{}^3He+\eta$ shows a very striking energy dependence near threshold [1, 2]. Despite the angular distribution remaining essentially isotropic, the square of the amplitude decreases by a factor of three over a few MeV in excess energy. The general feeling is that this is due to a very strong FSI, which suggests that this system has a nearby pole in the complex momentum plane. Now close to threshold there are two independent $d+p\rightarrow{}^3He+\eta$ amplitudes A and B. The moduli-squared of these amplitudes can be separated by measurements of the diffential cross sections and tensor analysing power t_{20} [3].

Before submitting a dedicated experimental proposal to determine the energy dependence of A and B, the feasibility of the measurements of t_{20} has to be shown. The first measurement has been carried out parasitically at an ANKE beam time on the deuteron charge-exchange reaction in February 2005 [4]. This reaction was studied for different energies and among other beam momenta at one setting corresponding to the $d+p\rightarrow{}^3He+\eta$ production at an excess energy of Q = 7.4 MeV (p = 3,17 GeV/c).

To search for the events of the reaction channel of interest the ^{3}He nuclei were identified using the ANKE forward detector. The reaction $\vec{d}+p\rightarrow{}^3He+\eta$ can be isolated by plotting the transversal versus the longitudinal reconstructed momentum, as shown in figure 1. For a reaction with two particles in the exit channel, one expects a momentum ellipse with a fixed radius. The calculated momentum ellipse of the exit channel $^3He+\eta$ is sketched in the plot (black line).

The identification of the η events is done using the missing mass distribution. To describe the background behaviour subthreshold data (Q = -4 to 0 MeV) from the ^{3}Heη beam time of January 2005 were used. An explanation of this method can be found in ref. [5]. Preliminary missing mass plots for the spin-mode 4 ($P_z = 0$ and $P_{zz} = 1$) and different $\cos\vartheta^{CM}$ intervals are plotted in figure 2.

The current results of the analysis show a clear η-signal on a background that can be described by the available subtreshold data. Hence the determination of t_{20} is feasible. Future measurements at different excess energies should be considered to study the FSI effects separately for the A and B terms [3].

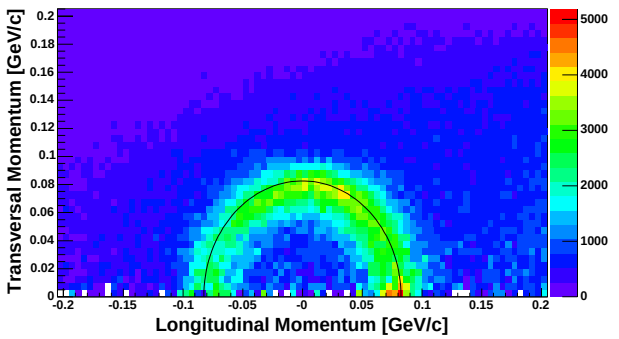

Fig. 1: ^{3}He momentum plot to identify a momentum ellipse. Preliminary results of the analysis at an average excess energy of Q = 7.4 MeV.

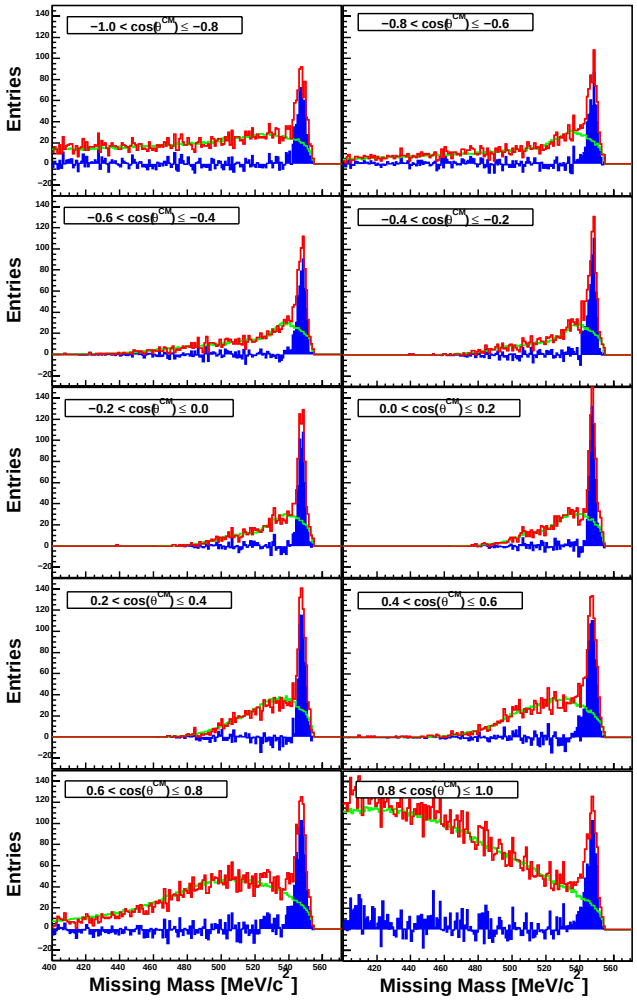

Fig. 2: Missing mass plots (red lines) for spin-mode 4 in various $\cos\vartheta^{CM}$ intervals at an excess energy of Q = 7.4 MeV, the background description (green lines) and the difference (blue filled histograms) are also included. The results are still preliminary.

References:

[1] J. Berger et al., Phys. Rev. Lett. **61** (1988) 919.
[2] B. Mayer et al., Phys Rev C **53** (1996) 2068.
[3] J.-F. Germond & C. Wilkin, J. Phys. **G14** (1988) 181.
[4] A. Kacharava et al., *The Polarised Charge-Exchange Reaction* $\vec{d}+p\rightarrow(pp)n$, COSY-Proposal, 2004
[5] T. Mersmann et al., *Investigation of the* $^3He\,\eta$ *final state in the dp-Reactions at ANKE*, IKP Ann. Rep. 2005

[1] IKP Westfälische Wilhelms-Universität, Münster, Germany
[2] IKP Forschungszentrum Jülich, Germany
[3] Phys. Inst. II, Universität Erlangen, Germany
[4] Physics Dept., UCL, London, UK
* Supported by FZ Jülich FFE

Final results of the first $dd \to {}^4He\eta$ measurement at ANKE[a]

A.Wrońska*, V.Hejny, and C. Wilkin†

In 2003 the ANKE collaboration performed measurements of the $dd \to {}^4He\eta$ reaction close to threshold [1] in two weeks of beam time, in January and November. The analysis of the first data set, *i.e.* that taken at the excess energies of -2.6 MeV, $+2.6$ MeV and $+7.7$ MeV, has been finalised. The details can be found in refs. [2, 3] and only the main results are summarised here.

Tracks and momenta of ^{4}He were reconstructed from signals in the multiwire drift chambers, while energy losses and time-of-flights were measured using the three–layer scintillation hodoscope. A set of two–dimensional cuts was exploited in order to select ^{4}He particles: three ΔE–p cuts and two ΔT–p cuts (signals from the 1st layer provided a reference time). The number of events with an η meson accompanying the ^{4}He particle was determined by studying the missing–mass spectra in individual angular bins. The shape of the background beneath the η peaks was deduced from analogous spectra obtained below threshold. The absolute normalisation was deduced by comparing the interpolated inclusive ^{4}He production data of ref. [4] with the yields observed in our experiment. This normalisation was confirmed through the analysis of another observed process, the $dd \to {}^3He\,n$ yields being compared to the data of ref. [5]. The total cross sections obtained were

$$\sigma_1 = \left(13.1 \pm 0.7_{\rm stat} \pm 1.8_{\rm syst}\right) \text{ nb} \quad \text{at} \quad Q_1 = 2.6\,\text{MeV},$$
$$\sigma_2 = \left(16.4 \pm 1.0_{\rm stat} \pm 2.1_{\rm syst}\right) \text{ nb} \quad \text{at} \quad Q_2 = 7.7\,\text{MeV}.$$

Fig. 1 is a graphical representation of our results and those of previous experiments [6, 7]. However, the SPESIV results [6] cover only lower excess energies and those of SPESIII were obtained with a polarised deuteron beam of helicity $m = \pm 1$. The latter can only be compared to our cross sections after making certain assumptions on the partial wave composition of the reaction amplitude. These can only be verified through the determination of angular distributions and deuteron tensor analysing powers.

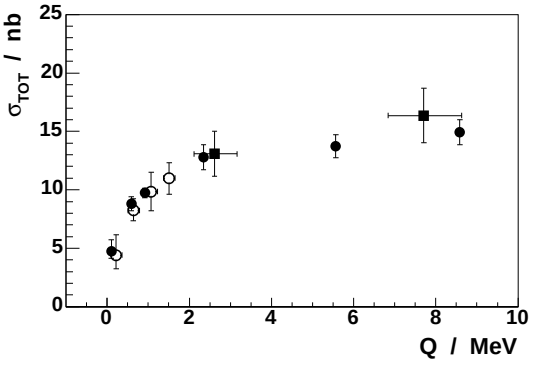

Fig. 1: Our results (squares) compared to the data on the $dd \to {}^4He\eta$ total cross section obtained at Saclay ([6] – open circles, [7] – full circles, data obtained with polarised beam).

Fig. 2 presents the angular distributions of the η meson from the $dd \to {}^4He\eta$ reaction measured in our experiment. Statistical errors are attached to the data points and the systematic errors, obtained by varying the analysis conditions within their uncertainties, are shown as histograms. Solid lines represent a constant and quadratic fits for the lower and higher excess energy, respectively. The two types of errors were added in quadrature for fitting purposes.

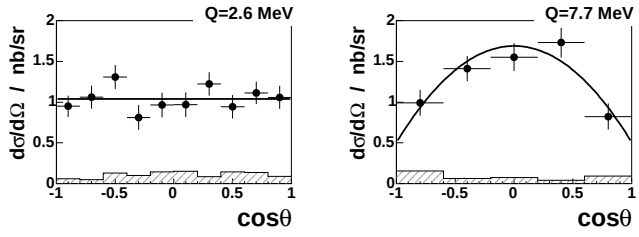

Fig. 2: Angular distributions of the η meson produced in the $dd \to {}^4He\eta$ reaction at the two excess energies investigated in the January beam time. Error bars represent statistical errors and the systematic ones are drawn as histograms.

While consistent with isotropy at the lower energy, *i.e.* with *s*-wave production, the angular distribution at the higher energy reveals a strong anisotropy, indicating the onset of higher partial waves. This result brings into question the scaling used in ref. [7] to obtain the unpolarised cross section from the polarised one.

The possibility of higher partial waves influences also the determination of the *s*–wave $\eta\alpha$ scattering length, which is a key quantity in studying the $\eta\alpha$ quasi–bound state hypothesis. This requires the *s*-wave production to be isolated. However, as we showed in ref. [3], the knowledge of the angular distributions alone is insufficient to decompose unambiguously the reaction amplitude into partial waves. For this purpose one needs also polarisation observables. Our experiment has shown, at which energies such measurements should be started. An experiment performed in autumn 2003 by the GEM collaboration [8] is designed to provide such deuteron analysing powers.

The data collected in the November run at $Q = 22$ MeV and $Q = 43$ MeV are still under analysis. Due to the smaller statistics, we will probably extract only total cross sections at these energies.

References:

[1] V. Hejny *et al.*, IKP Annual Report 2003.
[2] A. Wrońska, PhD thesis, Jagiellonian Univ., Cracow, 2005.
[3] A. Wrońska *et al.*, Eur. Phys. J. A 26 (2005) 421.
[4] J. Banaigs *et al.*, Nucl. Phys. B 105 (1976) 52.
[5] G. Bizard *et al.*, Phys. Rev. C 22 (1980) 1632.
[6] R. Frascaria *et al.*, Phys. Rev. C 50 (1994) 537.
[7] N. Willis *et al.*, Phys. Lett. B 406 (1997) 14.
[8] H. Machner *et al.*, COSY proposal 124 (2003).

[a] project supported by EU
* Institute of Physics, Jagiellonian University, Cracow, Poland
† Physics & Astronomy Department, UCL, London, U.K.

Near threshold π production in $dd \to {}^3HN\pi$ and $dd \to {}^3HeN\pi$

M. Śmiechowicz* for the ANKE collaboration

Recently two experiments observing charge symmetry breaking (CSB) reactions were successfully performed. Those are the measurement of the forward-backward asymmetry in $pn \to \pi^0 d$ [1] and the observation of a non-zero total cross section in $dd \to \alpha\pi^0$ [2]. In order to analyse these reactions in the framework of Chiral Pertubation Theory a big theory collaboration has been formed. However, to succesfully carry out the theoretical analysis, and, especially, to isolate the isospin violating matrix elements of interest, more information on related isospin conserving interactions is needed. In case of $dd \to \alpha\pi^0$ the reactions of interest are $dd \to {}^3HN\pi$ and $dd \to {}^3HeN\pi$. Obtaining the energy dependence of the total cross sections of these reactions will allow to better understand the isospin-conserving part of the initial-state interaction relevant for the analysis of the reaction $dd \to \alpha\pi^0$. In addition, the data may provide new insights into four nucleon dynamics in large-momentum transfer reactions, like role of the 4-body forces.

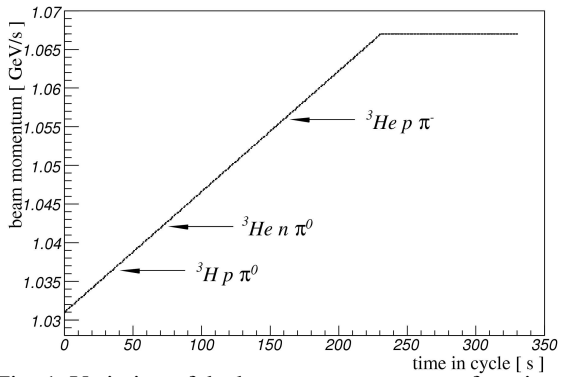

Fig. 1: Variation of the beam momentum as a function of time in one COSY cycle. Arrows mark the corresponding thresholds for all three reactions.

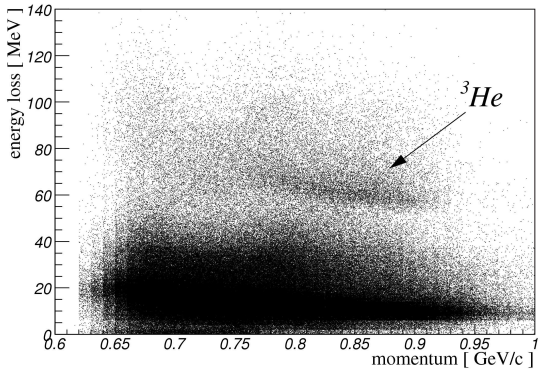

Fig. 2: Energy loss versus reconstructed momentum. The region containing ${}^3He$ is indicated.

The experiment was carried out in March 2005 using the internal zero-degree facility ANKE[3]. At beam momenta close to threshold ANKE has almost 100% acceptance for the investigated reactions. In order to extract full excitation functions close to threshold COSY provided a deuteron beam, which was smoothly ramped between 1.031 GeV/c and 1.067 GeV/c during one COSY cycle (see Fig.1). This enabled us to measure the following three reactions simultaneously: $dd \to {}^3Hp\pi^0$, $dd \to {}^3Hep\pi^-$ and $dd \to {}^3Hen\pi^0$.

Current status:

Energy-loss and time-of-flight calibrations for all counters are done. In order to improve the resolution in energy loss and to take into account effects of light propagation the detector signal has been corrected for the vertical coordinate of the impact point. Particle identification was then done by means of energy loss versus momentum and time-of-flight. In Fig.2 the energy loss is plotted versus the reconstructed momentum. The identified ${}^3He$ events are clearly visible. In Fig.3 the same events (i.e. those identified as ${}^3He$) are presented in a spectrum showing energy loss versus time-of-flight. The preliminary estimated number of detected ${}^3He$ particles is about $6 \cdot 10^4$.

The data analysis is still in progress. In order to extract energy-dependent total cross sections for all measured channels, the determination of luminosity, detector acceptance and analysis efficiency still has to be done.

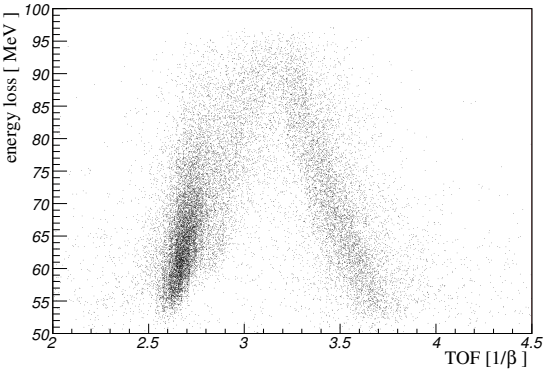

Fig. 3: Identification of ${}^3He$ on the energy loss versus time of flight spectrum.

References:

[1] A. K. Opper *et al.*, Phys. Rev. Lett. **91**, 212302 (2003).
[2] E. J. Stephenson *et al.*, Phys. Rev. Lett. **91**, 142302 (2003).
[3] S. Barsov *et al.*, Nucl. Inst. and Meth. A **462/3** (2001) 364.

* Institute of Physics, Jagellonian University, 30–059 Cracow, Poland

Production of the $^1S_0$ diproton in the $pp \to pp\pi^0$ reaction at 0.8 GeV

S. Dymov[a], V. Komarov[a], V. Kurbatov[a], Yu. Uzikov[a] and C. Wilkin[b]

Single pion production in NN collisions is the first inelastic process that can be used to test our understanding of the underlying meson–baryon dynamics [1]. By far the clearest reaction to study is $pp \to d\pi^+$, where the differential cross section and multitude of spin observables that have been measured over the years [2] can confront the different theoretical models.

In contrast, much less is known about the $pp \to pp\pi^0$ reaction. Now in cases where the excitation energy E_{pp} of the final protons is very small, due to the Pauli principle, this reaction can excite only the $J^p = 0^+$ ($^1S_0$) diproton state, so that the number of partial waves is restricted. Despite having kinematics very similar to those of $pp \to d\pi^+$, this reaction involves different transitions in the NN system. In particular, the role of the Δ isobar is expected to be much suppressed because the S–wave ΔN intermediate state is forbidden. Data here would thus provide a crucial extra test of pion production models in nucleon–nucleon collisions.

The $pp \to (pp)\pi^0$ differential cross section has been measured with the ANKE spectrometer for pion cms angles between 0° and 15.4° at a proton beam energy of 0.8 GeV [3] using techniques developed in our programme to study large momentum transfer deuteron breakup reactions [4, 5]. The measurement of the momenta of two charged particles, based on information from the forward detector, lead to a clean identification of about 5000 π^0 events, with a background of only a few percent. The value of the luminosity needed to determine the cross section was found from the yield of pp elastic scattering, which was measured simultaneously.

The spectra in the diproton excitation energy E_{pp} showed the expected pp final state enhancement in the $^1S_0$ state. This could be described by the Watson-Migdal factor while leaving the possibility of a very small P-wave contamination at the higher E_{pp}.

The cross sections reported here correspond to the sum over the range $0 < E_{pp} < 3$ MeV. Due to the identity of the initial protons, the differential cross section is an even function of $\cos\theta_\pi^{cm}$ and in the figure it is plotted *versus* $\cos^2\theta_\pi^{cm}$. The results show a monotonic decrease towards the forward direction and, as seen from the figure, this can be well parameterised by the linear function $a(1 + b\sin^2\theta_\pi^{cm})$, where $a = (704 \pm 22_{\rm stat} \pm 32_{\rm syst})$ nb/sr and $b = 5.6 \pm 1.2$. With the same E_{pp} cut as used here, a similar forward dip was observed in this reaction at lower energies, $T_p \leq 425$ MeV [6, 7], though for these energies the value of b was found to be much smaller.

Preliminary theoretical predictions for the cross section at 800 MeV have been made in a model that includes contributions from P–wave ΔN intermediate states [8]. The overall magnitude is similar to that which we have observed and, in particular, the forward slope, driven by the pion d–wave, is well reproduced.

There is a real lack of data on the ratio $R(\pi^0/\pi^+)$ of the forward $pp \to (pp)\pi^0$ cross section to that of $pp \to d\pi^+$ in the range between 425 MeV and 800 MeV, *i.e.* the region where the Δ dominates the $pp \to d\pi^+$ reaction. This could be very efficiently filled in by measurements at ANKE, possibly involving polarisation observables. At 800 MeV $R(\pi^0/\pi^+)$ is only about 0.5%, and this small size means that it is very doubtful whether one would be able to extract the isobaric analogue cross section from a study of the spectrum of the pn excitation energy in the $pp \to \pi^+X$ reaction [9]. Direct measurement of π^0 production is required.

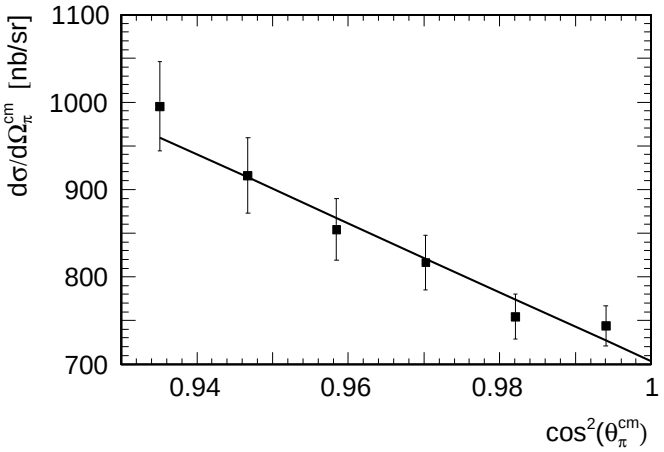

Fig. 1: The measured $pp \to (pp)\pi^0$ differential cross section for $E_{pp} < 3$ MeV as a function of $\cos^2(\theta_\pi^{cm})$. The curve is a straight–line fit to the data.

It is intriguing to note that the ratio of backward dinucleon production in the $pd \to (pp)n$ and $pd \to dp$ reactions at intermediate energies has a very similar value to $R(\pi^0/\pi^+)$ [4]. Such a connection would be natural within a one–pion–exchange mechanism, where the large momentum transfer $pd \to dp$ reaction is driven by a $pp \to d\pi^+$ subprocess [10, 11], and this relationship is currently under investigation [12].

References:

[1] *see e.g.* C. Hanhart, Phys. Rep. **397** (2004) 155.
[2] R.A. Arndt *et al.*, Phys. Rev. C **48** (1993) 1926.
[3] S. Dymov *et al.*, submitted to Phys. Lett. B.
[4] V. Komarov *et al.*, Phys. Lett. B **553** (2003) 179.
[5] S. Yaschenko *et al.*, Phys. Rev. Lett. **94** (2005) 072304.
[6] Y. Maeda, N. Matsuoka, and K. Tamura, Nucl. Phys. A **684** (2001) 392c.
[7] R. Bilger *et al.*, Nucl. Phys. A **693** (2001) 633.
[8] J.A. Niskanen, Phys. Rev. C **43** (1991) 36, and *in preparation*.
[9] M. Abdel-Bary *et al.*, Phys. Lett. B **610** (2005) 31.
[10] N.S. Craigie and C. Wilkin, Nucl. Phys. B **14** (1969) 477.
[11] V.M. Kolybasov and N.Ya. Smorodynskaya, Yad. Fiz. **17** (1973) 1211.
[12] Yu.N. Uzikov and C. Wilkin (*in preparation*).

[a] LNP, JINR, 141980 Dubna, Russia
[b] Physics Dept., UCL, London, WC1E 6BT, UK

Tensor Analysing Power Measurement in Charge–Exchange Reaction $\overrightarrow{d}\,p \to (pp)n^*$

D. Chiladze[a], A. Kacharava[b], F. Rathmann[a], and C. Wilkin[c] for the ANKE collaboration

One major feature of the polarised deuteron charge–exchange break–up reaction $\overrightarrow{d}\,p \to (pp)n$ is that the differential cross section and the two deuteron Cartesian analysing powers A_{xx} and A_{yy} are directly related to the magnitudes of the spin–spin neutron–proton charge–exchange amplitudes, which govern the spin–transfer observables in $\overrightarrow{n}\,p \to \overrightarrow{p}\,n$ at small momentum transfers [1].

A first measurement was carried out at ANKE with a 1170 MeV polarised deuteron beam [2]. Having determined their vector and tensor polarisations before and during the acceleration of deuterons in the COSY ring, measurements of three tensor and two vector analysing powers showed that any depolarisation of the circulating beam is definitely less than 2%. The vector and tensor polarisations are typically about 74% and 59%, respectively, of the ideal values that could be provided by the polarised source.

After identifying the $dp \to (pp)n$ events, these were binned in intervals of diproton excitation energy E_{pp} and three–momentum transfer $q = -\sqrt{t}$. With a stable spin axis in the beam line oriented along the y-direction, the numbers $N(q,\phi)$ of diprotons produced at an azimuthal angle ϕ are, after correcting for luminosity with the help of the beam current monitor,

$$N(q,\phi) = N_0(q)\,\big[1 + \tfrac{3}{2}P_z A_y(q)\cos\phi + \tfrac{1}{2}P_{zz}\big\{A_{yy}(q)\cos^2\phi + A_{xx}(q)\sin^2\phi\big\}\big], \qquad (1)$$

where P_z and P_{zz} are the beam polarisations for the seven different source states, $N_0(q)$ the numbers obtained with the unpolarised beam, and A_y and A_{yy} are vector and tensor analysing powers of the reaction.

The results for the two $\overrightarrow{d}\,p \to (pp)n$ tensor analysing powers are shown in fig. 1 in 20 MeV/c bins in q for two cuts in the excitation energy, *viz.* $0 < E_{pp} < 1\,\mathrm{MeV}$ and $1 < E_{pp} < 3\,\mathrm{MeV}$. In contrast to the strong and rapidly varying tensor analysing powers shown there, the vector A_y is consistent with zero for all momentum transfers.

For low excitation energy E_{pp} of the final pp pair, and small momentum transfers, the $\overrightarrow{d}\,p \to (pp)n$ reaction mainly excites the $^1S_0$ state of the final pp system. This involves a spin–flip from the pn triplet to pp singlet and thus provides a *spin–filter* mechanism. In single–scattering approximation, the results depend only upon the np spin–dependent amplitudes β, γ, δ and ε. If we neglect the deuteron D–state, we expect that at low E_{pp}

$$\begin{aligned} A_{xx} &= \frac{|\beta|^2 + |\gamma|^2 + |\varepsilon|^2 - 2|\delta|^2}{|\beta|^2 + |\gamma|^2 + |\delta|^2 + |\varepsilon|^2}\,, \\ A_{yy} &= \frac{|\delta|^2 + |\varepsilon|^2 - 2|\beta|^2 - 2|\gamma|^2}{|\beta|^2 + |\gamma|^2 + |\delta|^2 + |\varepsilon|^2}\,, \\ A_y &= 0\,. \end{aligned} \qquad (2)$$

Since in the forward direction $\beta = \delta$ and $\gamma = 0$, the value of $A_{xx} = A_{yy}$ at $q = 0$ should depend only upon the ratio of $|\beta|$ to $|\varepsilon|$, which changes smoothly with energy. However, the δ amplitude, which contains the one–pion–exchange pole, varies very rapidly with momentum transfer. Given that the dominant real part of this amplitude vanishes when q is of the order of the pion mass, it is to be expected that in this region

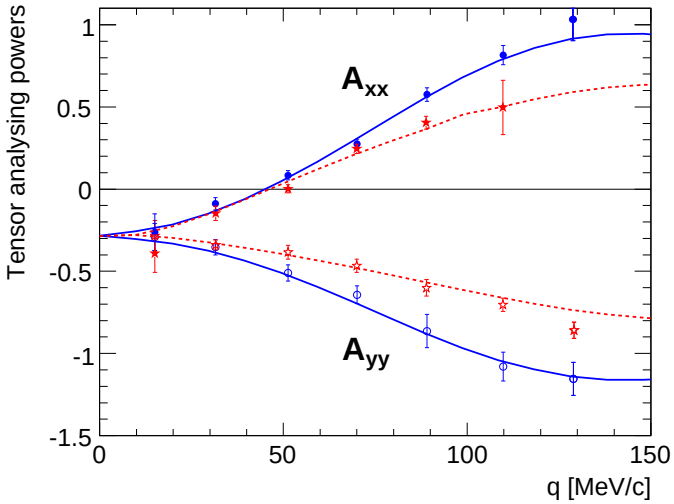

Fig. 1: Values of the tensor analysing powers A_{yy} and A_{xx} extracted for the $dp \to (pp)n$ reaction for $0 < E_{pp} < 1$ MeV (circles) and $1 < E_{pp} < 3$ MeV (stars). The curves correspond to the predictions of the impulse approximation program, for which the input amplitudes at 585 MeV were taken from SAID; $0 < E_{pp} < 1$ MeV (solid) and $1 < E_{pp} < 3$ MeV (broken).

A_{xx} should approach its kinematical limit of $+1$, as suggested by our data in fig. 1.

The spin–triplet final states generally produce the opposite signs for the analysing powers to the singlet and so, as soon as one departs from the very small E_{pp} limit, a dilution of the A_{xx} and A_{yy} signal is predicted. This effect depends sensitively upon the final state interactions in the low energy pp system. These, together with the Paris S+D–state deuteron wave function, are included in our full analysis program

The predictions of fig. 1 were made using amplitudes from the current SAID NN phase shift solution. All the features of both A_{xx} and A_{yy} are reproduced for $q \leq 130\,\mathrm{MeV/c}$ provided that $E_{pp} < 1\,\mathrm{MeV}$. Less dilution of the signal with E_{pp} is seen than predicted by the program, especially in the case of A_{xx}. However, due to the experimental acceptance, there is some correlation between the directions of the diproton relative momentum and the momentum transfer and the program indicates that this can lead to the observed weaker dilution.

References:

[1] A. Kacharava et al., COSY Proposal #152: *Spin Physics from COSY to FAIR*, nucl-ex/0511028.

[2] D. Chiladze et al., submitted to PR ST-AB, nucl-ex/0511052.

[a] IKP FZJ, Germany
[b] Erlangen University, Germany
[c] University College London, U.K.

* supported by FZ–Jülich FFE

First results of analysis of the deuteron break-up reaction $dp \to ppn$ with detection of low relative energy proton pairs in the Side Detector of ANKE

S.Dymov[a], D.Gusev[a], A.Kulikov[a]

Study of the deuteron break-up reaction $pd \to ppn$ at ANKE with a high momentum transfer to a proton pair has been reported in [1]. In this experiment proton pairs of small relative energies were detected in the Forward Detector. In the c.m. system this corresponds to forward emission of a proton pair.

Another reaction with a high momentum transfer (but involving the same physics process) which could provide similar data for understanding the interaction mechanism is $dp \to ppn$ with emission of low relative energy proton pairs in the backward direction in c.m.s. Such protons could be detected in the Side Detector. These measurements have been done in February 2005 using a polarized deuteron beam and a hydrogen jet cluster target.

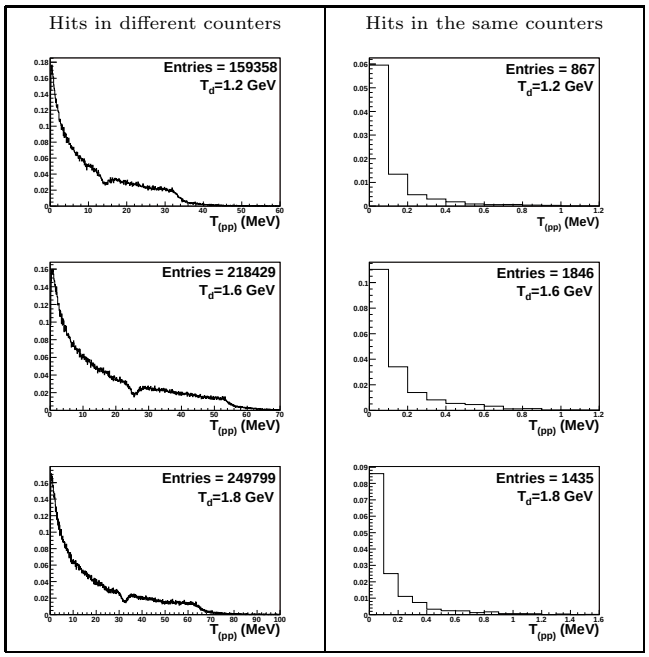

Fig. 1: Acceptance for different deuteron beam energies and for different combinations of hit counters

As a first step of data analysis, simulations have been done with GEANT4 for conditions of the beam-time, i.e. for deuteron energies T_d=1.2, 1.6, and 1.8 GeV, ANKE at an angle of 5.9 degree and using real detector and target coordinates. The acceptance in terms of the proton pair relative energy T_{pp} has been obtained at the condition that two tracks in the Side Detector are found hitting Start counters in combination with the Stop telescopes or Side Wall counters. Ionization losses and multiple scattering were taken into account. In Fig.1 the acceptance for three beam energies is shown for events with particles hitting different Start and Stop counters and those with two hits in the same Start and the same Stop counters. It is seen that the number of events with hits in the same counter (for which the analysis of timing is complicated) is much less than for different counters and T_{pp} for such events is extremely small. The dip in the 15-30 MeV region of T_{pp} is explained by transition from the telescopes to the Side Wall counters. In Fig.2 the calculated resolution of the proton pair relative energy $\sigma_{T_{pp}}$ is shown for T_d=1.6 GeV, this value is very close at all three beam energies. It increases with T_{pp} but for all beam energies is below 1 MeV at T_{pp}<20 MeV.

In Fig.3 the results of a preliminary analysis of experimental data are presented for the beam energy of 1.2 GeV. Only part of statistics is used here. In the left panel a TOF spectrum for one of the Start-Stop combinations is shown. Events from the region of a proton peak in all Start-Stop combinations are selected for further analysis. The right panel is the plot of the measured time difference between two protons versus the calculated one. The right panel is the missing mass distribution which is peaked, as expected, near the neutron mass. Cuts on ionization losses, not yet applied here, will definitely improve the process identification.

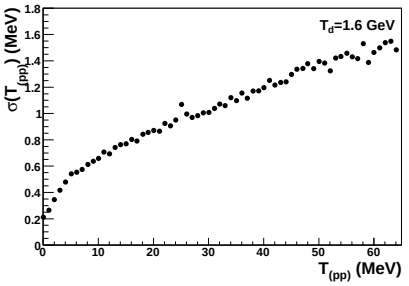

Fig. 2: Resolution on T_{pp} for different beam energies

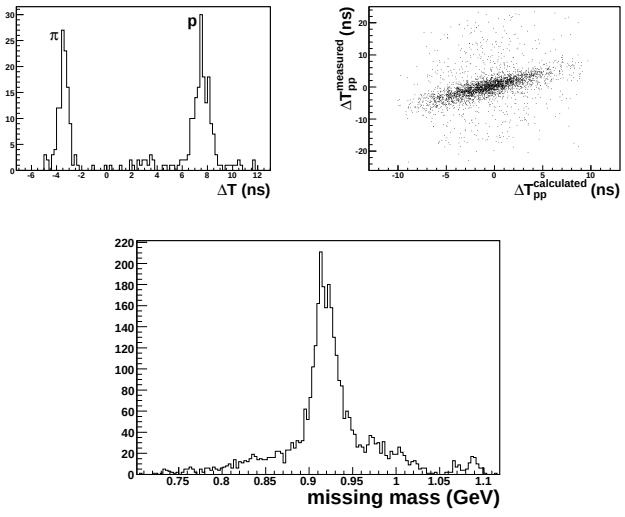

Fig. 3: Experimental distributions: TOF spectrum (left), measured versus calculated time difference between two protons (right), missing mass distribution (central).

[a] Joint Institute for Nuclear Research, Dubna, Russia

References:

[1] V.Komarov et al. Phys. Lett. B**553**(2003)179-185.

Development of a method to determine the polarization of the ANKE storage cell target

S. Dymov[a] and D. Gusev[a] for the ANKE collaboration

Commissioning of the ABS and the storage cell [1] at ANKE includes investigations of the atomic hydrogen density distribution in the cell and the nucleon polarization. The $pp \to d\pi^+$ process with detection of both secondaries was chosen for this aim, and a simulation has been performed to find the optimum conditions for the measurement [2]. At a proton beam energy of 600 MeV and deflection angle of 9.2°, the jet polarization can be determined with an accuracy (RMS) of 4% after 5 hours of data taking at a luminosity of $4 \times 10^{28}\mathrm{cm}^{-2}\mathrm{s}^{-1}$. The polarization would be measured by detecting both particles in the ANKE Forward Detector at $\Theta_\pi^{cm} = 17 - 22°$, while monitoring of the luminosity will be done with pions at 0°, which go to the Positive Detector.

The $pp \to d\pi^+$ events can be identified via reconstructed momenta, the arrival time difference and the energy loss in the scintillation counters. Trajectories of both particles together with their arrival times allow, with the use of kinematical constraints, to reconstruct the coordinates of the interaction point. This is accomplished by minimizing the following expression:

$$\chi^2 = \Sigma\frac{(\Delta w)_i^2}{(\sigma^2 w)_i} + \mathrm{HW}\cdot\Sigma(\Delta\mathrm{P})_\mathrm{i}^2 + \Sigma\frac{(\Delta\mathrm{TOF})_\mathrm{i}^2}{(\sigma^2\mathrm{TOF})_\mathrm{i}},$$

where the first term includes the deviations of the trajectories in the MWPCs, the second one is the kinematical term, applied with a "heavy weight" HW. ΔTOF was calculated as $\Delta\mathrm{TOF} = \tau(\vec{\mathrm{p}},\mathrm{l},\mathrm{m}) - \mathrm{TDC}\cdot\mathrm{channel}$, where $\tau(p,l,m)$ is the TOF from the vertex, calculated from the particle momentum, trajectory length and the mass assumed, and $TDC \cdot channel$ is the measured arrival time. This procedure provides a measurement of the gas density distribution inside the cell and a separation of the background $d\pi^+$–pairs originating from the rest gas in the target and magnet chambers. An appropriate software for the vertex reconstruction has been developed.

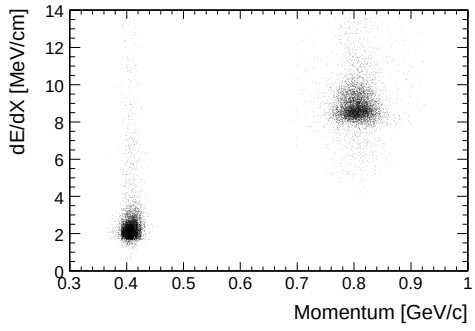

Fig. 1: Identification of $d\pi^+$ by energy loss.

The method was tested during a beam time in November 2005 [3]. A calibration run with a point-like CH_2 strip target allowed to tune the $d\pi^+$ events separation and confirmed that the obtained detector acceptance corresponds to the simulated one. The data showed that the resolution of the reconstructed vertex coordinate is $\sigma_z = 3.6$ cm longitudinally and $\sigma_x = 0.8$ cm transversely. These values have been obtained with the use of the FD MWPC only; the inclusion of the newly built MWDC into the analysis should improve σ_x up to ≈ 0.5 cm.

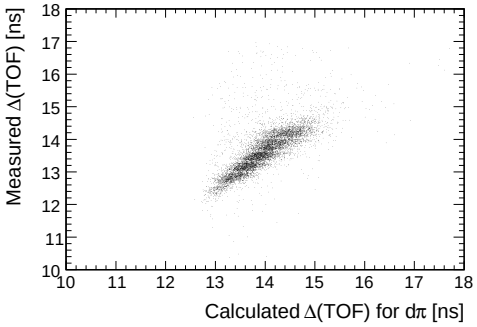

Fig. 2: Identification of $d\pi^+$ by TOF.

The $d\pi^+$ pairs are well separated due to the high deuteron energy loss, as shown in Fig. 1. In Fig. 2, the comparison of the measured arrival time difference with the one calculated for pion and deuteron masses is shown for the storage cell data. The large ΔTOF of $d\pi^+$ pairs allows to identify them practically without dilution from pairs of other particles. The distribution of coordinates in Fig. 3, obtained with the storage cell, shows the events produced inside the cell as well as the background. The origin in the figure corresponds to the ABS jet position and the x and y coordinates follow the positions of the COSY beam.

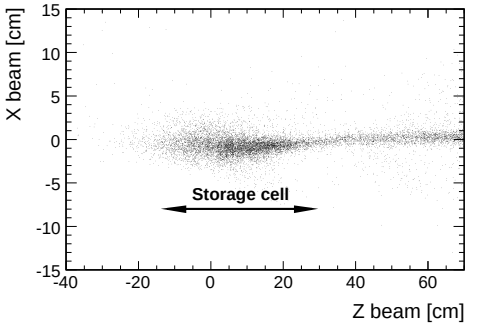

Fig. 3: Reconstructed vertex coordinates for the cell measurement.

[a] Joint Institute for Nuclear Research, Dubna, Russia

References:

[1] Commissioning and Initial Research with the Polarized Gas Target at ANKE. COSY Proposal #146.
[2] S. Dymov et al, Simulation of ABS polarization measurement in Week 47, 2005. ANKE internal report.
[3] K. Grigoryev et al, Storage cell tests and commissioning of the Polarized Internal Gas Target. IKP Annual report, 2005.

The Polarized Internal Target at ANKE

R. Engels, K. Grigoryev[a], P. Jansen[b], F. Klehr[b], H. Kleines[c], M. Mikirtychyants[a], F. Rathmann, J. Sarkadi, H. Seyfarth, and A. Vasilyev[a]

During spring of 2005 all components of the polarized internal target (PIT) have been transferred from the laboratory in the IKP office building to the LKW-Schleuse inside the COSY hall, but outside of the accelerator area. There, the polarized atomic beam source (ABS) using its central flange has been fixed to the new supporting bridge, which allows one to move the system of bridge and ABS as one unit by crane. It can be positioned either between the ANKE spectrometer dipole magnets D1 and D2, or on a special support in the LKW-Schleuse for tests or polarization studies in the framework of an ISTC project [1]. Test measurements, performed after reassembling of the ABS, have shown that the earlier values of ABS-beam intensity and polarization are reproduced. All the supply units and the components of the control and interlock system [2] are mounted on a crane-transportable platform. Thus, fast transfer of the whole setup to and from the ANKE-target position becomes possible, requiring only a few crane movements.
During the summer shutdown of 2005, the bridge with the ABS was moved (Fig. 1) to the ANKE-target position (photograph in Fig. 2). In order to test the movement of the complete setup with the lateral shift of the central dipole magnet D2, also the Lamb-shift polarimeter (LSP) was mounted at the ANKE-target chamber as shown in Fig. 2. The supply platform is positioned nearby outside the accelerator tunnel on an elevated support to keep the lengths of cables and supply-lines as short as possible.

Fig. 1: ABS and supporting bridge with suspension frame in flight to the ANKE target place. The main designer (F.K.) stands below in the opened COSY tunnel, trusting his constructions.

Measurements of the magnetic stray field, mainly caused by the 20 cm gap width of the magnet D2, have shown values near or above the critical values of ABS components, like turbo pumps, displacer-driving motors of the cryogenic pumps, and vacuum gauges. With sufficient soft-iron shielding, the ABS now delivers the laboratory $\vec{H}$ beam intensity of $\sim 7 \cdot 10^{16}$ atoms/s (two hyperfine states) at the highest D2-gap field of 1.6 T. Another sensitive component of the ABS is the medium field transition unit (MFT), which is used to depopulate one of the two hyperfine states of the $\vec{H}$ beam. Its soft-iron shielding (designed using the computer code MAFIA [3]) avoids any measurable influence of the magnetic stray fields up to the highest value.
In late 2005, first tests and commissioning measurements with the PIT at ANKE have been performed with promising results [4].

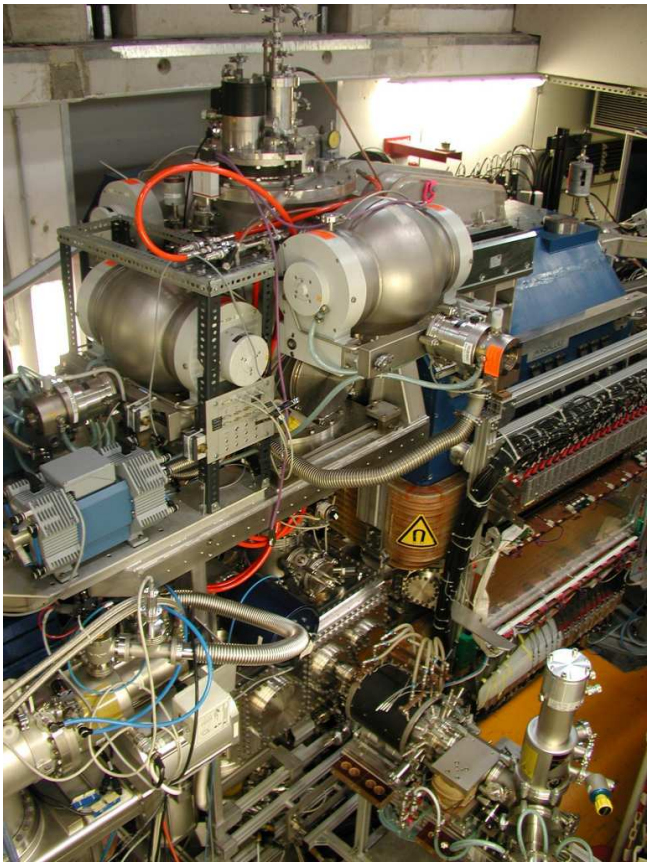

Fig. 2: ABS (vertical, carried by the support bridge) and components of the Lamb-shift polarimeter (horizontal) at the ANKE-target chamber. The COSY beam circulates from left to right through the setup, the spectrometer magnet D2 is at the right-hand side.

References:

[1] **I**nternational **S**cience and **T**echnology **C**enter, Moscow, Russia, project No. 1861.
[2] H. Kleines et al., Nucl. Instr. Methods A (2006, in print).
[3] V. Nelyubin, internal report IKP II (1998).
[4] K. Grigoriev et al., contribution to this report.

[a] St. Petersburg Nuclear Physics Institute, Gatchina, Russia.
[b] Zentralabteilung Technologie, FZ Jülich.
[c] Zentralinstitut für Elektronik, FZ Jülich.

Storage cell tests and commissioning of the Polarized Internal Gas Target

K. Grigoryev[1], S. Dymov[2], R. Engels, D. Chiladze[3], D. Gusev[2], A. Kacharava[4], B. Lorentz, M. Mikirtytchiants[5], S. Mikirtytchiants[5], D. Prasuhn, F. Rathmann, J. Sarkadi and A. Vasilyev[5]

In order to study the lateral dimensions of the COSY beam at the ANKE–target position and its intensity with the storage cell at the target position, a setup has been developed which allows one to position diaphragms and storage cells onto the COSY–beam axis, to move them perpendicular to the beam axis in horizontal ($\Delta X = \pm 75$ mm) and vertical ($\Delta Y = \pm 12.5$ mm) direction, and to tilt the cell–tube axis against the beam axis (Fig. 1). The remote-control system is part of the PIT control and interlock installation [1].

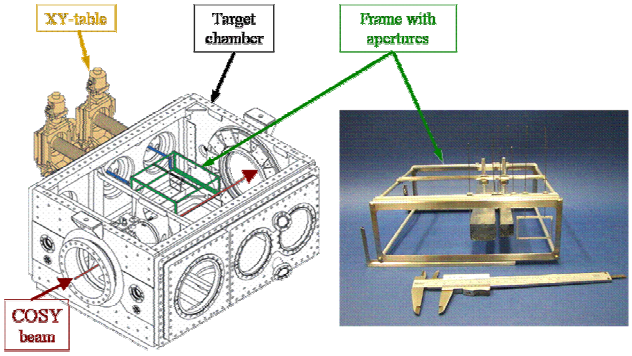

Fig. 1: The new ANKE target chamber (width 60 cm, length 80 cm, and height 40 cm) with the motorized, remote–controlled XY manipulators, used to position the target frame (left–hand part). Various apertures or storage cells can be suspended in the frame (right–hand part).

In February 2005, a second cell test run at ANKE was carried out. Based on the results from previous tests in 2004, new storage cell prototypes were built. Two storage cells made from 25µm thick pure aluminum foil and one aperture with inner size of 40x25 mm^2 were installed in the supporting frame (see right–hand part of Fig. 1) and implemented into the target chamber at ANKE. Both cells had an unpolarized gas feeding tube with a connection to a gas supply to simulate a hydrogen or nitrogen target of a density similar to what is obtained with the Atomic Beam Source (ABS) [2].

After acceleration of an unpolarized deuteron beam through the large cell (30x20 mm^2) at an energy of about 2.1 GeV, the size of the beam did not change much compared to earlier tests with a 2.7 GeV proton beam. It was possible to store and accelerate more than 2/3 of the injected deuterons into the ring (~9x10^9 deuterons). By scraping, the dimensions of the stored beam in the cell were decreased to 13x11 mm^2. After that, about 15% of the injected deuterons (1.7x10^9 deuterons) were successfully stored in the COSY ring with the small cell of 15x15 mm^2. The length of both cells was 220 mm and there are no restrictions to use cells up to a length of about 400 mm.

Based on the result of these tests, a new storage cell prototype was built (see Fig. 2.). An aluminum foil, covered with Teflon® PTFE suspension to minimize depolarization on the surface was used. This cell prototype has a feeding tube for the ABS beam and an extraction tube to the Lamb–Shift Polarimeter [3], which is planned to be used for polarization measurements of the target atoms. Since the major tasks for these tests were completed, first measurements with hydrogen gas in the target cell were carried out.

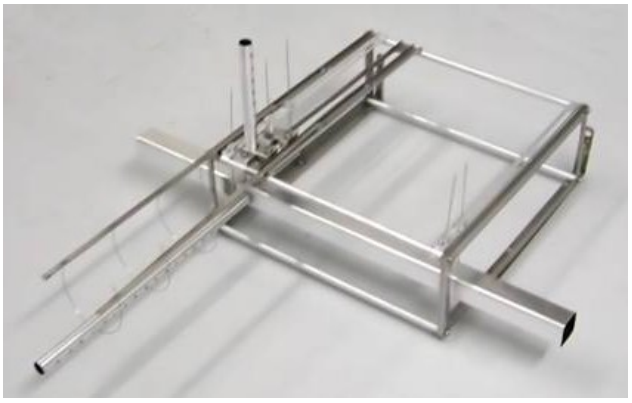

Fig. 2: Storage cell prototype with a feeding and an extraction tubes for tests in November 2005.

In June 2005, the polarized atomic beam source has been installed at the ANKE–target chamber for commissioning and test measurements [4]. Based on earlier studies, using different apertures to determine the lateral COSY–beam dimensions at the ANKE–target position, more extensive measurements were performed with a rectangular 40x25 mm^2 aperture and a storage–cell tube of 20x20 mm^2 cross section and 400 mm length. Cutting the beam by stepwise moving the left, right, upper, and lower edges of the apertures frame towards the beam axis gave lateral and vertical widths of the proton beam at injection energy of 40 MeV of 16 mm horizontal and 15 mm vertical. At its centered position, the aperture reduces the number of stored protons to ~87%. Application of electron cooling [5, 6] results in a reduction of the beam size to ~13 mm horizontal and ~11 mm vertical.

Table 1: The number of stored protons N_p at injection energy without cell, with the empty cell tube and with the cell tube fed by gas for the undeflected beam through ANKE ($\alpha = 0°$) and a chicane angle of $\alpha = 9.2°$ with stacking injection (s) and electron cooling at injection (c).

α	beam	N_p at injection		
		no cell	empty cell	gas–fed cell
0°	c	8.3x10^{10}	6.6x10^9	
9.2°	s+c		8.5x10^9	8.8x10^9

With the storage cell, with stacking injection [5, 6] and with electron cooling, the number of stored protons was measured using the beam–current transformer. These numbers are to be compared with those, achieved without the cell. As an essential step, an appreciable number of protons could be stored with the COSY beam deflected to 9.2° in the ANKE chicane. The data, measured at injection, are collected in Tab. 1, whereas Tab. 2 shows those achieved after acceleration to 600 MeV.

Table 2: The number of stored protons N_p after acceleration to 600 MeV (further explanations see caption of Table 1).

α	beam	N_p at 600 MeV		
		no cell	empty cell	gas–fed cell
0°	c	1.4×10^{10}	3.5×10^{9}	
0°	s+c	2.6×10^{10}	2.0×10^{9}	
9.2°	s+c		6.0×10^{9}	6.4×10^{9}

The number of 6.4×10^{9} stored and accelerated protons yields an appreciable luminosity up to 10^{30} cm^{-2} s^{-1} for double polarization experiments. Further studies will focus on the additional application of stochastic cooling.

The evaluation of the data from the pp → dπ^{+} reaction, measured with injection of hydrogen into the storage cell, is described here.

Prior to the tests with the storage cell filled with hydrogen, a few calibration runs were taken with a polyethylene strip target. The strip target setup was installed at the target chamber at the opposite flange of the cell supporting setup to be able to change the storage cell target with the strip target without breaking the vacuum and to avoid any changes in the cyclotron setup. That exchange can be done within a couple of minutes.

The results of the vertex reconstruction along the X-coordinates (perpendicular to the beam) and Z-coordinates (along the beam), with the origin in the CH_2 target position are shown in Fig. 3. The reconstructed vertex is very close to the real target coordinates. The resolution of the longitudinal coordinate is $\sigma_{\parallel} \sim 3.5 - 4$ cm and transversal $\sigma_{\perp} \sim 0.8$ cm.

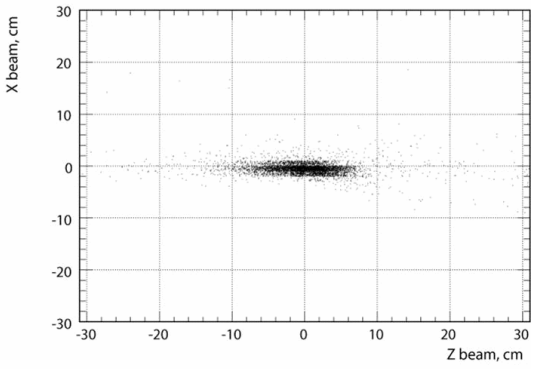

Fig. 3: CH_2 strip target vertex reconstruction.

Events from the storage cell were analyzed to study the vertex distribution. Results of these analyses show the expected ratio when the target consists of atoms of states 1+2 of the hydrogen beam and when into the cell only state 1 is injected (Fig. 4).

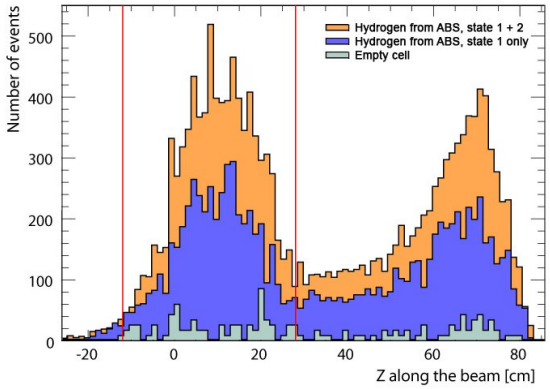

Fig. 4: Number of events from the cell as function of coordinate (along the COSY beam).

The observed event distribution in the cell region (area between two vertical lines in Fig. 4) possesses a triangular shape – well known for the density distribution of a cell target. Its apex is shifted to the right because of the higher acceptance at the cell exit (right vertical line in Fig. 4).

Acknowledgements:

The authors want to acknowledge the important help by the infrastructure divisions of FZJ and IKP in the development and installation of the PIT. Thanks go to members of the ANKE collaboration, who enabled the installation and the commissioning studies. The authors thank E. Steffens, Universität Erlangen-Nürnberg, and H. Paetz gen. Schieck, Universität zu Köln, for their contributions to the development of the PIT.

References:

[1] H. Kleines *et al.*, Nucl. Instr. Methods A (2006, in print).
[2] F. Rathmann *et al.*, Proc. 15th Int. Spin Physics Symposium, Upton, NY, USA, 2002. AIP Conf. Proc. **675** (2003) 553.
[3] R. Engels *et al.*, Rev. Sci. Instrum. **74** (2003) 4607.
[4] R. Engels *et al.*, contribution to this report.
[5] R. Maier *et al.*, IKP+COSY Annual Report 1999. Report Jül-3744 (2000) 147.
[6] H.J. Stein *et al.*, Proc. 18th Conf. on Charged Particle Accelerators,(RUPAC 2002), Obninsk, Russia, 2002. I.N. Meshkov (Ed. in chief), NRCRF Obninsk (2004) 220.

[1] PhD student from Petersburg Nuclear Physics Institute, 188300 Gatchina, Russia
[2] PhD student from Joint Institute for Nuclear Research, 141980 Dubna, Russia
[3] PhD student from Tbilisi State University, 380662 Tbilisi, Georgia
[4] Erlangen University, 91054 Erlangen, Germany
[5] Petersburg Nuclear Physics Institute, 188300 Gatchina, Russia

Timing Performance of the ANKE Silicon Tracking Telescopes.

V. Leontyev[a], S.Merzliakov[b], A. Mussgiller[a], D.Oellers[a], R.Schleichert[a] and S.Trusov[c]
for the ANKE-Collaboration.

An important application of the ANKE Silicon Tracking Telescopes (STT) will be a time-of-flight particle identification. Reactions of type $pd \to p_s pX$ or $pd \to p_s dX$ are investigated in ANKE, detecting a fast proton or a deuteron in FD ANKE and a spectator proton p_s in STT ANKE. The time resolution (FWHM) of FD is about 600 ps. If the STT will have a similar accuracy, the reactions can be clearly identified, measuring their time difference, because even fast (3 GeV/c) deuterons, detected in FD, have a time-of-flight at least 3 ns larger than the fast protons. Two experimental setups were realized in laboratory in order to directly measure the STT timing accuracy.

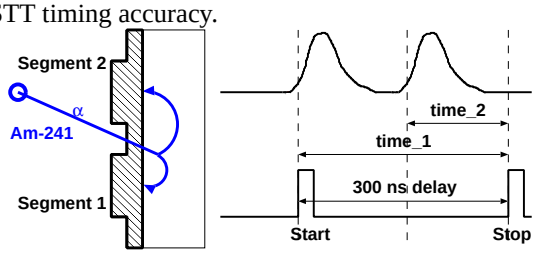

Fig. 1: Experimental setup and simplified time diagram of measurements with the α-source.

The first setup allows to study the dependence of a time walk and the standard deviation on the deposited energy in the sensitive detector zone from 400 keV up to 2 MeV, typical for spectator protons. Front-end electronics, based on the MATE3 chip [1], provides simultaneous time and energy measurement. The measurement uses an ^{241}Am α-source in air, in order to provide an energy variation of α-particles from the mono-energetic source. Particles, detected in the same segment, have different path length in air and consequently different energies, when they impinge on the detector. The experimental scheme is presented in Fig.1. α-particles, which impinge between two adjacent segments, were detected, and the difference between two measured times was studied. Due to the fact, that the desired accuracy is close to the limits of the read-out electronics performance, a dedicated procedure of handling of time peaks and a compensation for the ADC differential non-linearity were applied.

A standard deviation of the time difference $\sigma_{\Delta t}$ can be expressed as:

$$\sigma_{\Delta t}(E_{st}, E_{sm}) = \sqrt{\sigma_{st}^2(E_{st}) + \sigma_{sm}^2(E_{sm})}, \quad (1)$$

where σ_{st} is the resolution of a segment ST, produced the trigger, and σ_{sm} is the resolution of a measured segment (SM).

The dependence $\sigma_{sm}(E_{sm})$ for one segment alone was extracted from Eq.1 and described as:

$$\sigma_{sm}(E_{sm}) = \sigma_0 + exp(p_1 + p_2 \cdot E_{sm}), \quad (2)$$

where p_1 and p_2 are fit parameters. σ_0 is the standard deviation of the used electronics. The dependence of $\sigma_{sm}(E_{sm})$ is presented in Fig.2 and data points for two arbitrary chosen ranges of E_{st} are also shown in order to illustrate the independence of the obtained σ_{sm} on E_{st}, the energy in a different segment .

A similar procedure was made to obtain the time walk of the SM, the dependence of the time peak position T_{sm} on the deposit E_{sm}. This dependence is depicted in Fig.3, it was expressed as:

$$T_{sm}(E_{sm}) = p_0 + exp(p_1 + p_2 \cdot E_{sm}), \quad (3)$$

Data points for different E_{st} values show some systematic deviations from the function, fitting all events. It indicates that the description of the $T_{sm}(E_{sm})$, provided by the investigation method, is not completely independent on the responses of other segments. The deviations are significant (about 1 ns) only near the MATE3 threshold (0.4 MeV), so may be the behavior of the electronics introduces this uncertainty in that region.

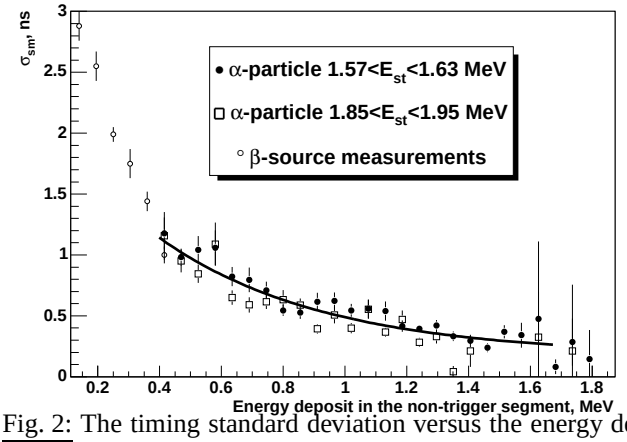

Fig. 2: The timing standard deviation versus the energy deposit. The dependence for the α-measurements is shown by a solid line.

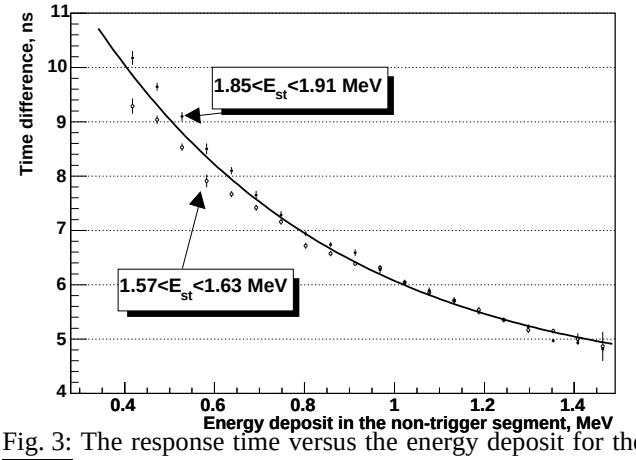

Fig. 3: The response time versus the energy deposit for the measurements with the α-source.

An inverse negative relationship of the deviation value and sum energy deposit ($E_{st} + E_{sm}$) was found, so another possible explanation is, that this systematical deviation results from a skin-deep penetration of α-particles in a detector sensitive region. Actually, α-particles with an energy deposit of 500 keV have a penetration depth of less than 1 μm, taking into account its inclination in the measurements. The internal electric field of the detector may be affected at that depth by surface effects, that influences the drift time. A planned measurement with a proton beam of the Cologne Tandem-Accelerator will provide a wide range of the penetration depths and will test this hypothethis.

Measurements with a β-source are also free of the surface effects. The second setup was developed in order to study

the timing for electrons. Since the electron energy losses are rather small, these data can be used only as a reference. It was estimated, using Ref.[2] data, that the proposed setup provides data for the deposited energy up to 500 keV. Electrons from a ^{90}Sr source were detected by two scintillator counters and the investigated silicon detector (Fig.4). A scintillator signal coincidence was used as reference time and as trigger for the silicon detector read-out. The scintillator time resolution (FWHM) was measured to be 600 ps.

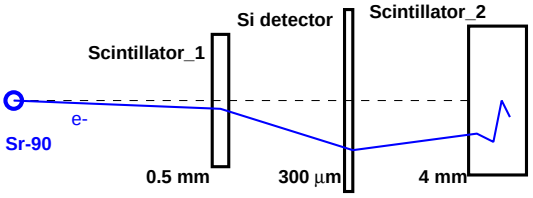

Fig. 4: Experimental setup for the β-source measurements.

The dependence of the time walk on the energy deposit in the range 0.14 MeV$\leq E_{sm} \leq$0.4 MeV was described in the form of Eq.3 and the resolution dependence as in Eq.2. The results forσ_{sm} of both methods are in agreement in the overlap region (see Fig.2).

Thus, the performed measurements allow to estimate the time resolution (FWHM) to better than 1 ns for an energy deposit above 1 MeV. The dependence of the time walk on the energy deposit is also obtained with the suitable uncertainty. The accuracy of the STT timing, obtained in the laboratory measurements, is high enough for the time-of-flight particle identification. The timing for protons will be tested at the Cologne Tandem-Accelerator during 2006.

References:

[1] P.Baron *et al*. MATE, a single front-end ASIC for silicon strip, Si(Li) and CsI detectors. *Nuclear Science Symposium Conference Record*, v.1, p.386-390. IEEE, October 2003.

[2] Casino - Monte Carlo Simulation of Electron Trajectory in Solids, Version 2.0, http://www.gel.usherbrooke.ca/casino/index.html

[a] IKP FZ Jülich, Germany
[b] JINR, Dubna, Russia
[c] IKP FZ Rossendorf, Germany

Absolute Energy Calibration of Micron Detectors for the ANKE Silicon Tracking Telescopes.

V. Leontyev[a], S. Barsov[b], S. Merzliakov[c], A. Mussgiller[a], D. Oellers[a], R. Schleichert[a] and S. Trusov[d]
for the ANKE-Collaboration.

The ANKE Silicon Tracking Telescopes (STT) are designed to measure the total energy of a stopped particle with a precision of about 1%. A calibration method, which has been applied up to now [1], is using a test-pulse and additional adjustments by fitting real data to the expected values, in particular dE/E plots. Due to the absence of an absolute energy reference, the achieved accuracy was of the order of 6%. The method described in this article provides a calibration point, detecting radiation an from α-source.

At this level of precision not only the calibration of energy losses in the sensitive detector zones (E_{meas}) have to be done carefully, but also losses in dead layers (E_{dead}) have to be taken into account. Information from Micron Semiconductor (UK) asserts a dead layer thickness on each detector side of about 4-5 μm, which varies by about 1 μm across the detector as shown in Fig. 1. An exact measurement of the dead layer thickness is necessary to provide the E_{dead} reconstruction. Due to the fact, that the dead layer has a two-step structure, two independent measurements are needed, which was achieved by a combination of two α-sources.

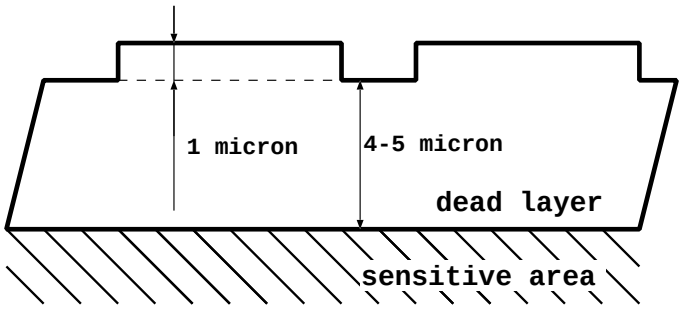

Fig. 1: Principle dead-layer structure on the surface of the detectors.

Measurements under vacuum with an ^{241}Am α-source were made in April 2005. Figure 2 presents a typical spectrum of the detected energy. The two-step structure of the dead layer results to a clear splitting of the α-peak. An estimation of a difference between the peak mean values is 160 keV and of peak standard deviations σ are 50 keV, assuming the dead layer of 5 μm.

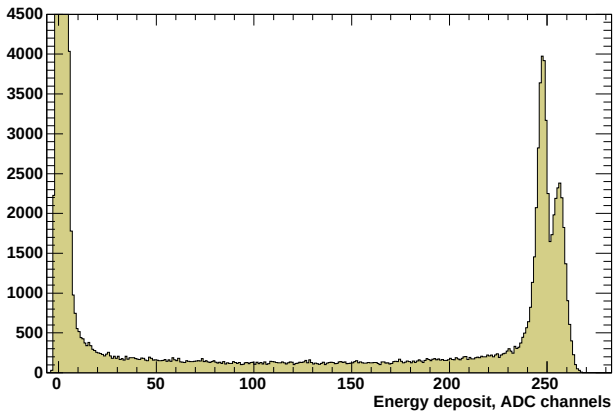

Fig. 2: Energy deposit of particles from ^{241}Am is presented in arbitrary units.

As shown in [2], E_{meas} can be described as $k \cdot f(N_{ADC})$, where $f(N_{ADC})$ is a read-out responce function, defined by the test-pulse calibration, and k is a calibration factor, introduced by the difference between the effectively used test pulse capacitance and the nominal capacitance. A dead layer energy loss can be calculated from the initial particle energy E and the dead layer thickness d. So, it can be expressed as $F(E,d)$. In vacuum E is equal to the sum of E_{meas} and E_{dead}:

$$E = k \cdot f(N_{ADC}) + F(E,d), \quad (1)$$

Due to the two-step structure, two values for the thickness d_1 and d_2, are required, and three values (k, d_1, d_2) are to be determined.

A combination of ^{239}Pu (E_α = 5.156 MeV) and ^{244}Cm (E_α = 5.805 MeV) can be applied to obtain a set of four peak with a good resolution. A non-linear system of equations can be created, and a numerical method was developed to solve this system and calculate d_1, d_2 and k with an error, much smaller than 1%. In a general way $F(E,d)$, expressed as an integral over the Bethe-Bloch formula [3] is very complicated, so it was approximated taking into account the confines on the dead layer thickness and fitting SRIM data [4]. The numerical method applies an iteration process of analytical solutions for the system, linearized in each iteration by linear interpolations of $F(E,d)$.

Knowing the dead layer thickness and measuring E_{meas}, the approximated $F(E,d)$ function can be used in experiments to reconstruct E_{dead} for particles of different types. In experiments, a proton with a primary energy of 8 MeV will pass through all four dead layers of the detectors and total loss E_{dead} there will be about 3% of the original energy. The energy straggling in the dead layers will be negligibly small.

Thus, the absolute values of the energy loss in sensitive zones of the STT detectors will be measured and the losses in the dead layers will be reconstructed with high precision. An installation of α-sources near the STT at ANKE will provide monitoring of the energy measurement stability during the time of experiments.

References:

[1] A.Mussgiller, 'Identification and Tracking of low Energy Spectator Protons', Ph.D. Thesis, Universität zu Köln, Hamburg, 2005.

[2] A.Mussgiller at al., Readout of silicon detector telescopes with a new frontend chip. IKP/COSY Annual Report 2003.

[3] W.R.Leo 'Techniques of Nuclear and Particle Physics Experiments', p.24. Springer-Verlag, 2 Printing, 1992.

[4] SRIM - The Stopping and Range of Ions in Matter. Ver. SRIM-2003, http://www.srim.org

[a] IKP FZ Jülich, Germany
[b] PNPI, Gatchina, Russia
[c] JINR, Dubna, Russia
[d] IKP FZ Rossendorf, Germany

Serial Check of Micron Silicon Strip Detectors

V. Leontyev[a], S. Barsov[b], S. Merzliakov[c], A. Mussgiller[a], D. Oellers[a], R. Schleichert[a] and S. Trusov[d]
for the ANKE-Collaboration.

Part of the ANKE Silicon Tracking Telescopes (STT) are 69, 300 and 500 μm thick double-sided structured silicon-strip detectors from Micron Semiconductor (UK). Each detector provides 128 on one and 151 segments on the other side. To guarantee a precise energy measurement by each segment, a semi-automatic method to check the performance has been developed.
The first five 300 μm detectors were received in Spring 2005. Their performance check has been realized in laboratory. In vacuum an α-source (^{241}Am) was placed at a distance of 5 cm from the approximate center of the p-side of every detector. Energy spectra of every segment and 2D-plots of energy distributions between adjacent segments were analyzed. Different irregularities of segment responses were found and classified.

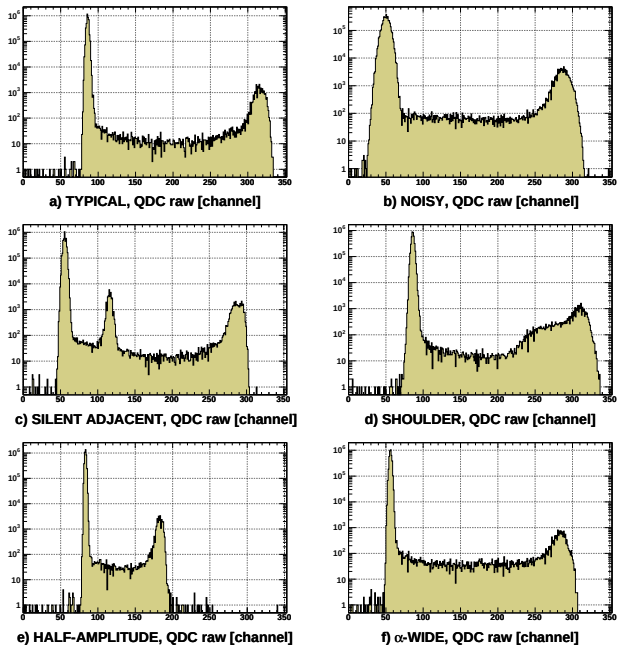

Fig. 1: a) Typical energy spectrum; b-f) Energy spectra of peculiar segments.

A regular energy spectrum (Fig.**??**.a) contains beside some small background two peaks of gaussian shape: one from the pedestal and the other from the α-particle energy deposit. Five kind of deviations from this regular spectrum have been found:

- **Noisy Segments** (Fig.**??**.b). Both peaks are 2-3 times wider than usual together with an about 5 times increased background.
- **Silent Segments** with no α-peak. Neighbours of silent segment have apparently a kind of short-cut with it, because they have always an additional peak of signals with an amplidute approximately 4 times smaller then the α-peak.
- **Shoulder Segments** have a non-typical shape of the α-peak with an additional significant tail to the left side. The background around the peak is increased by about a factor 10.
- **Half-Amplitude Segments** have peaks of regular shape and intensity, but the amplitude is approximately two times smaller then usual.
- **α-Wide Segments** have a normal pedestal peak, but the α-peak is wider and of less intensity together with an increased background.

Any of the described irregularities leads to a non-precise energy measurement for the affected segment. It was found that all these peculiar effects appear along the whole segment. A two-dimensional plot like Fig.**??** gives an impression on the performance of each detector. It shows the number of detected α-particles in dependence on the segment numbers on both detector sides. An entry is generated whenever the deposited α-energy is close as one σ to the peak-position. All regular segments have equal α counting rates after geometrical acceptance corrections.

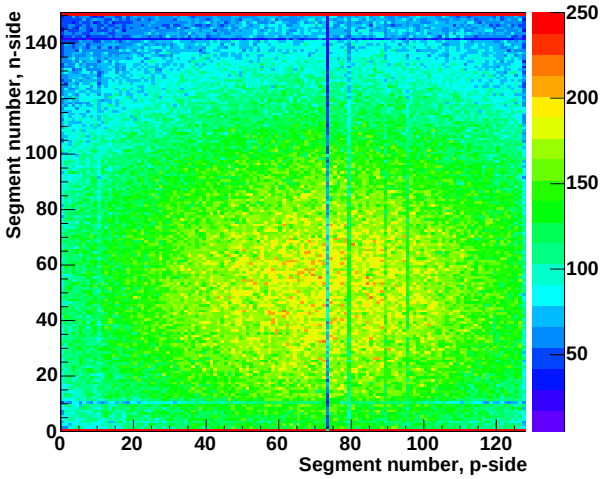

Fig. 2: α-particle distribution over a detector.

97 % of all detector segments are faultless. Nevertheless none of the detectors fullfills the given specification of 99 % fully working segments. The losses are typically of about 6 % per detector for a 2-d reconstruction and therefore about 12 % in a track reconstruction with two involved detector.
The obtained results together with the voltage-current characteristics have been delivered to Micron Semiconductor. They are the basis for an on-going discussion to improve the production technology for the next sample of detectors for the ANKE Silicon Tracking Telescopes.

[a] IKP FZ Jülich, Germany
[b] PNPI, Gatchina, Russia
[c] JINR, Dubna, Russia
[d] IKP FZ Rossendorf, Germany

Parametrisation of the Silicon-Detector Temperature

D. Oellers, S. Barsov[a], V. Leontyev, S. Merzliakov[b], R.Schleichert and S. Trusov[c]
for the ANKE-Collaboration.

The Silicon Tracking Telescopes (STT) of ANKE compose lithium drifted silicon semiconductor (Si(Li)) with a thickness of up to 7 mm. The operation parameters of such a diode depends on the silicon temperature.
For example the drift velocity of electrons e^- and holes (temperature T, detector thickness s and voltage U) have been parametrized as [1]

$$v_{e^-} = 2.1 \cdot 10^9 \cdot T[K]^{-2.5} \cdot \frac{U[V]}{s[cm]}$$
$$v_{holes} = 2.3 \cdot 10^9 \cdot T[K]^{-2.7} \cdot \frac{U[V]}{s[cm]}$$

As the peaking time of the amplifier is in the order of $1\,\mu s$ and the trigger needs around $600\,ns$, the drift time should be less than $500\,ns$ to give a negligible contribution in the energy resolution. Moreover different velocities lead to variations of the drift time. The drift time differences from electrons and holes will be used to obtain the penetration depth of stopped particles. Temperature stability is necessary to get a 3-dimensional information of the place where the measured particle is stopped. As it is impossible to mount a temperature sensor directly onto the detector one needs to find an indirect way to deduce the temperature of the Si(Li).

The experimental setup should be such that it provides the possibility to measure temperatures of the Si(Li) detector, of the Si(Li) frame, of the cooling liquid, of the environment as well as the power consumption of the silicon. This has

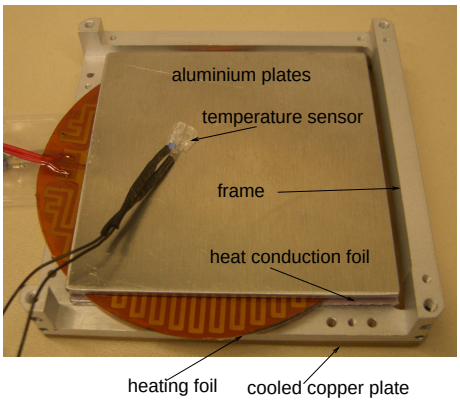

Fig. 1: Photograph of the main part of the experimental setup

been achieved by using an existing frame for the Si(Li) as the central part of the setup (See figure 1). The Si(Li) has been replaced by two aluminium plates (2 mm thick) with the area of the Si(Li). To simulate the power consumption P_{al} of the Si(Li), the plates have been equipped with a heating foil in-between. For good thermal conductivity additional heat conduction foils [2] have been used.
On the back side of the frame an actively cooled copper plate has been mounted. Here heat conducting foils have been used, too.
The setup was equipped with four temperature sensors:

- one $20\,\text{mm} \times 20\,\text{mm}$ thin sensor on the outer side of the aluminium: T_{al}
- one $2\,\text{mm} \times 10\,\text{mm}$ sensor on the frame: T_{fr}
- one $20\,\text{mm} \times 20\,\text{mm}$ thin sensor on the cooled copper plate: T_{liquid}
- one free hanging SMD-sensor to measure the temperature of the environment: T_{env}

This setup has been mounted on a DN 150CF-flange and put into vacuum. By externally heating up the vaccum test stand, the environment temperature could be increased.
The temperatures and the heating power have been taken after obtaining thermal equilibrium.

In the first step an independent linear fit for the liquid and environment temperature and the heating power has been done. With respect to the correlations between the parameters small corrections of the fitted coefficients have been established. The formular for the aluminium temperature is:

$$\mathrm{T_{al}} = 0.8 \cdot \mathrm{T_{liquid}} + 0.2 \cdot \mathrm{T_{env}} + 2.0\,\tfrac{\mathrm{K}}{\mathrm{W}} \cdot \mathrm{P_{al}}$$

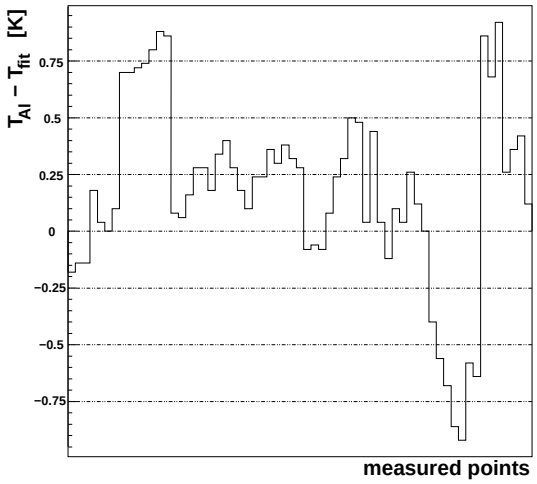

Fig. 2: Difference between the temperature of the aluminium and the fitted temperature.

Since the power consumption of the silicon will be less than 100 mW the third term can be neglected and the final formula is:

$$\mathrm{T_{al}} = 0.8 \cdot \mathrm{T_{liquid}} + 0.2 \cdot \mathrm{T_{env}}$$

Fig.2 shows that the discrepancy is less than ± 1 K and that it is possible to operate the silicon detector at any chosen temperature with a precision of better than ± 1 K. This corresponds to a systematic error in the drift time of less than ± 20 ns.

References:

[1] G. W. Ludwig and R .L. Watters, Phys. Rev **101** (1956) 1699.
[2] *http://www.alfatec.de/www_alfatec/kerafol_14_14_0_f.htm*
Keratherm_en_03_2006.pdf

[a] PNPI, Gatchina, Russia
[b] JINR, Dubna, Russia
[c] IKP FZ Rossendorf, Germany

Verification of the Drift Time Parametrisation in a 5 mm Si(Li)-Detector

D. Oellers, S. Barsov[a], V. Leontyev, S. Merzliakov[b], R.Schleichert and S. Trusov[c]
for the ANKE-Collaboration.

In the Silicon Tracker Telescope (STT) for the ANKE-spectrometer a lithium drifted silicon detector with a thickness s of up to 7 mm will be installed. It has a sensitive area of $64 \times 64\,\mathrm{mm}^2$ equipped with 96 strips on both sides.
By measuring the drift times in this detector the penetration depth of stopped particles will be deduced. This contribution shows that the drift times could be measured with a shaped signal and the drift velocities could be predicted as described in [1].

The energy loss in a depleted semiconductor leads to electron-hole pairs in the conducting band. The electric field pulls this free charges towards the electrodes with an average velocity v ([2]). Before the charges reach the electrodes, mirror charges are influenced on these. The overall mirror charge is distributed over all strips of the segmented detector. Thus one expects a fast, but rather low signal from the mirror charge, which does not change much in time. The signal will increase strongly when the free charge reaches the electrodes. It will finally decrease when no free charges are left in the detector.
This behaviour could be observed by connecting two or more strips together since this should cause a small increase in the mirror charges and no difference on the signal caused by the free charge itself.
Since the α-particles are stopped at the very surface of the detector, the drift time could be calculated by $t = \frac{s}{v}$. By irradiation one or another side of the detector either the electron drift or the hole drift is examined.

For the test measurements a 5 mm thick Si(Li)-detector was biased over a 1 MΩ resistor. An ^{241}Am source was placed near the detector to either irradiate the p- or n-doped side. The signals of each side were read out over kapton foils and the high voltage decoupling board. One strip per side was selected and connected to the preamplifier [3].
From here the energy output was shaped with a fast timing amplifier with 50 ns integration and differentiation time. The oscilloscope was used to create the delayed coincidence and to generate the plot of the signals.
The detector frame was cooled and several temperature sensors were placed on the setup. This provided the possibility to calculate the detector temperature [1].

The measurements were done with the environment at room temperature. The cooling temperature has been set at 1, 5, 10, 15, 19 °C and for each temperature several bias voltages have been applied. With the oscilloscope an average of 200 coincident signals were taken. In Fig. 1 an example of such a concident signal is shown.
One can clearly see the fast signal caused by the electrons, since the n-side is irradiated. The holes need to drift through the detector and cause the delayed signal. The signals caused by the mirror charges are also clearly visible in the plot, too.

The peaks are localised and the drift times measured (In Fig. 1 the measured drift time is 833 ns). The comparisation with

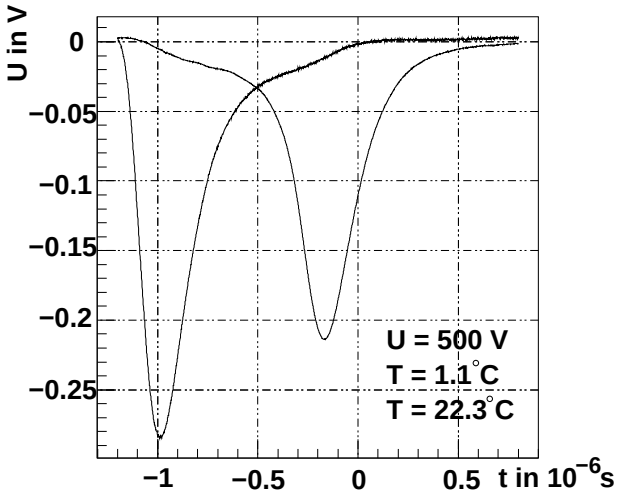

Fig. 1: Signal from ^{241}Am in the 5 mm Si(Li) with $U_{Bias} = 500\,V$ and $T_{liquid} = 1\,^{\circ}C$.

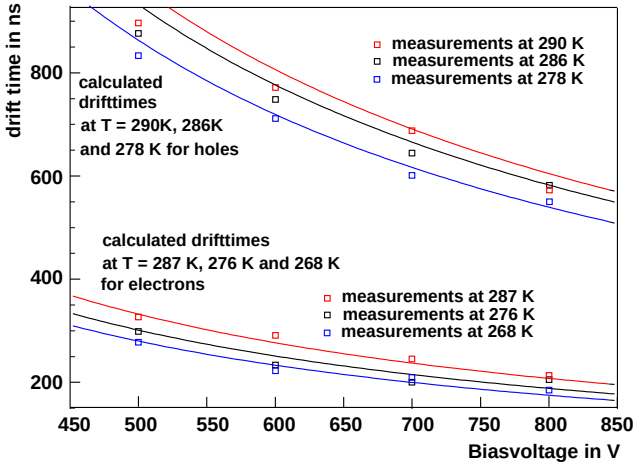

Fig. 2: Calculated and measured drifttimes in comparisation.

the expectation shows an agreement better than 10 % (see Fig. 2).
These measurements show, that the drift velocities can be stabilised by using the cooling temperature and the bias voltage as free parameters. This method allows to measure the drift time with a precision of ≈ 60 ns for the holes and ≈ 30 ns for the electrons. This corresponds to a systematic error of less than ±0.5 mm in penetration depth.

References:

[1] **Parametrisation of the Silicon-Detector Temperature**, D. Oellers et al., Annual Report IKP 2005
[2] G. W. Ludwig and R .L. Watters, Phys. Rev **101** (1956) 1699.
[3] CANBERRA 2003BT

[a] PNPI, Gatchina, Russia
[b] JINR, Dubna, Russia
[c] IKP FZ Rossendorf, Germany

COSY Vacuum-Break Detection to Protect the ANKE Silicon Tracking Telescopes

S. Merzliakov[1], H. Hadamek[2] and R. Schleichert[2]
for the ANKE-Collaboration

At COSY several severe vacuum breaks have happened over the last years of operation. In 2003 such an a ccident destroyed a complete setup of two Silicon Tracking Tel e-scopes at ANKE. Meanwhile an e xtended new setup is in preparation. To protect the ANKE Silicon Tracking Tel e-scopes against future COSY vacuum breaks, it is planned to install Fast Shutters arou nd the ANKE section [1]. These shutters shall close the se ction in less then 10ms in both directions: COSY against ANKE but also ANKE against COSY. This seems feasible within a re -design of the existing prototype. Measurements with this prototype shutter show the fast response time of the shutter (< 10ms) but the vacuum sensors are not fast enough [2].

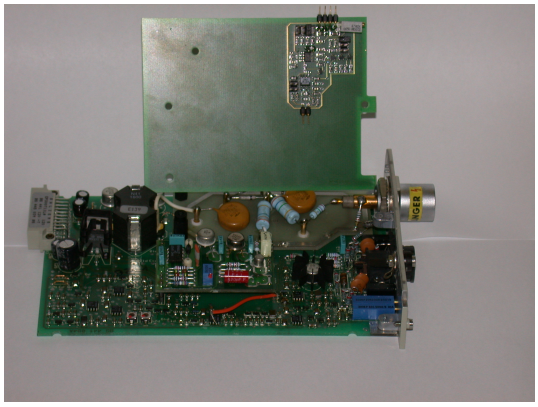

Fig. 1: Balzers TPG300 electronics (front) together with the add-on electronics (behind).

For the vacuum sensors the pr oposal now is to use the COSY standard Balzers vacuum gauges IKR070 together with an add -on electronics for the total pressure co ntrols TPG300 (Fig. 1). It provides a parasitic linear voltage output in a pressure range from 10^{-7} to 10^{-5} mbar. It is designed to detect a pressure i ncrease at a pressure of 10^{-6} mbar within 2ms.

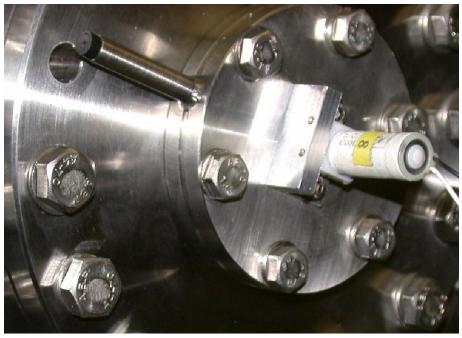

Fig. 2: Fast valve mounted on a DN40-CF flange.

To check the development a 'vacuum -break' has been stimulated by a fast valve [3]. Triggered by an electrical signal, it opens a diam eter of 0.8mm within 1.3ms and closes it again after a minimum time of 3.2ms, providing a controlled fast pressure i ncrease from 10^{-7} to 10^{-5} mbar. Fig. 2 shows a picture of this valve mounted on a DN40 -CF flange.

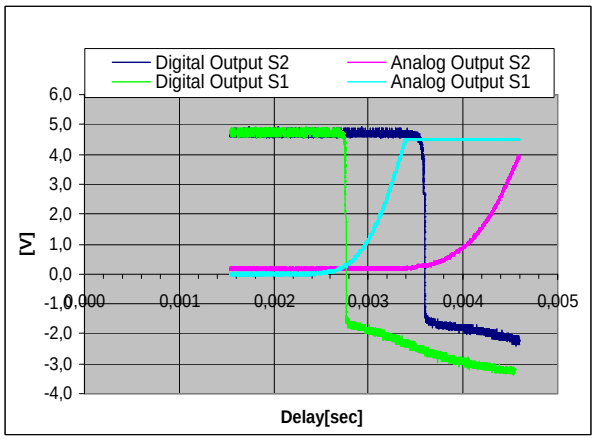

Fig. 3: Electrical signals on the oscilloscope.

Results of the measurements are illustrated In Fig. 3. Zero is defined by the time when the voltage is applied to the fast valve. The light blue curve 'Analog Output S1' shows the analogue output of the add -on electronics in case where the IKR070 gauge is mou nted as close as 0.2m. The green curve 'Digital Output S1' reflects the time -mark crossing a pressure level of 10^{-6} mbar. So the time delay to detect the 'vacuum -break' is T_0=2.8ms. The magenta curve 'Analog Output S1' and the dark blue curve 'Digital Output S2' are the corresponding signals if the IKR070 is mounted at a distance of 0.7m. Here the time delay is T(0.5m)=3.6ms. Taking into account the r esponse time of the fast valve of about 1.3ms, the pressure increase is d e-tected after 1.5ms. From the secon d mea surements one deduces a speed of about 0.6m/ms for the air-front.

This add-on electronics is prepared to upgrade the existing total pressure controls TPG300 at COSY. Once equipped, a vacuum break along the COSY ring can be detected at a selectable pressure level from 10^{-7} to 10^{-5} mbar with a time delay of less then 2 ms. This signal can be used to close the fast shutters within 10ms and to shut down the high voltage of the Silicon Tracking Telescopes at ANKE in a comparable time.

References:

[1] 'Schnellschliessendes UHV-Ventil für COSY', ZAT-Wissenschaftlicher Ergebnisbericht 2003
[2] 'Schnellschliessendes UHV-Ventil für COSY', ZAT-Wissenschaftlicher Ergebnisbericht 2004
[3] LFAA1203218H, 2-way injector valve, THE LEE CO. http://www.theleeco.com/

[1]Laboratory of Nuclear Problems, Joint Institute for N u-clear Research, 141980 Dubna, Russia
[2] Institut für Kernphysik, Forschungszentrum Jülich, 52428 Jülich, Germany

Search for transition region in exclusive reactions with high p_T at COSY energies

Yu. N. Uzikov[a] for ANKE collaboration

The structure of the lightest nuclei at short distances ($r_{NN} < 0.5$ fm) or for high relative momenta ($q > 1/r_{NN} \sim 0.4$ GeV/c) constitutes a fundamental problem in nuclear physics. Experimental investigation employ processes where the momentum transfer to the nucleus is large ($Q \sim 1$ GeV/c). One of the most interesting questions is the following: at which values of the Mandelstam variables s and t (or, more precisely, relative momenta q of nucleons in nuclei) does the transition region from the meson-baryon to the quark-gluon picture of nuclei set in? A possible signature for this transition is given by the constituent counting rules (CCR) [1]. According to dimensional scaling [1] the differential cross section of a binary reaction $AB \to CD$ at high enough incident energy can be parameterized for a given c.m.s. scattering angle θ_{cm} as

$$\frac{d\sigma}{dt}(AB \to CD) = \frac{f(t/s)}{s^{n-2}}, \qquad (1)$$

where $n = N_A + N_B + N_C + N_D$ and N_i is the minimum number of point-like constituents in the ith hadron (for a lepton one has $N_l = 1$), $f(s/t)$ is a function of θ_{cm}.

The CCR follows from perturbative QCD (pQCD) [2]. Recently these rules were also obtained within nonperturbative theories which are dual to QCD [3]. Existing high energy data for many measured hard scattering processes with free hadrons appear to be consistent with the CCR [4]. In the nuclei sector only electromagnetic processes and only on the deuteron were found to be compatible with the CCR. So, the deuteron photodisintegration reaction $\gamma d \to pn$ follows the s^{-11} scaling behaviour in the SLAC data [5] at energies $E_\gamma > 0.8 - 2.8$ GeV at $\theta_{cm} \approx 90^\circ$ and in the Jlab data at photon energy $E = 1 - 5$ GeV and high transversal momenta $p_T > 1.1$ GeV/c (see [7, 8] and references therein). Meson-exchange models fail to explain the $\gamma d \to pn$ data at $E_\gamma > 1$ GeV (see, for example, [6]). Recent models based on quark degrees of freedom have become quite successful in describing these data [9].

The pQCD (and, consequently, the scaling behaviour within the pQCD) is expected to be valid at very high transferred momenta which are not yet reached in existing data for nucleon and deuteron form factors [10]. From this point of view the origin of the observed scaling behaviour in the reactions with the deuteron at moderate transferred momenta is unclear. On the other side, in these reactions the 3-momentum transfer $Q = 1 - 5$ GeV/c is large enough to probe very short distances between nucleons in nuclei, $r_{NN} \sim 1/Q < 0.3\,fm$, where $0.3\,fm$ is a size of a constituent quark. One may expect that nucleons loose their separate identity in this overlapping region and, therefore, multi-quark components of a nucleus can be probed in these reactions. In order to get more insight into the underlying dynamics of the scaling behaviour new data are necessary, in particular, for hadron-nuclei interactions.

Very recently it was found [11] that the cross section of the reaction $dd \to {}^3He n$ (and $dd \to {}^3Hp$), measured in an old experiment at SATURNE [12], also perfectly demonstrates the scaling behaviour s^{-22} at transversal momenta $p_T \sim 0.6 - 0.9$ GeV/c (Fig.1).

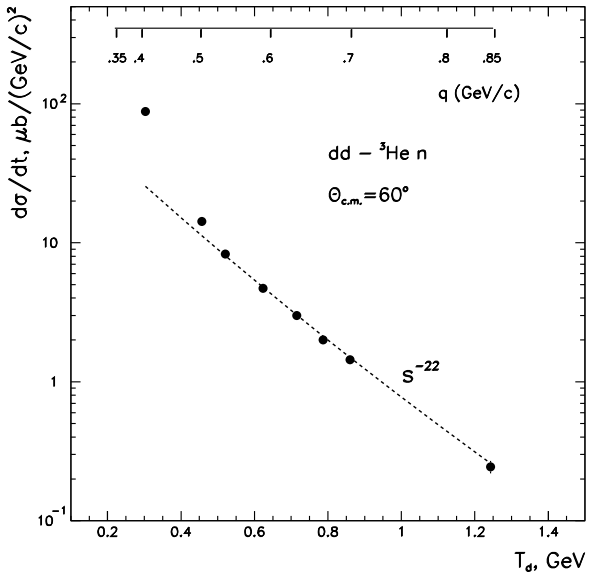

Fig. 1: The differential cross section of the $d + d \to {}^3He + n$ and $d + d \to {}^3H + p$ reactions at $\theta_{c.m.} = 60^o$ (•) [12]. The dashed curve gives the s^{-22} behaviour.

In Fig.1 we show the experimental data from Ref.[12] obtained at SATURNE at beam energies 0.3 – 1.25 GeV for the maximum measured scattering angle $\theta_{cm} = 60^\circ$. Shown on the upper scale is the relative momentum q_{pn} in the deuteron for the one nucleon exchange (ONE) diagram. One can see that at beam energies $0.5 - 1.25$ GeV the data perfectly follow the s^{-22} dependence. (In this reaction $n = 6+6+9+3 = 24$). In Fig. 1 the dashed curve represents the s^{-22} dependence with arbitrary normalization fitted on the data with $\chi^2_{n.d.f.} = 1.18$. *Up to now, the reaction $dd \to {}^3Hen$ (${}^3Hp$) is only purely hadronic process which involves the deuteron and ${}^3He({}^3H)$ nuclei and is found to follow the CCR.* At $\theta_{cm} = 90^\circ$ the ONE mechanism involves higher momenta $q_{pn} = 0.7$ - 1.1 GeV/c and $q_{Nd} = 0.80 - 1.22$ GeV/c for the same beam energies 0.5 – 1.25 GeV. Therefore, continuation of measurements up to $\theta_{cm} = 90^\circ$ is very desirable to confirm the observed s^{-22} behaviour.

An important task addressed to experiment is to search for similar beaviour of others exclusive reactions with the lightest nuclei at large p_T (> 0.6 GeV/c). As shown in Ref. [11], the cross section of the reaction $pd \to pd$ demonstrates $\sim s^{-16}$ behaviour at $T_p = 1 - 2.5$ GeV and $\theta_{cm} = 120^\circ - 130^\circ$. At these scattering angles a maximum contribution of the three-body forces is expected. The χ^2-parameter is too large, however, for the $pd \to pd$ reaction, probably, because of the data were obtained in various experiments. Others interesting reactions are the following: $d^3He \to {}^4Hep$, $dd \to dd$, $pd \to {}^3H\pi^+$, $pd \to {}^3He\eta$, $dd \to {}^4He\eta$, $pp \to d\rho^+$, $pp \to \{pp\}({}^1S_0)\gamma$. The last two of them, $pp \to d\rho^+$, $pp \to \{pp\}({}^1S_0)\gamma$, are nontrivial generalization of the $\gamma d \to pn$ reaction.

[a] Joint Institute for Nuclear Research, Dubna, Russia

References:

[1] V.A. Matveev, R.M. Muradyan and A.N. Tavkhelidze, Lett. Nuovo Cim. **7**, 719 (1973); S.J. Brodsky and G.R. Farrar, Phys. Rev. Lett. **31**, 1153 (1973).

[2] G.P. Lepage, S.J. Brodsky, Phys. Rev. D **22** (1980) 2157.

[3] J. Polchinski, M.J. Strassler, Phys. Rev. Lett.**88** (2002) 031601.

[4] R.L. Anderson et al., Phys. Rev. **D 14**, 679 (1976).

[5] J. Napolitano et al., Phys. Rev. Lett. **61**, 2530 (1988).

[6] C. Bochna et al., Phys. Rev. Lett. **81**, 4576 (1998).

[7] M. Mirazita et al., Phys. Rev. **C 70**, 014005 (2004).

[8] P. Rossi, et al., hep-ph/0405207.

[9] V.Yu. Grishina et al. Eur. Phys. J. **A10**, 355 (2001) and **A19**, 117 (2004).

[10] N. Isgur and C.H. Llewellyn Smith, Phys. Rev. Lett. **52** (1984) 1080; Phys. lett. **B 217**, 535 (1989).

[11] Yu.N. Uzikov, JETP Lett. **87** (2005)

[12] G. Bizard et al., Phys. Rev. **C 22**, 1632 (1980).

The analysing power for the $\vec{p}p \to pp\eta$ reaction at Q=10 MeV

R. Czyżykiewicz[a] and P. Moskal[a] for the COSY-11 collaboration

Polarisation observables for the reactions of meson creation in the elementary proton-proton collisions are the tool in studying the production mechanism of these mesons. So far there exist two predictions of the analysing power function in the close-to-threshold energy region [1, 2]. Both calculations start from the different assumptions concerning the production mechanism of η meson (pseudoscalar or vector mesons exchange dominance) and they conclude in different shapes of the analysing power function.

The analysing power formula reads:

$$A_y(\cos\theta) = \frac{1}{P}\frac{L_{rel}N_L(\cos\theta) - N_R(\cos\theta)}{L_{rel}N_L(\cos\theta) + N_R(\cos\theta)}, \qquad (1)$$

where P is the proton beam polarisation, N_L and N_R are the number of events scattered to the left and right side, respectively and L_{rel} is the relative spin-up/spin-down luminosity (as the detection system used in the measurements was asymmetric, which required the spin flip in the neighbouring cycles in order to register events scattered to the left and to the right side with respect to the polarisation plane).

The experiment have been performed utilizing the COSY facility and the COSY-11 detection setup. The polarised proton beam at the beam momentum equal to $p_{beam} = 2010$ MeV, corresponding to the excess energy $Q = 10$ MeV has been used in the measurement. The detailed method of the analysis is reported elsewhere [3, 4], here we would like to show only the major results. The spin averaged beam polarisation for the whole period of measurement was found to be P=0.680$\pm$ 0.010, while the relative luminosity was equal to $L_{rel} = 0.96468 \pm 0.00065$.

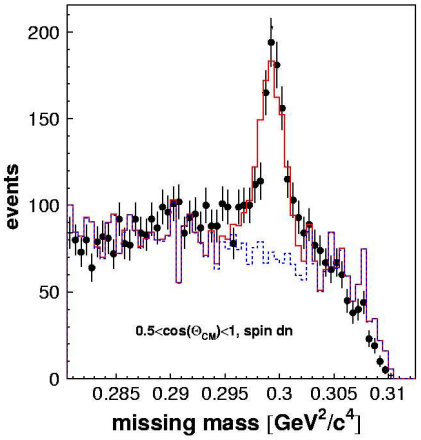

Fig. 1: An example of the background reconstruction. Points depict the experimental data. The dotted line represents the Monte-Carlo background simulation, whereas the solid line is the sum of the background and signal as it was obtained in Monte-Carlo calculations.

The missing mass spectrum for one out of the four ranges that the polar angle of η meson was divided into, is presented in Fig. 1. In order to calculate the production rates to the left and to the right side (N_L and N_R), first of all the multipionic background simulations as well as the signal Monte-Carlo simulations have been performed and subsequently a multidimensional fit of the sum of the background and signal to the experimental histograms has been applied. This method has been described in more details in [3].

The preliminary results concerning the production rates as the function of the η polar angle in the overall center-of-mass system ($\cos\theta_{CM}$), obtained as the result of the best fit, along with the analysing powers, calculated according to the eq. 1 are shown in Tab. 1.

$\cos\theta_{CM}$	N_R	N_L	A_y
[-1;-0.5)	533 ± 45	493 ± 44	-0.084 ± 0.090
[-0.5;0)	307 ± 28	323 ± 30	0.011 ± 0.096
[0;0.5)	278 ± 26	303 ± 28	0.037 ± 0.097
[0.5;1]	588 ± 47	592 ± 51	-0.021 ± 0.086

Table 1: Number of events scattered to the individual θ_{CM} angle and corresponding analysing powers for the $\vec{p}p \to pp\eta$ reaction at the excess energy Q=10 MeV. The results are preliminary.

Preliminary results of the analysing power function $A_y(\cos\theta)$ are presented in Fig. 2 as the full dots. The dotted line shows the predictions determined according to the vector meson exchange model [1], whereas the solid line refers to the pseudoscalar meson exchange model [2]. The errors are of the statistical nature only.

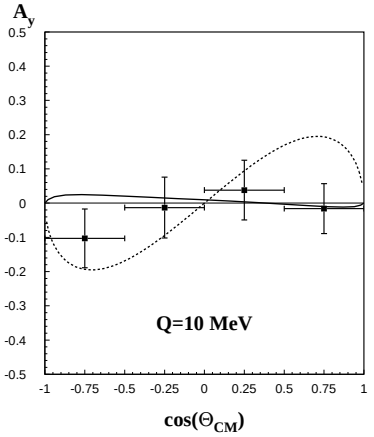

Fig. 2: The preliminary results of the analysing power for the $\vec{p}p \to pp\eta$ reaction at Q=10 MeV. The vertical bars show the statistical error, whereas the horizontal bars denote the ranges of averaging.

The preliminary analysing power data (see fig. 2) tend to slightly prefer the pseudoscalar vector exchange model [2]. The results show rather small values of the analysing power in the close-to-threshold region, which may be the indication of the η production to the *s*-wave final state, solely. However, for this statement the exact partial wave analysis remains to be done.

References:

[1] G. Fäldt and C. Wilkin, Phys. Scripta **64** (2001) 427.
[2] K. Nakayama et al., Phys. Rev. **C65** (2002) 045210.
[3] R. Czyżykiewicz et al., Acta Physica Slovaka (2006) in print.
[4] R. Czyżykiewicz et al., PhD Dissertation, in preparation.

[a] M. Smoluchowski Institute of Physics, Jagellonian University, 30–059 Cracow, Poland

Preparations for the study of the isospin dependence of the η' meson production via $pn \to d\eta'$ reaction

J. Przerwa[1], P. Moskal[1] for the COSY-11 collaboration

Over the last few years, the η' meson production was studied in nucleon–nucleon collisions at several experiments. The main interest has been given to the reaction mechanism and proton–η' interaction, which both remain essentially unknown.

Precise η' cross section data for nucleon–nucleon collisions are available for the proton–proton reaction channel only. From the existing $pp \to pp\eta'$ data it is not possible to draw univocal conclusions about the mechanism responsible for the η' production and therefore complementary data from the proton–neutron channel are needed. Such data will contribute significantly to the understanding of the η' meson production mechanism and its isospin dependence. During the year 2005, using the COSY-11 facility [1], a measurement of the η' meson production in the proton-neutron collision has been conducted [2]. At present the analysis of the data and simulation calculations are in progress.

Now we intend to extend the investigation to the close-to-threshold excitation function for the $pn \to d\eta'$ reaction channel corresponding to the isospin zero of the colliding nucleons. A measurement of the $pn \to d\eta'$ reaction is possible at the COSY-11 detection system using the spectator detector and the deuteron chamber (denoted as D4 in fig 1) installed initially for study of the $pd \to pd\eta$ reaction.

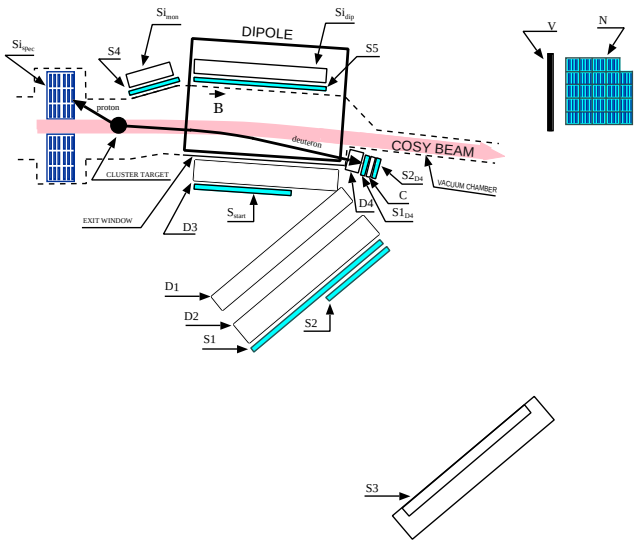

Fig. 1: Schematic view of COSY-11 detection setup . D1 – D4 denote drift chambers; S1 – S5, S_{start}, $S1_{D4}$, $S2_{D4}$ and V scintillation detectors; C Cerenkov counter; N the neutron detector and Si_{mon}, Si_{spec} and Si_{dip} silicon strip detectors to detect elastically scattered, spectator protons and negatively charged particles, respectively.

During the last experiment we examined the possibility to perform such a study and found that the trigger counting rate, based on the registration of one particle only, is a factor 200 too large to be accepted by the data acquisition system. However, based on the test performed during the run, we have elaborated a solution to reduce this rate by a factor of about 300. During the last run the triggering system was based on the coincidence between two close scintillator detectors indicated as $S1_{D4}$ and $S2_{D4}$ in figure 1 and the thresholds on discriminators were adjusted such that only noise was rejected. However, after careful calibration, one can set a threshold such that the significant fraction of signals originating from protons and pions will be rejected but still most of the impulses induced by deuterons will be registered. The ionization power of deuterons is only 30% larger than that of protons in the relevant momentum range (2.2GeV/c), but the energy resolution of the detectors (25% FWHM) allows for an efficient separation of signals from protons and deuterons (see Fig. 2). Thus, by adjusting appropriately the discriminator threshold we can e.g. cut about 3/4 of protons and pions loosing only about 1/10 of deuterons. Doing so on four scintillators which we plan to install could reduce the trigger rate by a factor of 256, decreasing simultaneously the efficiency of deuteron registration by 34% only. The bias to the deuteron energy spectrum could be reconstructed accurately from calibration measurements with decreased thresholds for the given detectors.

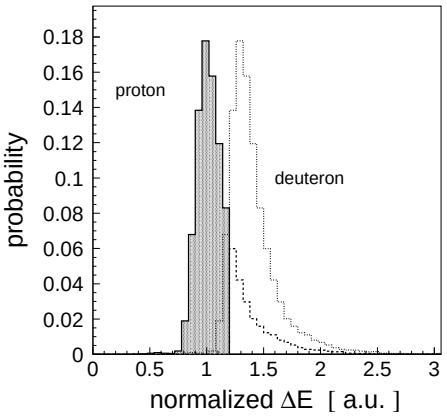

Fig. 2: Energy loss for protons and deuterons with momentum of 2.2 GeV/c normalized to the average energy loss of protons.

A corresponding proposal to perform a $pn \to d\eta'$ measurement was approved at the COSY Programme Advisory Committee in November 2005 and the experiment will be conducted in the year 2006. An additional outcome of this measurement will be an increase of the statistics for the $pn \to pn\eta'$ channel and a consistency check of the obtained results. The expected registered rate for the $pn \to d\eta'$ reaction is similar to the one for the $pn \to pn\eta'$ reaction. The estimated acceptance is about factor of 2.5 lower, however, by analogy to the η production [3] we expect the total cross section for the $pn \to d\eta'$ reaction to be few times larger than the one for the $pn \to pn\eta'$ process.

References:

[1] S. Brauksiepe et al., Nucl. Instr. & Meth. **A 376** (1996) 396.
[2] J. Przerwa et al., AIP Conf. Proc. **796** (2005) 164.
[3] H. Calén et al., Phys. Rev. Lett. **79** (1997) 2642.

[1] M. Smoluchowski Institute of Physics, Jagellonian University, 30-059 Cracow, Poland

Preparations for studies of the η' meson width via measurements of the $pp \to pp\eta'$ reaction at the COSY–11 facility

E. Czerwiński*, D. Grzonka, P. Moskal* for the COSY–11 collaboration

In the last issue of the Review of Particle Physics only two direct measurements of the natural width of the η' meson are reported [1]. In the first experiment the width was established from the mising mass spectrum of the $\pi^- p \to nX$ reaction measured close to the threshold for the production of the η' meson [2]. The experimental mass resolution achieved was equal to 0.75 MeV(FWHM) and the extracted value of $\Gamma_{\eta'}$ amounts to 0.28 ± 0.10 MeV/c^2. In the second experiment the value of $\Gamma_{\eta'}$ was derived from the threshold excitation function of the $pd \to {}^3HeX$ reaction [3]. The study was performed at 20 different beam momenta and although the experimental mass resolution was estimated to be 0.1 MeV/c^2 the error of the $\Gamma_{\eta'}$ was larger than in the previous measurement due to the large relative monitoring uncertainities. In this experiment $\Gamma_{\eta'} = 0.40 \pm 0.22$ MeV/c^2 was determined. At the COSY–11 facility we intend to combine both techniques. We can determine the threshold excitation function for the $pp \to pp\eta'$ reaction changing slowly the beam momentum during the measurement cycle and simultaneously we can construct missing mass spectra at various excess energies with an experimental precision better than 0.7 MeV/c^2 (FWHM) [4]. The slow ramping of the beam momentum during each cycle would allow to decrease significantly possible luminosity monitoring uncertainities due to target density variations.

A test measurement was already done at a fixed beam momentum equal to 3.210 GeV/c corresponding to about 0.6 MeV excess energy for the $pp \to pp\eta'$ reaction. At present the data are under analysis.

Figure 1 presents simulations performed in order to study the effects on the missing mass uncertainty due to the beam momentum spread and due to the experimental resolution of the momentum determination of the outgoing protons. One sees that the resolution of the missing mass due to the spread of the beam momentum is independent of the polar emission angle of the η' meson, and that the smearing of the missing mass due to the uncertainty of the proton momentum reconstruction does depend on this variable. This example illustrates that having high statistics data, even from a measurement at fixed beam momentum, we would be able to distinguish effects at least from some sources of the experimental uncertainities. The smearing of the missing mass due to the natural width of the η' is also independent of any variable and so one will be able to deconvolute the width of the η' meson from the missing mass spectrum only to the extent to which the smearing of the beam momentum is known. This can be monitored by the measurement of the Schottky frequency spectra and the known beam optics. The knowledge of the shape of the beam momentum spectrum would also be sufficient provided that it is different from the Breit-Wigner function expected for the mass distribution of the meson η'.

By scanning the threshold energy range the accuracy of the $\Gamma_{\eta'}$ determination can be farther improved. The scan will permit to fix the errors due to the beam momentum spread since this will change strongly with the momentum above threshold (in first approximation linearly) whereas the spread of the missing mass due to the natural width will remain unaltered. So with such a measurement we expect to reach an accuracy better than quoted in reference [2].

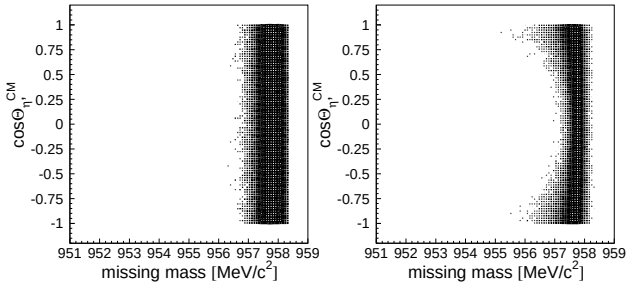

Fig. 1: Missing mass distributions of the $pp \to ppX$ reaction simulated for $X = \eta'$ as a function of the cosine of the centre-of-mass polar angle of the emission of the η' meson. The calculations were performed at a beam momentum of 3.210 GeV/c (1.7 MeV/c above the threshold for the η' meson production). (**left**) In the simulation only the smearing of the beam momentum $\sigma_{pb} = 2$ MeV/c was taken into account. (**right**) The beam momentum was fixed to 3.210 GeV/c. Only the experimental resolution of the proton momentum reconstruction was considered. Temporarily, for the calculations a covariance matrix [4] obtained for the $pp \to pp\eta$ reaction was utilized. As pointed out in reference [2] the advantage of a study close to the threshold is that the experimental uncertainities for the measurement of ejectiles are much reduced since ∂(mm)/∂p tends to zero. Here by mm we denoted the missing mass and by p the momentum of the outgoing proton. We see here, that indeed the smearing of the missing mass due to the uncertainities in the determination of the proton momenta is equal to about 0.3 MeV/c^2 only.

Even though a standard COSY–11 operation would permit to determine the $\Gamma_{\eta'}$ with a competitive accuracy, we hope to improve significantly the experimental resolution and to decrease drastically the spread of the beam momentum by using the cluster target with a diameter of about 1 mm which is to be compared with the normal operation with a target diameter of 9 mm for which a covariance matrix was extracted and used to prepare Figure 1(right). In this manner we would be able to increase the accuracy of the momentum measurement of the outgoing protons by a factor of about 1.4. Also the spread of the beam which hits the target is reduced due to the fact that the beam horizontal width is in the order of five milimeters (FWHM) and the target with a diameter of 1 mm would interact only with a part of the beam momentum distribution due to the finite dispersion at the COSY–11 interaction region.

References:

[1] S. Eidelman et al., Phys. Lett. **B 592** (2004) 1.
[2] D. M. Binnie et al., Phys. Lett. **B 83** (1979) 141.
[3] R. Wurzinger et al., Phys. Lett. **B 374** (1996) 283.
[4] P. Moskal, e-Print Archive: hep-ph/0408162.

* M. Smoluchowski Institute of Physics, Jagellonian University, 30-059 Cracow, Poland

The multi-pion background subtraction method for the two-proton correlation function.

P. Klaja[a] and P. Moskal[a] for the COSY-11 collaboration

Subtraction of the physical background and corrections for the limited acceptance of the detection system constitute the two main challenges when deriving the correlation function from high statistics data for the $pp \to pp\eta$ reaction [1]. The two-proton correlation function $R(q)$ depends on the two-proton relative momentum and can be defined [2] as the ratio of the reaction yield $Y_{pp\eta}(q)$ to the uncorrelated yield $Y^*(q)$.

$$R(q)+1 = C^* \frac{Y_{pp\eta}(q)}{Y^*(q)}, \quad (1)$$

where C^* denotes an appropriate normalization constant. For the $pp \to pp\eta$ experiment under discussion, only the four-momenta of the two protons in the final state were measured and the unobserved meson was identified via the missing mass technique [1, 3]. The entire accessible information of an event is contained in the momentum vectors of the registered protons. Therefore, it is in principle impossible to decide whether a given event corresponds to the η meson production or whether it is due to the multi-pion creation. However, statistically, on the basis of the missing mass spectra, one can derive a number of events originated from the production of $pp\eta$ system, for a chosen region of the phase-space. Therefore, $Y_{pp\eta}(q)$ can be easily extracted for each studied interval of q by dividing the sample of measured events according to the value of q, followed by calculating the missing mass spectra of the $pp \to ppX$ reaction for each sub-sample separately, and counting the number of $pp\eta$ events from these spectra. An example of such histogram for one interval of q is presented in the left panel of the figure 1. The derivation of the denominator of eq. 1 is more complicated. Applying a mixing technique one can construct an uncorrelated reference sample by combining two momentum vectors of protons corresponding to different real events. A real event is determined by the momentum vectors of two protons registered in coincidence, and an uncorrelated event will thus comprise momentum vectors of two protons ejected from different events. Unfortunately, in such a sample of uncorrelated momentum vectors, due to the loss of the kinematical bounds, the production of the η meson will be not reflected on the missing mass spectrum and hence it can not be used to extract a number of mixed-events corresponding to the production of the η meson. Therefore, in order to determine a background-free correlation function for the $pp \to pp\eta$ reaction the analysis has been performed in the following manner: First, for each event, a probability ω that this event corresponds to the $pp \to pp\eta$ reaction was determined. The probability ω_i, that the i^{th} $pp \to ppX$ event (with a missing mass m_i, and a relative momentum of q_i) corresponds to a $pp \to pp\eta$ reaction was estimated according to the formula:

$$\omega_i = \frac{N_\eta}{N_\eta + N_B}(m_i, q_i), \quad (2)$$

where N_η stands for the number of the $pp \to pp\eta$ reactions and N_B is the number of events corresponding to the multi-pion production. The values of N_η and N_B were extracted from the missing mass distributions produced separately for each of the studied intervals of relative momentum q. The pictorial definition of N_B and N_η is presented in the left panel of the figure 1. Now having introduced the weights we can calculate also the value of $Y^*(q)$ without a bias of the multi-pion background. We can achieve this by sorting an uncorrelated sample according to the q values similarly as in the case of the correlated events and next for each sub-sample we construct background free $Y^*(q)$ as a sum of the probabilities that both protons in an uncorrelated event originate from the reaction where the η meson was created. Specifically, if in a given uncorrelated event denoted by k, the momenta are taken from the real events $k1$ and $k2$, than the probability that both correspond to the reactions where the η was created equals to $\omega_{k1} \cdot \omega_{k2}$, and hence the uncorrelated yield $Y^*(q)$ may be constructed as a $\sum_k \omega_{k1} \cdot \omega_{k2}$, where k enumerates events in the uncorrelated sub-sample with a relative protons momentum q. The correlation function derived from the data is presented in the right panel of the figure 1 and is compared to the calculations, performed assuming a simultaneous emission of the two protons and the η meson and approximating tentatively the effective spatial shape of the emission zone by the Gaussian distribution. A rough comparison between the theoretical correlation functions simulated with $r_0 = 2\ fm$ and $4\ fm$, respectively, and the experimental correlation data indicates that the size of the reaction volume can be approximated by the Gaussian distribution with $r_0 \approx 3$ fm. The results presented in the right panel of the figure 1 have not yet been corrected for the acceptance of the COSY-11 detection setup, and the theoretical calculations have been performed without taking into account the experimental spread of the momenta. These corrections can significantly influence the final results.

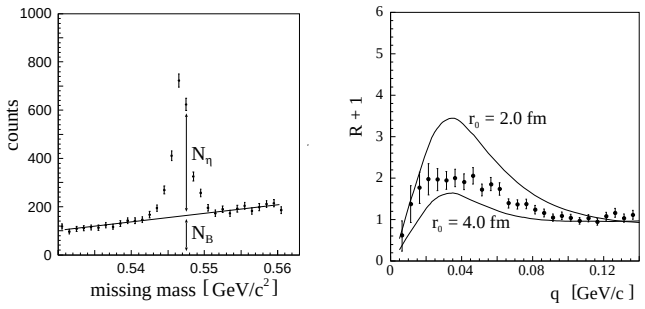

Fig. 1: **(Left panel):** The example of missing mass spectrum measured [1] for the $pp \to pp\eta$ reaction at $q \in (0.06;\ 0.07)$ GeV/c. **(Right panel):** Comparison of the experimental correlation function for the $pp \to ppX$ reaction, without acceptance correction represented by full dots and theoretical calculations indicated as two solid lines for emission sources parametrized by Gaussian distribution with $r_0 = 2.0$ and 4.0 fm.

References:

[1] P. Moskal et al., Phys. Rev. **C 69**, 025203 (2004)
[2] D. H. Boal et al., Rev. Mod. Phys. **62**, 553 (1990)
[3] P. Moskal: e-Print Archive: hep-ph/0408162

[a] M. Smoluchowski Institute of Physics, Jagellonian University, 30-059 Cracow,Poland

Energy Dependence of the $pp \to ppK^+K^-$ Total Cross Section Close to Threshold

D. Gil[a], D. Grzonka, P. Moskal[a], J. Smyrski[a] for the COSY-11 collaboration

Investigation of the K^+K^- interaction is of special interest due to the long standing puzzle on the nature of the $f_0(980)$ meson and its possible interpretation as a $K\bar{K}$ bound state (mesonic molecule) [1, 2]. For a study of the K^+K^- interaction the COSY-11 collaboration conducts a programme of measurements of the total cross section for the reaction $pp \to ppK^+K^-$ in the energy domain below the threshold for ϕ-meson production. Up to now, we measured the total cross sections at four excess energies in the range from $Q = 6$ MeV to 28 MeV [3, 4, 5]. The COSY-11 data points as well as the DISTO result [6], measured above the ϕ-threshold, are shown in Fig. 1.

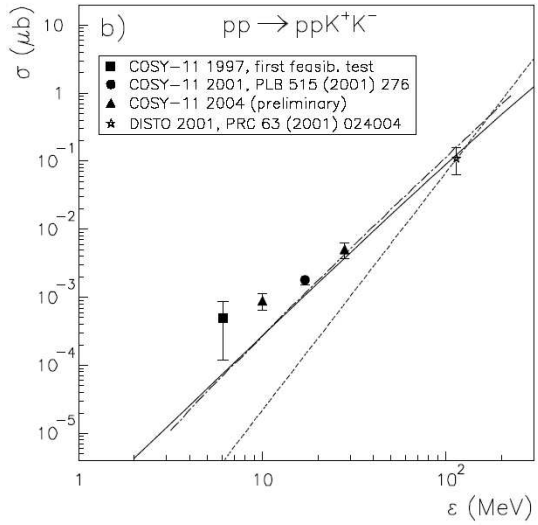

Fig. 1: The $pp \to ppK^+K^-$ cross section. The data are taken from [3, 4, 5, 6], the solid line shows the calculations of [7], the dashed line indicates the phase space $Q^{7/2}$- dependence, whereas the dash-dotted line results from a parametrization of the pp-FSI.

For the excess energy region below $Q = 10$ MeV, the cross section data seem to be enhanced by almost two orders of magnitude compared to a 4-body phase space dependence normalized to the DISTO data point. The cross sections are also by almost one order of magnitude too high compared with parametrization of the proton-proton final state interaction (pp-FSI) as well as with theoretical predictions of Sibirtsev et al. [7]. This situation is different than in the case of the $pp \to pp\eta'$ near-threshold cross section for which the energy dependence below 100 MeV arises mainly from the 3-body phase-space behavior weighted with a factor describing the interaction between the final state protons (see Fig. 2).

In order to prove the observed enhancement, it was of high importance to have further data closer to the threshold due to the low statistics at $Q = 6$ MeV of only two counts. Therefore, in November 2005 we performed a measurement of the $pp \to ppK^+K^-$ reaction at an excess energy of 3 MeV. The measurement was conducted at the COSY-11 detection system. It was based on the coincident detection of the pair of the outgoing protons and the positively charged kaon. The negatively charged kaons are identified via a missing mass determination. For the luminosity monitoring the elastic proton-proton scattering was registered. The data were collected during a 10 days run with an average luminosity of about $2 \cdot 10^{30}\mathrm{cm}^{-2}\mathrm{s}^{-1}$. The data analysis is in progress. We expect that the number of the collected K^+K^- events should be on the level of about 30 under the assumption that the corresponding $pp \to ppK^+K^-$ cross section is 30 pb. This would result in an error of about 20% for the cross section determination which is a drastic improvement compared to the 70% of the lowest data point.

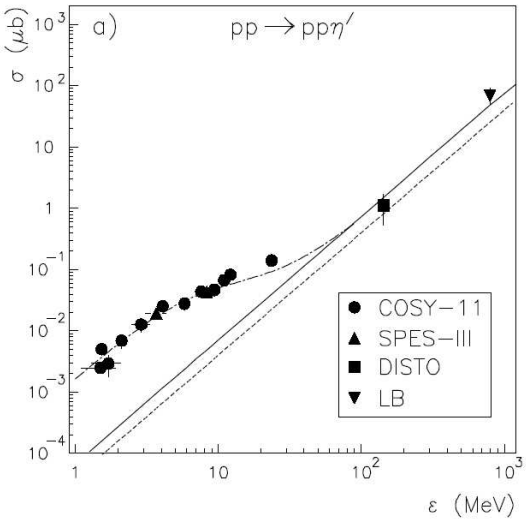

Fig. 2: The $pp \to pp\eta'$ cross section as a function of the excess energy. The dashed line shows the phase space Q^2 dependence, the solid line indicates calculations without FSI, the dash-dotted line includes a parametrization of the pp-FSI. The data are from [8, 9, 10, 11, 12, 13]

References:

[1] J. D. Weinstein and N. Isgur, Phys. Rev. **D 41**, 2236 (1990).
[2] D. Lohse, J. S. Durso, K. Holinde and J. Speth, Nucl. Phys. **A 516**, 513 (1990).
[3] M. Wolke, PhD Thesis, Westfalische Wilhelms-Universitat Munster, 1997, IKP Jul-3532.
[4] C. Quentmeier et al., Phys. Lett. **B 515**, 276 (2001).
[5] P. Winter, PhD Thesis, University of Bonn (2005).
[6] F. Balestra et al., Phys. Rev. **C 63**, 024004 (2001).
[7] A. Sibirtsev, W. Cassing and C. M. Ko, Z. Phys. **A 358**, 101 (1997).
[8] A. Khoukaz et al., Eur. Phys. J. **A 20**, 345 (2004).
[9] P. Moskal et al., Phys. Rev. Lett. **80**, 3202 (1998)
[10] P. Moskal et al., Phys. Lett. **B 474**, 416 (2000)
[11] F. Hibou et al., Phys. Lett. **B 438**, 41 (1998)
[12] F. Balestra et al., Phys. Lett. **B 491**, 29 (2000)
[13] A. Baldini et al., Total cross-sections for reactions of high-energy particles, Landolt-Bornstein, New Series Vol. I/12 (Springer, Berlin, 1988).

[a] M. Smoluchowski Institute of Physics, Jagellonian University, 30–059 Cracow, Poland

General thoughts to the Kaon pair production in the threshold region

W. Oelert, P. Winter, H.-H. Adam[1], A. Budzanowski[2], R. Czyżykiewicz[3], D. Grzonka, M. Janusz[3], L. Jarczyk[3], B. Kamys[3], A. Khoukaz[1], K. Kilian, P. Klaja[3], P. Moskal[3], C. Piskor-Ignatowicz[3], J. Przerwa[3], J. Ritman, T. Rożek[4], T. Sefzick, M. Siemaszko[4], J. Smyrski[3], A. Strzałkowski[3], A. Täschner[1], M. Wolke, P. Wüstner[5], Z. Zhang, W. Zipper[4]

Total cross sections [1 – 4] of the reaction $pp \to ppK^+K^-$ at excess energies below $Q = 120$ MeV are given in Figure 1. At

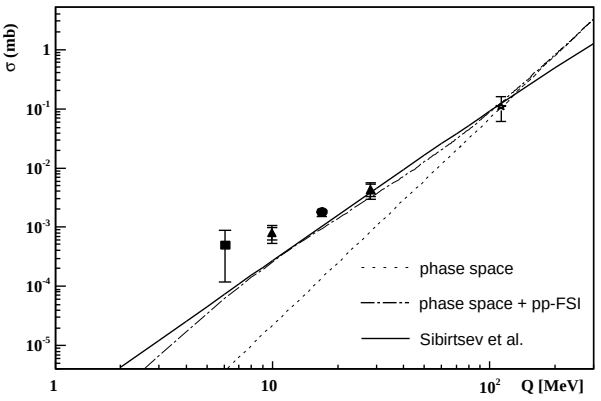

Fig. 1: Total cross section as a function of the excess energy Q for the reaction $pp \to ppK^+K^-$ [1, 2, 3, 4].

low excess energies the data points lie significantly above the various expectations indicated by the different lines as long as these predicted curves are all normalized to the DISTO point [4] at $Q = 114$ MeV. The pure phase space (dashed line) differs by two orders of magnitude at $Q = 10$ MeV and a factor of five to ten at $Q = 28$ MeV. In comparison to that, the inclusion of the pp-FSI (dashed-dotted line) by folding its parameterization known from the three body final state with the four body phase space is already closer to the experimental results but does not fully account for the difference. The solid line representing the calculation within a one-boson exchange model [5] reveal a similar discrepancy as the pp-FSI parameterization. This model includes an energy dependent scattering amplitude derived from the fit of the total cross sections in $K^{\pm}p \to K^{\pm}p$ [6] while the pp-FSI was not included, yet. Up to now, there is no full calculation available but the new data demands for further theoretical efforts in order to give a complete picture of the K^+K^- production.

An important aspect might be the mass splitting between the neutral K^0K^0 and charged K^+K^- kaons being in the order of 8 MeV. Based on the theoretical observation that the opening neutral kaon production channel shows a substantial influence on the $\pi\pi \to K^+K^-$ transition (c.f. Figure 2. in reference [7]), we tried a simple–minded Ansatz for the energy dependence of the excitation function for the $pp \to ppK^+K^-$ reaction assuming that with the opening of the neutral kaon channel (at 8 MeV excess energy) some yield is taken out of the charged kaon channel. As long as the total energy is large enough to produce the charged kaon pair but is below the neutral kaon channel all strength for the associated strangeness production is devoted to the K^+K^- creation. At 8 MeV excitation energy the charged channel faces the competition of the neutral one. For estimating such a coupled channel effect, we postulated the two simple assumptions. First, we assume that the excitation function for the neutral $pp \to ppK^0\bar{K}^0$ channel follows exactly the dashed-dotted line in figure 1 for the charged kaon production case, but shifted by 8 MeV. If $f(Q)$ describes the excitation function of the dashed-dotted line, we simply assume that the energy dependence for the neutral channel is given by $g(Q) = f(Q - 8\,\mathrm{MeV})$ where Q refers here to the K^+K^- system. Second, the opening channel is incorporated by the idea that the modified description $\bar{f}(Q)$ of the $pp \to ppK^+K^-$ channel is given by a subtraction of the neutral channel via $\bar{f}(Q) := c \cdot [f(Q) - g(Q)]$ with an arbitrary normalization c. This is certainly an extreme scenario since the influence of the $K^0\bar{K}^0$ channel is assumed to be an uncorrelated sum of the K^+K^- and $K^0\bar{K}^0$ cross sections; and, since the inverse transition $K^0\bar{K}^0 \to K^+K^-$ is not considered to take place. The resulting energy dependence $\bar{f}(Q)$ as shown in Figure 2 just happens to pass through the experimental data. This good agreement should be taken with caution since a

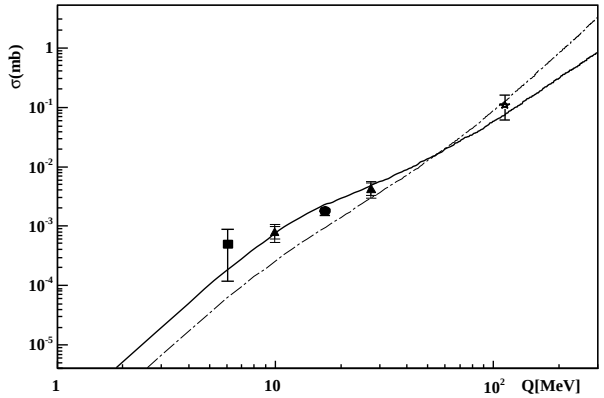

Fig. 2: Experimental data together with a simplified Ansatz for the incorporation the $K^0\bar{K}^0$ channel (solid line).

full coupled channel calculation has to be performed to determine quantitatively the effect of the $K^0\bar{K}^0$ channel, which is expected to be rather small [8] and can not account for the full enhancement seen in the data. Furthermore other effects are not considered which should certainly be taken fully into account such as final state interactions between the subsystems $p - K^+, p - K^-$ and $K^+ - K^-$ as well as the influence of intermediate resonances.

References:

[1] P. Winter et al., submitted for publication to Phys. Lett.
[2] C. Quentmeier et al., Phys. Lett. **B 575** 276 (2001)
[3] M. Wolke, Dissertation, Münster, 1997, IKP JÜL. 3532
[4] F. Balestra et al., Phys. Rev. **C 63** 024004 (2001)
[5] A. Sibirtsev, et al., Z.Phys. **A 358** 1001 (1907)
[6] A. Baldini et al., Landolt–Börnstein, Vol I/12, New Series, Springer, Berlin, 1988
[7] O. Krehl, et al., Phys. Lett. **B 390** 23 (1997)
[8] J. Haidenbauer, private communication

[1] IKP, Westfäl. Wilhelms–Universität, Münster, Germany
[2] Institute of Nuclear Physics, Cracow, Poland
[3] IP, Jagellonian University, Cracow, Poland
[4] IP, University of Silesia, Katowice, Poland
[5] ZAT, Research Center Jülich, Germany

Preparations for investigations of the $^4He-\eta$ bound state

P. Klaja[a], J. Złomańczuk[b], R. Czyżykiewicz[a], M Janusz[a], P. Moskal[a], W. Oelert, J. Przerwa[a], J. Smyrski[a]
for the COSY-11 and WASA-at-COSY collaborations

A bound state between nucleus and meson was predicted twenty years ago [1]. However, until now its existence has not been confirmed experimentally. Recent theoretical elaborations indicate a possibility of the existence of such states for light nuclei even for helium. Therefore, the nucleus-meson bound state production in deuteron-proton and deuteron-deuteron collisions could be possible. During three weeks of April 2005, the COSY-11 collaboration performed measurements of the $dp \rightarrow {}^3H\pi^+$ and $dp \rightarrow {}^3He\pi^0$ cross sections near the η meson production threshold. The ^3He ejectiles and $^3H-\pi^+$ pairs were registered with the COSY-11 detection setup during slow ramping of the COSY deuteron beam. The deuteron beam momentum was continously varied from 3.099 GeV/c to 3.179 GeV/c, around the threshold for the $dp \rightarrow {}^3He\eta$ reaction at 3.139 GeV/c. In the ongoing analysis, the determination of the total and differential cross sections for the $dp \rightarrow {}^3He\eta$ reaction channel for excess energies in the range from threshold up to Q = 9.0 MeV is in progress [2]. In the preliminary results a structure originating from the $^3He-\eta$ bound state decays has not been observed in the excitation curve for pion production in the reaction $dp \rightarrow {}^3He\pi^0$.

In November 2005 the COSY-11 collaboration presented at the COSY-PAC meeting a proposal [3] to extend investigations on the reactions induced by a deuteron beam on a deuteron target. The primary goal of these measurements is a search for a $^4He-\eta$ bound state via a measurement of the excitation function for the $dd \rightarrow {}^3He\,p\pi^-$ reaction where the outgoing $p-\pi^-$ pair originates from the conversion of the η meson on a neutron inside the ^4He nucleus and the ^3He ejectile is an "observer". An enhancement in the corresponding cross section at beam momenta below the η production threshold would indicate an existence of the $^4He-\eta$ nucleus. Such a state is foreseen e.g. by S. Wycech et al. [4] on the basis of the multiple scattering theory. The proposal

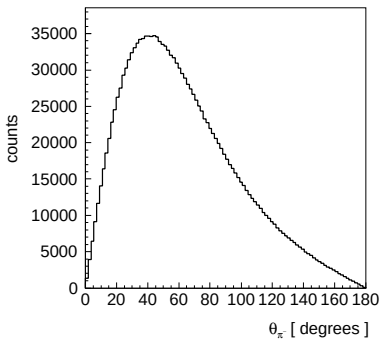

Fig. 1: Distribution of the polar emission angle of the π^- meson from the $dd \rightarrow {}^3He p\pi^-$ reaction.

was judged positively, however, the committee suggested to check the possibility of performing this experiment at the WASA-at-COSY facility which allows for the registration of all ejectiles from the $dd \rightarrow {}^3He p\pi^-$ reaction. For this aim we are conducting simulations of the $dd \rightarrow {}^3He p\pi^-$ reaction applying the ODIN system [5], a software package for acquisition and analysis of data in the WASA experiments. At present the investigations are still in progress and here in figures 1, 2 and 3 we present only distributions of the polar angle of the outgoing particles. Indeed, the figures indicate that significant part of the ejectiles could be registered in the forward detector with the angular range from 2.5 to 18 degrees and a central detector with an angular acceptance ranging from 20 to 140 degrees. The simulations were performed assuming the homogenous phase space population of the $dd \rightarrow {}^3He p\pi^-$ reaction. Yet in the case of the formation of the bound $^4He-\eta$ state and its subsequent decay into ^3He, proton and π^- we expect that the ^3He nucleus will move with the Fermi momentum possessed at the moment of the decay. In this case most of the ^3He would be emitted with the polar angle smaller than 2.5 degree and could not be detected. At present we are continuing the study and performing simulations for other possible decay channels in order to optimize the search for the bound state of the η meson with the helium nucleus at COSY.

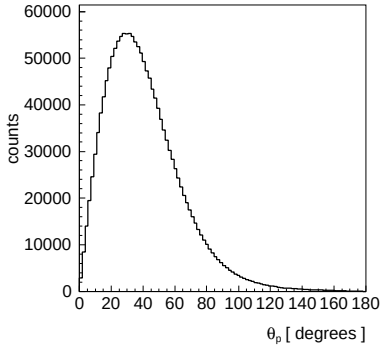

Fig. 2: Distribution of the polar emission angle of the proton from the $dd \rightarrow {}^3He p\pi^-$ reaction.

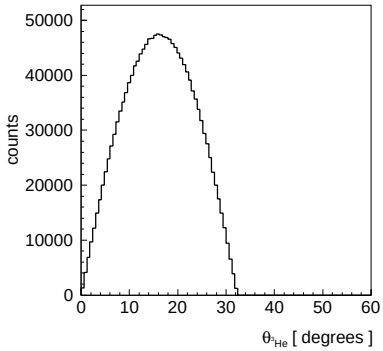

Fig. 3: Distribution of the polar emission angle of the ^3He nucleus from the $dd \rightarrow {}^3He p\pi^-$ reaction.

References:

[1] Q. Haider, L. C. Liu, Phys. Lett. **B 172** (1986) 257.
[2] J. Smyrski et al., Acta Phys. Slovaca, in print.
[3] J. Smyrski, P. Moskal et al., COSY Proposal No. 156.
[4] S. Wycech et al., Phys. Rev. **C 52** (1995) 544.
[5] J. Złomańczuk, Internal WASA report, Uppsala (2003).

[a] M. Smoluchowski Institute of Physics, Jagellonian University, 30-059 Cracow, Poland
[b] Department of Radiation Sciences, Uppsala University, S-751 21 Uppsala, Sweden

Threshold hyperon production in proton–proton collisions at COSY–11

T. Rożek[1], D. Grzonka, H.-H. Adam[2], A. Budzanowski[3], R. Czyżykiewicz[4], M. Janusz[4], L. Jarczyk[4], B. Kamys[4], A. Khoukaz[2], K. Kilian, P. Klaja[4], P. Kowina[1 *], P. Moskal[4], W. Oelert, C. Piskor-Ignatowicz[4], J. Przerwa[4], J. Ritman, T. Sefzick, M. Siemaszko[1], J. Smyrski[4], A. Strzałkowski[4], A. Täschner[2], P. Winter, M. Wolke, P. Wüstner[5], Z. Zhang, W. Zipper[1]

The Σ^0 and Λ hyperon production near the kinematical threshold was studied by the COSY-11 collaboration in $pp \to pK^+\Lambda/\Sigma^0$ reactions [1, 2, 3]. The cross section ratio $\sigma(pp \to pK^+\Lambda)/\sigma(pp \to pK^+\Sigma^0)$ below excess energies of 15 MeV was measured to be around 28 in contrast to the value of about 2.5 determined for excess energies higher than $Q = 300$ MeV [5]. Beside that, the $pp \to pK^+\Lambda$ excitation function close-to-threshold shows a clear deviation from the pure phase space distribution and a proton–hyperon final state interaction (FSI) has to be included to describe the data [1, 2, 3, 4]. In the $pp \to pK^+\Sigma^0$ channel the pY FSI seems to be negligible and the pure phase space calculations follow reasonably well the data points.

To explain this threshold behaviour, various theoretical scenarios within meson exchange models were proposed. Calculations have been performed with pion and kaon exchange added coherently [11] or incoherently [6], including the excitation of nucleon resonances [7, 10] and heavy meson exchange (ρ, ω and K^*) [8, 10]. Although the various descriptions differ even in the dominant basic reaction mechanism, all more or less reproduce the trend of an increase in the cross section ratio in the threshold region. In order to exclude possible explanations further studies e.g. in the other isospin projections are required. Therefore the production of the Σ^+ hyperon via the $pp \to nK^+\Sigma^+$ channel was measured.

After the installation of a neutron detector, the $pp \to nK^+\Sigma^+$ channel became accessible at the COSY–11 detection system. The measurement of the Σ^+ hyperon production was performed at two beam momenta i.e. P_{beam} = 2.6 GeV/c and P_{beam} = 2.74 GeV/c, corresponding to the excess energies of 13 MeV and 60 MeV, respectively.

The Σ^+ hyperon was identified via the missing mass technique by detecting the K^+ and the neutron. The momentum vector of the K^+ meson can be established by tracking back the K^+ trajectory reconstructed in the drift chambers through the known magnetic field back to the target point. Assuming a hit in the neutron detector being due to a neutron, the four momentum vector of the neutron is given by the measured velocity, the direction of the neutron (given by the first hit module) and the known mass. The background from charged particles hitting the neutron detector is discriminated by veto scintillators.

In figure 1a) and 2a) the experimental distributions of the squared missing mass (m_x^2) of the $pp \to nK^+X$ system for the two beam momenta are shown. In order to determine the number of Σ^+ events in the higher energy data set, a fit has been done with a polynomial function superposed by the expected missing mass distribution of the nK^+ system for the $pp \to nK^+\Sigma^+$ reaction obtained from simulation studies. Figure 1b shows the result of the subtraction of the fitted polynomial from the experimental missing mass distribution together with the MC distribution.

In order to understand the background distribution, 22 reaction channels (mostly multi-pion reactions but also $pp \to pK^+\Lambda$ $(\Sigma^0, \Lambda\gamma)$) were simulated and their contributions to the missing mass distribution were determined.

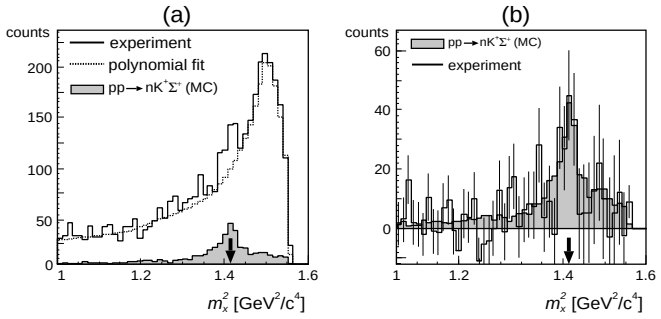

Fig. 1: Background determination for the $pp \to nK^+\Sigma^+$ reaction at P_{beam} = 2.74 GeV/c. (a) The experimental squared missing mass spectrum of the nK^+ system with a polynomial background fit and the simulated $pp \to nK^+\Sigma^+$ spectrum. (b) Result of the subtraction of the fitted background from the experimental distribution compared with the simulated spectrum. The arrows show the nominal squared mass of the Σ^+ hyperon. Only statistical errors are shown.

These studies showed that the reactions $pp \to pK^+\Lambda$ and $pp \to pK^+\Lambda\gamma$ (γ's) are the dominant background channels in the Σ^+ region. All background channels result in a rather smooth distribution of the missing mass spectrum.

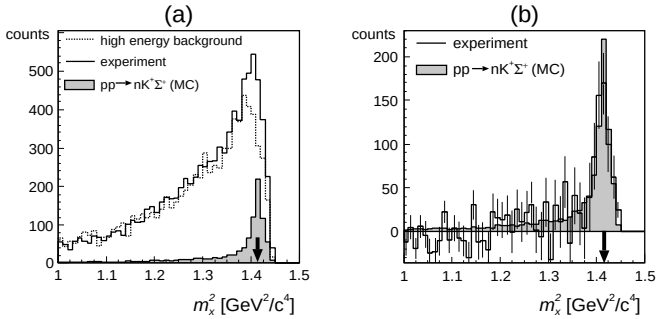

Fig. 2: Background investigation for the $pp \to nK^+\Sigma^+$ reaction at P_{beam} = 2.6 GeV/c. (a) The experimental squared missing mass spectrum of the $pp \to nK^+X$ system compared to the assumed background taken from the data at Q = 60 MeV and the simulated $pp \to nK^+\Sigma^+$ distribution. (b) Result of the subtraction of the fitted background from the experimental distribution compared to the simulated spectrum. The arrows show the nominal squared mass of the Σ^+ hyperon. Only statistical errors are shown.

For the lower energy data set a Σ^+ peak is not obviously visible via the missing mass distribution and a simple polynomial background fitting cannot be used. To determine the number of Σ^+ events it was assumed that the background shape for this data set is the same as that at the higher energy (see figure 2). This assumption is justified since there is no new open channel for the higher energy. For the considered

background reactions the form of the missing mass distributions does not change (within the error bars) for both beam momenta.
In table 1 the total cross sections for both beam momenta are given. The detection efficiency of the COSY–11 apparatus for the two excess energies were determined in the MC studies and the luminosity by a simultaneous measurement of proton-proton elastic scattering.

Table 1: Values of the total cross section for the $pp \to nK^+\Sigma^+$ reaction obtained in the present work. Both, statistical and systematical errors are presented, however, for the systematical uncertainty only lower limits are given, since they are still under discussion.

Beam momentum P_{beam} $[GeV]$	Excess energy Q $[MeV]$	Total cross section σ $[nb]$
2.60	13	$4559.7 \pm 940.9 \pm > 359.8$
2.74	60	$44812.0 \pm 10687.9 \pm > 1573.0$

Theoretical predictions available for this Σ^+ production channel are far below the experimental data. Calculations of the Σ^+ production within the *Jülich meson exchange model* [11], where the π- and K-exchange amplitudes interfere predict a total cross section of σ = 229 nb at Q = 13 MeV for a destructive interference (which was necessary to describe the high Λ/Σ^0 cross section ratio at threshold). That is about a factor of 20 below the experimental value of about σ_{exp} = 4560 nb. A constructive interference would result in a cross section even a factor of 53 too low. For the *resonance model* [6, 9], where π, η and ρ meson exchange with the excitation of intermediate baryonic resonances are taken into account, the data point for the $pp \to nK^+\Sigma^+$ channel at Q = 13 MeV is underestimated by the calculated total cross section by about a factor of 500 and for Q = 60 MeV by about a factor of 50.
In the investigation of the hyperon production in COSY–11 it was observed [1, 2, 3] that a pure 3-body phase space (PS) dependent cross section expressed as [12]:

$$\sigma = K \cdot Q^2, \tag{1}$$

where K is a normalization factor and Q the excess energy cannot describe the $pp \to pK^+\Lambda$ data, and therefore a modification is needed which takes into account the *proton - hyperon* FSI. In order to compare the Σ^+ data with the FSI analyses of the Λ and Σ^0 channels, the parametrisation of the excitation function including the FSI proposed by Fäldt-Wilkin [4] was used. It is expressed by:

$$\sigma = C \cdot \frac{Q^2}{(1+\sqrt{1+Q/\varepsilon})^2}, \tag{2}$$

where C and ε are parameters related to the FSI strength. In figure 3 the cross sections for different production channels of the hyperons Λ, Σ^0, and Σ^+ are compared to predictions of the three-body phase space (PS, dotted line) and the three-body phase space calculations modified by the proton-hyperon final state interaction (solid line) following equation 2 with ε and C as free parameters which were adjusted to the experimental data for each channel and which are directly related to the scattering length and range parameters of the scattering.

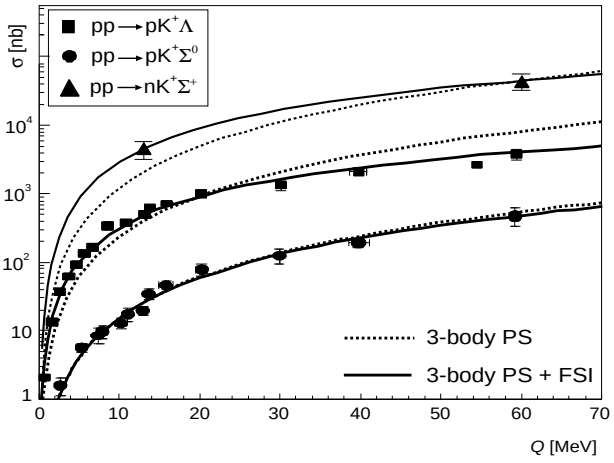

Fig. 3: The $pp \to nK^+\Sigma^+$, $pp \to pK^+\Lambda$ and $pp \to pK + \Sigma^0$ excitation functions. The experimental data were taken from [1, 2, 3, 13, 14] The lines represent calculations corresponding to three-body phase space distribution with (solid line) and without (dashed line) final state interaction.

For the $pp \to nK^+\Sigma^+$ data the resulting ε and C parameters are of similar values as for the $pp \to pK^+\Lambda$ channel. It indicates that in the case of the Σ^+ production via the $pp \to nK^+\Sigma^+$ reaction a rather strong $n\Sigma^+$ FSI seems to be present.

References:

[1] J. T. Balewski et al., Phys. Lett. **B420** (1998) 211.
[2] S. Sewerin et al., Phys. Rev. Lett. **83** (1999) 682.
[3] P. Kowina et al., Eur. Phys. J. **A22** (2004) 293.
[4] G. Fäldt and C. Wilkin, Z. Phys. **A357** (1997) 241, nucl-th/9612019.
[5] A. Baldini et al., *Total Cross-Section for Reactions of High-Energy Particles*, Springer, Berlin, 1988.
[6] A. Sibirtsev et al. Nucl. Phys. **A646** (1999) 427.
[7] A. Sibirtsev et al. nucl-th/0004022 **v2** (2000).
[8] R. Shyam et al., Phys. Rev. **C63** (2001) 022202.
[9] N. Tsushima et al., Phys. Rev. **C59** (1999) 369.
[10] R. Shyam, hep-ph/0406297 (2004).
[11] A. Gasparian et al., Nucl. Phys. **A684** (2001) 397.
[12] E. Byckling, *Particle Kinematics*, John Wiley & Sons Ltd., London 1973.
[13] T. Rozek, PhD Thesis, University of Silesia, Katowice, Poland, 2006.
[14] R. Bilger et al., Phys. Lett. **B 420** (1998) 217.

[1]IP, University of Silesia, Katowice, Poland
[2]IKP, Westfäl. Wilhelms–Universität, Münster, Germany
[3]Institute of Nuclear Physics, Cracow, Poland
[4]IP, Jagellonian University, Cracow, Poland
[5]ZAT, Research Center Jülich, Germany

Compared to other light mesons, the mass of the η is surprisingly poorly known. Though the Particle Data Group (PDG) quote a value of $m_\eta = 547.75 \pm 0.12$ MeV/c^2 in their 2004 review [1], this error hides differences of up to 0.7 MeV/c^2 between the results of some of the modern counter experiments quoted. This is shown in Fig. 1. The early values

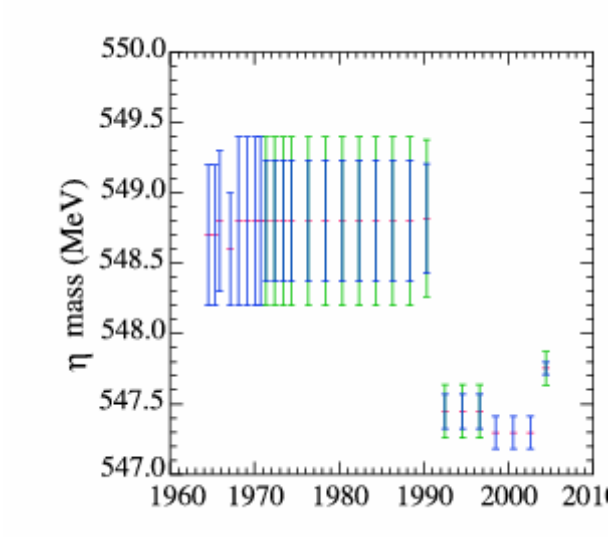

Fig. 1: The PDG value of the η mass as function of PDG publication year (taken from PDG).

are from bubble chamber measurement. No new data were added in the seventieths and eighties. Only in the nineties the first counter experiments determined the η mass and PDG rejected the old data. The 2004 PDG average is in fact dominated by the result of the CERN NA48 experiment, $m_\eta = 547.843 \pm 0.051$ MeV/c^2, which is based upon the study of the kinematics of the six photons from the $3\pi^0$ decay of 110 GeV η-mesons [2]. In the other experiments employing electronic detectors, which typically suggest a mass ≈ 0.5 MeV/c^2 lighter, the η was produced much closer to threshold and its mass primarily determined through a missing-mass technique where, unlike the NA48 experiment, precise knowledge of the beam momentum plays an essential part. In the Rutherford Laboratory experiment the momentum of the pion beam in the $\pi^- + p \to n + \eta$ reaction was fixed macroscopically using the floating wire technique [3]. In the measurement making use of the photoproduction reaction $\gamma + p \to p + \eta$, the energy of the electrons that were the source of the bremsstrahlung photons was fixed to a relative precision of 2×10^{-4} by measuring the distance of the beam paths in the third race track microtron of the MAMI accelerator [4]. In the Saclay SATURNE experiment a high resolution, but small acceptance, spectrometer was used and, through an ingenious series of measurements on different nuclear reactions, the beam energy and spectrograph settings were both calibrated. The value of the η mass was then extracted from the missing-mass peak in the $p + d \to {}^3\mathrm{He} + X$ reaction [5]. The Big Karl spectrograph and the high brilliance beam at COSY are ideally suited to perform a high precision experiment. The underlying idea of the study is

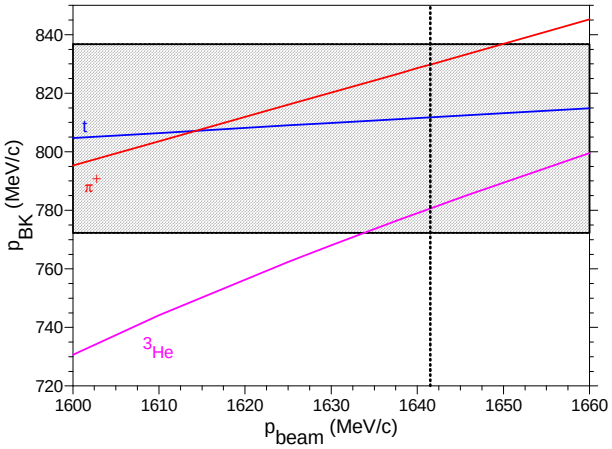

Fig. 2: The momenta of the three particles of interest at zero degrees in the laboratory system as function of the beam momentum. The acceptance of the spectrograph for a central momentum of 804.5 MeV/c is shown as the shaded area. Also a beam momentum of 1641.4 MeV/c is indicated.

a self calibrating experiment. Three reaction products were measured at the same time with one setting of the spectrometer and one setting of the beam momentum. The reaction were

$$\begin{aligned} (1)+(2) &\to (3)+(4) \\ p+d &\to t+\pi^+ \quad (1) \\ p+d &\to \pi^+ + t \quad (2) \\ p+d &\to {}^3He+\eta \quad (3) \end{aligned}$$

It was always the third particle which was measured. Input are the well known masses of the proton, deuteron, π^+, triton and ^3He. Fig. 2 shows the momenta of the third particle being emitted at zero degree in the laboratory system. Pions and ^3He are emitted into the forward direction, tritons into the backward direction in the center of mass system. For ^3He the momenta were divided by two in order to account for the double charge. The momentum acceptance of the spectrograph is also shown. Clearly, for a beam momentum close to 1641 MeV/c all three particles are within the acceptance of the spectrograph. The pion is used to deduce the absolute beam momentum. Then the triton is used to fix the spectrograph setting and finally from the ^3He one obtains the mass of the η meson. In the analysis the target thickness, as measured from the triton momentum, was studied as function of measuring time. It was found that it increased with time most probably due to freezing out of air. This is shown in Fig. 3. The upper part of the figure shows the variation of the COSY beam with time as estimated from measuring the pions (reaction 2). The middle part shows the variation of the target thickness as deduced from the measurement of tritons (reaction 1). The lowest part shows the measurement of the η mass as deduced from the detected ^3He ions (reaction 3). A thinner target at approximately half of the measuring time coincides with a cleaning of the target windows. In order to investigate the properties of the spec-

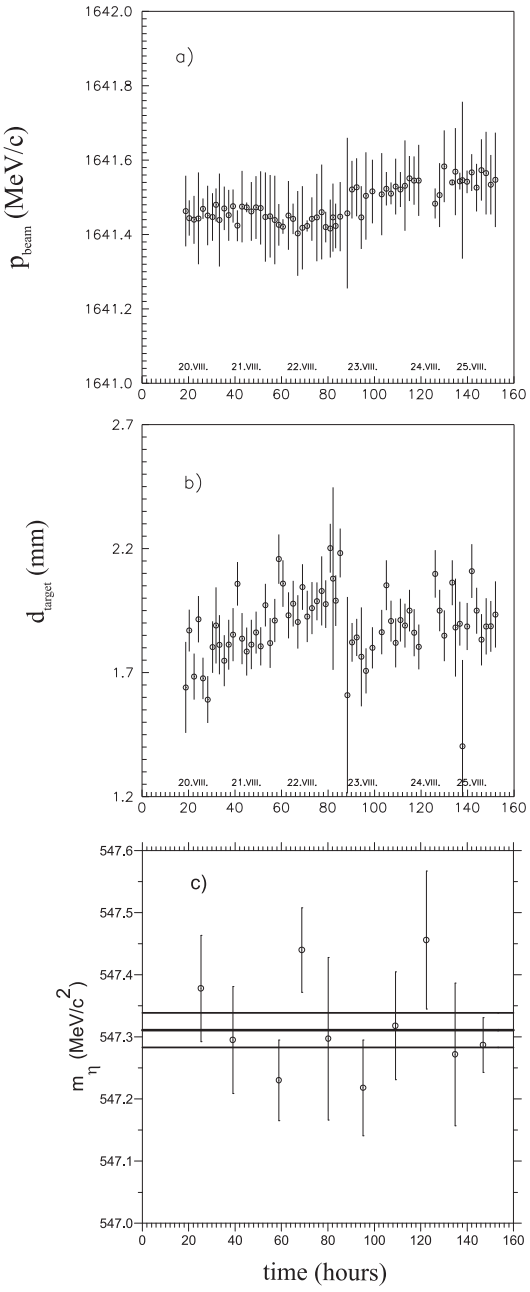

Fig. 3: Upper part: variation of the accelerator beam momentum with time as deduced from the pion momenta. Middle part: variation of the target thickness with time as deduced from the triton momenta. Lower part: same as above but for values of the η mass as deduced from the measured ^3He measurements. The thick line is the statistical mean value and the thin lines indicate the $\pm 1\sigma$ band.

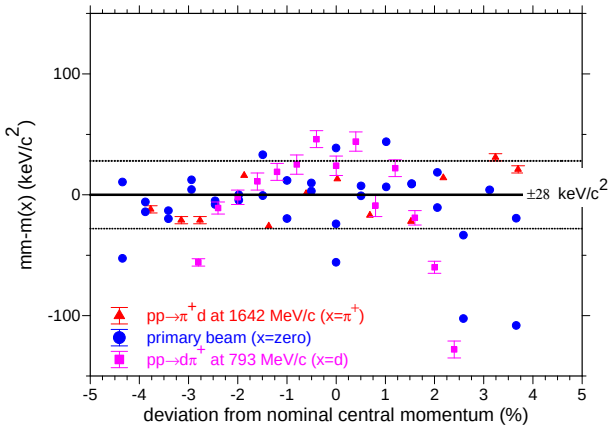

Fig. 4: The systematic error as function of deviation from the central momentum of the spectrograph.

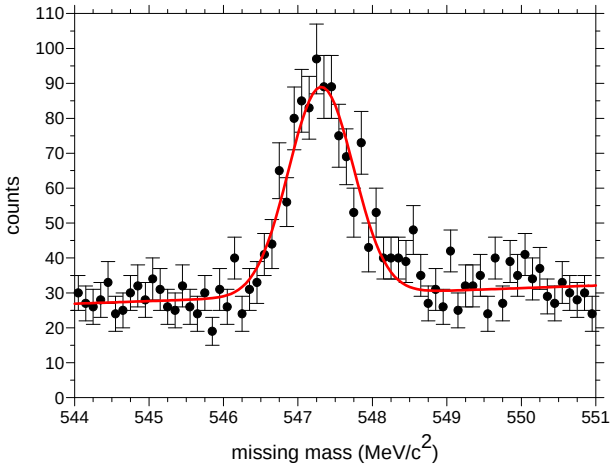

Fig. 5: The missing mass spectrum. The solid curve is a linear background plus a Gaussian.

trograph a series of calibration runs were performed. These include sweeping with the primary beam over the focal plane without a target at a beam momentum of 793 MeV/c. This corresponds to a reaction $p+0 \rightarrow p+0$. Then the full ellipse of deuterons from the reaction $p+p \rightarrow d+\pi^+$ at the same beam momentum was measured. Finally, pions from the reaction $p+p \rightarrow \pi^+ + d$ were measured at 1640 MeV/c with again sweeping the deuteron loci over the whole focal plane. The the following procedure was adopted. It is assumed that the spectrograph is known. The three calibration reactions were now used to fix the beam momentum, the target thickness and the η mass. In a second step the assumption (known spectrograph) was studied by determining the missing mass of the unobserved particle in the calibration runs. These are the masses 0, π^+ and d. The deviations of the nominal masses (taken to be the PDG values) as function of the position in the spectrograph, measured in terms of deviation from the central momentum, are shown in Fig. 4. Deviations have an uncertainty of $\sigma = \pm 28$ keV/c^2, which is the main contribution to the systematical error which in total is 32 keV/c^2. The missing mass measurement yields a statistical error of the same order of magnitude. This is shown as band in the lower panel of Fig. 3. The same result is achieved of course if we take all data for the missing mass together (see Fig. 5). This figure shows also the fit curve: a linear background and a Gaussian.

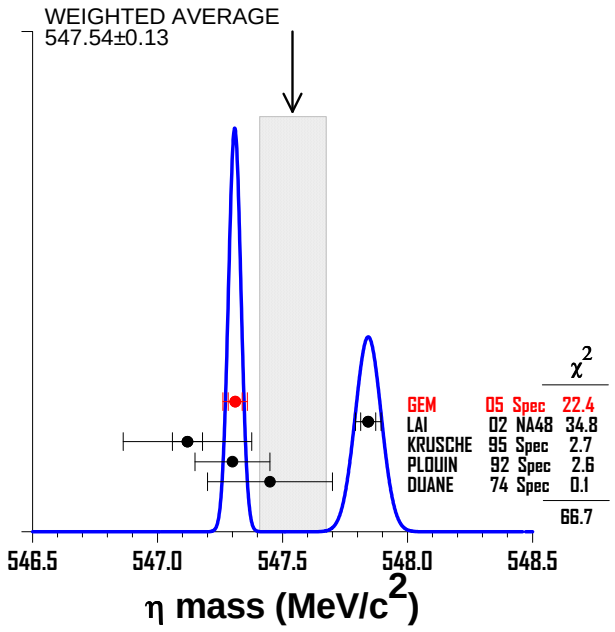

Fig. 6: Ideogram in the style of the PDG.

Its width is given almost completely by the scattering of the ^3He ions in the target.

The final result is [6]:

$$m(\eta) = 547.311 \pm 0.028 \text{ (stat.)} \pm 0.032 \text{ (syst.) MeV/c}^2.$$

This final result is compared in the ideogram 6 with all other recent data. The total average and its uncertainty is also indicated. The data fall into two groups. One consists of only one measurement and the other contains all remaining experiments. The width of the latter is dominated by the present result.

References:

[1] S. Eidelman et al.: Phys. Lett., **B 592** (2004) 1.
[2] A. Lai et al.: Phys. Lett., **B 533** (2002) 196.
[3] A. Duane et al.: Phys. Rev. Lett., **32** (1972) 425.
[4] B. Krusche et al.: Z. Physik, **A 351** (1995) 327.
[5] F. Plouin et al.: Phys. Lett., **B 276** (1992) 526.
[6] M. Abdel-Bary et al. (GEM Collaboration): Phys. Lett., **B 619** (2005) 281.

Study of the reaction $\vec{d}+d \to \eta+\alpha$

GEM Collaboration

The study of the $\vec{d}+d \to \eta+\alpha$ reaction is driven by the quest wether a strongly bound η-nucleus system exists. Theory predicts that a heavier system should result into a stronger binding. Close to threshold only total cross sections existed so far [1, 2]. Only recently the first angular distributions become available [3]. GEM has a preliminary value for the total cross section measured at a beam momentum of 2.39 GeV/c. All the known points are included into Fig. 1. It is interesting

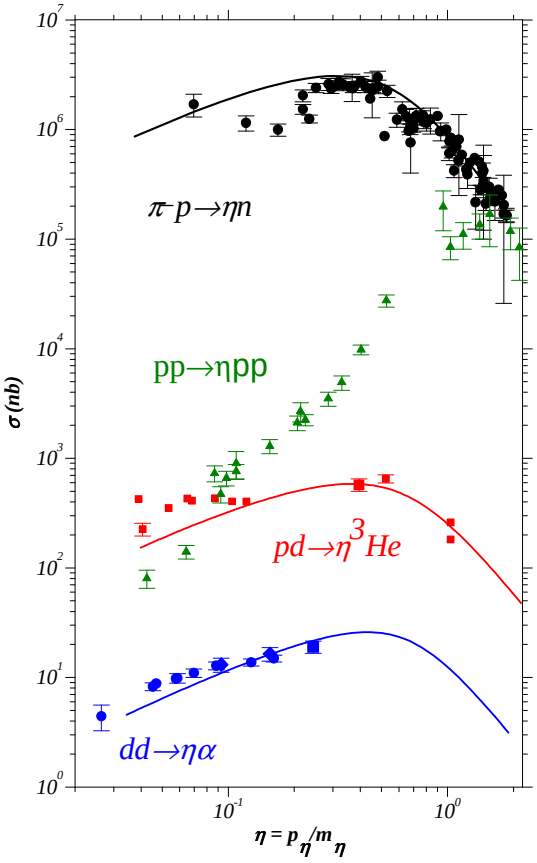

Fig. 1: Excitation functions for the indicated reactions. Points from GEM are always indicated by squares, the new data from ANKE [3] as rhombi. Data for the reaction $pd \to {}^3He\eta$ from Refs. [4] and [5] have been omitted. The solid curves are the predictions of the resonance model discussed in the text.

to note that the new data follow the resonance model originally developed for the $pd \to {}^3He\eta$ reaction [6]. It also accounts for the $\pi^- p \to \eta n$ cross sections. However, the excitation curve for $pp \to \eta pp$ shows a completely different behavior. We can summarize the present observations that reactions with two particles in the final state seem to have a quite similar behavior that reactions with three particles in the final state. The $dd \to \eta\alpha$ reaction allows to extract the real and imaginary parts of the partial wave amplitudes, if one measures the vector and tensor analyzing powers in addition to the differential cross section. Suppose one is dealing with only s- and p-wave in the initial state. The polarized differential cross section for transversal polarized deuterons is given by

$$\left(\frac{d\sigma}{d\Omega}(\theta,\varphi)\right)_{pol} = \left(\frac{d\sigma}{d\Omega}(\theta)\right)_{unpol.} \times \left[1 - \frac{1}{2}\tau_{20}T_{20} + i\sqrt{2}\tau_{10}T_{11}\cos\varphi - \sqrt{\frac{3}{2}}\tau_{20}T_{22}\cos 2\varphi\right] \quad (1)$$

with τ_{10} and τ_{20} the vector and tensor polarization of the beam. The unpolarized cross section is the sum of the amplitudes squared. A recent analysis of the scattering length from $pd \to {}^3He\eta$ yielded a very small imaginary part and uncertainty about the sign of the real part [7]. This is surprising since the original pionic inelasticity of ηN scattering is large and seems to decouple in the case of nuclei. This decoupling or very weak absorption was recently attributed to a suppression of the two main inelasticity channels [8]. These are the pion inelasticity due to the process $\eta N \to \pi N$ and the nuclear inelasticity $\eta d \to NN\pi$ with d a quasi deuteron state.

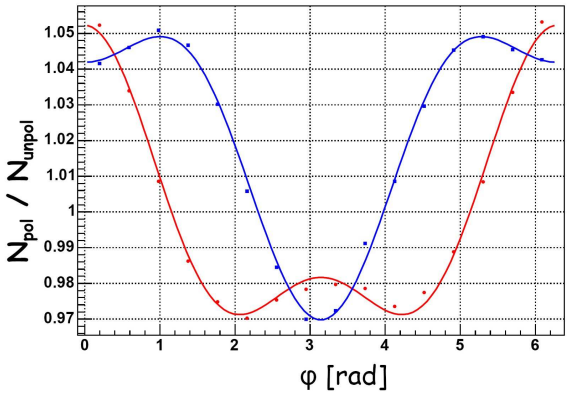

Fig. 2: Ratio of counting rates for polarized to unpolarized deuteron beam as measured with the wedge detector. The curve with the minimum at $\phi = \pi$ is for nominal $p_{zz} = -1$ the other for $p_{zz} = +1$

An experiment employing vector and tensor polarized deuteron beams was performed by GEM earlier this year. The data are presently under evaluation. In order to continuously monitor the polarization an additional detector was mounted downstream behind the target consisting of 16 wedge shaped scintillators. The result of such a measurement is shown in Fig. 2for $p_{zz} = \pm 1$. The curves are fits with the function $\sigma(\phi) = A(1 + B\cos\varphi + C\cos 2\varphi)$ to the data.

References:

[1] R. Frascaria et al.: Phys. Rev., **C 50** (1994) R537.
[2] N. Willis et al.: Phys. Lett., **B 406** (1997) 14.
[3] A. Wrońska et al.: archive, **ex** (2005) 0510056.
[4] R. Bilger et al.: Phys. Rev., **C 65** (2002) 044608.
[5] A. Khoukaz: priv. communication to H. M., (2004).
[6] M. Betigeri et al.: Phys. Lett., **B 472** (2000) 267.
[7] A. Sibirtsev, J. Haidenbauer, C. Hanhart, J. A. Niskanen: The European Physical Journal, **A 22** (2004) 495.
[8] J. Niskanen: arXiv, **nucl-th** (2005) 0508021.

Charge independence studied in $NN \to d\pi$ reactions

H. Machner and J. A. Niskanen*

The isospin invariance as introduced originally by Heisenberg is only an approximate symmetry even in the case of strong interactions. The break-down of the symmetry is due to mass differences of different charge states of hadrons, electromagnetic interactions and particle mixings, which in turn are intimately related to e.g. the difference of the *u* and *d* quarks. While the violation of charge symmetry (mirroring of neutrons and protons) has been seen at the level of a few per mille in pion production, the more general charge independence, expected to break at a higher level of a few per cent, has never been unambiguously observed there.

Charge independence requires that the ratio of the cross sections of the two reactions $pp \to d\pi^+$ and $np \to d\pi^0$ is exactly two. Optimally one would compare differential cross sections at the same final momenta for these reactions. (The final state is considered to be more relevant in this comparison because of the stronger dependence of the matrix elements on the final than initial momentum.) However, such data do not exist. Therefore, in the hope of bridging data at different energies to overlap we have resorted to fits of the total cross sections (or "reduced" cross sections where the effect of different phase spaces and Coulomb interaction has been removed) and angular dependencies as functions of the final state momentum [1]. In this we have followed the prescription

$$\frac{d\sigma(\theta)}{d\Omega} = \underbrace{\frac{1}{4(2\pi)^2\hbar^4}\frac{p_\pi^*}{p_N^*}\frac{E_N E_p E_d E_\pi}{s}}_{\equiv\ P_{Np}} \underbrace{\sum_{\mu SM} |\ \langle \psi_d^\mu \mid H^\pi \mid \phi^{SM}\rangle\ |^2}_{R_{Np}}$$

of Ref. [2] to separate the matrix elements without these obvious charge dependencies.

Lacking accurate *np* data it is not possible to perform a meaningful comparison of total cross sections. In this the uncertainty of the neutron beam normalization is paramount. However, in relative quantities, such as angular and energy dependence, it is possible to minimize this shortcoming. In particular, in the parametrization of the reduced total cross section as

$$R = \alpha_0(1+\alpha_1\eta^2)$$

the parametre α_1 gives a possibility of normalization independent comparison of the reactions. A similar parametrization can be made for the angular dependence. It should be noted that this presentation minimizes the error in the energy and angular dependence part absorbing the normalization uncertainty to the first overall parametre α_0. Unfortunately this is not often done and this uncertainty is present also in the second parametre.

Fig. 1 shows a compilation of the low energy world data together with our fits to the two reactions. Clearly the energy dependencies differ significantly. It is interesting to compare this against a prediction from a calculation without explicitly charge dependent forces [2]. This comparison is conducted in Fig. 2 for the relative change in the reduced cross sections

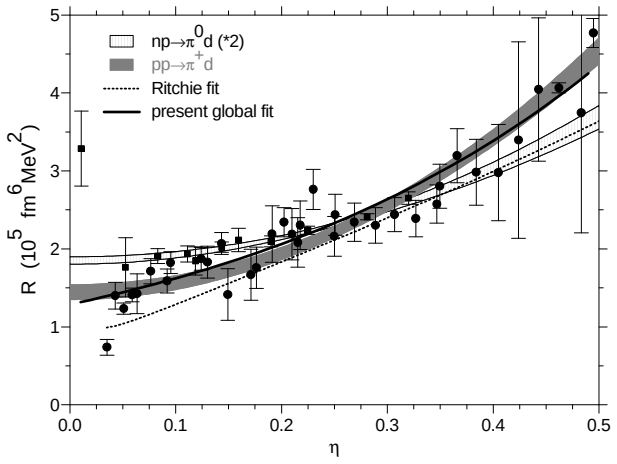

Fig. 1: Low energy data and fits for the reactions $pp \to d\pi^+$ (dots) and $np \to d\pi^0$ (squares, *np* multiplied by 2).

R using the above fits directly and also with α_0 renormalized by factors 0.9 and 1.1 to account for the normalization uncertainty. The fits based on the data and the model prediction cannot be made to agree. Also this deviation should be outside the model dependence of Ref. [2]. Possibly it can be considered as an indication for a need for charge dependent interactions to describe pion production.

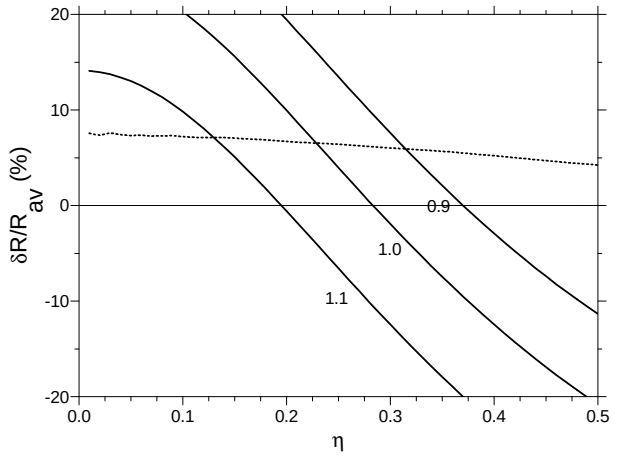

Fig. 2: Comparison of the relative change between the model results of Ref. [2] (dashed curve) and the above fit (solid curves) directly and with $\alpha_0(np)$ renormalised by factors 0.9 and 1.1.

This work was supported in part by grants from DAAD (Germany, number DB000379) and the Academy of Finland (numbers 211592 and 54038).

References:

[1] H. Machner and J. A. Niskanen, nucl-ex/0511027.
[2] J. A. Niskanen, M. Vestama, Phys. Lett., **B 374** (1997) 253.

Search for η-bound nuclei

GEM Collaboration

A large acceptance plastic scintillator detector "ENSTAR" with state-of-art fibre optics readout has been designed and built at Bhabha Atomic Research Centre (BARC) in Mumbai for studies of a new form of nuclear matter: an η-mesic nucleus($\eta \otimes A$) which is a bound system of an η-meson and a nucleus. The η-mesic nuclei, which are solely the result of strong interactions unlike the pionic atoms, are a new kind of atomic nuclei and their research has fundamental significance in studying in-medium properties of hadrons, in particular, medium modification of meson masses The experimental confirmation of the existence of such an η-bound system will lead to new possibilities of studying the interaction between a nucleus and the short lived ($t_{1/2} \approx 10^{-18}$ s) η meson. This system should be produced in a

$$p + A \rightarrow^3 He + \eta \otimes (A-2) \quad (1)$$

where all beam momentum is carried away by the ^3He and the η as well as the $A-2$ spectator nucleons at rest in the laboratory system. The beam momentum for such a situation of recoil free kinematics is also known as magic momentum. The ^3He ion will be detected by the magnetic spectrograph BIG KARL thus allowing to identify the mesic nucleus via missing mass technique. A huge background from nuclear fragmentation is expected to superimpose the small signal from the mesic nuclei. A second detector ENSTAR is foreseen to reduce this background. One expects the following chain of reactions to occur:

$$\eta + n \rightleftarrows N^*(1535) \rightleftarrows \pi^- + p \quad (2)$$

with eventually two charged particles which will be emitted back to back. These particles will be detected with ENSTAR.

ENSTAR has a cylindrical shape around the beam pipe. It consists of three segmented layers of plastic allowing modest azimuthal angle resolution and good polar angle resolution [1]. The construction of the ENSTAR detector has been completed in December 2003 and the detector was mounted in the COSY beam line in March 2004. A number of test measurements have been carried out at BARC during the construction of the detector. First, variation of signal pulse height from a scintillator tile was studied as a function of the number of fibers. The pulse height, which depends on the amount of light collected by the fibers, is observed to increase with the increase of number of fibers, and it saturates when the fibers cover $\approx 30-40\%$ of the scintillator tile surface. The number of fibers in the present detector has been optimized accordingly. Light output of different pieces of ENSTAR was also tested at BARC with α sources.

The in-beam testing of the detector in full assembled condition with its all 122 pieces was performed at COSY, Jülich in March 2004. Different nuclear reactions ($p+p$ elastic scattering, $p+p \rightarrow d+\pi^+$, $p+$ "heavy target") were used, in addition, cosmic ray data were collected. Coincidence data (a coincidence between

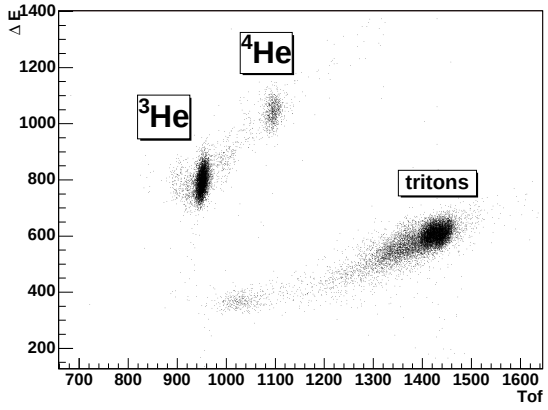

Fig. 1: Particle identification with the BIG KARL spectrograph. Shown is the energy loss in the first layer of the scintillator hodoscope in the focal plane versus the flight time (TOF) between hodoscope layers.

ENSTAR and BIG KARL spectrometer and a 2-fold coincidence between different elements in ENSTAR) were also collected. A good light output has been obtained even for cosmic muons for which energy loss in the plastic scintillator is only ≈ 1.8 MeV/cm. Pions were seen in the ENSTAR from the reaction $p+p \rightarrow d+\pi^+$. The methodology was established for obtaining relative gains between different pieces and absolute calibration.

The experiment was performed in May 2005 in order to look for the η-bound state. A 1 mm thick Aluminium foil was chosen to as target. This thickness is a compromise: it gives acceptable counting rate and does not decrease considerably the energy resolution. The beam was selected to be protons at a momentum of 1745 MeV/c which is close to the magic momentum.

Also a number of test runs were performed for purpose of ENSTAR energy calibration and BIG KARL spectrometer adjustment. This includes proton-proton elastic scattering and pion production on a CH_2 target, and also measurements of cosmic rays .

Particle identification in the BIG KARL focal plane detectors is shown in Fig. 1. A time spectrum is shown for coincident events with ENSTAR and the focal plane of the spectrograph achieved during the experiment in Fig. 2.

Data from cosmic muons have been used for the absolute energy calibration of ENSTAR scintillator pieces. Experimental data from *pp*-elastic scattering were used for the relative energy calibration. Hereby the following method was applied: The thick outer layer consists of wedge shaped scintillators. The overlap between two neighboring elements has a rectangular shape and thus constant thickness. The response of two neighboring elements as well as the coincident signal for cosmics is shown in Fig. 3.

Two different BIG KARL settings were used during

measurements. This allows us to cover wide range in missing mass spectra: 70 MeV area, while $\approx$ 10 MeV peak is suspected to appear near $\eta + ^{25}Mg$ production threshold (Fig.4). Further analysis is required in order to obtain the experimental signature of bound η. This includes: application of calibrated ENSTAR cuts and corrections of BIG KARL acceptance.

References:

[1] IKP Annaual Report 2004

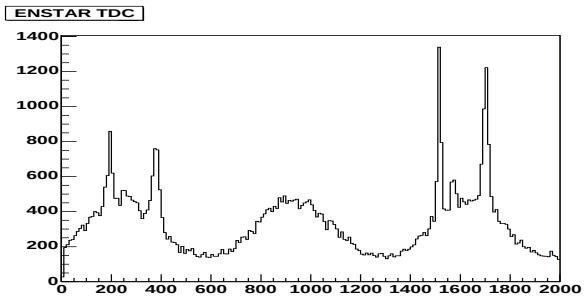

Fig. 2: Time spectrum of coincident events between ENSTAR and focal plane detectors. The maxima of the continuous distribution belong to different revolutions in the accelerator ring. The peaks correspond to different particle types with ^3He, ^4He and ^3H (from left to right). A gate on the energy loss (compare Fig. 1) reduces the ^4He events.

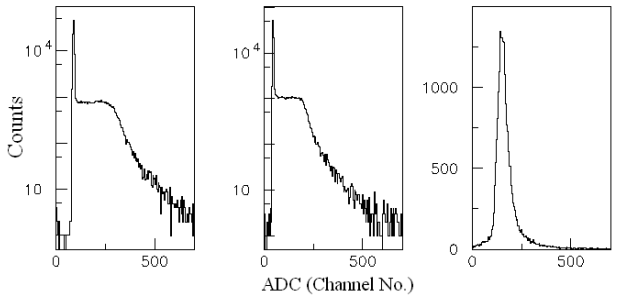

Fig. 3: Left and middle: The energy loss of cosmic rays in two neighboring elements of the thick outer layer of ENSTAR. Right: the total energy loss of the two elements when a coincidence between them is required.

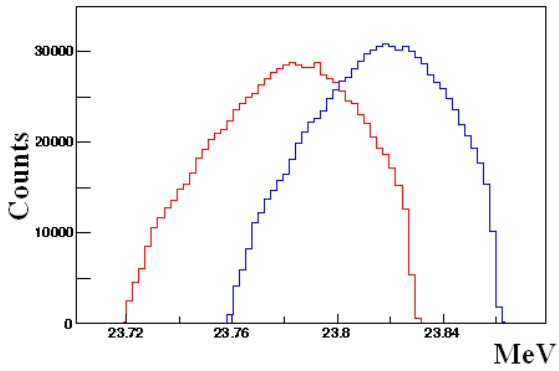

Fig. 4: Missing mass spectra for two different settings of the magnetic spectrograph BIG KARL. The shapes represent the acceptance of the spectrograph.

N*-resonances in the strangeness production in the reaction pp ® K+Lp

W. Eyrich, M. Krapp, A. Lehmann, C. Pizzolotto, P. Schönmeier, W. Schroeder, A. Teufel,
Physikalisches Institut, Universität Erlangen-Nürnberg, for the COSY-TOF-Collaboration

The main interest in the investigation of the associated strangeness production in elementary reactions close to threshold is to get insight into the dynamics of the $\bar{s}s$ production. The questions especially concern the role of N*-resonances and the hyperon-nucleon final-state interaction which is known to be of special importance close to threshold. To come to conclusive results precise observables are needed, concentrating on exclusive data, covering the full phase space.

The external experiment COSY-TOF is a wide angle, non magnetic spectrometer with an inner detector system, which is optimized for strangeness production measurements. This system with small beam holes as well as the outer detector system covers the full angular range of the reaction products and allows the complete reconstruction of the pp $\rightarrow K^+\Lambda p$ events, including a precise measurement of the delayed decay of the Λ-hyperon. The reaction pp $\rightarrow K^+\Lambda p$ has been investigated at several beam momenta between 2.5 GeV/c and 3.3 GeV/c [1,2], that means from threshold up to nearly the COSY-limit for the external beam. For reactions with more than two particles in the final state, as in the case of the reaction pp $\rightarrow K^+\Lambda p$, Dalitz plots are a powerful tool to extract information about the reaction mechanism. Where-as pure phase-space leads to a homogeneous strength distribution, in particular resonances should lead to significant deviations from this. Fig. 1 (left side) shows the Dalitz plots extracted from the experiment at the beam momenta of 2.85, 2.95, 3.20 GeV/c and 3.30 GeV/c, respectively. They obviously show strong deviations from phase space.

Using a parametrization of A. Sibirtsev [3], which includes the N*(1650, 1710, 1720)-resonances, a non-resonant term and the pΛ-final state interaction on the amplitude base, the strengths of the various contributions were adjusted individually to achieve a best fit for the various Dalitz plots. The results are shown on the right side of Fig. 1. The data are well described by the model fits. The obtained reduced χ^2-values are between 1.4 and 2.0. The most interesting result is that the strength of the contribution of the N*(1650) resonance compared to the sum of the contributions of the N*(1710) and N*(1720) changes dramatically with the beam momentum. The given bands correspond to a 3σ-error interval of the extracted strengths of the resonances. The amplitude of the non-resonant contribution is smaller by a factor of about ten compared to the sum of the three contributing resonances. The influence of the pΛ-final state interaction is significant even for the highest momentum; the corresponding amplitude is within errors independent of the beam momentum. From these results it has to be concluded that there must be a dominant exchange of non-strange mesons. Only they are able to contribute to the observed leading mechanism via N*-resonances.

Data corresponding to much larger data samples, which are under investigation, will allow to study the resonance parameters in detail and to search for unknown resonances. In this context the use of a polarized beam and the inclusion of other reaction channels, which have already been started, will be of special importance.

We are very optimistic, that COSY-TOF will strongly contribute in gaining more insight into the N*-resonances and their parameters in the mass range up to about 1.9 GeV/c^2.

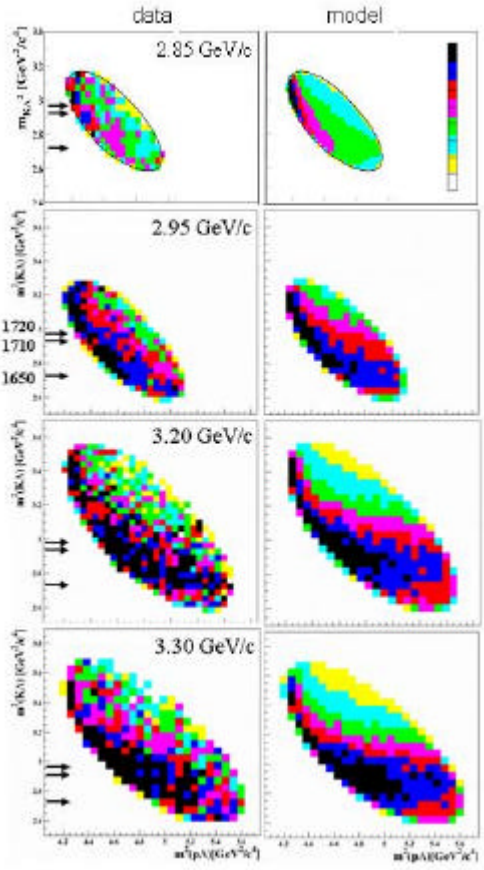

Fig. 1: Dalitz plots of the reaction pp $\rightarrow K^+\Lambda p$; data (left side) compared to model-fits (right side).

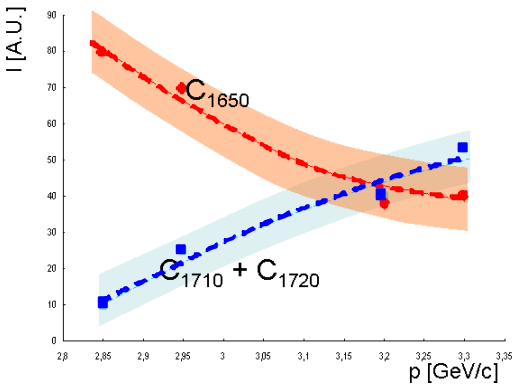

Fig. 2: Contribution of N*(1650) compared to the sum of N*(1710)+N*(1720) as a function of the beam momentum

References:

[1] COSY-TOF coll., Phys. Lett. B 420 (1998) 217
[2] COSY-TOF coll., Phys. Lett. B 632 (2006) 27
[3] A. Sibirtsev, private communication, 2002, 2005

Dynamics of ω Meson Production in Proton Proton Reactions[α]

M. Schulte-Wissermann[β], K.-Th. Brinkmann[β], J. Dietrich[β], S. Dshemuchadse[β], H. Freiesleben[β], R. Jäkel, L. Karsch[β], E. Kuhlmann[β], S. Reimann[β], W. Ullrich[β], R. Wenzel[β] for the COSY-TOF collaboration

The TOF detector is located at an external beam line and stands out for versatility and high acceptance (approx. 2π in the laboratory frame). Instead of direct particle identification, the detector rather aims at measuring the velocity-vectors of all charged particles in order to completely reconstruct event patterns. This strategy allows TOF to access multiple hadronic channels, starting from threshold up to excess energies as high as 1GeV.

One of the experimental programs at TOF is dedicated to the ω meson production in proton-proton collisions ($pp \to pp\omega$). For this reaction a considerable interest on the part of theory arose during the last years (e.g. [1][2]), where the focus is on the following aspects: (1) Do $p\omega$ resonances exist? (2) The general reaction mechanism of (neutral) vector meson production is of fundamental interest. (3) The strangeness content of the nucleon is still an open question.

All these questions can be addressed in the study of total and differential distributions of, not only the ω meson, but all neutral vector mesons in SU(3), i.e. ρ, ω, ϕ. COSY is currently the only facility in the world which can contribute data for vector meson production, and the TOF detector is very well suited to examine ω-meson production.

The current data base on neutral vector meson production in pp-reactions is rather scarce. The DISTO collaboration has published a set of differential observables at $\varepsilon = 83\,MeV$ ($pp \to pp\phi$) and $\varepsilon = 320\,MeV$ ($pp \to pp\omega$) [3]. TOF extended

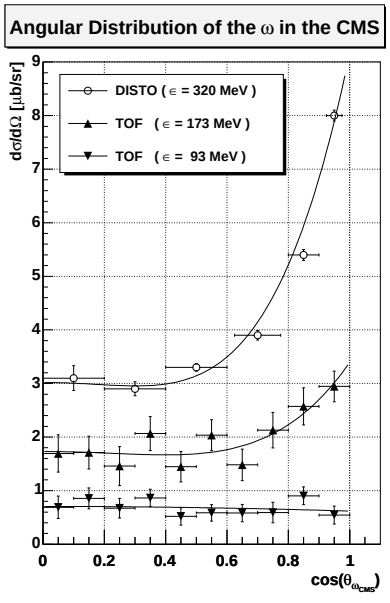

Fig. 1: Energy dependence of the angle of the ω-meson in the overall CMS with respect to the beam-axis.

the experimental data base for ω production with total cross sections and angular distributions for two excess energies ($93\,MeV$ and $173\,MeV$)[4][5]. From this, it is possible to observe, for example, the development of the angular distribution with energy. This is shown in Fig. 1. It is important to point out that the energy dependence of differential observables is the key to an understanding of the reaction dynamics.

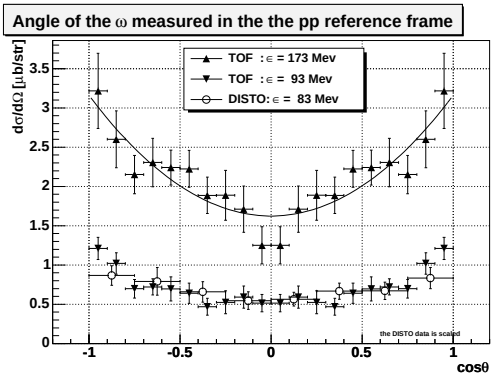

Fig. 2: The TOF data shows the angle of the ω-meson measured in the pp-reference frame. The DISTO data refers to the same observable, however for the reaction $pp \to pp\phi$ (scaled by a factor 50).

Due to many small (but in total significant) software improvements during the analysis of the Θ^+ beamtime of October 2004, many formerly not accessible differential observables are now within reach (including: angle of the protons with respect to the beam axis, angle between the protons and the ω, invariant mass distributions of the $p\omega$- and the pp-system, angle of the ω-meson measured in the pp-reference frame). This new data now provides a much broader data base to test, tune, and improve the different theoretical approaches on vector meson production. One of the new results is shown in Fig. 2 together with data from [3]. The angular distribution of the ω in the pp-reference frame shows only a small deviation from pure phase-space for the smaller excess energy, while at $\varepsilon = 173\,MeV$ the ω-distribution shows a strong anisotropy. Theory is now challenged to not only reproduce this experimental fact, but in addition, to simultaneously describe the distribution of the φ-meson as well. In Fig. 2, the φ-meson distributions shows a similar behavior ($\varepsilon = 83\,MeV$). However, this might not be true for other angular distributions.

Currently, the reaction $pp \to pp\omega$ is analyzed using the data of all previous beamtimes. This will yield total and differential observables for five different excess energies, ranging from below the ω-threshold (background studies) up to $\varepsilon \approx 200\,MeV$. In addition, one of the beamtimes was performed with a polarized beam [6] which will give access to polarization observables, for which so far no data exists.

References:

[1] K. Tsushima and N. Nakayama, Phys.Rev.C **68**, 034612 (2003)
[2] A. Faessler et al., Phys. Rev. C **70**, 035211 (2004)
[3] The DISTO collaboration, Phys. Rev. C **63** 024004 (2001)
[4] The COSY-TOF collaboration, Phys. Lett. B **522** 16 (2001)
[5] M. Schulte-Wissermann, Dissertation, TU Dresden, http://nbn-resolving.de/urn:nbn:de:swb:14-1098884274765-15485
[6] W. Ullrich, Annual Report 2005

[α] Supported by FZ Jülich and BMBF

[β] Institut für Kern- und Teilchenphysik,TU Dresden, 01069 Dresden, Germany

Determination of the beam polarization with the external COSY-TOF detector[α]

W. Ullrich[β], K.-Th. Brinkmann[β], J. Dietrich[β], S. Dshemuchadse[β], H. Freiesleben[β], R. Jäkel[β] , L. Karsch[β], E. Kuhlmann[β], S. Reimann[β], M. Schulte-Wissermann[β] , R. Wenzel[β] for the COSY-TOF collaboration

For experiments with polarized beams a precise knowledge of the polarization is important. At COSY the polarization is measured utilizing the EDDA detector. However this procedure has two drawbacks: 1) EDDA can only determine the internal polarization and 2) the low luminosity due to the very thin target and the rapidly decreasing cross section of proton proton elastic scattering with increasing beam momenta leads to relatively long beam-tuning cycles.
The TOF detector is an external experiment and very well suited for polarization measurements as it covers the full azimuthal angular range (ϕ) and polar angles θ up to 60°. This has already been shown in [1] where the *online*-determination of the asymmetry was described (beam time April 2004, proton beam, $p_{beam} = 3065\frac{MeV}{c}$, liquid hydrogen target). The orientation of the proton beam polarization was flipped in this beam time after each operation cycle of COSY and each cycle took about 120s.
In the offline analysis the data from the elastic scattering were used to determine the asymmetry, which was measured for different θ intervals and for each interval in 24 ϕ bins. For each bin the asymmetry can be expressed as:

$$a = \frac{\frac{N_\uparrow}{\Sigma N_\uparrow} - \frac{N_\downarrow}{\Sigma N_\downarrow}}{\frac{N_\uparrow}{\Sigma N_\uparrow} + \frac{N_\downarrow}{\Sigma N_\downarrow}}$$

were $N_\uparrow$ and $N_\downarrow$ are the count rates in the given (θ, ϕ) interval for spin up and spin down. $\Sigma N_\uparrow$ and $\Sigma N_\downarrow$ are the total count rates summed over all ϕ bins. The asymmetry in ϕ can be fitted with a cosine function as shown in figure 1. In order to

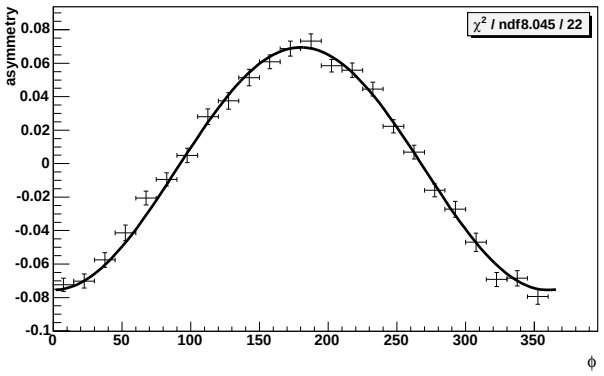

Fig. 1: *Asymmetry versus ϕ for $42° < \theta_{CMS} < 46°$.*

determine the polarization from the measured asymmetry, the data were compared with the analyzing power measured by EDDA [2] as shown in figure 2. The scaling factor between EDDA and TOF is the polarization which, on average, is $P = 0.330 \pm 0.012$. The uncertainty is mainly due to the statistical uncertainty of the EDDA data. A polarization of $P \approx 0.30$ is quite satisfactory in view of the high momentum of the extracted beam. Within uncertainty limits the TOF data agree perfectly with the EDDA result.
For figure 2, a large dataset of ~7,500,000 elastically scattered events is used which was collected during six days,

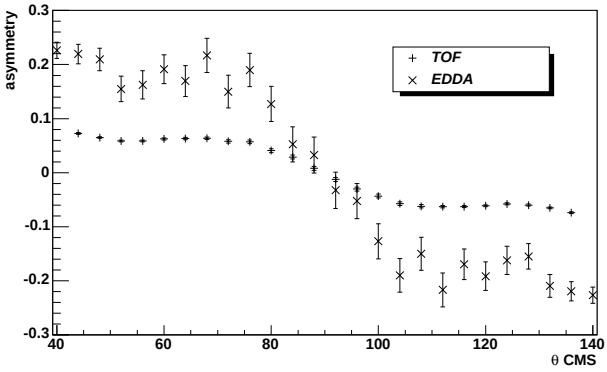

Fig. 2: *Asymmetry from TOF and analyzing power from EDDA versus θ_{CMS}.*

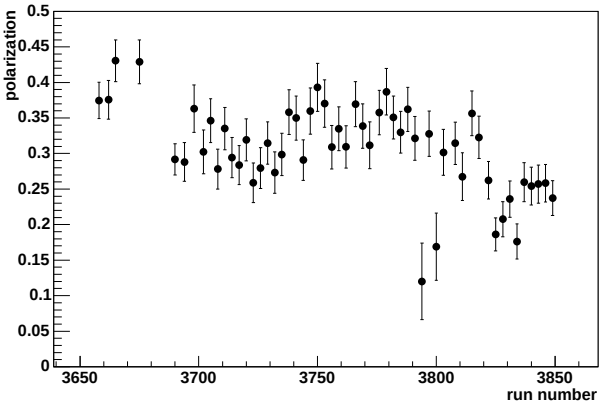

Fig. 3: *Polarization versus run number, the data was taken during six days.*

however it is possible to monitor the polarization in much shorter time slices. This is shown in figure 3 where for the same data the polarization is plotted against the run number. During beam tuning, the trigger is set for elastic scattering and the polarization can be determined already after 30 min, using the online analysis of the Dresden Online Monitor [3]. Thus, an extracted polarized beam can be prepared within a rather short period.

References:

[1] M. Schulte-Wissermann, annual report 2004
[2] M. Altmeier et al. (EDDA) Eur. Phys. J. A23, 351-364 (2005)
[3] M. Schulte-Wissermann, Dissertation, Dresden 2004
http://nbn-resolving.de/urn:nbn:de:swb:14-1098884274765-15485

[α] Supported by FZ Jülich and BMBF
[β] Institut für Kern- und Teilchenphysik,TU Dresden, 01069 Dresden, Germany

A Frozen-Spin Polarized Target for COSY-TOF

H. Dutz[1], J. Heckmann[2], Ch. Hess[2], F. Klein[1], R. Krause[3], W. Meyer[2],
A. Raccanelli[1], E. Radtke[2], G. Reichertz[2]

The scattering experiments for which a high beam intensity and collimation are required demand challenging performance of a frozen-spin polarized target. The requirements are not only in terms of radiation resistance but also and especially on the thermal transport properties, as localized beam heating causes inhomogeneous depolarization of the target.

For the experiment under preparation at COSY to measure the parity of the pentaquark $\Theta^+(1540)$, the required luminosity and accuracy in the vertex reconstruction correspond to a beam intensity of 10^7 protons/s at a beam spot of about 1 mm^2. Under these conditions, ammonia and lithium compounds are the only materials that offer suitable radiation resistance [1].

The efficiency of the thermal transport in the target material for dissipating the heat deposited by the beam toward the cryogenic bath is strongly limited by the Kapitza resistance. The amplitude of this thermal discontinuity on the boundary, due to an acoustic mismatch between the speed of sound in liquid helium and in solid materials, is proportional to the inverse of the third power of the temperature and proportional to the surface area. Therefore, at the very low temperature required by the frozen-spin operation mode, the only way to reduce the Kapitza resistance is to maximize the surface area of target, e.g. by preparing it as a series of thin slices of material. In this case, lithium compounds appear to be the most suitable choice due to their easier handling and preparation, since ammonia is in the gaseous state at room temperature.

Since the relaxation time quickly decreases with increasing temperature, the choice of size and shape of the target, and in particular of its thickness, must be based on the evaluation of the temperature profile inside the target for the specific experimental conditions. Unfortunately, the thermal conductivity of irradiated lithium compounds at very low temperature is not known. Furthermore, if one uses the known thermal conductivity of butanol and the approximations generally adopted [2] to evaluate the temperature profile, the estimated temperature at the centre of the target turns out to be too high (fig. 1) and shows that the experiment is apparently unfeasible [3].

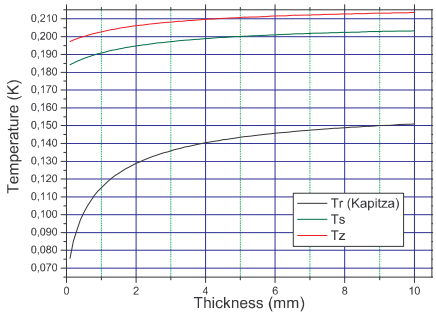

Fig. 1: Temperature dependence of the target outer surface (black), of the beam surface in the target (green), and of the center of the target (red) as function of the target thickness. The estimate is done for a cylindrical target of 6mm diameter, at an operating temperature of 55 mK.

Driven by the need for a more realistic way to estimate the temperature profile inside the target, the Polarized Target Group in Bonn and the Institute for Numerical Simulation are completing a new finite element model to study the thermal transport properties as a function of size and shape of the target and of the thermal conductivity parameters. The implementation of the model is based on the UG package [4] and includes the Kapitza resistance as a boundary condition (fig. 2).

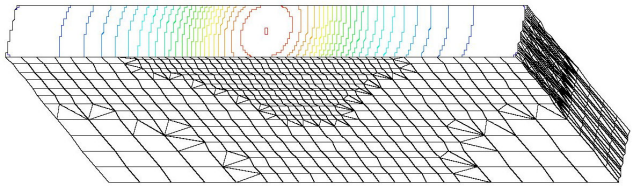

Fig. 2: Simulation of the temperature profile in the target on a section along a plane containing the beam axis.

According to the results provided by this new model, the required constraints on the temperature can be matched for thicknesses less than 500 μm, even with the reduced thermal conductivity adopted for the calculation.

The Polarized Target Group in Bochum, in cooperation with the Bochum Institute for Mineralogy, has polished a sample of ^{6}LiD to a thickness of 200 μm and a commercial sample of LiH to a thickness of 500 μm (fig. 3).

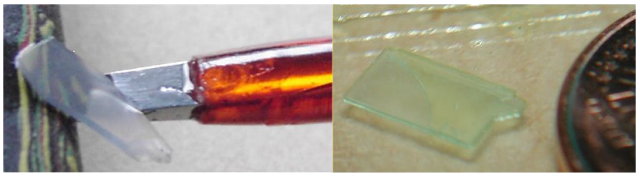

Fig. 3: A sample of ^{6}LiD polished to a thickness of 200 μm (right) and one of LiH polished to a thickness of 500 μm (left).

The result obtained with the 200 μm thick ^{6}LiD could hardly be repeated and a series production cannot be guaranteed. However, it is possible that the thickness of ^{7}LiH could be reduced below 500 μm when using new samples of material, carefully protected from atmospheric contamination.

References:

[1] H. Dutz et al., IKP Ann. Rep. (2004)
[2] M. Plückthun, PhD-thesis, Bonn (1998).
[3] A. Raccanelli et al., to be published in Proc. of PST05.
[4] P. Bastian et al., Comput. visual. sci. (1997).

[1] Physikalisches Institut, Universität Bonn.
[2] Institut für Experimentalphysik I, Ruhr-Universität Bochum.
[3] Institut für Numerische Simulation, Universität Bonn.

Stopping time criteria for cascade model calculations on proton induced reactions

PISA collaboration

It is planned to use the Boltzmann-Uehling-Uhlenbeck (BUU) [1], [2] or Hadron String Dynamics (HSD) [3] transport model combined with statistical model [4] in order to describe the light charged particles and intermediate mass fragment spectra, measured by the PISA collaboration [5]. The first, fast stage of proton-nucleus reaction, which proceeds as cascade of nucleon-nucleon collisions is described by BUU or HSD models, whereas the second stage of the reaction is treated as statistical evaporation of nucleons or composite fragments. The outcome of the transport model calculations serves as an input for the statistical model studies. Thus it is important to know, whether the information obtained from the transport models is sensitive to the time duration of the first stage of reaction which is a parameter of the theoretical analysis. Variation of three physical quantities: excitation energy per nucleon, angular momentum of the excited, residual nucleus, and mass number of this nucleus with the duration time of the first stage of reaction have been used as a test for this purpose. Dependence of the average excitation energy of the nucleus evaluated according to prescription of the ref. [6] is shown in Fig. 1.

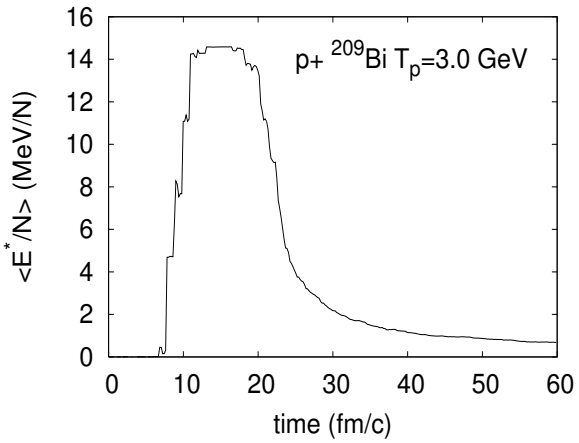

Fig. 1: Evolution of the average excitation energy per nucleon of the hot residual nucleus in $p + Bi$ collision at 3 GeV proton beam energy.

It is evident from the figure that E* drops very quickly in the range 20-30 fm/c of the duration time of the first stage of the reaction, whereas it is varying only a little at larger times. It seems that e.g. for targets as heavy as Bi, the first stage calculations should be terminated at time 35-40 fm/c, when the average excitation energy per nucleon starts to stabilize.

Very similar behavior is observed for the average angular momentum of the hot nucleus during first stage of the reaction. At around 18 fm/c and later the angular momentum lowers significantly due to nucleons escaping from the nucleus. This leakage of angular momentum stops at around 30 fm/c and angular momentum value stabilizes. At later time spurious slow increase of angular momentum is observed which is unphysical and results from building-up inaccuracies of numerical calculations.

From inspection of the Fig. 3, where the mass number evolution is presented, one can state that the mass of the residual nucleus decreases monotonically with duration time of the

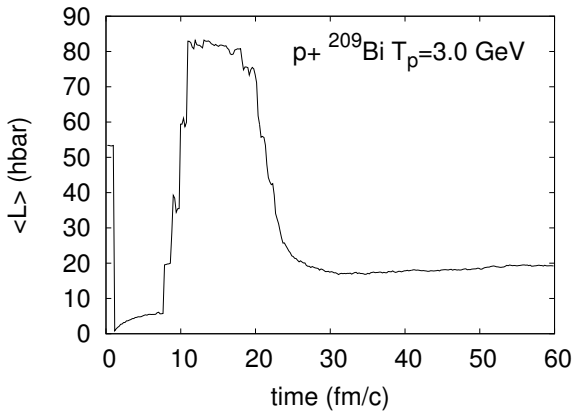

Fig. 2: Evolution of the average angular momentum of the hot residual nucleus in $p + Bi$ collision at 3 GeV proton beam energy.

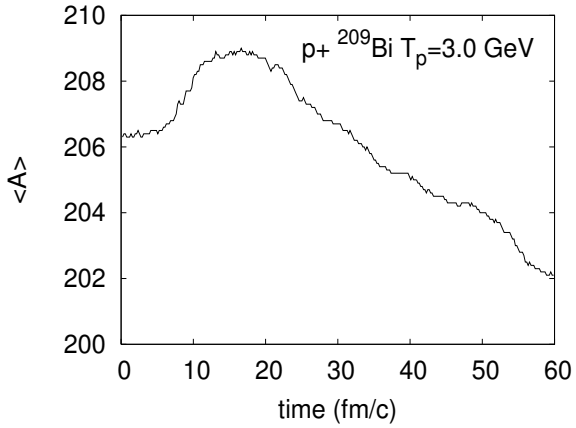

Fig. 3: Evolution of the average mass number of the hot residual nucleus, in $p + Bi$ collision at 3 GeV.

first stage of reaction starting from the time about 15 fm/c. Therefore duration time of the cascade of the nucleon-nucleon collisions cannot be determined on the basis of behavior of the average mass number of the nucleus. The mass number does not stabilize at larger times, as it was the case for the excitation energy. Thus we conclude that the behavior of excitation energy and angular momentum as a function of time suits better for determination of the duration time of the first stage of proton-nucleus collisions. The full simulation including also the final deexcitation of the nucleus by statistical evaporation will be studied in order to provide sensitivity of observables (like e.g. multiplicities, double differential cross sections,...) on the fast stage stopping time.

References:

[1] K. Niita et al. , Nucl. Phys. A 504(1989)391
[2] G. F. Bertsch and S. Das Gupta, Phys. Rep. 160(1988)189
[3] J. Geiss et al. Nucl. Phys. A 644(1998)107
[4] K. Langanke, J.A. Maruhn, S.E. Koonin, *Computational Nuclear Physics 2, Nuclear Reactions* (Springer Verlag, New York, 1993)
[5] R.Barna et al., Nucl. Instr. and Meth. A 519(2004)610
[6] Z.Rudy et al., Eur.Phys.J.A 18(2003)537

Absolute normalization of particle production cross-sections measured in PISA experiment

PISA Collaboration

The PISA experiment [1] is devoted for the determination of the proton induced spallation cross-sections. Since the experiment is performed at the internal beam of COSY, it was decided that the integrated beam-target luminosity will be measured by means of a reference reaction of well known cross-section. For the experimental geometry of PISA and the types and thicknesses of solid targets used in the measurements, the most feasible method seemed to be the measurement of the yield of δ-electrons knocked out from the target in the $p-e$ quasi-free scattering. Using cooled silicon detector telescopes for each experimental run simultaneously with the spallation products the respective δ-electron yield has been recorded.

The cross-section for this kind of $p-e$ interaction for a specified kinematics is given by an analytical formula. However, in order to avoid possible confusion created by complicated dependence of the electron detection efficiency on their kinetic energy and influence of the target thickness on the δ-electron energy spectra, it was decided that additional reference measurements of $p-p$ elastic cross sections have been performed for each proton-beam energy used in the experiment, in order to unambiguously calibrate the δ-electron yield. Advantage was taken of the knowledge of double-differential cross-sections for elastic $p-p$ scattering precisely measured by EDDA experiment [2] in broad ranges of energies and for the whole kinematic range of detection angles. The reference reaction - $p-p$ scattering - was measured with the use of a polyethylene (CH_4) target for each experimental energy by means of the two plastic-scintillator telescopes - one at a fixed detection angle of 35° (LAB) and second one - positioned according to the requirements of the reaction kinematics. In order to evaluate the contribution from the $p-C$ scattering in the polyethylene target, additionally, under exactly the same kinematical conditions, the $p-C$ scattering was measured with the use of the pure carbon target. The solid angles of the proton detectors were adjusted in the manner allowing the counting of the elastically scattered protons without recording their energy spectrum. During all reference measurements also the δ-electrons were registered. A typical δ-electron spectrum obtained with the use of the polyethylene target is shown in fig. 1. The proposed procedure of calibration is time consuming because it requires multiple exchanging of targets, beam energies and detection angles for protons. It has, however, a great advantage since it avoids the need for a direct measurement of the target thickness – a non-trivial problem. As it is shown in the report [3] the combination of quantities measured during the calibration of reference reaction allows to cancel the targets thicknesses in the final formula for the experimental beam-target luminosity. In effect the absolutely normalized double-differential cross-section has been obtained for various target-energy combinations and different detection angles. As an example, in fig. 2, the energy distribution is shown for the ^{7}Li isotope from the $p-Au$ reaction at 2.5 GeV energy and at the laboratory detection angle of 35°. Result of PISA experiment is compared with the spectrum obtained by NESSI experiment [4] at similar experimental conditions but at external COSY beam where the beam luminosity was measured directly by counting incoming protons by means of scintillation detector. The good agreement of both distributions permits the confidence about the cross-section normalization applied in PISA experiment.

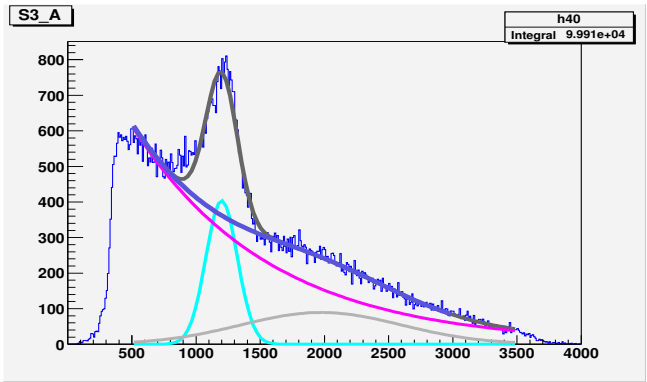

Fig. 1: Typical energy spectrum of δ-electrons from the quasi-free $p-e$ scattering in the polyethylene target at beam energy of 2.5 GeV. Horizontal axis represents the energy, whereas the vertical one - the yield. (The former one is scaled with the arbitrary units). The well visible electron peak(dark grey) is superimposed on the detection background(blue). The electron peak is fitted with the Gaussian curve(light blue) and the background is fitted with a combination of an exponent(magenta) and Gaussian(grey), and subtracted from the spectra allowing the determination of the net value of the δ-electron number.

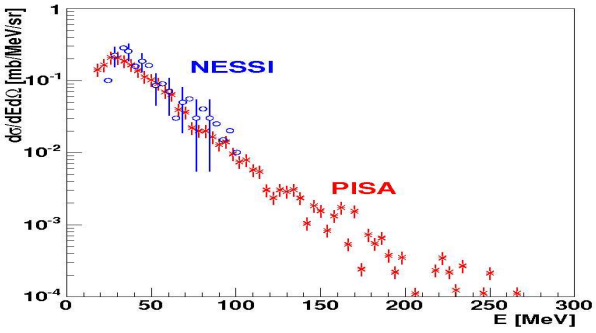

Fig. 2: Comparison of the double differential cross-section for the spallation reaction Au(p,^{7}Li)X at 2.5 GeV measured at laboratory detection angle of 35° in the internal beam experiment PISA (stars) with the results of the similar measurement performed at the external COSY beam in the NESSI experiment (open circles).

References:

[1] R. Barna et al, Nucl. Instr. Meth. **A519**(2004)610
[2] D. Albers et al., Phys. Rev. Lett. **78**(1997)1652, www.iskp.uni-bonn.de/gruppen/edda/publ/prl78data.html
[3] A. Magiera, PISA Collaboration internal note, http://www.fz-juelich.de/ikp/pisa/docu/luminosity_monitor.ps
[4] A. Letourneau et al., Nucl. Phys. **A712**(2002)133

Application of phoswich detectors for measurement of high energy spectra of light charged particles

PISA collaboration

The project PISA (Proton Induced Spallation) is devoted to measurements of double differential cross section $\frac{d\sigma}{d\Omega dE}$ for light charged particles and intermediate mass fragments in proton induced reactions. The detection system consisting of semiconductor telescopes is able to identify H, He, Li, Be, B, C, N reaction products and provides the energy spectra in the energy range of 2 MeV/nucleon - 25 MeV/nucleon (lower for d,t). Faster products do not stop in silicon telescopes employed here and therefore extraction of information on high energy spectra is hindered. Scintillator telescopes in the form of phoswich detectors were applied to detect high energy light particles (H and He isotopes). It was possible to calibrate energy of the particles combining information of the energy loss ΔE in the silicon detectors placed

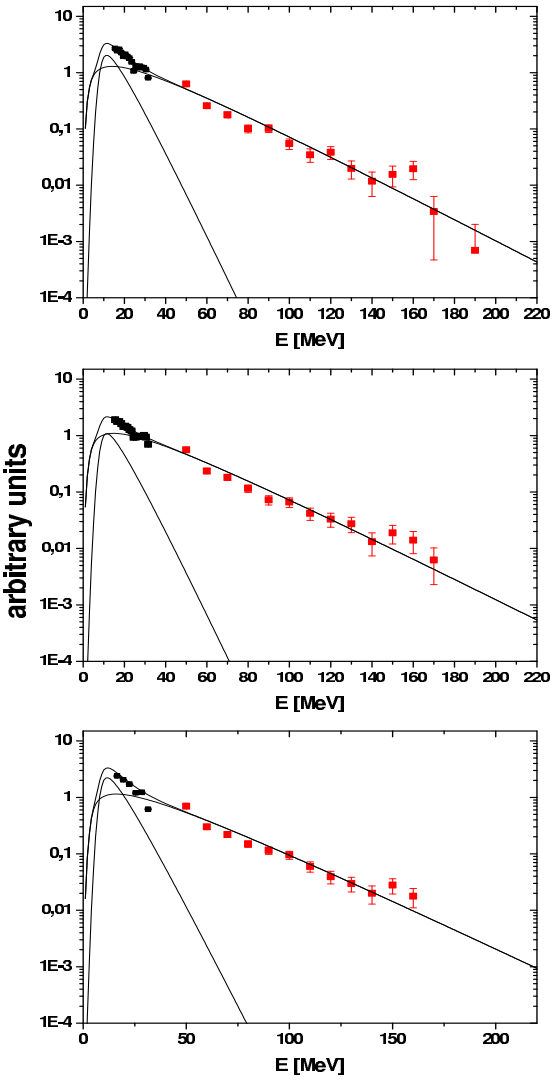

Fig. 1: Double differential cross section for Au(p,t)X reaction at 100 deg, for beam energies 1.2 (top), 1.9 (middle), 2.5 GeV (bottom). Curves present fits of the model of two moving sources [1]

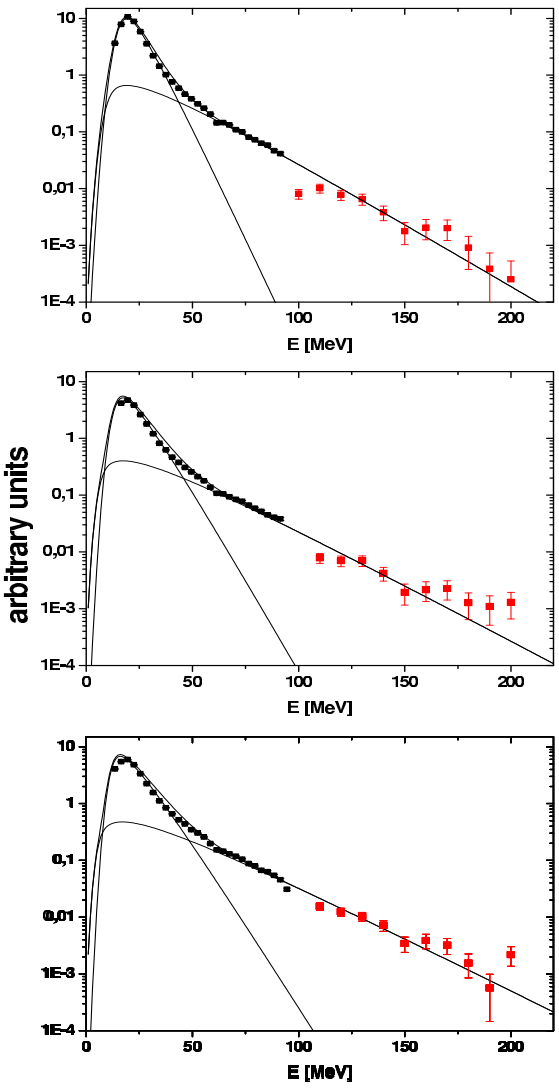

Fig. 2: Double differential cross section for Au(p,^{4}He)X reaction at 100 deg, for beam energies 1.2 (top), 1.9 (middle), 2.5 GeV (bottom). Curves present fits of the model of two moving sources [1]

in the front of phoswiches and total energy deposited in the phoswich detectors. The obtained spectra for tritons measured in proton induced reactions on Au target at three energies (1.2, 1.9, and 2.5 GeV) are shown in fig. 1 and spectra of α-particles from the same reactions are presented in fig. 2. Black symbols represent experimental cross sections obtained with use of silicon detectors whereas the red symbols show new data obtained by phoswich detectors. Lines indicate predictions of phenomenological model of two moving sources [1] emitting isotropically the particles. As can be seen in the figures, the application of phoswich detectors enabled us to extend significantly the range of energies of light charged particles.

References:

[1] G.D.Westfall, R.G.Sextro, A.M.Poskanzer, A.M. Zebelman, G.W.Butler, E.K.Hyde, Phys. Rev. C17 (1978) 1368

INC and BUU Model predictions on pion production in proton induced reactions

PISA collaboration

It is known that creation of pions is very important process in proton induced reactions on atomic nuclei due to the fact that they carry away a large part of the four-momentum deposited in the nucleus, during the first stage of the reaction. This is because the mass of pions ($\sim$ 140 MeV/c^2) is small enough to allow for copious production of pions in nucleon-nucleon collisions even at low beam energies, and large enough to contribute significantly to the energy and momentum transfer.
Studies of the pion production in proton-nucleus reactions have been performed with two theoretical models: **(i)** the Intranuclear Cascade model (INCL4.2) [1] which assumes static (time independent) mean field, and **(ii)** more sophisticated model comprising dynamically changing field, i.e. the Boltzmann-Uehling-Uhlenbeck (BUU) [2, 3] or Hadron String Dynamics (HSD) [4] transport model. All the models deal with the first, fast stage of proton-nucleus reaction, which proceeds as cascade of nucleon-nucleon collisions. Calculations of the first stage of the reaction are sufficient in order to receive realistic pion spectra, since all pions are produced only in this stage of reaction where the available amount of four-momentum is large enough. During the subsequent deexcitation of the hot matter via evaporation, no pion-production is expected.

An exemplary balance of the BUU model calculations, for the $p+Au$ collision at 2.5 GeV proton beam energy is presented below in order to show how significant the amount of momentum carried off by pions in nucleon-nucleus collisions is: The total initial momentum deposited in nucleus by incoming proton is equal to 3.31 GeV/c. At the end of the first stage of the reaction (here: after 40 fm/c), the total momentum of the excited nucleus is equal to 0.37 GeV/c. The rest of the initial momentum is carried away by nucleons and pions. Nucleons accumulate 2.54 GeV/c and pions 0.40 GeV/c. The multiplicity of nucleons is equal to 4.08 and the average momentum of one nucleon is equal to 0.62 GeV/c whereas the pion multiplicity, summed over all pion charges, is equal to 1.48, and the average momentum of one pion is equal to 0.27 GeV/c.

It should be emphasized that in spite of the fact that the momentum carried away by pions is several times smaller than the appropriate momentum of nucleons, the contribution of pions to the momentum and energy transfer may be comparable to that of nucleons because pions can be absorbed and emitted several times during the reaction. Therefore, the proper treatment of pion production and absorbtion may be crucial for realistic estimation of the residual nucleus excitation energy and other nuclear properties after fast cascade of nucleon-nucleon collisions.

One of the important features of the transport models which can influence the magnitude of pion production and absorption is the treatment of the nucleon-nucleus mean field. To check whether the assumptions concerning the mean field in transport calculations affect significantly the model results concerning multiplicity of produced pions the calculations have been done with two, mentioned above models. The results of the calculations for $p+Ni$ and $p+Au$ reactions are presented in the table 1 and 2, respectively.

Table 1: Multiplicity of pions produced in $p+^{58}Ni$ reactions at 2.5 GeV proton beam energy following INCL4.2 and BUU (HSD) model calculations

	INCL4.2 model	BUU (HSD) model
π^+:	0.35	0.51
π^0:	0.34	0.46
π^-:	0.18	0.38

Table 2: Multiplicity of pions produced in $p+^{197}Au$ reactions at 2.5 GeV proton beam energy following INCL4.2 and BUU (HSD) model calculations

	INCL4.2 model	BUU (HSD) model
π^+:	0.29	0.49
π^0:	0.35	0.53
π^-:	0.25	0.46

It is seen that *the relative behavior of the pion multiplicities obtained from the different models is similar: for lighter target (Ni) the* $\pi^+ : \pi^0 : \pi^-$ *ratio is equal to 1:0.97:0.51 for INCL4.2 and 1:0.90:0.75 for BUU (HSD), and for the heavy target (Au) 1:1.21:0.86 (INCL4.2) and 1:1.08:0.94 (BUU). However,* absolute values of pion multiplicities obtained from the BUU (HSD) model are always higher by a factor of $\sim$1.5 than the values received with the INCL4.2 model.

Since, the properties of hot, residual nuclei after the first stage of the reaction may be affected by the difference in pion multiplicities, the experimental verification of model predictions is very desirable. Unfortunately the appropriate data on pion production in proton-nucleus collisions for proton beam energies in the range of GeV are not available. In addition to light charged particles and intermediate mass fragments measured by the PISA collaboration [5] for a broad range of target nuclei and beam energies, the experimental investigation of pions would increase the comprehension of the complete reaction mechanism and put further strong constraints to any model calculations.

References:

[1] J. Cugnon et al., Nucl. Phys. A, 620(1997)475
[2] K. Niita, W. Cassing and U. Mosel, Nucl. Phys. A 504(1989)391
[3] G. F. Bertsch and S. Das Gupta, Phys. Rep. 160(1988)189
[4] J. Geiss, W. Cassing, C. Greiner, Nucl. Phys. A 644(1998)107
[5] R.Barna et al., Nucl. Instr. and Meth. A 519(2004)610

Timescale of fission in GeV proton induced reactions on Au, Bi, and U

NESSI collaboration

The fission probability P_f of highly excited targetlike nuclei produced in reactions of 2.5 GeV protons on Au, Bi, and U was studied as a function of excitation energy E^*, whereby E^* is deduced eventwise from the multiplicity of evaporated light particles[1]. The overall time elapsed from the equilibrium deformation up to the scission (10^{-20}s) is known to be quite long compared to other processes like the emission of neutrons [2]. Although the entire fission process is slow, the decision to fission can be fast. For the three targets the dependance of the inelastic cross section $\sigma_{\rm inel}$, and the fission cross section, $\sigma_{\rm f}$, as a function of E^* [3, 4] is studied. Their ratio, the fission probability $P_f(E^*) = \sigma_{\rm f}(E^*)/\sigma_{\rm inel}(E^*)$, provides the best possible evidence for the presence of dissipative or transient effects in fission and is shown in Fig. 1. Fission fragments have been seperated from heavy residues and intermediate mass fragments by constraints as discussed in more detail in ref. [1]. The total fission cross sections deduced amount to $\sigma_{\rm f} = 200 \pm 60, 320 \pm 50$, and 1350 ± 120 mb for Au, Bi and U, respectively, in agreement with ref. [5]. Despite the large differences in fissility and fission barriers $B_f \approx 5$, 12 and 21 MeV of the initial nuclei U, Bi and Au, respectively, at the highest E^* of 1000 MeV, P_f amounts to 30% for all 3 target nuclei. INC+statistical-model calculations satisfactorily reproduce the observed evolution of P_f with E^*provided that no extra transient delay is introduced. A dynamical fission hindrance or transient time which suppresses fission at higher E^* or reduces $\sigma_{\rm f}$, might be compensated for by a larger value of the level density at saddle. As for example the chain dotted line for Au target nuclei in Fig. 1 shows that for $\tau_d = 2 \times 10^{-21}$s and $a_f/a_n = 1.05$ the calculation fails to describe the actual Au fission data. Our method—the differential observation of $dP_f(E^*)/dE^*$—allows an *independent* determination of a_f/a_n and τ_d. Concluding, fission is decided upon very fast and early in the long deexcitation chain towards scission, i.e. at high excitations. Consequently the large amount of remaining excitation must be carried off, either during the descent from saddle to scission or after scission. Indeed according to the calculation at $E^* = 800$ MeV, only between 11%(Au) and 23%(U) of all light particles are emitted before reaching the saddle, or, expressed in terms of pre- and post-saddle multiplicities, $M^{LCP}_{\rm presaddle} = 1.9, 1.9, 3.3$ and $M^{LCP}_{\rm postsaddle} = 11.0, 10.4, 7.6$ for Au, Bi and U, respectively. In the present experiment, postscission LCP emission can be deduced from the angular correlation with the fission axis. The energy spectra of α- particles for three ranges of emission angles relative to the motion direction of the light fission fragment is shown in Fig.2. The spectra are plotted in the center-of-mass system of the FFs from the reaction 2.5 GeV p+Au at $E^* = 600 - 900$ MeV. The different contributions from the compound nucleus prior to scission (uncorrelated to the scission axis), and from the two FFs which vary in shape and intensity with $\theta_{\alpha-\rm LF}$ are indicated. The sum of all components (including the neck emission at 70° to 100°) shown in Fig.2 as histograms provides a good approximation at least to the lower-energy ($E_\alpha \leq 35$ MeV) part, i.e., to the evaporation part, of the spectra. The high energy tails in the measured spectra, instead, originate partly from pre-equilibrium processes. Further details can be found in ref. [1].

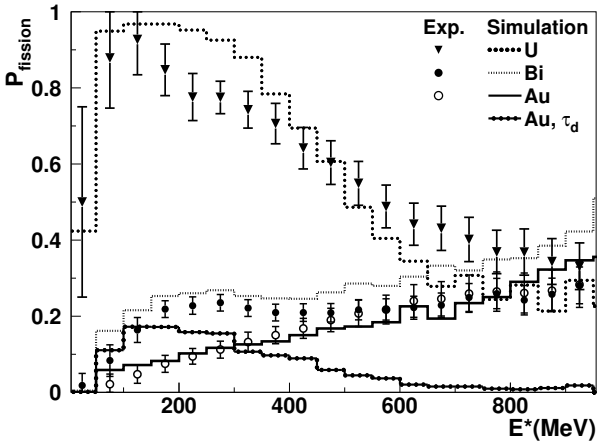

Fig. 1: Comparison of experimental (symbols) and simulated (histograms) fission probability as a function of E*. The simulation for p+Au with $a_f/a_n = 1.05$ and $\tau_d = 2 \times 10^{-21}$s according to ref. [6] is shown by the chain dotted histogram.

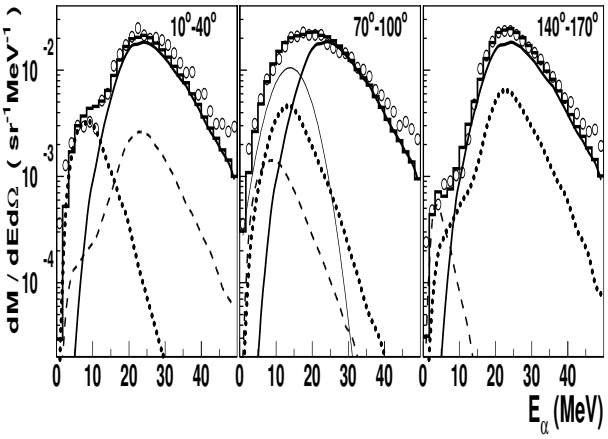

Fig. 2: α-particle energy spectra for 3 angular domains relative to the motion of the light fission fragment: $\theta_{\alpha-\rm LF}$ as indicated in the figure; dots: exp.data, lines: contribution from compound nucleus prior to scission (thick continuous lines), from the light (dashed lines) and from the heavy (dotted lines) fission fragments. At 70° to 100° a further component for neck emission is added(thin line). The total calculated spectrum is shown by the histogram. Example: 2.5 GeV p+Au at $E^* = 600 - 900$ MeV.

References:

[1] U. Jahnke et al.,Phys.Rev.Lett. 95, 162701, (2005).

[2] D. Hilscher and H. Rossner, Ann. Phys. (Paris) 17, 471 (1992).

[3] U. Jahnke et al., NIM Phys. Res., Sect. A 508, 295 (2003).

[4] C.-M. Herbach et al., NIM Phys. Res., Sect. A 508, 315 (2003).

[5] L. A. Vaishnene et al., Z. Phys. A 302, 143 (1981).

[6] J. Benlliure et al., Nucl. Phys. A700, 469 (2002).

Intermediate Mass Fragments from 200 MeV Protons

H. Machner, D. G. Aschman[1], K. Baruth-Ram[2], J. Carter[3], A. A. Cowley[4], F. Goldenbaum, B. M. Nangu[5], J. V. Pilcher[6], E. Sideras-Haddad[3], J. P. F. Sellschop[3], F. D. Smit[6], B. Spoelstra[5], D. Steyn[1]

Studies of spallation processes, both experimental and theoretical, are numerous. One reason for this may be the importance of knowledge of cross sections and reaction mechanisms for our understanding of cosmic rays and the production of cosmogenic radionuclides, and the process of neutron production in spallation sources. Recent reviews of the process can be found in Refs [1,2]. Most of the experimental data exist in the range above 1 GeV which is important for spallation neutron source construction and the understanding of very high energy cosmic rays. However, the energy of the maximum abundance of protons in cosmic rays is around 200 MeV [3,4]. We measured intermediate mass fragments at a proton beam energy of 200 MeV incident on three targets spanning the periodic table, namely, ^{27}Al, ^{59}Co and ^{197}Au. These data complement previous cross sections for proton, deuteron and tritium emission on ^{27}Al and ^{197}Au [5,6].

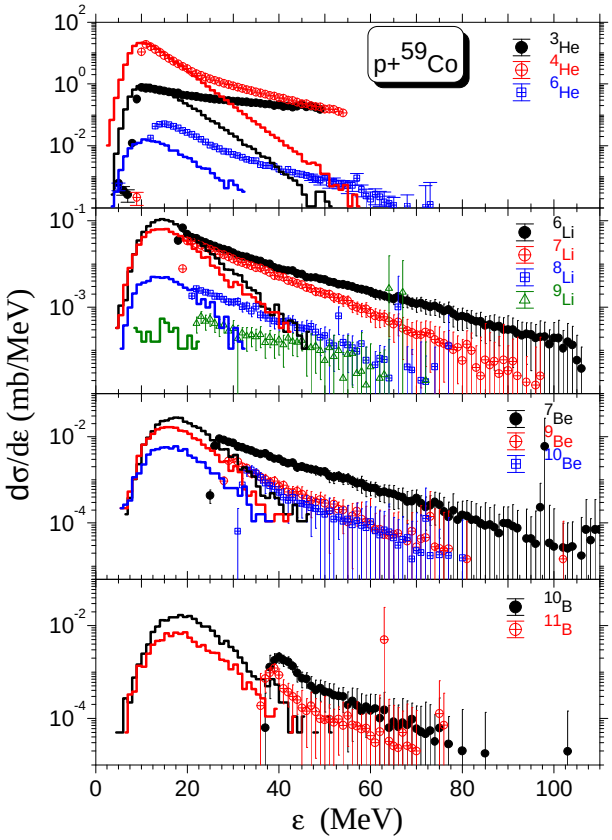

Fig. 1: Energy differential cross sections for the cobalt target. The data are shown as points with error bars, the calculations as histograms.

The experiment was performed at the sector focussing cyclotron of tThemba LABS in South Africa. Intermediate mass fragments (IMFs) were detected with a stack of silicon detectors in an angular range from 20 to 120 degree in the laboratory system. Energy calibration was performed with radioactive sources. Self supporting foils of ^{27}Al, ^{59}Co and ^{197}Au were used as targets. Particle identification was performed by the $\Delta E - E$ method.

Count rates were transformed to cross sections by known incident flux, target thickness and solid angle of the detector. From the double differential cross sections energy dependent cross sections were derived. As an example such angle integrated cross sections are shown in Fig. 1 for the case of the cobalt target.

The data were compared with model calculations. We have applied an intra nuclear cascade model INCL4.2 [7]. After equilibrium is reached we apply an evaporation model. It is the generalized evaporation model (GEM) of Furihata [**?**], which is based on the classical Weisskopf-Ewing approach including angular momentum coupling. Whereas the cascade treats only emission of nucleons and pions, in the evaporation we allow for fragments up to ^{28}Mg. The resulting energy spectra are compared against the data in Fig. 1. The absolute height for low energies, i. e. in the evaporation region is reproduced by the calculation while for higher energies the pre-equilibrium emission is missing.

In cosmic rays there is a large deviation of abundances for *Li*, *Be* and *B* compared to solar systems. All isotopes of these elements are either stable or short lived. Only ^{10}Be has a half life time of 1.8×10^6 years. The ratio ^{10}Be to ^{9}Be may thus be a clock. We compare the ratio between ^{10}Be and ^{9}Be for the different targets. The yield of the short lived ^{9}Li is added to the latter.

Table 1: The ratio $R = \sigma(^{10}Be)/[\sigma(^{9}Be)+\sigma(^{9}Li)]$ for the different targets in the energy range 30 to 50 MeV.

target	R
^{27}Al	0.654 ± 0.073
^{59}Co	0.577 ± 0.133
^{197}Au	0.918 ± 0.109

References:

[1] J. Hüfner: Phys. Rep., **125** 129 (1985).
[2] R. Silberberg, C.H. Tsao: Phys. Rep., **191** 351 (1990).
[3] S. Austin: Progress in Part. Nucl. Phys., **7** 1 (1981).
[4] J. A. Simpson: Ann. Rev. Nucl. Part. Sci., **33** 323 (1983).
[5] J. P. Didelez et al.: www.fz-juelich.de/ikp/gem under Conference Proceedings and Ricerca Scientifica ed Educazione Permanente, **Suppl. 28** 237 (1982).
[6] H. Machner et al.: Phys. Lett., **B 138** 39 (1984).
[7] A. Boudard, J. Cugnon, S. Leray, C. Volant: Phys. Rev., **C 66** 044615 (2002).

1. Dept. of Physics, University of Cape Town, Johannesburg, South Africa
2. Dept. of Physics, University of Durban-Westville, South Africa
3. Dept. of Physics, University of the Witwatersrand, Johannesburg, South Africa
4. Dept. of Physics, University of Stellenbosch, Stellenbosch, South Africa
5. Dept. of Physics, University of Zululand, KwaDlangezwa, South Africa
6. iThemba Labs, Faure, South Africa

Installation of an electrolytical deuterium generator for the cluster targets at COSY

T. Rausmann[1], W. Borgs[2], A. Khoukaz[1], T. Mersmann[1], M. Mielke[1], M. Papenbrock[1], R. Schleichert[2]
and the ANKE collaboration

For experiments at COSY two cluster targets have been built at the IKP of the University of Münster and installed within the internal experiments COSY-11 and ANKE in 1995 and 1999, respectively [1, 2, 3]. Due to the special design they allow to provide cluster beams of all gases except helium as targets for scattering experiments. For studies on elementary meson and hyperon production processes in the pp-, pn- and pd-scattering, hydrogen and deuterium gas is of special interest as target material.

In contrast to hydrogen, deuterium gas is comparatively expensive. Therefore, a regeneration system was build in order to reduce the consumption of deuterium gas by cleaning and compressing the used process gas available at the exhaust of the forepumps. By this only small deuterium gas losses have to be compensated by gas bottles in a gas cabinet. This system was successfully tested at a cluster target in Münster and installed at the COSY ring in summer 1999 [4].

To further reduce the cost for deuterium a electrolysis unit was installed and tested at the deuterium regeneration in 2005. With this unit the needed deuterium gas can be produced using comparatively cheap heavy water (D_2O).

A scheme of the regeneration with the new electrolysis unit is depicted in figure 1. Exhausted gas (1) is collected from the fore pump stages and feed into the regeneration. At this point the new unit is connected to the previously existing parts. The electrolysis (domnick hunter model 60H) provides deuterium with a pressure of 7 bar and volume flow of up to 500 ml/min. When one of the cluster targets is set into operation, a higher volume flow is needed for a short time. Therefore a buffer volume is connected to the electrolysis unit. The deuterium is then lead through a pressure reducer, which limits the overpressure to approximately 0.5 bar.

To automatically feed deuterium into the system when needed, a remote controlled pneumatic valve is used, placed between the electrolysis and the compression unit. The valve is controlled by a baratron at the gas cabinet. If the pressure drops below a certain value the valve is opened and deuterium from the electrolysis is feed to the compression unit.

The first test operation of the electrolysis unit at COSY was performed during a ANKE beam time in February 2005. During this two weeks of beam time a stable cluster beam was produced soleley using deuterium from the electrolysis of heavy water.

References:

[1] H. Dombrowski, D. Grzonka, W. Hamsink, A. Khoukaz, T. Lister, R.Santo, Nucl. Phys. **A 386**, 228 (1997)
[2] S. Brauksiepe et al., Nucl. Phys. **A 376**, 397 (1996)
[3] H.-H. Adam, A. Khoukaz, N. Lang, T. Lister, C. Quentmeier and R. Santo, *The Cluster Target for the ANKE-Experiment at COSY*, IKP Annual Report (1999)
[4] H.-H. Adam, A. Khoukaz, N.Lang, T. Lister, C. Quentmeier, R. Santo, W.Verhoeven, *Deuterium Recuperation for Cluster Targets at COSY*, IKP Annual Report (1999)

[1] Institut für Kernphysik, Universität Münster, 48149 Münster, Germany
[2] Institut für Kernphysik Forschngszentrum Jülich, 52428 Jülich, Germany

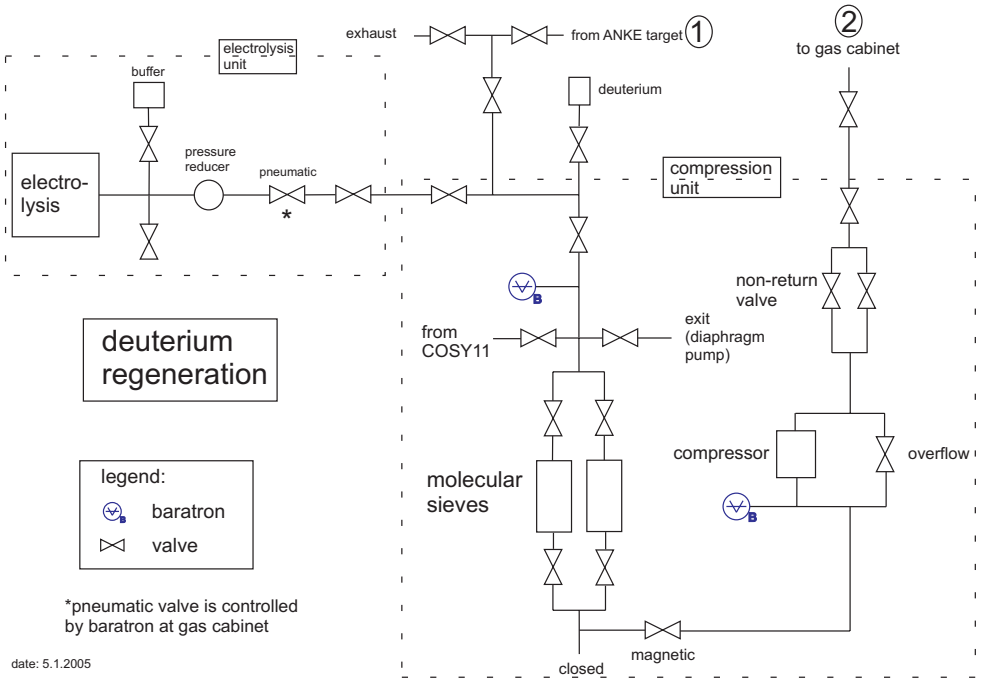

Fig. 1: Scheme of the deuterium regeneration system with the new electrolysis unit.

Status of the pellet target for the WASA@COSY experiment

T. Rausmann[1], U. Bechstedt[2], G. D'Orsaneo[2] , A. Khoukaz[1], D. Spölgen[2] , A. Täschner[1] and the WASA collaboration

In June 2005 the transfer of the WASA-detector from CELSIUS to COSY has been started and will be finished with the commissioning of WASA at COSY in the second half of 2006 [1]. An essential part of the WASA-experiment is the internal pellet target, which is the first and up to now only pellet target system which was operated as an internal target in an accelerator experiment [2, 3].

A scheme of the target generator where the pellets are produced is depicted in figure 1. Liquid hydrogen is pressed through a vibrating glass nozzle. The vibrations induce the break up of the jet into single droplets with a diameter of around 30 μm. During the injection of the droplet beam into the vacuum through a 7 cm long capillary, the droplets freeze due to evaporation and form a pellet beam. The beam is then collimated by a skimmer and lead through a thin 2 m long pipe into the scattering chamber to interact with the ion beam. The remaining pellets are collected 2m below the scattering chamber in the target beam dump. The effective pellet target thickness is in the order of 10^{16} atoms/cm^2 with a beam diameter of around 3 mm at the interaction point.

The transfer of the target began at the end of June with dismantling in Uppsala and shipment to COSY. After the arrival of the components in Jülich the pumps, cryo compressors and the hydrogen purifier were maintenanced. Furthermore, several components have to be modified to meet the later requirements at COSY.

In December 2005 the reassembly of the pellet station has been started in the "Bermuda triangle" at COSY for optimisation and test purposes. Here the size of the test frames have been choosen to simulate the later situation at COSY. By this information reflecting the final operation at COSY can be gained. The pellet generator, a test scattering chamber and

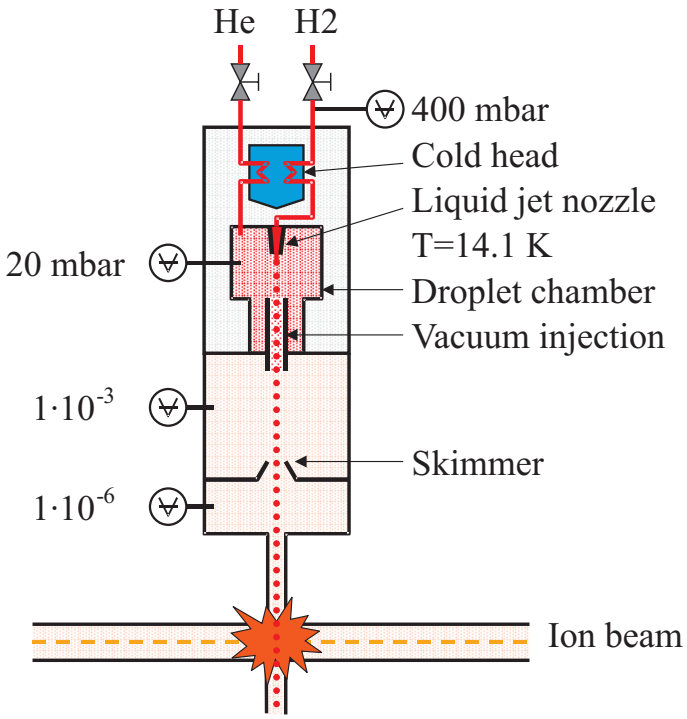

Fig. 1: Scheme of the WASA pellet generator

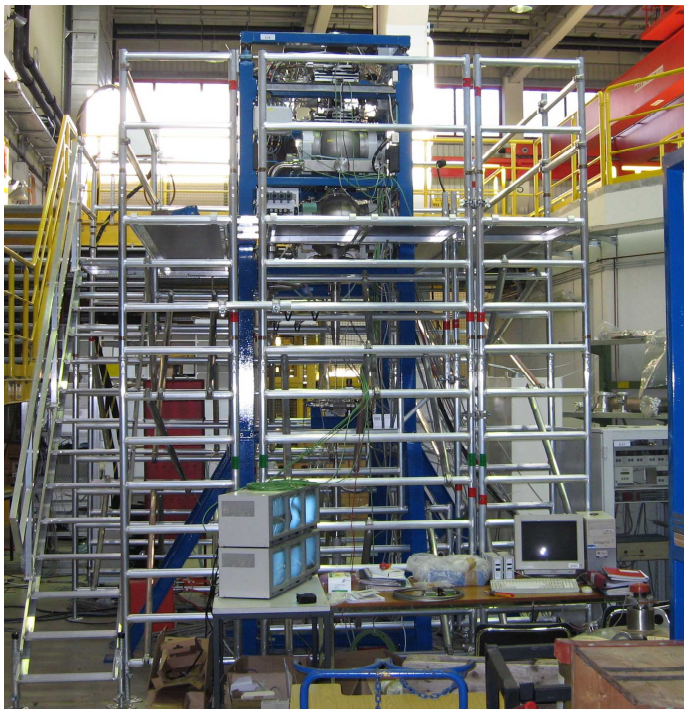

Fig. 2: Setup of the pellet target in the Bermuda triangle

the beam dump were aligned optically and the pipes between them were installed. For an optimal access to the generator a scaffold was installed around the target frame.

The current status of the test station is shown in figure 2. The assembly will be finished in the January of 2006 followed by test measurements with the pellet target. The development of a glas nozzle production line in Jülich will be finished in 2006. In Summer 2006 the WASA pellet target is scheduled to be installed at the WASA-Experiment at COSY.

References:

[1] B. Hoistad, J. Ritman *Proposal for WASA at COSY* COSY-PAC 29 (2004)
[2] B. Trostell , Nucl. Instr. and Meth. **A 362**, 41 (1995)
[3] C. Ekström et al. , Nucl. Instr. and Meth. **A 371**, 572 (1996)

[1] Institut für Kernphysik, Universität Münster, 48149 Münster, Germany
[2] Institut für Kernphysik Forschngszentrum Jülich, 52428 Jülich, Germany

Investigation of pellet parameters with the Moscow-Jülich Pellet Target*

M.Büscher[b], A.Bukharov[c], V.Chernetsky[a], V.Chernyshev[a†], A.Gerasimov[a], P.Fedorets[a,b], A.Semenov[c]

The tests with the Pellet Target in 2005 focused on the investigation of nozzle-sluice coaxiality and on the study of the pellet velocities, angular and radial distributions. In order to fulfill these tasks, special software has been developed for precise determination of the axes of sluice and nozzle, which is used for the nozzle-sluice adjustment. This program analyses the images from CCD cameras in two projections (X and Y), estimates the shapes of the nozzle and sluice, and calculates their axes. The program provides information about the radial displacement of axes and the angle between them. Figure 1 presents the working window of the program. The change of the position and inclination of the nozzle is performed with adjustment units operated manually (at the moment). With this program the adjustment accuracy of nozzle-sluice axis is better than 40μm.

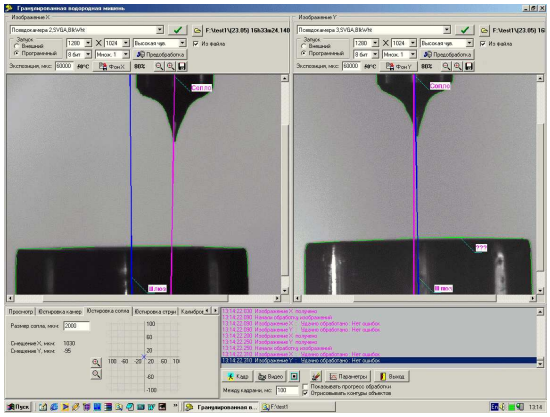

Fig. 1: CCD analysis program for precise determination of the axes of sluice (blue line) and nozzle (pink) in X and Y projections. Photos are taken before the adjustment.

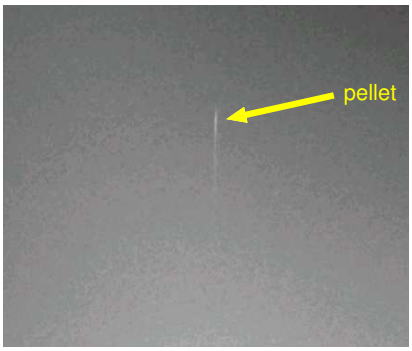

Fig. 2: Hydrogen pellet with diameter 25μm in the scattering chamber.

Two CCD cameras have been installed in addition to the two existing cameras. These cameras monitor the output from the sluice in the 1^{st} vacuum chamber. During tests with pellets any pair of CCD cameras can be moved for observation to the second vacuum chamber or to the scattering chamber.
In the test measurement in spring 2005, with improved coaxiality of the nozzle and sluice, hydrogen pellets with diameters of $\sim 25-30\mu$m have been observed in the scattering chamber for the first time (Fig. 2). This chamber is located ~ 1.3m below the triple-point chamber.
In April 2005 we started to investigate the velocity and angular distributions of pellets. Below we present the first results from the April test. The data from November test are currently under analysis.
In the first vacuum chamber, at the output of the sluice, the pellets are detected as a short tracks due to the sensitive time of the CCD. The track length depends on the velocity of the pellet. Thus the pellet velocities can be deduced by measuring the lengths of the track images. Figure 3 shows the measured velocity distribution of pellets in the 1^{st} vacuum chamber. The average velocity of hydrogen pellets is ~ 70m/s.

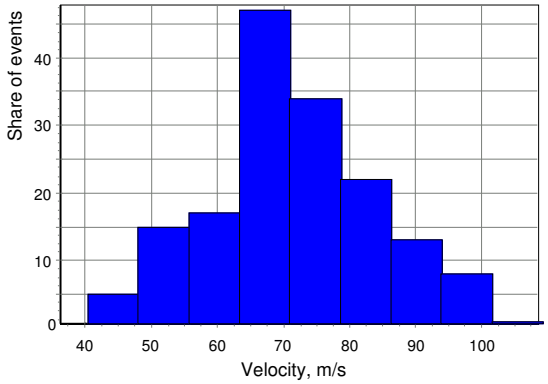

Fig. 3: Preliminary velocity distribution of pellets in the 1^{st} vacuum chamber.

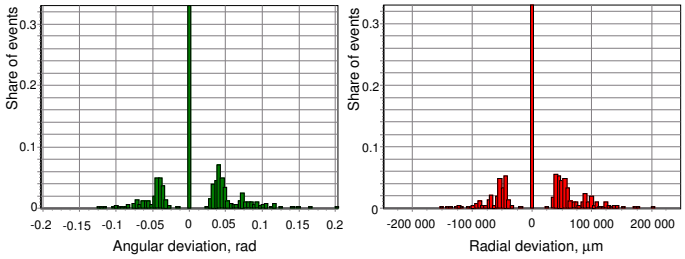

Fig. 4: Angular distribution of pellets in plane of the sluice (left) and the calculated distribution of radial displacement of pellets in a plane of the scattering chamber (L=120 cm from sluice)(right).

Figure 4(left) presents the measured angular distribution of pellets in the plane of the sluice. This angular distribution provides the possibility to calculate the radial displacement distribution of pellets at any distance from the sluice. For example, Fig. 4(right) shows the calculated radial displacement distribution in the scattering chamber. The angular distribution has a central line corresponding to direct pellets (about 30%) and tails from pellets, which interact with the sluice walls. Taking into account the geometrical acceptance of the channel (second sluice, diameter of the pipe) one finds, that only direct pellets are able to reach the scattering chamber. If one decreases the resolution, the shape of angular

distribution (and consequently the radial displacement distribution) changes and takes the shape of a broad Gaussian distribution.
Figure 5 shows the calculated distribution of radial displacement in the scattering chamber after taking into account the geometrical acceptance of the channel. Within of our resolution we can conclude that the radial displacement of pellets in the scattering chamber (distance 120 cm from sluice) is not worse than $\pm 200\mu$m.

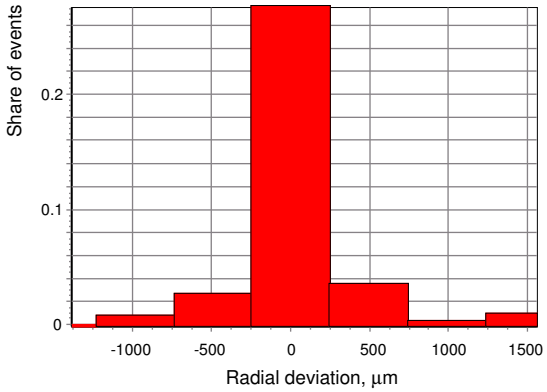

Fig. 5: Calculated distribution of a radial displacement of pellets in a plane of scattering chamber after taking into account the geometrical acceptance of the channel.

During the tests in the last two years stable (several hours) jet and pellet production from hydrogen and nitrogen with diameters of $\sim 25-30\mu$m has been achieved. The investigation of the regimes for jet and pellet production from argon is under way. An automatic filling system for liquid helium has been designed and is now being built in the workshops of FZJ. This system will allow long-term target operation (several days), which is limited now to a few hours due to the need to manually refill liquid helium.

[a]ITEP, Moscow
[b]IKP FZJ
[c]MPEI, Moscow
† deceased January 2006

∗Supported by grants EU-000419, RFFI03-02-04013, RFFI02-02-16349, DFG-436RUS-113/733.

1.2 Experiments at External Facilities

Remeasurement of the charged pion mass

D. F. Anagnostopoulos[a], A. Dax[b], J.–P. Egger[c], D. Gotta, M. Hennebach, P. Indelicato[d], Y.–W. Liu[b], B. Manil[d], N. Nelms[e], L. M. Simons[b], M. Trassinelli[d], A. Wells[e]

The measurement of the charged pion mass using X–rays from pionic nitrogen has been reanalysed after a critical survey of the experimental conditions [1]. The experiment is based on the precise knowledge of the muon mass, which is known to an accuracy of 0.05ppm, and on the fact that medium Z exotic atom have a completely ejected electron shell during the intermediate part of the atomic cascade [2]. Consequently, the electromagnetic transition energies are calculable with an uncertainty of ± 1 meV only in the few keV range.

A suitable pair of a muonic calibration line and a pionic one is found to be $\pi N(5g-4f)$ (4.055 eV) and $\mu O(5g-4f)$ (4.023 eV). The small energy difference allows the simultaneous measurement with a Johann–type Bragg crystal spectrometer equipped with a large area detector built up from 6 Charge–Coupled Devices (CCDs) [3]. Pions of the $\pi E5$ beam line at PSi were stopped in a target cell inside the cyclotron trap. The cell was filled with an N_2/O_2 gas mixture (10%/90%) in order to obtain similar count rates for the pionic and the muonic transition (Fig. 1). Such a measurement is basically free of systematic errors originating from mechanical drifts during the 4 weeks data taking.

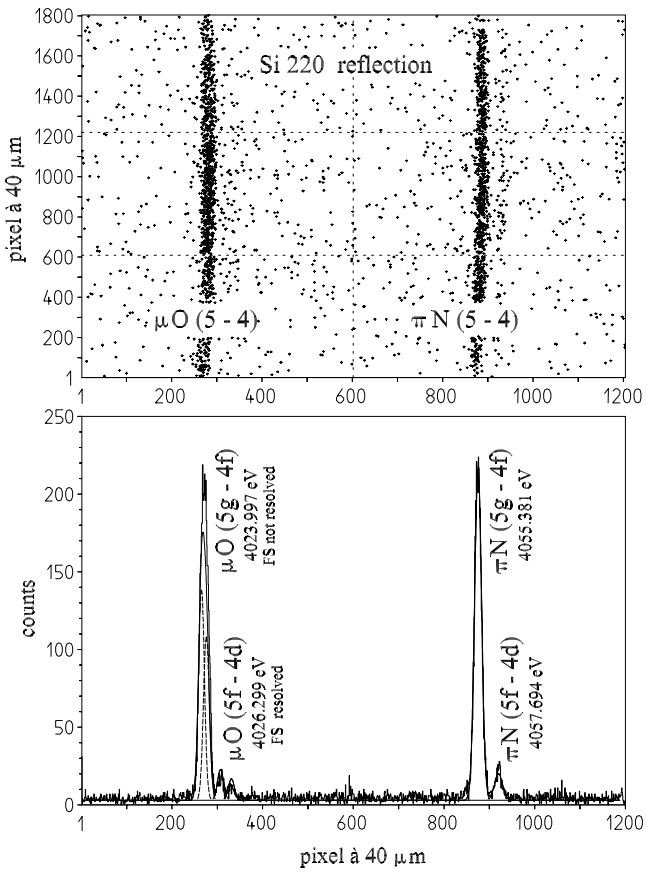

Fig. 1: Simultaneous measurement of the $\pi N(5g-4f)$ and $\mu O(5g-4f)$ transitions in a large area CCD array.

The energy of the $\pi N(5g-4f)$ transition and with that of the pion's mass is given by the angular distance of pionic and calibration line, determined from the position distance of the Bragg reflections. Hence, the relative positions of the CCDs itself and the size of the individiual pixel have to be known to high accuracy and have been determined in dedicated measurement [4].

The statistical accuracy achieved of 1.54ppm is mainly limited by the count rate of the muonic transition. The main systematic errors are due to the spectrometer focus (0.7ppm), the geometry of the CCD array (0.3) and the QED transition energies (0.4ppm). The total systemetic error is 0.95ppm. Assuming uncorrelated errors the total error amounts to 1.81ppm resulting in

$$m_\pi = 139.57095 \pm 0.000253\, MeV/c^2 \qquad (1)$$

for the charged pion mass (Fig. 2). This value is 5.5ppm larger than world average value [5], which is obtained from a measurement of pionic nitrogen using Cu $K\alpha$ radiation for energy calibration [6] and a pionic magnesium transition calibrated by a nuclear γ–ray [7]. The new large value for m_π results in a non zero value for the muon neutrino mass, however with a significance of less than 2 standard deviations ($m_{\nu_\mu} = 210 \pm 131$ keV).

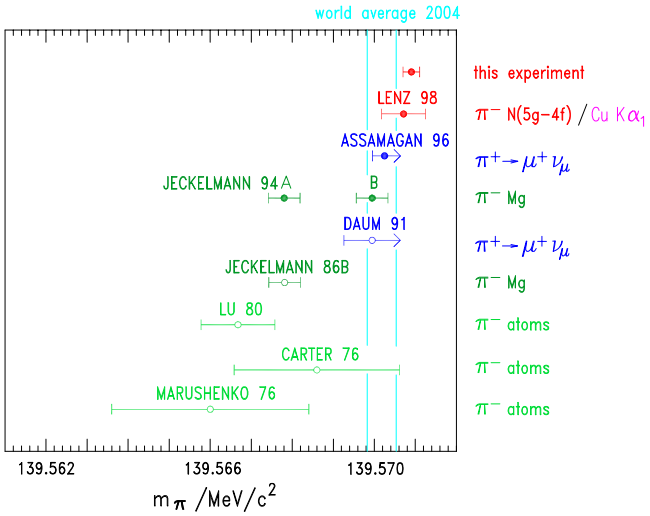

Fig. 2: Recent results for the charged pion mass.

References:

[1] PSI experiment R–97.02: pion mass.
[2] R. Bacher et al., Phys. Rev. Lett. (1985) 2087; R. Bacher et al., Phys. Rev. A 39 (1989) 1610.
[3] N. Nelms et al., Nucl. Instr. Meth. A 484 (2002) 419.
[4] C. David et al., this report and submitted to Rev. Sci. Instr.
[5] S. Eidelmann et al.(PDG), Phys. Lett. B 592 82004) 1.
[6] S. Lenz et al., Phys. lett. B 416 (1998) 50.
[7] B. Jeckelmann et al, Phys. Lett. B 335 (1994) 326.

[a] Dept. Mat. Sc., Univ. Ioannina, Greece
[b] PSI, Switzerland
[c] Inst. de Phys. Univ. Neuchâtel, Switzerland
[d] Lab. Kastler–Brossel, Univ. P. et M. Curie, Paris
[e] Dept. Phys. and Astr., Univ. of Leicester, England

High statistics measurement of the Kα transition in pionic hydrogen

D. Covita[a], D. Gotta, A. Hirtl[b], A. Gruber[b], P. Indelicato[c], E.-O. Le Bigot[c], M. Nekipelov, Th. Pask[b], J. M. F. dos Santos[d], Th. Strauch, L. M. Simons[e], J. F. C. A. Veloso[d], J. Zmeskal[b]

Experiment R-98.01 aims at a precision determination of the hadronic effects in the ground state of pionic hydrogen by stopping pions in the cyclotron trap and measuring pionic K X–ray transitions with a high–resolution crystal spectrometer [1]. The first data taking periods in 2001 and 2002 for pionic hydrogen and in 2004 an additional measurement of muonic hydrogen to study cascade effects yielded an improvement of a factor of about 3 compared to the previous experiment [2]. The results from these periods are

$$\varepsilon_{1s} = 7116 \pm 8\,(stat.) \pm 7\,(sys.)\ meV \quad (1)$$

$$\Gamma_{1s} = 785 \pm 27\ meV\ (\pm 3.5\%). \quad (2)$$

The final error of the hadronic shift ε_{1s} of $\pm 11\,meV$ results from the reduction of the systematic error by an improved calculation of the electromagnetic transition energy. This value is now given with an uncertainty of $\pm 1\,meV$ (previously $\pm 6\,meV$).

The measured line shape results from the convolution of the crystal spectrometer response, the hadronic widths Γ_{1s} itself (a Lorentzian), and up to 4 different contributions from Doppler broadening owing to Coulomb de–excitation. Significant progress in the determination of the hadronic width was achieved (i) from the precise determination of the spectrometer response with helium–like X–rays excited in an electron–cyclotron resonance source [3] and (ii) from the inclusion of various contributions from Doppler broadening in the fit of the line shape. The general picture of the atomic cascade was essentially supported by the analysis of the line broading of the $\mu H(3p-1s)$ transition as measured in 2004 [4]. Depending on the pionic transition measured different Doppler contributions must be taken into account. Such an analysis results in a set of consistent values both for different transitions and at different densities (Fig.1) which, however, are significantly smaller than the results of the previous experiment (ETHZ–PSI [5]). Presumably, the much higher background level in that measurement was absorbed partly into the tails of the Lorentzian.

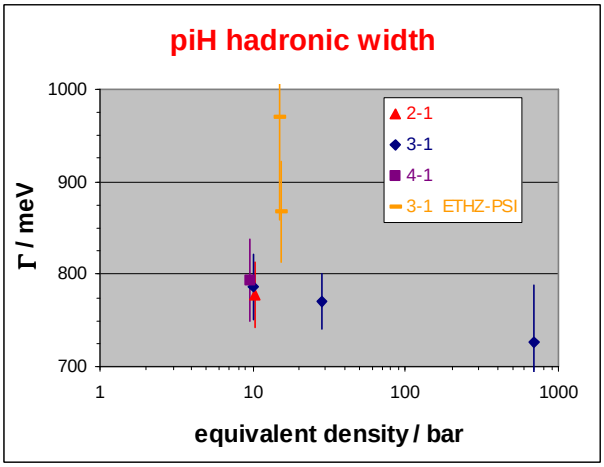

Fig. 1: Hadronic broadening as determined from various πH transitions and at different target densities (without the recent $\pi H(2p-1s)$ measurement).

From the shift and broadening the isoscalar and isovector scattering length a^+ and a^- were calculated following an approach within the framework of chiral perturbation theory [6]. Preliminary values of $a^+ = 0.009 \pm 0.003\,m_\pi^{-1}$ and $a^- = 0.084 \pm 0.002\,m_\pi^{-1}$ are obtained indicating a positive value with 3 standard deviations for the isoscalar scattering length. From a^- a rather small value is derived for the πN coupling constant $f^2_{\pi N} = 0.074 \pm 0.008$.

In order to improve on the accuracy of Γ_{1s}, a high statistics measurement of the Kα transition was performed in autumn 2005, which constitutes the last data taking period within the proposal pionic hydrogen [1]. Within a 5 weeks data taking period at the πE5 channel of the ring cyclotron of the Paul Scherrer Institut (PSI) about 40000 events have been accumulated in the $\pi H(2p-1s)$ transition (Fig. 2). The high statistics together with a further substantially reduced background will allow a better fit to the tails of the Lorentzian. Another factor of 2 improvement for Γ_{1s} is expected. This in turn will result in more accurate values for the scattering lengths and with that for the pion–nucleon sigma term (from a^+) and the πN coupling constant (from a^-).

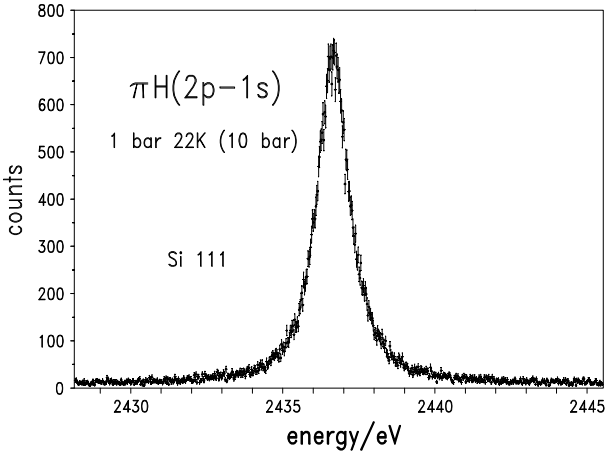

Fig. 2: The spectrum of Kα transition in pionic hydrogen measured with a Si 111 crystal at a target density equivalent to 10 bar.

References:

[1] http://pihydrogen.web.psi.ch.
[2] D. Gotta et al., Int. J. Mod. Phys. A 20 (2005) 349; D. F. Anagnostopoulos et al., Proc. EXA05, Vienna, 2005, p. 107.
[3] D. F. Anagnostopoulos et al., Nucl. Instr. Meth. A 545 (2005) 217; S. Boucard et al., annual report IKP, 2004.
[4] D. F. Anagnostopoulos et al., annual report IKP, 2004.
[5] H. C. Schröder et al., Eur. Phys. J. C 21 (2001) 473.
[6] J. Gasser et al., Eur. Phys. J. C 26 (2003) 13.

[a] Dept. of Phys., Univ. Coimbra, Portugal
[b] SMI, Österr. Akademie d. Wiss., Vienna
[c] Lab. Kastler–Brossel, Univ. P. et M. Curie, Paris
[d] PSI, Switzerland

Characterisation of a CCD array for Bragg spectroscopy

C. David[a], D. Gotta, M. Hennebach, P. Indelicato[b], E.-O. Le Bigot[b], N. Nelms[c], L. M. Simons[a], M. Trassinelli[b]

The energies of the two exotic–atom transitions $\pi N(5g-4f)$ and $\mu O(5g-4f)$ (4 keV) differ by 32 eV only. When using a crystal spectrometer, the Bragg angle difference is about 0.5° for the Si 220 reflection and both lines can be detected simultaneously in a large area X–ray detector [1]. Such a detector was set up as an array of 6 charge–coupled devices of 24 mm×24 mm each, arranged as a 2×3 matrix (Fig. 1). The 6 individual CCD mountings are fixed on an INVAR plate which is connected to a liquid nitrogen dewar.

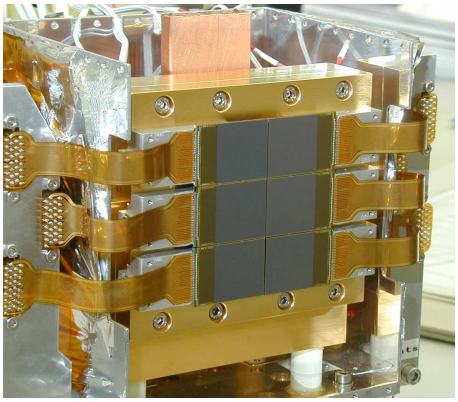

Fig. 1: CCD array used as focal–plane X–ray detector of a crystal spectrometer for exotic–atom experiments.

For an accurate determination of the angular difference among other things both the relative orientation and the pixel distance have to be known precisely. The distance between the devices is about 0.3 mm and the nominal pixel size is 40 μm as given by the lithographic mask used to fabricate the surface structure (at room temperature). The CCDs are produced in the so called 0.5 μm technology, i. e., the distance between the first and last row or column (one device consists of 600×600 pixels) is given with to precision of 0.5 μm. Hence, the average pixel distance should be $40.0000 \pm 0.0008\,\mu m$. However, no data could be found at the operating temperature of – 100°C.

In order to measure the average pixel distance at – 100°C the detector was illuminted by light through a quartz nano mask (Fig. 2). Linearity and distances of the two–dimensional line pattern on this mask is determined to at least 0.05 μm [4]. In addition, the size of the wafer overlapping the whole array allows to verify the alignment of the six devices measured earlier using sulphur Kα X-rays and a wire eroded aluminum mask [2, 3].

The nano mask was installed 4 cm in front of the CCD array inside the cryostat and monitored to stay always at room temperature. The light bulb was at a distance of more than 6 m in order to avoid parallax effects. The diffraction pattern produced by the lines of the mask was fitted by a model taking into account main and side maxima together with a background contribution. (Fig. 3). A non–negligible background originates from reflected light.

About 180 individual pairs of straight sections were evaluted per CCD yielding a value for the average pixel distance of $39.9775 \pm 0.0006\,\mu m$ at – 100°C [5], which differs significantly from the nominal value. The inter device distances and relative rotations were consistent with the earlier measurement using X–rays, but are a factor of about two more precise.

Fig. 2: Quartz wafer used for the determination of the average pixel size and relative orientation of the CCD array. The spacing of the grating is 2 mm.

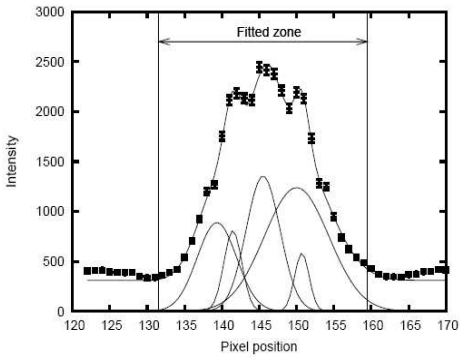

Fig. 3: Typical diffraction pattern and fit.

Furthermore, the temperature dependence of the pixel distance was determined by additional measurements at – 105°C, – 80°C, – 60°C, and – 40°C. The deduced average thermal extension coefficient is about a factor of two larger than the one for pure silicon or INVAR ($\approx 1.2 \cdot 10^{-6}/K$ and $\approx 1.5 \cdot 10^{-6}/K$). As expected the complex structure of CCDs build up of various silicon types in combination with other materials does not allow a detailled calculation. It must be concluded, that for precision experiments relying on the exact knowledge of the CCD structure, an individual characterisation is essential.

References:

[1] D. F. Anagnostopoulos et al., this report.
[2] D. Gotta et al., ann. rep. IKp 2001.
[3] M. Hennebach, PhD thesis, Univ. zu Köln, 2003.
[4] C. David, PSI nano laboratory, priv. comm.
[5] C. David et al., submitted to Rev. Sci. Instr.

[a] PSI, Switzerland
[b] Lab. Kastler–Brossel, Univ. P. et M. Curie, Paris
[c] Dept. Phys. and Astr., Univ. of Leicester, England

Developments for trapping antihydrogen atoms

U. Bechstedt, F.M. Esser*, H. Glückler*, F. Goldenbaum, D. Grzonka, G. Hansen*, S. Martin, W. Oelert, T. Sagefka, M Schmitt*, T. Sefzick, H. Soltner*, Z. Zhang, for the ATRAP-Collaboration

Since the start of the dedicated Antiproton Decelerator (AD) at CERN in 2000 the ATRAP collaboration [1] is in the process of producing antihydrogen atoms via the cooling of antiprotons with positrons [2] and its background free identification [3]. The collaboration made large progress in the driven production of cold antihydrogen atoms and the first measured distribution of states of antihydrogen [4] and the determination of the velocity of slow antihydrogen atoms [5]. Though several thousands of antihydrogen atoms were produced during one experiment in this three body recombination process, the created atoms were still about two orders of magnitude too high in velocity to be captured in field gradients of todays technology. Slower antihydrogen atoms were produced in a first laser–controlled double charge exchange experiment [6], but the production rate was rather slow. The main experimental disadvantage of the investigations performed till now was the use of a recycled super-conduction solenoid (from the former TRAP experiment at LEAR) with a bore as small as about 10 cm in diameter. The new experiments in 2006 will have available a magnet with a much larger bore of 50 cm giving ample of space for additional detection [7], laser access and especially magnetic traps with a gradient of the magnetic field overlaying the homogeneous field of the super conducting solenoid. The new magnet is shown in figure 1 during its installation. The photo multipliers of the outer scintillator paddles are clearly seen.

Fig. 1: The new magnet of the ATRAP collaboration with its 50 cm-bore.

There is the principal conflict that for the trapping of high density antiproton and positron clouds a homogeneous magnetic field is essential whereas the neutral antihydrogen can only be captured by the gradient of a magnetic field increasing from the trap center in all directions. An optimal solution has to be worked on and is part of the present research. The magnetic field gradient (B) produces a repulsive force (F) onto the magnetic moment (μ) of the antihydrogen atom (essentially of the positron) according to: $\vec{F} = -\vec{\nabla}\ (\vec{\mu}\vec{B})$. Figure 2 a) shows the principle of a magnetic trap. Whereas figure 2 b) presents a design worked out at the ZAT from the Research Center Jülich in cooperation with the ATRAP team where great care has to be given in view of the tremendous forces acting. The figure shows the inner body where the trap will be placed and which will be produced out of Ti-

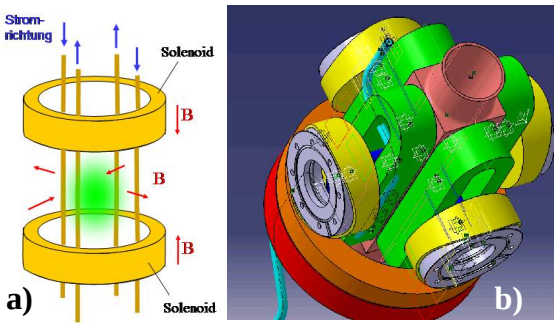

Fig. 2: Left: Principle functioning of an magnetic trap, right: three dimensional display of the design as prepared by the ZAT Research Center Jülich.

tanium surrounded by coils with four openings for the laser access. The entire design will be encapsulated by an Aluminum holder, which shrinks stronger than the Titanium material in order to prevent movements of the coils which would result in quenching of the system.
It is planed that the new trap will be built during the first few months of 2006 for installation into the ATRAP apparatus in August/September this year. The team is well aware of the fact that the present design might only be a prototype which likely must be changed after the first experiences in the experimental performance. It might even turn out that a quadrupole field is not sufficient and higher order multi-poles have to be used.

References:

[1] http://hussle.harvard.edu/∼ atrap
[2] G. Gabrielse, J. Estrada, J.N. Tan, P. Yesley, N.S. Bowden, P. Oxley, T. Roach, C.H. Storry, M. Wessels, J. Tan, D. Grzonka, W. Oelert, G. Schepers, T. Sefzick, W.H. Breunlich, M. Cargnelli, H. Fuhrmann, R. King, R. Ursin, J. Zmeskal, H. Kalinowsky, C. Wesdrop, J. Walz, K.S.E. Eikema und T.W. Hänsch. Phys. Lett. **B 507** 1 (2001)
[3] G. Gabrielse, N.S. Bowden, P. Oxley, A. Speck, C.H. Storry, J.N. Tan, M. Wessels, D. Grzonka, W. Oelert, G. Schepers, T. Sefzick, J. Walz, H. Pittner, T.W. Hänsch, E.A. Hessels. Phys. Rev. Lett. **89** 213401 (2002)
[4] Authors as in ref [3] Phys. Rev. Lett. **89** 23340 (2002)
[5] G. Gabrielse, A. Speck, C.H. Storry, D. Le Sage, N. Guise, D. Grzonka, W. Oelert, G. Schepers, T. Sefzick, H. Pittner, J. Walz, T.W. Hänsch, D. Comeau, E.A. Hessels. Phys. Rev. Lett. **93** 073401 (2004)
[6] C.H. Storry, A. Speck, D. Le Sage, N. Guise, G. Gabrielse, D. Grzonka, W. Oelert, G. Schepers, T. Sefzick, H. Pittner, M. Herrmann, J. Walz, T.W. Hänsch, D. Comeau, E.A. Hessels. Phys. Rev. Lett. **93** 63401 (2004)
[7] F. Goldenbaum, D. Grzonka, W. Oelert, T. Sefzick, Z. Zhang, Contribution in this annual report.

* ZAT, Research Center Jülich, Germany

Track reconstruction in the ATRAP-II experiment

F. Goldenbaum, D. Grzonka, W. Oelert, T. Sefzick, Z. Zhang
for the ATRAP-Collaboration

The ATRAP experiment at the CERN antiproton decelerator AD aims for a test of the CPT invariance by a high precision comparison of the 1s-2s transition between the hydrogen and the antihydrogen atom [1]. The experimental studies at ATRAP are performed at two separate installations, ATRAP-I, a system with severe space limitation, where routinely antihydrogen was produced [2], [3] and ATRAP-II, which will go into full operation during the year 2006. ATRAP-II includes a much larger superconducting solenoid bore allowing the installation of an extended detection system as well as an optimized combined magnetic/Penning trap. The antihydrogen annihilation detector system consists of 10 layers of scintillating fibres, grouped in 3 detector rings. Each detector ring contains 2 layers straight fibers to get the coordinates perpendicular to the magnetic field and in addition the inner and outer detector rings include helical fibers for the axial coordinates. With this diagnostic element the annihilation vertex of the antiprotons will be determined which allows to optimize the production of cold antihydrogen.

A reliable Monte Carlo simulation is essentially important both for detector design and physics analysis. In order to take advantages of the powerful physics processes and modern software engineering, the main framework of the ATRAP-II simulation package is developed using Geant4 simulation tool-kit and the Object-Oriented C++ language. Extensive Monte Carlo simulations concerning the track reconstruction have been performed using this developed simulation package. Some crucial parameters such as the average charged primary meson multiplicity and the energy loss of charged particles in the scintillating fiber are studied [4].

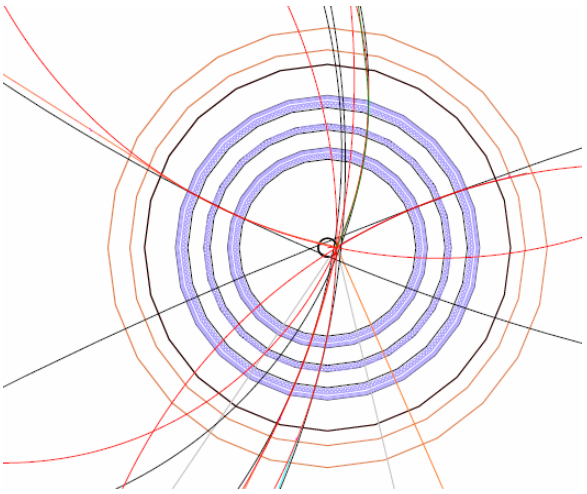

Fig. 1: Typical simulated event of antiproton annihilation on the gold plated trap wall within a 3 T magnetic field. Non-constrained fitting tracks (black curves) and Constrained fitting tracks (red curves) are also shown.

Fig. 1 shows an example of a typical simulated event of antiproton annihilation on a nucleus of the trap wall in a 3 Tesla magnetic field. Antiproton annihilations produce a large amount of charged and neutral particles due to secondary interactions. The tracks of high energy charged primary particles which pass through all three detector rings have to be identified. The three coordinates in radial direction allow to fit a circle to determine the track in the plane perpendicular to the magnetic field and with the two coordinates in axial direction the full track in 3 dimension is determined. From the intersection of two or more charged tracks, the annihilation “vertex” can be deduced.

To improve the position resolution, a constraint-fit procedure was adopted. All primary tracks from the antiproton annihilation have to start in a common space point which was fixed to lie at the trap wall. As shown in fig. 2, this fit procedure results in a vertex position resolution of about 6 mm FWHM. The backward rise toward 25 mm distance results from a misidentification of the vertex point nearly opposite to its origin. Since 100,000 input annihilations result in 4485 reconstructed events, the efficiency is as low as only 4.5%. This is due to the condition used that each particle track has to produce a signal in at least 5 of the 6 straight layers. Relaxing this strong condition would increase the efficiency by decreasing the spacial resolution. Further possible improvements by applying certain cuts on the Monte Carlo event samples are presently studied.

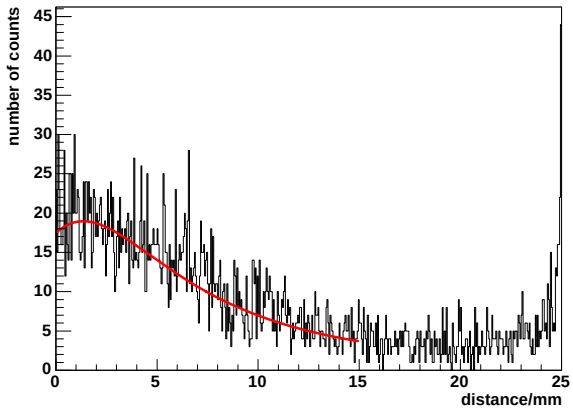

Fig. 2: Distribution of the distance between original and reconstructed vertices following 100,000 input events and 4485 resulting entries.

References:

[1] ATRAP Proposal, CERN-SPSC 97-8/P306
[2] G. Gabrielse et al., Phys. Rev. Lett., 89, 213401 (2002)
[3] G. Gabrielse et al., Phys. Rev. Lett., 89, 233401 (2002)
[4] Z. Zhang et al., AIP Conference Proceedings Vol. 796, 417-420 (2005)

2 Theoretical Physics

2.1 Hadron Structure and dynamics

Near threshold enhancement of the $p\bar{p}$ mass spectrum in J/Ψ decay

A. Sibirtsev, J. Haidenbauer, S. Krewald, Ulf-G. Meißner, A.W. Thomas (Jlab)

We investigate the nature of the near-threshold enhancement in the $p\bar{p}$ invariant mass spectrum of the reaction $J/\Psi \to \gamma p\bar{p}$ reported recently by the BES Collaboration. Using the Jülich $N\bar{N}$ model we show that the mass dependence of the $p\bar{p}$ spectrum close to the threshold can be reproduced by the S-wave $p\bar{p}$ final state interaction in the isospin I=1 state within the Watson-Migdal approach. However, because of our poor knowledge of the $N\bar{N}$ interaction near threshold and of the $J/\Psi \to \gamma p\bar{p}$ reaction mechanism and in view of the controversal situation in the decay $J/\Psi \to \pi^0 p\bar{p}$, where no obvious signs of a $p\bar{p}$ final state interaction are seen, explanations other than final state interactions cannot be ruled out at the present stage. The results are published in Ref. [1].

References:

[1] A. Sibirtsev, J. Haidenbauer, S. Krewald, U.-G. Meißner and A. W. Thomas, Phys. Rev. D **71**, 054010 (2005) [arXiv:hep-ph/0411386].

Analysis of Θ^+ production in $K^+ - Xe$ collisions

A. Sibirtsev, J. Haidenbauer, S. Krewald, Ulf-G. Meißner

The reaction $K^+Xe \to K^0pX$ is investigated in a meson-exchange model including rescattering of the secondary protons with the aim to analyze the evidence for the $\Theta^+(1540)$ resonance reported by the DIANA collaboration. We confirm that the kinematical cuts introduced by the DIANA collaboration efficiently suppress the background to the $K^+n \to K^0p$ reaction which may contribute to the $\Theta^+(1540)$ production. We find that these kinematical cuts do not produce a narrow structure in the K^0p effective mass spectra near 1540 MeV. We study the effect of a narrow Θ^+ resonance of both positive and negative parity in comparison with the DIANA data. We show that the $K^+Xe \to K^0pX$ calculations without Θ^+ contribution as well as the results obtained with a Θ^+ width of 1 MeV are in comparably good agreement with the DIANA results. More dedicated experiments are called for to establish this exotic baryon resonance. The results are published in Ref. [1]

References:

[1] A. Sibirtsev, J. Haidenbauer, S. Krewald and U.-G. Meißner, Eur. Phys. J. A **23**, 491 (2005) [arXiv:nucl-th/0407011].

Parity nonconserving observables in thermal neutron capture on a proton

C. H. Hyun (Seoul), S. J. Lee (Seoul), J. Haidenbauer, S. W. Hong (Seoul)

We calculate parity nonconserving observables in the processes where a neutron is captured on a proton at the threshold energy radiating a photon. Various potential models such as Paris, Bonn and Argonne $v18$ are used for the strong interactions, and the meson-exchange description is employed for the weak interactions between hadrons. The photon polarization P_γ in the unpolarized neutron capture process and photon asymmetry A_γ in the polarized neutron capture process are obtained in terms of the weak meson-nucleon coupling constants. A_γ turns out to be basically insensitive to the employed strong interaction models and thus can be uniquely determined in terms of the weak coupling constants, but P_γ depends significantly on the strong interaction models. The results are published in Ref. [1]

References:

[1] C. H. Hyun, S. J. Lee, J. Haidenbauer and S. W. Hong, Eur. Phys. J. A **24**, 129 (2005) [arXiv:nucl-th/0411102].

Resonances and final state interactions in the reaction pp→pK$^+\Lambda$

A. Sibirtsev, J. Haidenbauer, H.-W. Hammer (Bonn) and S. Krewald

A study of the strangeness production reaction $pp \to pK^+\Lambda$ for excess energies of $\epsilon \leq 150$ MeV, accessible at high-luminosity accelerator facilities like COSY, is presented. Methods to analyze the Dalitz plot distribution and angular spectra in the Jackson and helicity frames are worked out and suitable observables for extracting information on low lying resonances that couple to the $K\Lambda$ system and for determining the Λp effective-range parameters from the final state interaction are identified and discussed. Furthermore, the chances for identifying the reaction mechanism of strangeness production are investigated. The results are available at Ref. [1].

References:

[1] A. Sibirtsev, J. Haidenbauer, H.-W. Hammer and S. Krewald, arXiv:nucl-th/0512059.

Interaction of slow J/Ψ and Ψ' with nucleons.

A. Sibirtsev, M.B. Voloshin (Minnesota U.)

The interaction of the charmonium resonances J/Ψ and Ψ' with nucleons at low energies is considered using the multipole expansion and low-energy theorems in QCD. A lower bound is established for the relevant gluonic operator average over the nucleon. As a result we find the discussed interaction to be significantly stronger than previously estimated in the literature. In particular we conclude that the cross section of the J/Ψ-nucleon elastic scattering at the threshold is very likely to exceed 17 mb and that existence of bound states of the J/Ψ in light nuclei is possible. For the Ψ' resonance we estimate even larger elastic scattering cross section and also a very large cross section of the process $\Psi'+N\to\Psi+N$ giving rise to the decay width of tens of MeV for the Ψ' resonance in heavy nuclei. The results are published in Ref. [1].

References:

[1] A. Sibirtsev, M.B. Voloshin, Phys. Rev. D **71** (2005) 076005 [hep-ph/0502068].

The Fubini-Furlan-Rosetti sum rule and related aspects in light of covariant baryon chiral perturbation theory

V. Bernard (Strasbourg), B. Kubis (Bonn), Ulf-G. Meißner

We analyze the Fubini-Furlan-Rosetti sum rule in the framework of covariant baryon chiral perturbation theory to leading one–loop accuracy and including next-to-leading order polynomial contributions. We discuss the relation between the subtraction constants in the invariant amplitudes and certain low-energy constants employed in earlier chiral perturbation theory studies of threshold neutral pion photoproduction of nucleons. In particular, we consider the corrections to the sum rule due to the finite pion mass and show that below the threshold they agree well with determinations based on fixed-t dispersion relations. We also discuss the energy dependence of the electric dipole amplitude E_{0+}. These results are published in Ref. [1].

References:

[1] V. Bernard, B. Kubis and U.-G. Meißner, Eur. Phys. J. A **25** (2005) 419 [arXiv:nucl-th/0506023].

$K\bar{K}$ photoproduction from protons

A. Sibirtsev (Bonn), J. Haidenbauer, S. Krewald, Ulf-G. Meißner and A. W. Thomas (Jefferson Lab)

we study the contribution of the Drell mechanism driven by K^+ and K^- exchange to the reaction $\gamma N \to K\bar{K}N$. Our calculation implements the full KN and $\bar{K}N$ reaction amplitudes in the form of partial wave amplitudes taken from a meson-exchange model (KN) and a partial wave analysis ($\bar{K}N$), respectively. Comparing our results to data of the LAMP2 collaboration we observe that the Drell mechanism alone cannot describe the large $\Lambda(1520)$ photoproduction rate observed experimentally. We argue that the discrepancy could be due to significant contributions from K^*-meson exchange with subsequent excitation of the $\Lambda(1520)$ resonance. After adding such contributions to our model a good agreement of the LAMP2 experiment is achieved. When applying the same model to the recent SAPHIR data we find an excellent description of the K^+p spectrum and can determine the parameters of the $\Lambda(1600)$ P_{01} resonance, $M_R = 1617 \pm 2\,\mathrm{MeV}$ and $\Gamma_R = 117 \pm 4\,\mathrm{MeV}$, from the K^-p mass distribution. These results [1] are submitted for publication.

References:

[1] A. Sibirtsev, J. Haidenbauer, S. Krewald, U.-G. Meißner and A. W. Thomas, arXiv:hep-ph/0509145.

Novel evaluation of the two-pion contribution to the nucleon isovector form factors

M. A. Belushkin (Bonn), H.-W. Hammer (Bonn) and Ulf-G. Meißner

We calculate the two-pion continuum contribution to the nucleon isovector spectral functions drawing upon the new high statistics measurements of the pion form factor by the CMD-2, KLOE, and SND collaborations. The general structure of the spectral functions remains unchanged, but the magnitude increases by about 10%. Using the updated spectral functions, we calculate the contribution of the two-pion continuum to the nucleon isovector form factors and radii. We compare the isovector radii with simple ρ-pole models and illustrate their strong underestimation in such approaches. Moreover, we give a convenient parametrization of the result for use in future form factor analyses. These results are published in Ref. [1].

References:

[1] M. A. Belushkin, H. W. Hammer and U.-G. Meißner, Phys. Lett. B **633** (2006) 507 [arXiv:hep-ph/0510382].

Aspects of ϕ-meson production in proton-proton collisions

A. Sibirtsev (Bonn), J. Haidenbauer, Ulf-G. Meißner

We analyze near threshold data for the reaction $pp \to pp\phi$ published by the DISTO collaboration and the data recently presented by the ANKE Collaboration as a preliminary results. We formulate a procedure to evaluate the OZI ratio at low energies taking into account kinematical and final-state interaction corrections. Combining the new data with the few measurements available at higher energies we give a limit for OZI rule violation and estimate the possible contribution from five-quark baryonic resonances coupled to the ϕp system. These results [1] are submitted for publication.

References:

[1] A. Sibirtsev, J. Haidenbauer and U.-G. Meißner, arXiv:hep-ph/0512055.

Baryon octet masses, chiral extrapolations and all

M. Frink (Bonn), Ulf-G. Meißner and I. Scheller (Bonn)

We calculate the baryon octet masses to fourth order in chiral perturbation theory employing dimensional and cut-off regularization. We analyze the pion and kaon mass dependences of the baryon masses based on the MILC data. We show that chiral perturbation theory gives stable chiral extrapolation functions for pion (kaon) masses below 550 (600) MeV. The results are published in Ref. [1].

References:

[1] M. Frink, U.-G. Meißner and I. Scheller, Eur. Phys. J. A **24** (2005) 395 [arXiv:hep-lat/0501024].

Chiral extrapolations and the covariant small scale expansion

V. Bernard (Strasbourg), T. R. Hemmert (München), Ulf-G. Meißner

We calculate the nucleon and the delta mass to fourth order in a covariant formulation of the small scale expansion. We analyze lattice data from the MILC collaboration and demonstrate that the available lattice data combined with our knowledge of the physical values for the nucleon and delta masses lead to consistent chiral extrapolation functions for both observables up to fairly large pion masses. This holds in particular for very recent data on the delta mass from the QCDSF collaboration. The resulting pion-nucleon sigma term is $\sigma_{\pi N} = 48.9$ MeV. This first quantitative analysis of the quark-mass dependence of the structure of the $\Delta(1232)$ in full QCD within chiral effective field theory suggests that (the real part of) the nucleon-delta mass-splitting in the chiral limit, $\Delta_0 = 0.33\,\mathrm{GeV}$, is slightly larger than at the physical point. Further analysis of *simultaneous* fits to nucleon and delta lattice data are needed for a precision determination of the properties of the first excited state of the nucleon. These results are published in Ref. [1].

References:

[1] V. Bernard, T. R. Hemmert and U.-G. Meißner, Phys. Lett. B **622** (2005) 141 [arXiv:hep-lat/0503022].

Quark mass dependence of baryon properties

Ulf-G. Meißner

I discuss the quark mass dependence of various baryon properties derived from chiral perturbation theory. Such representations can eventually be used as chiral extrapolation functions when lattice data at sufficiently small quark masses become available. The quark mass dependence is encoded in loop and contact term contributions, the latter given in terms of low-energy constants. I stress the importance of utilizing phenomenological input to constrain a certain class of low-energy constants and discuss the ensuing theoretical uncertainty for various baryon observables, like the nucleon and the baryon octet masses, the nucleon isovector anomalous magnetic moment and the axial-vector coupling of the nucleon. I stress the role of resonance decoupling and present first results for the delta mass based on an effective field theory in which the nucleon-delta mass splitting is counted as a small parameter. I also discuss breifly the pion mass dependence of the nuclear force as derived from chiral nuclear effective field theory. These results are published in Ref. [1].

References:

[1] U.-G. Meißner, PoS **LATT2005** (2005) 009 [arXiv:hep-lat/0509029].

The pion-nucleon scattering lengths from pionic deuterium

Ulf-G. Meißner, U. Raha (Bonn) and A. Rusetsky (Bonn)

We use the framework of effective field theories to discuss the determination of the S-wave πN scattering lengths from the recent high-precision measurements of pionic deuterium observables. The theoretical analysis proceeds in several steps. Initially, the precise value of the pion-deuteron scattering length $a_{\pi d}$ is extracted from the data. Next, $a_{\pi d}$ is related to the S-wave πN scattering lengths a_+ and a_-. We discuss the use of this information for constraining the values of these scattering lengths in the full analysis, which also includes the input from the pionic hydrogen energy shift and width measurements, and throughly investigate the accuracy limits for this procedure. In this paper, we also give a detailed comparison to other effective field theory approaches, as well as with the earlier work on the subject, carried out within the potential model framework. These results are published in Ref. [1].

References:

[1] U.-G. Meißner, U. Raha and A. Rusetsky, Eur. Phys. J. C **41** (2005) 213 [arXiv:nucl-th/0501073] and erratum, Eur. Phys. J. C, in print.

Isospin-breaking corrections in the pion-deuteron scattering length

Ulf-G. Meißner, U. Raha (Bonn) and A. Rusetsky (Bonn)

It is shown that isospin-breaking corrections to the pion-deuteron scattering length can be very large, because of the vanishing of the isospin-symmetric contribution to this scattering length at leading order in chiral perturbation theory. We further demonstrate that these corrections can explain the bulk of the discrepancy between the recent experimental data on pionic hydrogen and pionic deuterium. We also give the first determination of the electromagnetic low-energy constant f_1. These results [1] are submitted for publication.

References:

[1] U.-G. Meißner, U. Raha and A. Rusetsky, arXiv:nucl-th/0512035.

OZI violation in photoproduction

A. Sibirtsev (Bonn), Ulf-G. Meißner and A. W. Thomas (Jefferson Lab)

We investigate OZI rule violation in ω and ϕ-meson photoproduction off nucleons. Data on the total cross sections indicate a large ϕ/ω ratio of about 0.8 at the maximal available photon energy that is in good agreement with expectations from QCD. On the other hand, data at large four momentum transfer exhibit a ratio of about 0.07, showing that the perturbative QCD regime is not approached at $|t|>2$ GeV^2 and photon energies $E_\gamma<4$ GeV. The anomanously large ϕ/ω ratio at low energies, that is close to the reaction threshold, remains to be explained within nonperturbative QCD. These results are published in Ref. [1].

References:

[1] A. Sibirtsev, U.-G. Meißner and A. W. Thomas, Phys. Rev. D **71** (2005) 094011 [arXiv:hep-ph/0503276].

Soft-core meson-baryon interactions. II. πN and K^+N scattering

H. Polinder and Th. A. Rijken (Nijmegen, The Netherlands)

The πN potential includes the t-channel exchanges of the scalar mesons σ and f_0, vector meson ρ, tensor mesons f_2 and f_2' and the Pomeron as well as the s- and u-channel exchanges of the nucleon N and the resonances Δ, Roper, and S_{11}. These baryonic resonances are not generated dynamically. We consider them, at least partially, as genuine three-quark states, and we treat them in the same way as the nucleon. The Roper and S_{11} resonances were needed to find the proper behavior of the phase shifts at higher energies in the corresponding partial waves. The soft-core πN model gives an excellent fit to the empirical πN S- and P-wave phase shifts up to $T_{\rm lab} = 600$ MeV. Also, the scattering lengths have been reproduced well, and the soft-pion theorems for low-energy πN scattering are satisfied. The soft-core model for the K^+N interaction is an $\mathrm{SU}_f(3)$ extension of the soft-core πN model. The K^+N potential includes the t-channel exchanges of the scalar mesons a_0, σ, and f_0, vector mesons ρ, ω, and ϕ, tensor mesons a_2, f_2, and f_2' and the Pomeron as well as u-channel exchanges of the hyperons Λ, Σ, $\Sigma(1385)$, and $\Lambda(1405)$. The fit to the empirical K^+N S-, P-, and D-wave phase shifts up to $T_{\rm lab} = 600$ MeV is reasonable and certainly reflects the present state of the art. Since the various K^+N phase shift analyses are also not very consistent, scattering observables are also compared with the soft-core K^+N model. A good agreement for the total and differential cross sections as well as the polarizations is found.
The results are published in Ref. [1].

References:

[1] H. Polinder and Th. A. Rijken, Phys. Rev. C **72**, 065211 (2005) [arXiv:nucl-th/0505083].

Soft-core meson-baryon interactions. I. One-hadron-exchange potentials

H. Polinder and Th. A. Rijken (Nijmegen, The Netherlands)

The Nijmegen soft-core model for the pseudoscalar meson-baryon interaction is derived, analogous to the Nijmegen NN and YN models. The interaction Hamiltonians are defined and the resulting amplitudes for one-meson exchange and one-baryon exchange in momentum space are given for the general mass case. The partial wave projection is carried through and explicit expressions for the momentum space partial wave meson-baryon potentials are presented. The results are published in Ref. [1].

References:

[1] H. Polinder and Th. A. Rijken, Phys. Rev. C **72**, 065210 (2005) [arXiv:nucl-th/0505082].

Analysis of the reaction $\gamma p \to \eta' p$

K. Nakayama[1,2] and H. Haberzettl[2,3]

The recent high-precision data for the reaction $\gamma p \to p\eta'$ at photon energies in the range 1.5–2.3 GeV obtained by the CLAS collaboration at the Jefferson Laboratory [1] have been analyzed [3] within an extended version of the photoproduction model developed previously by the authors based on a relativistic meson-exchange model of hadronic interactions [2]. As shown in Fig. 1, the η' photoproduction can be described quite well over the entire energy range of available data by considering S_{11}, P_{11}, P_{13}, and D_{13} resonances, in addition to the t-channel mesonic currents. The observed angular distribution is due to the interference between the t-channel and the nucleon s- and u-channel resonance contributions. The $j = 3/2$ resonances are required to reproduce some of the details of the measured angular distribution. For the resonances considered, our analysis yields mass values compatible with those advocated by the Particle Data Group [4]. We emphasize, however, that cross-section data alone are unable to pin down the resonance parameters and it is shown that the beam and/or target asymmetries impose more stringent constraints on these parameter values. It is found that the nucleonic current is relatively small and that the $NN\eta'$ coupling constant is not expected to be much larger than 2. Details of our analysis can be found in Ref.[3].

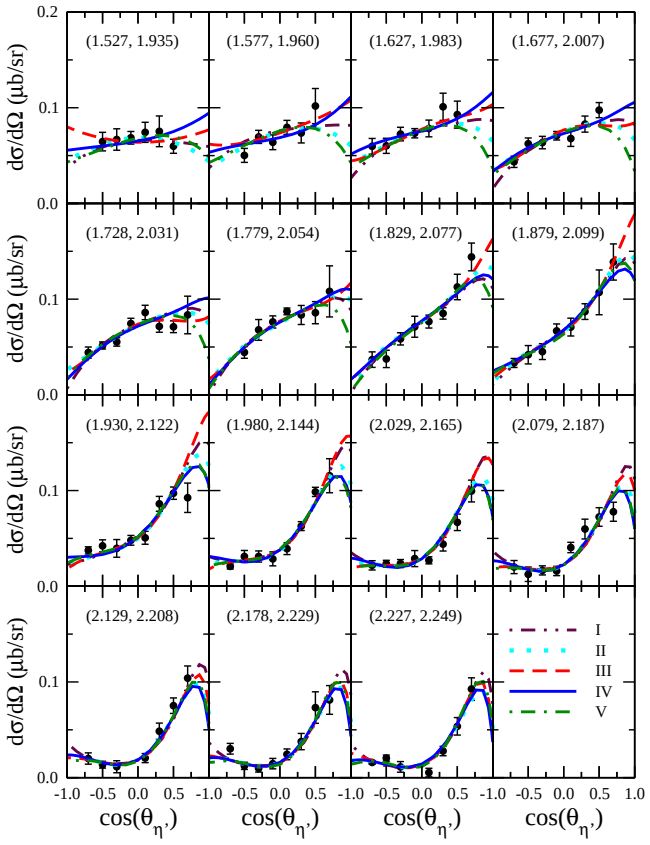

Fig. 1: Comparison of the model results for the differential cross section for $\gamma p \to p\eta'$. The numbers (T_γ, W) in parentheses are the incident photon energy T_γ and the corresponding s-channel energy $W = \sqrt{s}$, respectively, in GeV. The various curves represent different parameter sets of the model. The data are from Ref. [1].

References:

[1] M. Dugger *et al.* (CLAS collaboration), nucl-ex/0512019.
[2] K. Nakayama and H. Haberzettl, Phys. Rev. C **69**, 065212 (2004).
[3] K. Nakayama and H. Haberzettl, nucl-th/0507044.
[4] S. Eidelman et al., Phys. Lett.**B 592**, 1 (2004).

1. Department of Physics and Astronomy, University of Georgia, Athens, GA 30602, USA
2. Institut für Kernphysik (Theorie), Forschungszentrum Jülich, D-52425 Jülich, Germany
3. Center for Nuclear Studies, Department of Physics, The George Washington University, Washington, DC 20052, USA

Gauge-invariant approach to meson photoproduction including the final-state interaction

H. Haberzettl[1,2], K. Nakayama[2,3] and S. Krewald[2]

Photoproduction of mesons off nucleons has been studied for many years since the pioneering work by Chew, Goldberger, Low, and Nambu on pion production [1]. The major purpose of studying such a reaction is to learn about the nucleon excited states. In order to extract accurate information on nucleon resonances, such a study requires, in addition to precise and extensive measurements, a reliable reaction theory which allows us to disentangle the resonance contribution from the background contribution to the observables. There are a number of different approaches to describe meson photoproduction reactions, ranging from Chiral Perturbation Theory to three level Effective Lagrangian to K-matrix to dynamical model approaches. The present work concerns the latter approach. More specifically, we concentrate on the dynamical model approach within meson-exchange models of hadronic interactions. This approach requires the introduction of the so-called form factors at hadronic vertices which account, among other things, for the composite nature of hadrons. At present, the lack of a theoretical understanding of these vertex form factors forces us to introduce phenomenological form factors - usually parameterized in terms of a monopole or dipole form - whose parameters are adjusted to fit the data. The presence of such form factors spoils gauge invariance of the photoproduction amplitude. Furthermore, the presence of the final state interaction (FSI) poses an additional difficulty in preserving gauge invariance of the total amplitude, since the construction of the interaction current consistent with the FSI requires the knowledge of the underlying structure, a requirement that is impossible to be fulfilled in a approach where phenomenological form factors are introduced. Therefore, within such an approach, one proceeds to find a prescription for ensuring gauge invariance of the reaction amplitude. Such a prescription, however, is not unique and therefore it requires to find one that works best in reproducing the data. We emphasize that this is an unavoidable procedure within such a phenomenological approach. Indeed, there are a number of prescriptions which have been applied in the photoproduction as well as in electroproduction reactions.

However, most of the existing calculations based on phenomenological dynamical models are actually not gauge invariant. In fact, they revert to a variety of *ad hoc* recipies for the sole purpose of enforcing current conservation, but not the gauge-invariance condition expressed by the generalized Ward–Takahashi (WT) identity [2, 3, 4]

$$\begin{aligned} k_\mu M^\mu \quad &= -[F_s\tau]S_{p+k}Q_iS_p^{-1} + S_{p'}^{-1}Q_fS_{p'-k}[F_u\tau] \\ &\quad + \Delta^{-1}_{p-p'+k}Q_\pi\Delta_{p-p'}[F_t\tau] \ , \end{aligned} \tag{1}$$

which is an *off-shell* condition. In the above equation, p and k are the four-momenta of the incoming nucleon and photon, respectively, and p' and q are the four-momenta of the outgoing nucleon and pion, respectively, related by momentum conservation $p'+q=p+k$. S and Δ are the propagators of the nucleons and pions, respectively, with their subscripts denoting the available four-momentum for the corresponding hadron; Q_i, Q_f, and Q_π are the initial and final nucleon and the pion charge operators, respectively. The index x at $[F_x\tau]$ labels the appropriate kinematic situation for πNN vertex in the s-, u-, or t-channel diagrams.

In the present work, we construct a photoproduction amplitude based on the field-theoretical approach given by Haberzettl [4]. The full formalism is gauge-invariant as a matter of course. However, in view of its complexity and high nonlinearity, its practical implementations require that some reaction mechanisms need to be truncated and/or replaced by phenomenological approximations. Our objective here is to preserve full gauge invariance, in the sense of Eq. (1), for this approximate treatment, but allowing for the presence of explicit hadronic FSIs. The resulting amplitude can be written as

$$M^\mu = M_s^\mu + M_u^\mu + M_t^\mu + M_{int}^\mu \ , \tag{2}$$

where the first three terms describe the coupling of the photon to external legs of the underlying πNN vertex (with subscripts s, u, and t referring to the appropriate Mandelstam variables of their respective intermediate hadrons). They are usually referred to as the s-, u- and t-channel diagrams, respectively. These terms are relatively straightforward and easy to implement in a practical application. However, the last term, the interaction current M_{int}^μ, where the photon couples inside the vertex, explicitly contains the hadronic FSI; its structure is, therefore, more complex than that of any of the first three terms. The approximated interaction current, which respects gauge invariance in the sense of Eq. (1) reads [5]

$$M_{int}^\mu = M_c^\mu + T^\mu + XG_0\left[(M_u^\mu - m_u^\mu) + (M_t^\mu - m_t^\mu) + T^\mu\right] , \tag{3}$$

where M_c^μ can be *any* contact current satisfying

$$k_\mu M_c^\mu = -F_s e_i + F_u e_f + F_t e_\pi \tag{4}$$

and T^μ is an undetermined transverse *contact* current that is unconstrained by Eq. (1). X denotes the meson-nucleon FSI and G_0, the meson-nucleon propagator. m_u^μ and m_t^μ stand for the longitudinal part of M_u^μ and M_t^μ, respectively. The operators $e_i = \tau Q_i$, $e_f = Q_f\tau$ and $e_\pi = Q_\pi\tau$ describe the respective hadronic charges in an appropriate isospin basis. Charge conservation for the meson production process simply reads $e_i = e_f + e_\pi$. The explicit form of M_c^μ adopted in our approach may be found in [5]. In this scheme, therefore, the choice one makes for M_c^μ (and T^μ) corresponds to an implicit approximation of the full dynamics contained in the interaction current. Moreover, beyond this actual choice, the only explicit effect of the FSI X is from explicitly *transverse* loop contributions.

As an example of the present approach, Fig. 1 shows the total cross section result for the reaction $\gamma + p \to \pi^0 + p$ from the threshold up to $T_\gamma \approx 400$ MeV. As we can see, the agreement with the data is very good except for energies above $T_\gamma \sim 360$ MeV, where the prediction tends to underestimate the data. In particular, around $T_\gamma \approx 390$ MeV, the discrepancy is about 10%. We also see that the FSI loop contribution is relatively small compared to the Born contribution. However, it plays a crucial role in reproducing the observed energy dependence through its interference with the dominant Born term.

References:

[1] G. F. Chew, M. L. Goldberger, F. E. Low, and Y. Nambu, Phys. Rev. **106**, 1345 (1957).

Pentaquark $\Theta^+(1540)$ production in $\gamma N \to K\overline{K}N$ Reactions

Kanzo Nakayama*, Yongseok Oh*, and T.-S. H. Lee**

The production of putative pentaquark state, $\Theta(1540)$, has been attracted much attention in hadron physics [1, 2]. (For a brief review, see Ref. [3].) In this research, we have investigated the production of such an exotic state in the reaction of $\gamma N \to K\bar{K}N$ [3]. We focus on the study of how the exotic pentaquark $\Theta(1540)$ baryon production can be identified in the $\gamma N \to K\overline{K}N$ reactions, paying attention to the influence of the background (non-Θ production) mechanisms. Our background production mechanisms include the so-called t-channel Drell diagrams, $K\overline{K}$ production through the intermediate vector meson and tensor meson photoproduction, and the mechanisms involving intermediate baryons (mostly hyperons). By imposing flavor SU(3) symmetry and using various quark model predictions as well as available experimental data, we are able to fix the coupling constants for evaluating the backgrounds.

The vector meson photoproduction part, especially ϕ meson photoproduction background, is known to be very important as it can contribute to the reaction via $\gamma N \to VN \to K\bar{K}N$. This part is calculated from a phenomenological model which describes well the experimental data at low energies. The model we use includes the Pomeron exchange, pseudoscalar meson and tensor meson exchanges as well as the nucleon terms, which is known to be successful to describe the total cross sections and differential cross sections at forward scattering angles of vector meson (ρ, ω, ϕ) photoproduction [4, 5].

Tensor meson photoproduction can also contribute via $\gamma N \to TN \to K\bar{K}N$ and its importance was anticipated as the kinematic region of $\gamma N \to K\bar{K}N$ at low energies covers the physical region of several tensor mesons, $a_2(1320)$ and $f_2(1275)$. Furthermore, it was claimed that the observed Θ peak in the reaction of $\gamma N \to K\bar{K}N$ might be a false peak coming from the tensor meson photoproduction background [6]. We first point out that the neutral tensor meson production can not be due to π^0-exchange as done by Dzierba *et al.* [6] because of C parity. The neutral tensor meson production is estimated by considering the vector meson exchange and found to be too weak to generate any peak at the position near $\Theta(1540)$. Therefore, any peak in the KN invariant mass distribution, if confirmed, can hardly come from the kinematic reflection.

Finally, for the hyperon backgrounds, $\gamma N \to KY \to K\bar{K}N$, we consider $\Lambda(1116)$, $\Lambda(1405)$, $\Lambda(1520)$, $\Sigma(1193)$, and $\Sigma(1385)$ states as the intermediate Y state. We also consider the photo-transition of $\Delta \leftrightarrow N\gamma$ as a background of $\gamma N \to \Delta N \to KY \to K\bar{K}N$ (and the crossed diagram). The couplings are estimated from the decay widths if the experimental data are available. If there is no experimental data or the data are not precise enough, we rely on the quark model predictions. We have verified that the intermediate $\Lambda(1520)$ is the most important background (with the ϕ meson background) in $\gamma N \to K\bar{K}N$ as expected.

Since $\Theta(1540)$ has strangeness $+1$, its minimal quark content must include $q^4\bar{q}$. The quark model then states that there can be pentaquarks in the flavor multiplets of **1**, **8**, **10**, $\overline{\mathbf{10}}$, **27**, and **35** [7]. The Θ particles which have strangeness $+1$ can then take isospin 0 (in $\overline{\mathbf{10}}$), 1 (in **27**), and 2 (in **35**). For $\Theta(1540)$ production, we assume that it is an isoscalar

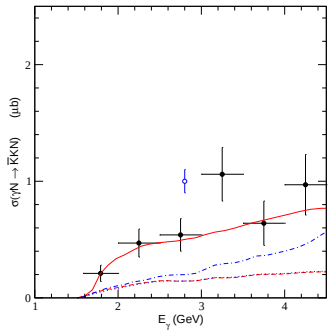

Fig. 1: Total cross sections for $\gamma N \to K\bar{K}N$ reactions. The solid line is for $\gamma p \to K^+K^-p$, dashed line for $\gamma p \to K^0\overline{K}^0 p$, dot-dashed line for $\gamma n \to K^+K^-n$, and dotted line for $\gamma n \to K^0\overline{K}^0 n$. The experimental data are for $\gamma p \to K^+K^-p$ reaction and from Ref. [9] ($\bullet$) and Ref. [10] ($\circ$). The dashed and dotted lines are close together and hard to be distinguished.

and hence can only be produced in $\gamma n \to K^+K^-n$ and $\gamma p \to K^0\overline{K}^0 p$ reactions, but not in $\gamma p \to K^+K^-p$ and $\gamma n \to K^0\overline{K}^0 n$. We also assume that it has spin-1/2 as the lowest state. The coupling of Θ with the kaon and the nucleon was estimated by assuming $\Gamma(\Theta) = 1$ MeV [8].

The form factors are included to regularize the vertices depending on the exchanged particles. The charge conservation condition is then recovered by employing the widely-used methods [11]. The cutoff parameters for vector meson and tensor meson photoproduction backgrounds are fixed by the data for meson production. The total cross section data of $\gamma p \to K^+K^-p$ is then used to fix the cut-off parameters of the intermediate baryon background amplitudes so that the signal of $\Theta(1540)$ in $\gamma n \to K^+K^-n$ and $\gamma p \to K^0\overline{K}^0 p$ cross sections can be predicted. The results are show in Fig. 1.

Then we compute the invariant mass distributions as well as the differential cross sections. We find that the predicted K^+K^- and K^+n invariant mass distributions of the $\gamma n \to K^+K^-n$ reaction can qualitatively reproduce the shapes of the JLab data. (Fig. 2) However, the predicted $\Theta(1540)$ peak can not be identified unambiguously with the data. High statistics experiments are needed to resolve the problem. We also find that an even-parity Θ is more likely to be detected, while it will be difficult to identify an odd-parity Θ, even if it exists, from the background continuum, if its coupling constants are small as in the present quark model predictions. The new measurements at CLAS [12] with higher statistics actually shows that the observed peak is not sharp enough and the upper limit of the cross section is suppressed, which leads to a doubt on the existence of $\Theta(1540)$.

References:

[1] LEPS Collaboration, T. Nakano *et al.*, Phys. Rev. Lett. **91**, 012002 (2003).
[2] CLAS Collaboration, S. Stepanyan *et al.*, Phys. Rev. Lett. **91**, 252001 (2003).
[3] Y. Oh, K. Nakayama, and T.-S. H. Lee, Phys. Rep. **423**, 49 (2006).

Nucleon resonances in $\pi N \to \omega N$

Yongseok Oh*, Kanzo Nakayama*, and T.-S. H. Lee**

The hadronic reactions $\pi N \to VN$, where V stands for a vector meson (ρ, ω, ϕ) have attracted much interest in understanding the hadron interactions at low energies. The existing experimental data can be hardly explained by simple t-channel vector meson exchanges and s- and u-channel nucleon terms only and the crucial contributions from the nucleon resonances are expected [1]. In addition, this reaction must be understood before we establish models for the final-state interactions (FSIs) of other reactions such as $\gamma N \to VN$ and $pp \to ppV$ [2], etc.

In this work we consider the reaction $\pi N \to \omega N$. This reaction has been studied by the Giessen group [3, 4], within a coupled channel approach in the K-matrix approximation. They included various channels below 2 GeV and all the model parameters are fixed by fitting the experimental data. In an effort to understand the essential underlying features of this reaction, we study it within a simple model by considering only two-channels, namely, πN and ωN channels. The full $\pi N \to \omega N$ transition amplitude can, then, be cast into the form

$$T_{21} \cong (1 + T_{22} G_2) V_{21} (1 + G_1 T_{11}), \qquad (1)$$

where the subscripts indicate the states as $1 \equiv \pi N$ and $2 \equiv \omega N$. Here, T_{ij} (V_{ij}) denotes the $j \to i$ transition amplitude (potential) and, G_i is the propagator of the intermediate state i. The right-most factor in the above equation corresponds to the πN initial state interaction (ISI), while the left-most factor to the ωN FSI. We use the empirical values of the πN phase-shifts and inelasticities from SAID for the πN ISI. The ωN FSI is included in the effective range approximation, whose scattering length and effective range are fitted to the available $\pi N \to \omega N$ data.

For the $\pi N \to \omega N$ transition potential, V_{21} in Eq. (1), we consider the t-channel ρ-meson exchange and the s- and u-channel nucleon contributions, in addition to the nucleon resonance contributions. The possible b_1 meson exchange was found to be suppressed in Ref. [5] and it is not considered in this calculation. We include the following nucleon resonances; $P_{11}(1440)$, $P_{11}(1710)$, $S_{11}(1535)$, $S_{11}(1650)$, $P_{13}(1720)$, $D_{13}(1520)$, $D_{13}(1700)$, $F_{15}(1680)$, and $D_{15}(1675)$. They are the 4-star or 3-star nucleon resonances listed in Particle Data Group with a mass lower than 2 GeV.

The total cross section results for the $\pi^- p \to \omega n$ reaction is shown in Fig. 1 together with the available data. Our calculation reveals the importance of the nucleon resonance contributions; in particular, the $D_{13}(1520)$ and $F_{15}(1680)$ resonances play a crucial role in reproducing the observed energy dependence. However, the nucleon resonances are not the only crucial ingredient in reproducing the observed feature of the cross section; in fact, the ωN FSI also plays a very important role. We found the averaged scattering length of $a = (0.5 - i\,0.1)$ fm and the effective range of $r_0 = 4$ fm for the F wave. (The effective range of the lower partial waves are suppressed.)

The results for the differential cross sections are shown in Fig. 2. Most of them can be understood by large contributions from the nucleon resonances, except in the very low energy region, where other contributions are relevant. A rather

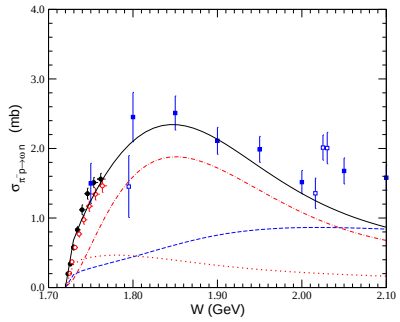

Fig. 1: Total cross section for $\pi^- p \to \omega n$ reaction. The dashed line is obtained without the nucleon resonances while the dotted and dot-dashed lines correspond to the contributions from $D_{13}(1520)$ and $F_{15}(1680)$ resonances, respectively. The solid line is the sum of all amplitudes considered in this work.

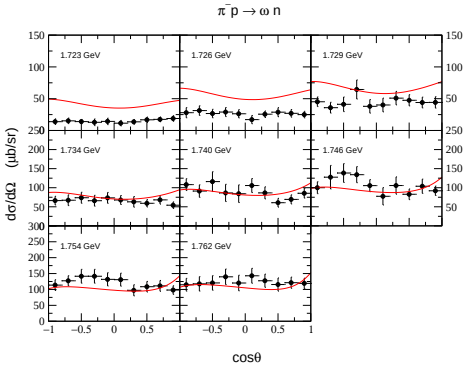

Fig. 2: Differential cross section for $\pi^- p \to \omega n$ reaction. The experimental data are from Ref. [1].

flat shape of the angular distributions is a result of the interference among various resonance contributions considered and not just the $D_{13}(1520)$ and $F_{15}(1680)$ resonances which dominate the total cross section.

A more detailed analysis of the total and differential cross sections is under progress and will soon be reported elsewhere.

References:

[1] H. Karami, J. Carr, N. C. Debenham, D. A. Garbutt, W. G. Jones, D. M. Binnie, J. Keyne, P. Moissidis, H. N. Sarma, and I. Siotis, Nucl. Phys. B **154**, 503 (1979).

[2] K. Tsushima and K. Nakayama, Phys. Rev. C **68**, 034612 (2003).

[3] G. Penner and U. Mosel, Phys. Rev. C **65**, 055202 (2002).

[4] V. Shklyar, H. Lenske, U. Mosel, and G. Penner, Phys. Rev. C **71**, 055206 (2005), **72**, 019903(E) (2005).

[5] Y. Oh and T.-S. H. Lee, Phys. Rev. C **66**, 045201 (2002).

Insights on scalar mesons from their radiative decays

Yu. Kalashnikova (Moscow), A. Kudryavtsev (Moscow), A. V. Nefediev (Moscow), J. Haidenbauer, C. Hanhart

We estimate the rates for radiative transitions of the lightest scalar mesons $f_0(980)$ and $a_0(980)$ to the vector mesons rho and omega. We argue that measurements of the radiative decays of those scalar mesons can provide important new information on their structure. The results are published in Ref. [1].

References:

[1] Y. Kalashnikova, A. Kudryavtsev, A. V. Nefediev, J. Haidenbauer and C. Hanhart, arXiv:nucl-th/0512028; Phys. Rev. C, in print.

The radiative decays $\phi \to \gamma a_0/f_0$ in the molecular model for the scalar mesons

Yu. Kalashnikova (Moscow), A. Kudryavtsev (Moscow), A. V. Nefediev (Moscow), J. Haidenbauer, C. Hanhart

We show on very general grounds that, contrary to earlier claims, the data on the radiative decays of ϕ mesons into scalars are compatible with a molecular nature of the light scalar mesons, in line with recent publications. We also show where the earlier analyses went wrong. The results are published in Ref. [1].

References:

[1] Y. Kalashnikova, A. Kudryavtsev, A. V. Nefediev, J. Haidenbauer and C. Hanhart, Eur. Phys. J. A **24** (2005) 437.

2.2 Nuclear forces and few body systems

Extraction of scattering lengths from final-state interactions

A. Gasparyan (Moscow), J. Haidenbauer, and C. Hanhart

A recently proposed method based on dispersion theory, that allows to extract the scattering length of a hadronic two-body system from corresponding final-state interactions, is generalized to the situation where the Coulomb interaction is present. The steps required in a concrete practical application are discussed in detail. In addition a thorough examination of the accuracy of the proposed method is presented and a comparison is made with results achieved with other methods like the Jost-function approach based on the effective-range approximation. Deficiencies of the latter method are pointed out. The reliability of the dispersion theory method for extracting also the effective range is investigated.

The results are published in Ref. [1].

References:

[1] A. Gasparyan, J. Haidenbauer, and C. Hanhart, Phys. Rev. C **72** (2005) 034006.

The $K^-\alpha$ scattering length and the reaction $dd \to \alpha K^+ K^-$

V. Yu. Grishina (Moscow), L.A. Kondratyuk (Moscow), A. Sibirtsev (Bonn), M. Büscher, S. Krewald, Ulf-G. Meißner and F. P. Sassen

We present first results for the the $K^-\alpha$ scattering length obtained within the framework of the multiple scattering approach. Evaluating the pole position of the $K^-\alpha$ scattering amplitude within the zero range approximation, we find a loosely bound $K^-\alpha$ state with a binding energy of $E_R = -2 \div -7$ MeV and a width $\Gamma_R = 11 \div 18$ MeV. We propose to measure the $K^-\alpha$ scattering length through the final state interaction between the α and K^--meson produced in the reaction $dd \to \alpha K^+ K^-$. It is found that the $K^-\alpha$ invariant mass distribution from this reaction at energies near the threshold provides a new tool to determine the s-wave $K^-\alpha$ scattering length. These results are published in Ref. [1].

References:

[1] V. Y. Grishina, L. A. Kondratyuk, A. Sibirtsev, M. Buscher, S. Krewald, U.-G. Meißner and F. P. Sassen, Eur. Phys. J. A **25** (2005) 159 [arXiv:nucl-th/0503076].

Isospin–violating nucleon–nucleon forces using the method of unitary transformation

E. Epelbaum (Jefferson Lab) and Ulf-G. Meißner

Recently, we have derived the leading and subleading isospin–breaking three–nucleon forces using the method of unitary transformation. In the present work we extend this analysis and consider the corresponding two–nucleon forces using the same approach. Certain contributions to the isospin–violating one– and two–pion–exchange potential have already been discussed by various groups within the effective field theory framework. Our findings agree with the previously obtained results. In addition, we present the expressions for the subleading charge–symmetry–breaking two–pion exchange potential which were not considered before. These corrections turn out to be numerically important. Together with the three–nucleon force results presented in our previous work, the results of the present study specify completely the isospin–violating nuclear force up to the order q^5/Λ^5. These results are published in Ref. [1].

References:

[1] E. Epelbaum and U.-G. Meißner, Phys. Rev. C **72** (2005) 044001 [arXiv:nucl-th/0502052].

The triton and three-nucleon force in nuclear lattice simulations

B. Borasoy (Bonn), H. Krebs (Bonn), D. Lee (North Carolina State Univ.), Ulf-G. Meißner

We study the triton and three-nucleon force at lowest chiral order in pionless effective field theory both in the Hamiltonian and Euclidean nuclear lattice formalism. In the case of the Euclidean lattice formalism, we derive the exact few-body worldline amplitudes corresponding to the standard many-body lattice action. This will be useful for setting low-energy coefficients in future nuclear lattice simulations. We work in the Wigner SU(4)-symmetric limit where the S-wave scattering lengths ${}^1S_0$ and ${}^3S_1$ are equal. By comparing with continuum results, we demonstrate for the first time that the nuclear lattice formalism can be used to study few-body nucleon systems. These results are published in Ref. [1].

References:

[1] B. Borasoy, H. Krebs, D. Lee and U.-G. Meißner, Nucl. Phys. A **768** (2006) 179 [arXiv:nucl-th/0510047].

Gauge invariance in two-particle scattering

B. Borasoy (Bonn), P. C. Bruns (Bonn), R. Nißler (Bonn) and Ulf-G. Meißner

It is shown how gauge invariance is obtained for the coupling of a photon to a two-body state described by the solution of the Bethe-Salpeter equation. This is illustrated both for a complex scalar field theory and for interaction kernels derived from chiral effective Lagrangians. These results are published in Ref. [1].

References:

[1] B. Borasoy, P. C. Bruns, U.-G. Meißner, and R. Nißler, Phys. Rev. C **72** (2005) 065201 [arXiv:hep-ph/0508307].

Towards a field theoretic understanding of $NN \to NN\pi$

V. Lensky, V. Baru (Moscow), J. Haidenbauer, C. Hanhart, A.E. Kudryavtsev (Moscow) and Ulf-G. Meißner

We study the production amplitude for the reaction $NN \to NN\pi$ up to next–to–leading order in chiral perturbation theory using a counting scheme that takes into account the large scale introduced by the initial momentum. In particular we investigate a subtlety that arises once the leading loop contributions are convoluted with the NN wavefunctions as demanded by the non–perturbative nature of the NN interaction. We show how to properly identify the irreducible contribution of loop diagrams in such type of reaction. The net effect of the inclusion of all next-to-leading ordr loops is to enhance the leading rescattering amplitude by a factor of 4/3, bringing its contribution to the cross section for $pp \to d\pi^+$ close to the experimental value. These results are published in Ref. [1].

References:

[1] V. Lensky, V. Baru, J. Haidenbauer, C. Hanhart, A. E. Kudryavtsev and U.-G. Meißner, Eur. Phys. J. A **27** (2006) 37 [arXiv:nucl-th/0511054].

The Jülich hyperon–nucleon model revisited

J. Haidenbauer and Ulf-G. Meißner

A one-boson-exchange model for the hyperon-nucleon (ΛN, ΣN) interaction is presented. The model incorporates the standard one boson exchanges of the lowest pseudoscalar and vector meson multiplets with coupling constants fixed by SU(6) flavor symmetry relations. As the main new feature of the model, the contributions in the scalar–isoscalar (σ) and vector–isovector (ρ) exchange channels are now constrained by a microscopic model of correlated $\pi\pi$ and $K\bar{K}$ exchange. Additional short-ranged ingredients of the model in the scalar–isovector (a_0) and scalar–isospin-1/2 (κ) channels are likewise viewed as arising from meson-meson correlations but are treated phenomenologically. With this model a satisfactory reproduction of the available hyperon-nucleon data can be achieved. These results are published in Ref. [1].

References:

[1] J. Haidenbauer and U.-G. Meißner, Phys. Rev. C **72** (2005) 044005 [arXiv:nucl-th/0506019].

The role of the nucleon recoil in low–energy meson–nucleus reactions

V. Lensky, V. Baru (Moscow), J. Haidenbauer, C. Hanhart, A.E. Kudryavtsev (Moscow) and Ulf-G. Meißner

The reaction $\gamma d \to \pi^+ nn$ was calculated up to order $\chi^{5/2}$ in chiral perturbation theory, where χ denotes the ratio of the pion to the nucleon mass. Special emphasis was put on the role of nucleon–recoil corrections that are the source of contributions with fractional power in χ. Using the known near threshold production amplitude for $\gamma p \to \pi^+ n$ as the only input, the total cross section for $\gamma d \to \pi^+ nn$ is described very well. A conservative estimate suggests that the theoretical uncertainty for the transition operator amounts to 3 % for the computed amplitude near threshold. The results are published in Ref. [1].

References:

[1] V. Lensky, V. Baru, J. Haidenbauer, C. Hanhart, A. E. Kudryavtsev and U.-G. Meißner, Eur. Phys. J. A **26** (2005) 107 [arXiv:nucl-th/0505039].

Spin observables of the reactions $NN \to \Delta N$ and $pd \to \Delta(pp)(^1S_0)$ in collinear kinematics

Yu.N. Uzikov (Dubna) and J. Haidenbauer

A general formalism for double and triple spin-correlations of the reaction $\vec{N}\vec{N} \to \vec{\Delta}N$ is developed for the case of collinear kinematics. A complete polarization experiment allowing to reconstruct all of the four amplitudes describing this process is suggested. Furthermore, the spin observables of the inelastic charge-exchange reaction $\vec{p}\vec{d} \to \vec{\Delta}^0(pp)(^1S_0)$ are analyzed in collinear kinematics within the single pN scattering mechanism involving the subprocess $pn \to \Delta^0 p$. The full set of spin observables related to the polarization of one or two initial particles and one final particle is obtained in terms of three invariant amplitudes of the reaction $pd \to \Delta(pp)(^1S_0)$ and the transition form factor $d \to (pp)(^1S_0)$. A complete polarization experiment for the reaction $\vec{p}\vec{d} \to \vec{\Delta}^0(pp)(^1S_0)$ is suggested which allows one to determine three independent combinations of the four amplitudes of the elementary subprocess $\vec{N}\vec{N} \to \vec{\Delta}N$. The results are available at Ref. [1].

References:

[1] Y. N. Uzikov and J. Haidenbauer, arXiv:nucl-th/0509023.

2.3 Nuclear structure

Electromagnetic strength of neutron and proton single- particle halo nuclei

S. Typel*, G. Baur

Light exotic nuclei are available as secondary beams at various radioactive beam facilities all over the world. These unstable nuclei are generally weakly bound with few, if any, bound excited states. Electromagnetic strength functions of halo nuclei are a low energy phenomenon and exhibit universal features that can be described in terms of a few characteristic parameters. For a nucleus with nucleon+core structure the reduced transition probability, as determined, e.g., by Coulomb dissociation experiments, shows a typical shape that depends on the nucleon separation energy and the orbital angular momenta in the initial and final states. In the case of neutron+core nuclei analytical results for the reduced transition probabilities are obtained by introducing an effective-range expansion. Many important features of the neutron halo case can be also obtained from a square well model. Rather simple analytical formulae are found. The nucleon-core interaction in the continuum affects the determination of astrophysical S factors at zero energy in the method of asymptotic normalisation coefficients (ANC). It is also relevant for the extrapolation of radiative capture cross sections to low energies. We expect that our model with its rather simple analytical results can serve as a good testing ground to investigate the validity of low energy expansions. The present work is published in [1], a detailed account, also with applications to proton halo nuclei is given in [2].

The most important parameter for halo nuclei is $\gamma = qR$, where q is related to the binding energy E_b by $E_b = \hbar^2 q^2/(2\mu)$ where μ is the reduced mass of the (A+n) system and R is the range of the (A+n) interaction. This parameter γ is small for halo nuclei with their large size $1/q$ and serves as a convenient expansion parameter. For low neutron energies we can use the effective range expansion for the phase shift. We restrict ourselves to the lowest order term, i.e.

$$tan(\delta_l) = -(xc_l\gamma)^{2l+1}$$

where $x = k/q$. The neutron wave number is k and c_l is a reduced scattering length which is treated as a free parameter and fitted to the experiment. We compare our approach to the Coulomb breakup data of ^{11}Be from GSI [3]. This nucleus shows a very pronounced halo structure with an $s_{1/2}$ -neutron bound by 504 keV. There is also a bound excited $p_{1/2}$-state at 320 keV excitation energy. Its presence is felt in the reduced scattering parameter $c_1^{1/2}$ which we extract [1] from the experimental results. In a square well potential with radius R the scattering length a_l ($l > 0$) is related to the bound state parameter q of a single neutron halo state in partial wave l by

$$a_l = \frac{2(2l-1)R^{2l-1}}{q^2(2l+1)!!(2l-1)!!}$$

The diffuseness of the Woods Saxon potential will modify this simple relation (or renormalize the value of R), the agreement to the result of [1] is satisfactory[4].

The present approach is also applied to the electromagnetic strength in the neutron rich isotope ^{23}O, which was recently studied at GSI [5].

In Fig.1 (Fig.21 of [2]) the reduced transition probability $dB(E1)/dE$ is shown as a function of the potential depth V_0 felt by the continuum particle. In the ANC method [6] the transition probability is calculated assuming that $V_0 = 0$. This figure shows the sensitivity of the transition probability (and hence also of the astrophysical S-factor) to the strength of the interaction in the continuum.

Due to the increasing Coulomb barrier, proton halo nuclei will tend to become less important for heavier nuclei. The halo effect for neutrons, on the other hand, is expected to be present for heavier nuclei also, where the present approach will find further applications.

Low lying E1 strength is also an important issue of s- and r-processes in nuclear astrophysics [7]. The methods developed in this work are potentially very useful in this context also.

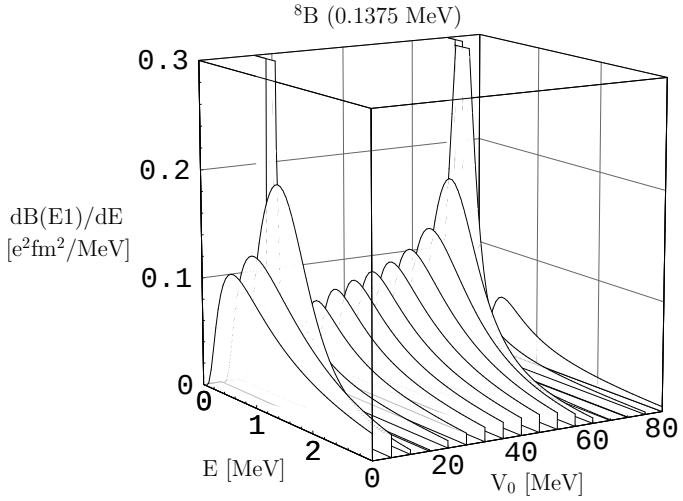

Fig. 1: Reduced transition probability for the breakup of ^{8}B into a proton and ^{7}Be as a function of the c.m. energy E for various depths V_0 of the potential in the continuum. For further explanation see [2]

References:

[1] S.Typel and G.Baur, Phys. Rev. Lett 93(2004)142502
[2] S. Typel and G. Baur, Nucl. Phys. A 759(2005)247
[3] R.Palit et al. Phys.Rev.C68(2003)034318
[4] G.Baur and S.Typel, proceedings of the ...Mumbai... nucl-th/05....., and in preparation
[5] C.Nociforo et al. Phys. Lett. B605(2005)79
[6] see e.g. A.M. Mukhamedzhanov, C.A. Gagliardi, R.E. Tribble Phys. Rev. C63(2001)024612
[7] S.Goriely Phys. Lett. B 436(1998)10

* GSI, Darmstadt.

Projectile electron losses in the collision with neutral targets

G. Baur, Th. Stöhlker *, D. Matrasulov **, Kh. Yu. Rakhimov **, V.I. Matveev†

We report on ongoing work in the framework of our INTAS collaboration.

An important issue in the acceleration of U^{28+}at the forthcoming FAIR/GSI [1] is the projectile electron loss in the collision with the rest gas atoms(molecules). It can lead to degraded focusing and loss of the beam to the walls. These charge-changed fast ions strike the accelerator container walls and give rise to sputtering and activation of the surface. Evidently, it is important to study the interaction of highly charged heavy ions with neutral (rest gas) targets, for practical as well as theoretical reasons. It is a theoretical challenge to treat the many-electron (relativisic) scattering problem in a realistic nonperturbative way.

In the spirit of high energy Glauber theory we present a nonperturbative approach for the treatment of single and multiple electron losses of intermediate as well as relativistic highly charged ions colliding with neutral atom targets[2].

We introduce an average impact dependent probabilty p(b) as

$$p(b) = \frac{1}{n_0}\sum_n \frac{1}{M_n}\sum_{l,m}\int d^3k| < \vec{k}|\exp -i\chi(\vec{b},\vec{r})|nlm > |^2 \quad (1)$$

where $\chi(\vec{b},\vec{r})$ denotes the eikonal phase. The number of all possible values of l and m in a given shell n is denoted by M_n, n_0 is the number of shells, further details can be found in [2].

Now we can write the probability W^{N_e} for the loss of $N_e = N_p - N$ electrons, where N_p is the number of electrons of the highly charged ion ($N_p = 64$, in the case of our application to $^{28+}$U) as

$$W^{N_e}(b) = \frac{N_p}{N!N_e!}p(b)^{N_e}(1-p(b))^N \quad (2)$$

The corresponding cross section is obtained by an integration over the impact parameter d^2b using the Laplace method [2]. In Fig.1(taken from [2]) we show the dependence of the multiple electron loss cross section on the number $N_e = N_p - N$ of electrons lost.

In our approach we used a parametrisation for p(b) where we have to fix two parameters[2]. This was done by fitting to the experimentally observed cross section [3] for $N_e = 14, 15$. The agreement is very good, in view of the approximations made.

It is our aim to calculate ionisation cross sections in a more detailed way using the LOSS code[4], which we intend to modify in order to include impact parameter depence as well as relativistic effects.

References:

[1] "An International Accelerator Facility for Beams of Ions and Antiprotons", Conceptual Design Report. GSI November 2001.

[2] V.I. Matveev, E.S. Gusarevich, D.U. Matrasulov, Kh. Yu. Rakhimov, Th. Stöhlker and G.Baur, submitted to J.Phys. B

[3] R.D. DuBois, A.C.F. Santos, Th. Stöhlker et al. Phys. Rev. A 70(2004)032712 ;R.E.Olson, et al. J.Phys. B37(2004)4539

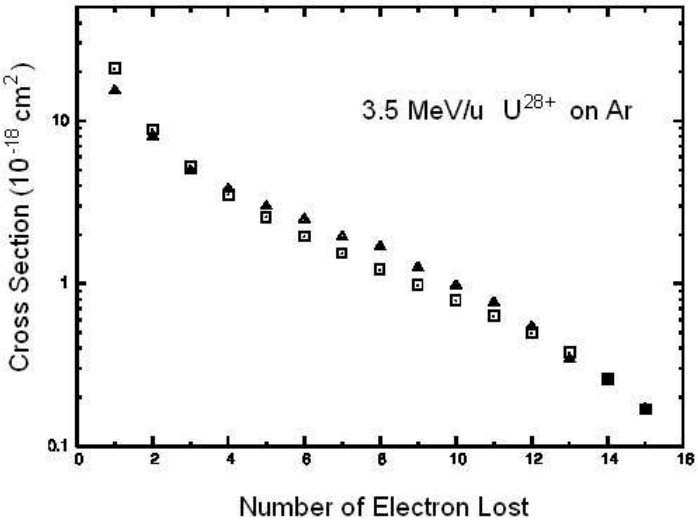

Fig. 1: Dependence of the multiple electron loss cross section(in $10^{-18}cm^2$) on the number of loss electrons. triangles are the experimental data [3], squares are the result of our calculation [2]. For further explanation see text and[2].

[4] V.P. Shevelko, I.Yu. Tolstikhina and Th. Stöhlker, Nucl. Inst. and Meth. in Phys. Res. B184(2001)295

* GSI Darmstadt

** Heat Physics Department of the Uzbek Academy of Sciences, 700135 Tashkent, Uzbekistan

† Physics Department, Pomor State University, 163002 Arkhangelsk, Russia

The investigation of subthreshold resonances with the Trojan Horse Method

G. Baur, S. Typel*

A similarity between cross sections for two-body and closely related three-body reactions under certain kinematical conditions [3] led to the introduction of the Trojan-Horse method [2](for a rather complete theoretical study in the DWBA framework and for further references, see [1]). In this indirect approach a two-body reaction

$$A + x \rightarrow C + c \tag{1}$$

that is relevant to nuclear astrophysics is replaced by a reaction

$$A + a \rightarrow B + b \rightarrow C + c + b \tag{2}$$

with three particles in the final state. One assumes that the Trojan horse a is composed predominantly of clusters x and b, i.e. $a = (x + b)$. This reaction can be considered as a special case of a transfer reaction to the continuum. It is studied experimentally under quasi-free scattering conditions, i.e. when the momentum transfer to the spectator b is small. The method was primarily applied to the extraction of the low-energy cross section of reaction (1) that is relevant for astrophysics. However, the method can also be applied to the study of single-particle states in exotic nuclei around the particle threshold.

It is of special interest to study the limit of stripping to bound and unbound states(continuum). We treat two cases, in the first there is only the channel $A + x$ at $E_{Ax} = 0$, in the second there is also absorption due to the presence of other open channels $C + c$.

To study the first case we imagine that the strength of the single particle potential V_{Ax} is decreased, so that the bound state close to threshold(a halo state), disappears and shows up as a resonance in the continuum. For $l > 0$ this bound state turns into a resonance, and the cross section to this resonance (defined as an integral over an energy region which is several times larger than the width) joins smoothly to the stripping to the bound states, see[4]. Due to the absence of the angular momentum barrier for $l = 0$ there are some peculiarites which we study now. Stripping to bound states is determined by the asymptotic normalization constant B (see eqs. A54-56 of [5]))of the bound state wave function and the behavior of the function $h_l(iqr)$ where q is related to the binding energy. Since

$$B \sim q^{3/2} \quad \text{for} \quad l = 0 \tag{3}$$

and

$$B \sim q^{l+1} R^{l-1/2} \quad \text{for} \quad l > 0 \tag{4}$$

the stripping cross section (see e.g. eq. 17 of [4] to a (halo) state with $l = 0$ tends to zero for q going to zero, while it stays finite for $l > 0$. We note that the presence of a bound state close to zero energy leads to a large scattering length in the $A + x$-system which leads to an enhancement of the elastic breakup cross section. When the strength of the potential is decreased, the bound state becomes a virtual state, which again leads to a very large scattering length, see also [6]. In this context it seems interesting to note that about 30 years ago a new type of threshold effects was predicted in [7](what is now called a halo state was referred to as a puffy state in those days).

In the second case we study the relation between transfer to bound and unbound states in the presence of inelastic channels at threshold. The system $B = (A + x)$ in eq. 2 can be a bound state B with binding energy $E_{bind} = -E_{Ax} (> 0)$, the open channel $A + x$, with $E_{Ax} > 0$, or another channel $C + c$ of the system $B = (A + x)$. In particular, the reaction $x + A \rightarrow C + c$ can have a positive Q value and the energy E_{Ax} can be negative as well as positive. As an example we quote the recently studied Trojan horse reaction d+^{6}Li [10] applied to the ^{6}Li$(p,\alpha)^3$He two-body reaction (the neutron being the spectator). In this case there are two charged particles in the initial state (^{6}Li+p). Another example would be the ^{6}Li + $^{12}C \rightarrow d + ^{16}$O +$\gamma$ reaction, which is relevant for the astrophysically relevant capture reaction $^{12}C(\alpha,\gamma)^{16}O$. The general question which we want to answer here is how the two regions $E_{Ax} > 0$ and $E_{Ax} < 0$ are related to each other. E.g., in Fig. 7 of [10] the coincidence yield is plotted as a function of the ^{6}Li-p relative energy. It is nonzero at zero relative energy. How does the theory [1] (and the experiment) continue to negative relative energies? With the Trojan horse method, subtreshold resonances can be investigated rather directly. We treat two cases separately, one where system B is always in the $(A + x)$ channel, with a real potential V_{Ax} between A and x. In the other case, there are also other channels $C + c$, at positive and negative energies E_{Ax}. This work is an extension of [9] to negative energies E_{Ax}, a preliminary account is given in [11].

One may also envisage applications of the Trojan-Horse method with exotic nuclear beams. Maria Grazia, SPIRAL 2?.... An unstable (exotic) projectile hits a Trojan-Horse target allowing to study specific reactions on exotic nuclei that are not accessible in direct experiments. We mention the d(^{56}Ni,p)^{57}Ni reaction studied in inverse kinematics in [12]. In this paper stripping to bound states was studied; an extension to stripping into the continuum would be of interest for this and other reactions of this type.

References:

[1] S. Typel and G. Baur, Ann. Phys. **305**, 228 (2003)
[2] G. Baur, Phys. Lett. B **178**, 135 (1986).
[3] H. Fuchs et al., Phys. Lett. **37B**, 285 (1971).
[4] G. Baur and D. Trautmann, Z. Physik **267**, 103 (1974).
[5] S.Typel and G.Baur, Nucl. Phys. A759(2005)247
[6] G.Blanchon, A. Bonaccorso, N. Vinh Mau Nucl. Phys. A 739(2004)259
[7] P.v. Brentano, B.Gyarmati and J.Zimanyi Phys. Lett. 46B(1973)177
[8] M.Ichimura, N.Austern and C.M. Vincent Phys. Rev. C32(1985)431
[9] A.Kasano and M.Ichimura Phys. Lett 115B(1982)81
[10] A.Tumino et al. Phys.Rev.C67(2003)065803
[11] G.Baur and S.Typel, Proceedings of Reaction Mechanisms for Rare Isotope Beams, East Lansing, Michigan 9-12 March 2005 CP791, AIP, p. 61
[12] K. E. Rehm et al., Phys. Rev. Lett. **80**, 676 (1998).

* GSI, Darmstadt.

A Toy Model for the Coulomb Dissociation of Neutron Halo Nuclei

G. Baur, R. Shyam*, D. Trautmann**, S. Typel***, and P. Chatterjee†

Coulomb dissociation is a valuable tool to determine electromagnetic matrix-elements in nuclei. A recent discussion of the theory of intermediate energy Coulomb dissociation and its applications is provided in [1, 2, 3, 4, 5]. Intermediate energy Coulomb excitation and dissociation is also of great interest for the radioactive beam facilities (existing, being built or planned) all over the world[6, 7]. Some new applications of Coulomb dissociation for nuclear astrophysics [8] and nuclear structure physics are also discussed in these references. Now there are various theoretical assumptions which enter in the analysis of experimental Coulomb dissociation data in terms of electromagnetic matrix-elements and much work has been done to clarify these assumptions, for a review see [3].

Coulomb dissociation is at least a three-body problem and therefore intrinsically difficult. We have started to study in detail the following simple but realistic model of the Coulomb dissociation of a neutron halo nucleus. We consider a three-body system consisting of a neutron n, a core c and an (infinitely heavy) target nucleus with charge Ze. The Hamiltonian is given by

$$H = T_r + T_{r_c} + V_{cZ}(r_c) + V_{nc}(r) \qquad (1)$$

where $T = T_r + T_{r_c}$ is the kinetic energy of the system. The Coulomb interaction between the core and the target is given by $V_{cZ} = ZZ_c e^2/r_c$ and V_{nc} is a zero-range interaction between c and n. The s-wave bound state of the $a = (c+n)$ system is given by the wave function $\Phi_0 = \sqrt{q/(2\pi)}\exp(-qr)/r$, where q is related to the binding energy E_b by $E_b = \hbar^2 q^2/(2\mu)$ and the reduced mass of the $c+n$ system is denoted by μ. The momentum of the incident particle a is denoted by $\vec{q}_a$, the momenta of the particles c and n in the final state are given by $\vec{q}_c$ and $\vec{q}_n$ respectively. The relative and c.m. momentum in the final state is given by $\vec{q}_{rel} = \frac{m_c\vec{q}_n - m_n\vec{q}_c}{m_n+m_c}$ and $\vec{q}_{cm} = \vec{q}_c + \vec{q}_n$.

This system can be described by a few parameters, the most important ones being the dimensionless Coulomb parameter η, the adiabaticity parameter ξ, the strength parameter y and the shape parameter x. The Coulomb parameter η is given by $\eta = \frac{Z_1 Z_2 e^2}{\hbar v}$ where v is the projectile velocity. The parameter ξ denotes the ratio of the collision time to the nuclear excitation time and it is defined by $\xi = \frac{2\eta q_{||}}{q_\perp}$ where $\vec{q}_{Coul} = \vec{q}_a - \vec{q}_{cm}$ is the momentum transfer. The shape parameter is given by $x = q_{rel}/q$ and the strength parameter y is defined by $y = \frac{m_n\eta}{(m_n+m_c)bq}$. The impact parameter b is introduced in the semiclassical treatment of the problem. It is given in terms of the kinematic quantities by $b = \frac{2\eta}{q_{Coul}}$.

This system can be studied analytically in various approximations. There are analytical results for the Born approximation, and the semiclassical straight line approximation. The post-form DWBA expression is evaluated analytically in terms of Sommerfeld's 'Bremsstrahlung integral'. These results can serve as a benchmark for the comparison of various analytical as well as numerical approaches in different regions of parameter space (η,ξ,x,y). E.g. an analytical expression is given for the higher order contribution in y for $\xi << 1$ and $\eta >> 1$ in eq.(2.7) of [9]. For further details we refer to [3] (see especially Ch. 4 there).

Of special interest is the study of the 'postacceleration effect'. It tends to diminish with increasing beam energy[10], it is intended to study this transition more closely in the future. it would also be very interesting to apply the three-body methods of [11] to this toy model.

Another very interesting point is also the derivation of the semiclassical approximation from the quantal post-form DWBA expression. It can be obtained from the quantal expression ('Bremsstrahlung integral') by letting the Coulomb parameter η go to infinity. We pursue various strategies to obtain this limit.

An essential aim of this study is to verify the high accuracy of semiclassical approximation for high energy forward scattering on high Z-targets. This semiclassical approximation (which also works for relativistic beam energies) is e.g. routinely used in the analysis of high energy breakup reactions on high Z targets. As examples we quote the precision study of the electromagnetic response of the halo nucleus ^{11}Be [12]and the recent discovery of the pygmy resonance in Sn isotopes[13]. We hope to present a detailed account in the next annual report.

References:

[1] G.Baur Breakup and Transfer of One Neutron Halo Nuclei invited talk at INFN Workshop on reactions and Structure with Exotic Nuclei Pisa 24-26 February 2005 transparencies at http://www.df.unipi.it/ angela/finalprogram.htm

[2] G.Baur and S.Typel Proceedings of the International Workshop on... in MSU

[3] G. Baur, K. Hencken and D.Trautmann, Prog. in Part. and Nucl. Phys., 51(2003) 487

[4] G.Baur NRRIB05: Neutron-Rich Radioactive Ion Beams- Physics with MAFF-, Kloster Banz, Germany 29 March-1 April 2005 Direct reactions with radioactive beams and astrophysics invited talk, transparencies at http://www.ha.physik.uni-muenchen.de/maff/workshop/

[5] G.Baur invited talk Mumbai 2005 transparencies...

[6] "An International Accelerator Facility for Beams of Ions and Antiprotons", Conceptual Design Report. GSI November 2001.

[7] RIA WEB page, `http://www.phy.anl.gov/ria/`

[8] G.Baur, C.A. Bertulani and H.Rebel, Nucl Phys. A**458** (1986) 188.

[9] S.Typel and G.Baur, Phys. Rev. C64(2001)024601

[10] P. Banerjee et al. Phys. Rev. C65(2002) 0646002

[11] E.O. Alt et al. Phys. Rev. C71(2005)024605

[12] R.Palit et al. Phys. Rev. C68(2003)034318

[13] P. Adrich et al. Phys. Rev. Lett. 95(2005)132501

* Theory Division Saha Institute of Nuclear Physics, Kolkata, India

* Institut für Theoretische Physik, Universität Basel, Klingelbergstraße 82, CH-4056 Basel, Switzerland

** GSI, D-64291 Darmstadt

† GANIL, F-14076, France

Nucleon-Nucleon Potential in Finite Nuclei

U.T. Yakhshiev (Pusan, Tashkent), U.-G. Meißner, A. Wirzba, A.M. Rakhimov (Tashkent),
and M.M. Musakhanov (Tashkent)

We consider the spin-isospin–independent central part of the residual nucleon-nucleon potential in finite spherical nuclei taking into account the deformation effects of the nucleons within the surrounding nuclear environment. It is shown that inside the nucleus the short-range repulsive contribution of the potential is increased and the intermediate-range attraction is decreased. We identify the growth of the radial component of the spin-isospin–independent short-range part of the in-medium nucleon-nucleon interaction as the responsible agent that prevents the radial collapse of the nucleus. The results are published in Ref. [1].

References:

[1] U. T. Yakhshiev, U.-G. Meißner, A. Wirzba, A. M. Rakhimov and M. M. Musakhanov, Phys. Rev. C **71** (2005) 034007.

2.4 High energy physics

Theoretical Studies of Ultraperipheral Collisions at Relativistic Heavy Ion Colliders

G. Baur, K. Hencken*, D. Trautmann*

We continue our studies on ultraperipheral heavy ion collisions('UPC'). Ultraperipheral relativistic heavy ion collisions are accompanied by very strong electromagnetic fields of very short duration. This electromagnetic pulse can be viewed as a spectrum of equivalent photons which extends to very high energies. The parameter which characterizes the strength of the interaction is the Coulomb parameter η:

$$\eta = \frac{Z_1 Z_2 e^2}{\hbar v} \approx Z_1 Z_2 \alpha \qquad (1)$$

where Z_1 and Z_2 are the charges of the nuclei and $v \approx c$ is the relative velocity of the ions. For heavy nuclei like Au-Au (RHIC) or Pb-Pb (LHC) we have $\eta \gg 1$.

A very promising channel is coherent vector meson production. A photon which is emitted by one nucleus is turned into a vector meson in a diffractive interaction with the other nucleus. Both nuclei can emit photons, which leads to an interesting interference effect. For heavy ions we have $\eta >> 1$ and semiclassical or Glauber methods can be used to describe this effect [1]. In [2] we also study vector meson production in pp and $p\bar{p}$ collisions, in this case we have $\eta << 1$ and the one-photon exchange approximation is sufficient. ρ^0production in UPC was studied experimentally at RHIC/STAR [7]. Preliminary results on transverse momentum distributions of the ρ^0's were presented at various conferences [6]. It is planned to study vector meson production in UPC also at the forthcoming LHC, see e.g. [8] Due to the higher beam energy as compared to RHIC, it will be possible to study J/Ψ or even Υ production in UPC. These processes will allow to study the gluon distribution in nuclei.

A review paper is planned on the subject of lepton pair production in UPC. Due to its strong field aspects this field has attracted a lot of interest recently and many groups published results, which were sometimes in conflict with each other. Not surprisingly, these conflicts were found to be spurious. The probability of electron-positron pair production calculated in lowest order perturbation theory exceeds the unitarity limit of one [9, 10, 11]. This means that multiple e^+e^- pair production is expected to be appreciable for heavy ions at RHIC and LHC conditions. e^+e^- pair production was studied experimentally at RHIC [12], for the high transverse momentum pairs lowest order perturbation theory was found to be sufficient [13]

At CERN a Yellow Report to document the physics potential of UPC is currently being prepared. The field is also reviewed in [3, 4, 14, 5].

Finally it should be mentioned that a NATO Advanced Research Workshop on the subject of UPC was organized to be held in Tashkent, Uzbekistan, 10-15 October 2005 [15]. However, due to reasons beyond our control, it had to be cancelled.

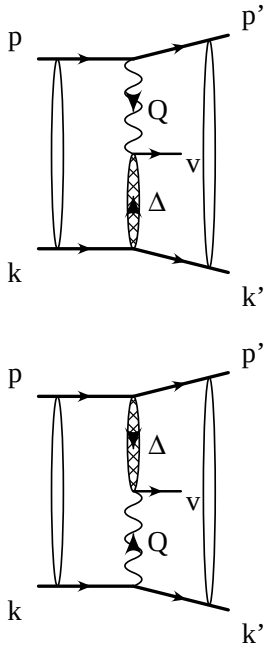

Fig. 1: A schematic Feynman diagram for the vector meson production in UPC. The corresponding exchange diagram is also shown. The initial and final state interactions are indicated by blobs.

References:

[1] K.Hencken, G. Baur and D.Trautmann, nucl-th/05, Phys. Rev. Lett. , in press
[2] K.Hencken, G. Baur and D.Trautmann in preparation
[3] G. Baur, K. Hencken, D. Trautmann, S. Sadovsky, Y. Kharlov, Phys. Reports 364 (2002) 359.
[4] F. Krauss, M. Greiner, G. Soff, Prog. Part. Nucl. Phys. 39 (1997) 503.
[5] C.A. Bertulani, S.Klein and J. Nystrand, Ann.Rev.Nucl. Part. Sci.,55(2005)271
[6] S.R. Klein et al. for the STAR collaboration , nucl-ex/0310020 and nucl-ex/0402007
[7] C. Adler et al., Phys. Rev. Lett.89 (2002) 272302.
[8] F.Carminati et al., for the ALICE collaboration, J.Phys. G, Nucl.Part. Phys. 30(2004)1517 and http://alice.web.cern.ch/Alice/ppr/web/ PPRVIICurrentVersion.html
[9] K. Hencken, D. Trautmann and G. Baur, Phys. Rev. A51 (1995) 998.
[10] K. Hencken, D. Trautmann and G. Baur, Phys. Rev. A51 (1995) 1874.
[11] A. Aste, G. Baur, K. Hencken, D. Trautmann and G. Scharf, Eur. Phys. J. C23 (2002) 545.
[12] J.Adams et al. Phys.Rev.C70(2004)031902(R)
[13] K.Hencken, G.Baur and D.Trautmann Phys.Rev.C 69(2004)054902
[14] K.Hencken, invited talk at the conference "Physics at LHC" 13-17 July 2004, Vienna, Austria, Kai Hencken, Gerhard Baur, Ute Dreyer and Dirk Trautmann: Ultraperipheral Collisions Proceedings of Physics at LHC to be published in Czechoslovak Journal of Physics Vol.54(2004) Suppl. A
[15] http://www.hiehic05.uzsci.net/

* Institut für Theoretische Physik, Universität Basel, CH-4056 Basel, Switzerland

Why Breakup of Photons and Pions into Forward Dijets Is so Different: Predictions from Nonlinear Nuclear k_t-factorization

N.N. Nikolaev, W. Schäfer, B.G. Zakharov (Chernogolovka) and V.R. Zoller (Moscow)

Based on an approach to non-Abelian propagation of color dipoles in a nuclear medium we formulate a nonlinear k_t-factorization for the breakup of photons and pions into forward hard dijets in terms of the collective Weizsäcker-Williams (WW) glue of nuclei. We find quite distinct practical consequences of nonlinear nuclear k_t-factorization for interactions of pointlike photons and non-pointlike pions. In the former case the large transverse momentum p_t of jets comes from the intrinsic momentum of quarks and antiquarks in the photon and nuclear effects manifest themselves as an azimuthal decorrelation with an acoplanarity momentum of the order of the nuclear saturation momentum Q_A. In the breakup of pions off free nucleons to the leading order in pQCD the spectator parton has a small transverse momentum and the hard dijet cross section is suppressed. In the breakup of pions off heavy nuclei the forward hard jets are predicted to be entirely decorrelated. We comment on the sensitivity of the pionic dijet cross section to the pion distribution amplitude. The predicted distinction between the breakup of photons and pions can be tested by the sphericity and thrust analysis of the forward hadronic system in the COMPASS experiment at CERN. The results are published in Ref. [1].

References:

[1] N. N. Nikolaev, W. Schäfer, B. G. Zakharov and V. R. Zoller, Phys. Atom. Nucl. **68** (2005) 661 [Yad. Fiz. **68** (2005) 692] [arXiv:hep-ph/0406085].

Breaking of $k_\perp$-factorization for Single Jet Production off Nuclei

N.N. Nikolaev and W. Schäfer

The linear $k_\perp$-factorization is part and parcel of the pQCD description of high energy hard processes off free nucleons. In the case of heavy nuclear targets the very concept of nuclear parton density becomes ill-defined as exemplified by the recent derivation [2] of nonlinear nuclear $k_\perp$-factorization for forward dijet production in DIS off nuclei. Here we report a derivation of the related breaking of $k_\perp$-factorization for single-jet processes. We present a general formalism and apply it to several cases of practical interest: open charm and quark and gluon jet production in the central to beam fragmentation region of $\gamma^* p, \gamma^* A, pp$ and pA collisions. We show how the pattern of $k_\perp$-factorization breaking and the nature and number of exchanged nuclear pomerons do change within the phase space of produced quark and gluon jets. As an application of the nonlinear $k_\perp$-factorization we discuss the Cronin effect. Our results are also applicable to the $p_\perp$-dependence of the Landau-Pomeranchuk-Migdal effect for, and nuclear quenching of, jets produced in the proton hemisphere of pA collisions. The results are published in Ref. [1].

References:

[1] N. N. Nikolaev and W. Schäfer, Phys. Rev. D **71** (2005) 014023 [arXiv:hep-ph/0411365].

Multiple exchanges in lepton pair production in high–energy heavy ion collisions

E. Bartos (Bratislava), S. R. Gevorkyan (Dubna), E. A. Kuraev (Dubna), N. N. Nikolaev

The recent analysis of nuclear distortions in DIS off nuclei revealed a breaking of the conventional hard factorization for multijet observable. The related pQCD analysis of distortion effects for jet production in nucleus-nucleus collisions is as yet lacking. As a testing ground for such an analysis we consider the Abelian problem of higher order Coulomb distortions of the spectrum of lepton pairs produced in peripheral nuclear collisions. We report an explicit calculation of the contribution to the lepton pair production in the collision of two photons from one nucleus with two photons from the other nucleus, $2\gamma + 2\gamma \to l^+l^-$. The dependence of this amplitude on the transverse momenta has a highly nontrivial form the origin of which can be traced to the mismatch of the conservation of the Sudakov components for the momentum of leptons in the Coulomb field of the oppositely moving nuclei. The result suggests that the familiar eikonalization of Coulomb distortions breaks down for the oppositely moving Coulomb centers, which is bad news from the point of view of extensions to the pQCD treatment of jet production in nuclear collisions. On the other hand, we notice that the amplitude for the $2\gamma + 2\gamma \to l^+l^-$ process has a logarithmic enhancement for the lepton pairs with large transverse momentum, which is absent for $n\gamma + m\gamma \to l^+l^-$ processes with $m, n > 2$. We discuss the general structure of multiple exchanges and show how to deal with higher order terms which cannot be eikonalized. The results have been published in Ref. [1].

References:

[1] E. Bartos, S. R. Gevorkyan, E. A. Kuraev and N. N. Nikolaev, J. Exp. Theor. Phys. **100** (2005) 645 [Zh. Eksp. Teor. Fiz. **100** (2005) 732] [arXiv:hep-ph/0410263].

Nonuniversality Aspects of Nonlinear $k_\perp$-factorization for Hard Dijets

N.N. Nikolaev, W. Schäfer, B.G. Zakharov (Chernogolovka)

The origin of the breaking of conventional linear $k_\perp$-factorization for hard processes in a nuclear environment is by now well established. The realization of the nonlinear nuclear $k_\perp$-factorization which emerges instead was found to change from one jet observable to another. Here we demonstrate how the pattern of nonlinear $k_\perp$-factorization, and especially the role of diffractive interactions, in the production of dijets off nuclei depends on the color properties of the underlying pQCD subprocess. The results are pubished in Ref. [1].

References:

[1] N. N. Nikolaev, W. Schäfer and B. G. Zakharov, "Nonuniversality aspects of nonlinear k(T)-factorization for hard dijets, Phys. Rev. Let. **95**, 221803 (2005) [arXiv: hep-ph/0502018].

Nonlinear $k_\perp$-factorization for Quark-Gluon Dijet Production off Nuclei

N.N. Nikolaev, W. Schäfer, B.G. Zakharov (Landau Institute) and V.R. Zoller (ITEP Moscow)

The breaking of conventional linear $k_\perp$-factorization for hard processes in a nuclear environment is by now well established. Here we report a detailed derivation of the nonlinear $k_\perp$-factorization relations for the production of quark-gluon dijets. This process is of direct relevance to dijets in the proton hemisphere of proton-nucleus collisions at energies of the Relativistic Heavy Ion Collider (RHIC). The major technical problem is a consistent description of the non-Abelian intranuclear evolution of multiparton systems of color dipoles. Following the technique developed in our early work [N.N. Nikolaev, W. Schäfer, B.G. Zakharov and V.R. Zoller, J. Exp. Theor. Phys. **97** (2003) 441], we reduce the description of the intranuclear evolution of the $qgg\bar{q}$ state to the system of three coupled-channel equations in the space of color singlet 4-parton states $|3\bar{3}\rangle, |6\bar{6}\rangle$ and $|15\bar{1}\bar{5}\rangle$ (and their large-N_c generalizations). At large number of colors N_c, the eigenstate $(|6\bar{6}\rangle - |15\bar{1}\bar{5}\rangle)/\sqrt{2}$ decouples from the initial state $|3\bar{3}\rangle$. The resulting nuclear distortions of the dijet spectrum exhibit much similarity to those found earlier for forward dijets in Deep Inelastic Scattering (DIS). Still there are certain distinctions regarding the contribution from color-triplet qg final states and from coherent diffraction excitation of dijets. To the large-N_c approximation, we identify four universality classes of nonlinear $k_\perp$-factorization for hard dijet production. The results are pubished in Ref. [1].

References:

[1] N. N. Nikolaev, W. Schäfer, B. G. Zakharov and V. R. Zoller, Phys. Rev. D **72** (2005) 034033 [arXiv: hep-ph/0504057].

Nonlinear $k_\perp$-factorization for Gluon-Gluon Dijets Produced off Nuclear Targets

N.N. Nikolaev, W. Schäfer and B.G. Zakharov (Chernogolovka)

The origin of the breaking of conventional linear $k_\perp$-factorization for hard processes in a nuclear environment is by now well established. The realization of the nonlinear nuclear $k_\perp$-factorization which emerges instead was found to change from one jet observable to another. Here we report on an important technical progress, the evaluation of the four-gluon color dipole cross section operator. It describes the coupled seven-channel non-Abelian intranuclear evolution of the four-gluon color-singlet states. An exact diagonalization of this seven-channel problem is possible for large number of colors N_c and allows a formulation of nonlinear $k_\perp$-factorization for production of gluon-gluon dijets. The momentum spectra for dijets in all possible color representations are reported in the form of explicit quadratures in terms of the collective nuclear unintegrated glue. Our results fully corroborate the concept of universality classes. The results are published in Ref. [1].

References:

[1] N. N. Nikolaev, W. Schäfer and B. G. Zakharov, arXiv: hep-ph/0508310. Phys. Rev. **D** (2005) accepted for publication.

Nonlinear $k_\perp$-factorization: a new paradigm for an in-nucleus hard QCD

N. N. Nikolaev, W. Schäfer, B.G. Zakharov (Chernogolovka) and V.R. Zoller (Moscow)

We review the origin, and salient features, of the breaking of the conventional linear $k_\perp$-factorization for an in-nucleus hard pQCD processes. A realization of the nonlinear $k_\perp$-factorization which emerges instead is shown to depend on color properties of the underlying pQCD subprocesses. We discuss the emerging universality classes and extend nonlinear $k_\perp$-factorization to AGK unitarity rules for the excitation of the target nucleus. The results are published in Ref. [1].

References:

[1] N. N. Nikolaev, W. Schäfer, B. G. Zakharov and V. R. Zoller, Proceedings of Gribov-75: Memorial Workshop On Quarks, Hadrons, And Strong Interactions, 22-24 May 2005, Budapest, Hungary arXiv: hep-ph/0511285.

$B_{s,d} \to \gamma\gamma$ decay in the model with one universal extra dimension

G. Devidze (Tbilisi), A. Liparteliani (Tbilisi) and Ulf-G. Meißner

We estimate the beyond the Standard Model (SM) contribution to the $B_{s,d} \to \gamma\gamma$ double radiative decay in the framework of the model with one universal extra dimension. This contribution gives a $\sim 3\,(6)\%$ enhancement of the branching ratio calculated in the SM for $B_{s\,(d)} \to \gamma\gamma$. These results are published in Ref. [1].

References:

[1] G. Devidze, A. Liparteliani and U.-G. Meißner, Phys. Lett. B **634** (2006) 59 [hep-ph/0510022].

2.5 Further studies

Spin Filtering in Storage Rings

N.N. Nikolaev and F.F. Pavlov

The spin filtering in storage rings is based on a multiple passage of a stored beam through a polarized internal gas target. Apart from the polarization by transmission, a unique geometrical feature of interaction with the target in such a filtering process, pointed out by H.O. Meyer, is a scattering of stored particles within the beam. A rotation of the spin in the scattering process affects the polarization buildup. We derive here a quantum-mechanical evolution equation for the spin-density matrix of the stored beam which incorporates scattering within the beam. We show how the interplay of transmission and scattering with the beam changes from polarized electrons to polarized protons in the atomic target. After discussions of the FILTEX results on the filtering of stored protons, we comment on the strategy of spin filtering of antiprotons for the PAX experiment at GSI FAIR. The results will be published in Ref. [1].

References:

[1] N. N. Nikolaev and F. F. Pavlov, Proceedings of the International Workshop on Transverse Polarization Phenomena in Hard Processes (Transversity 2005) Villa Olmo (Como), 7-10 September 2005, arXiv: hep-ph/0512051.

Fermionic Casimir Effect in Case of Andreev Reflection

A. Bulgac (Seattle), P. Magierski (Seattle, Warsaw), and A. Wirzba

We describe the fermionic Casimir effect in the case of two spherical superfluid scatterers immersed in a normal Fermi system. It is shown that due to the focusing property of Andreev reflection this new Casimir-like energy is significantly enhanced when compared to the case of normal scatterers with specular reflection. The results are published in Ref. [1].

References:

[1] A. Bulgac, P. Magierski and A. Wirzba, Europhys. Lett. **72** (2005) 327.

Casimir interaction between normal or superfluid grains in the Fermi sea

A. Wirzba, A. Bulgac (Seattle), and P. Magierski (Seattle, Warsaw)

We report on a new force that acts on cavities (literally empty regions of space) when they are immersed in a background of non-interacting fermionic matter fields. The interaction follows from the obstructions to the (quantum mechanical) motions of the fermions caused by the presence of bubbles or other (heavy) particles in the Fermi sea, as, for example, nuclei in the neutron sea in the inner crust of a neutron star or superfluid grains in a normal Fermi liquid. The effect resembles the traditional Casimir interaction between metallic mirrors in the vacuum. However, the fluctuating electromagnetic fields are replaced by fermionic matter fields. We show that the fermionic Casimir problem for a system of spherical cavities can be solved exactly, since the calculation can be mapped onto a quantum mechanical billiard problem of a point-particle scattered off a finite number of non-overlapping spheres or disks. Finally we generalize the map method to other Casimir systems, especially to the case of a fluctuating scalar field between two spheres or a sphere and a plate under Dirichlet boundary conditions. The results are published in Ref. [1].

References:

[1] A. Wirzba, A. Bulgac and P. Magierski, arXiv:quant-ph/0511057.

Scalar Casimir effect between Dirichlet spheres or a plate and a sphere

A. Bulgac (Seattle), P. Magierski (Seattle, Warsaw), and A. Wirzba

We present a simple formalism for the evaluation of the Casimir energy for two spheres and a sphere and a plane, in case of a scalar fluctuating field, valid at any separations. We compare the exact results with various approximation schemes and establish when such schemes become useful. The formalism can be easily extended to any number of spheres and/or planes in three or arbitrary dimensions, with a variety of boundary conditions or non-overlapping potentials/non-ideal reflectors. The results are published in Ref. [1].

References:

[1] A. Bulgac, P. Magierski and A. Wirzba, arXiv:hep-th/0511056.

A force from nothing onto nothing: Casimir effect between bubbles in the Fermi sea

A. Wirzba

We report on a new force that acts on cavities (literally empty regions of space) when they are immersed in a background of non-interacting fermionic matter fields. The interaction follows from the obstructions to the (quantum mechanical) motions of the fermions in the Fermi sea caused by the presence of bubbles or other (heavy) particles immersed in the latter, as, for example, nuclei in the neutron sea in the inner crust of a neutron star. This effect resembles the traditional Casimir effect, which describes the attraction between two parallel metallic mirrors in vacuum. Here, however, the fluctuating (bosonic) electromagnetic fields are replaced by fermionic matter fields. Furthermore, the Casimir energy is inferred from the geometry-dependent part of the density of states, and its sign is not fixed, but oscillates according to the relative arrangement and distances of the cavities. In fact, with the help of Krein's trace formula, the quantum field theory calculation is mapped onto a quantum mechanical billiard problem of a point-particle scattered off a finite number of non-overlapping spheres or disks; i.e. classically hyperbolic (or even chaotic) scattering systems. This topic is relevant to the physics of neutron stars (nuclei or quark bubbles embedded in a neutron gas), to dilute Bose-Einstein-condensate bubbles inside the background of a Fermi-Dirac condensate, to buckyballs in liquid mercury and to superconducting droplets in a Fermi liquid. The results are published in Ref. [1].

References:

[1] A. Wirzba, in *Non-Linear Dynamics and Fundamental Interactions*, edited by F. Khanna and D. Matrasulov, NATO Science Series II: Mathematics, Physics and Chemistry – Vol. **213** (2006) 229-241.

Wave Chaos in Elastodynamic Cavity Scattering

A. Wirzba, N. Søndergaard (Lund), and P. Cvitanović (Atlanta)

The exact elastodynamic scattering theory is constructed to describe the spectral properties of two- and more-cylindrical cavity systems, and compared to an elastodynamic generalization of the semi-classical Gutzwiller unstable periodic orbits formulas. In contrast to quantum mechanics, complex periodic orbits associated with the surface Rayleigh waves dominate the low-frequency spectrum, and already the two-cavity system displays chaotic features. The results are published in Ref. [1].

References:

[1] A. Wirzba, N. Søndergaard and P. Cvitanović, Europhys. Lett. **72** (2005) 534.

The effects of box diagrams in proton proton collision*

V.A. Nikonov[a]

Nucleon resonances and their couplings to different channels play a critical role for an understanding of nuclear interactions. The study of the resonances produced in proton-proton collisions is therefore an important contribution to nuclear physics which will be studied in the WASA experiment.

The analysis and interpretation of the data is a most interesting task which the collaboration will meet. For this purpose, the momentum operator expansion method will be used which was developed for the analysis of pion and photon induced production of baryons [1]. The approach is fully relativistically invariant and allow us to perform combined analyses of different reactions imposing directly analyticity and unitarity constraints.

A resonance corresponds to the pole singularity in the scattering amplitude: such singularities are the strongest ones. When it is situated close to the physical region, it can be identified with good reliability and accuracy. However, if the pole is situated far from the physical region (a broad state) or in situations with strong interferences between different states, it is necessary to control other singularities of the scattering amplitude as well. In particular two–body final–state amplitudes have threshold singularities which are proportional to $1/\sqrt{s}$ which need to be taken into account explicitly. The three–particle final–state has additionally triangle singularities which diverge logarithmically. They correspond resonance production with subsequent rescattering of one of the decay particles with the spectator particle. In the case of four particle final state there are singularities which are connected with the processes like shown in Fig. 1. Such amplitudes has a number of logarithmic singularities and a $1/\sqrt{s}$ singularity. The latter singularity can have an appreciably effect on the cross sections of the reactions with four body final states. A special aspect of this discussion is the possibility that the $\gamma\gamma$ signal observed by the WASA collaboration near $\pi\pi$ threshold could be explained by a contribution from the box diagram.

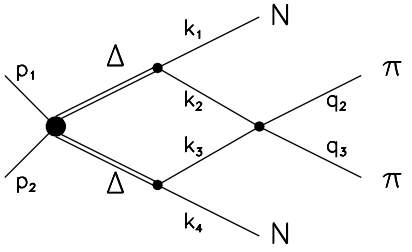

Fig. 1: Four-angle diagram for proton-proton collision.

The amplitude for the box diagram with initial protons and produced Δ resonances interacting in S-wave has the following form:

$$A = \int \frac{d^4k}{(2\pi)^4 i} \frac{\bar{u}(p_2)u(p_1)\, F_{\mu\nu}\, k_{12\nu}^{\perp}\, F_{\mu\eta}\, k_{34\eta}^{\perp}}{(M^2 - s_{12} - iM\Gamma)(M^2 - s_{34} - iM\Gamma)} \times \frac{u(k_1)X_{\alpha_1\ldots\alpha_n}(k_{23}^{\perp})X_{\beta_1\ldots\beta_n}(q_{23}^{\perp})\bar{u}(k_4)}{(\mu^2 - k_2^2 - i0)(\mu^2 - k_3^2 - i0)}$$

$$F_{\mu\nu} = \frac{1}{2}(g_{\mu\nu}^{\perp} - \frac{1}{3}\gamma_{\mu}^{\perp}\gamma_{\nu}^{\perp})(\sqrt{s_{12}} + \hat{k_1} + \hat{k_2}),$$
$$F_{\mu\eta} = \frac{1}{2}(g_{\mu\eta}^{\perp} - \frac{1}{3}\gamma_{\mu}^{\perp}\gamma_{\eta}^{\perp})(\sqrt{s_{34}} + \hat{k_3} + \hat{k_4}), \quad (1)$$

the operators $X_{\alpha_1\ldots\alpha_n}$ are orbital moment operators, their definition is given explicitly in [1].

In principle this integral can be calculated analytically, and for the case of spinless particles the result is given in [2]. However such calculations are very complicated and there is no general expression for the box amplitude contribution to a particular partial wave. At present we have developed numerical methods for the calculation of the diagrams like shown in Fig. 1. For the case of scalar particles the results can be directly compared with analytical calculations [2] and for proton-proton collision it can be checked for the present of expected singularities in the complex plane.

Below we present numerical results for the reaction $pp \to p\pi\pi p$ with two Δ resonances in the intermediate state.

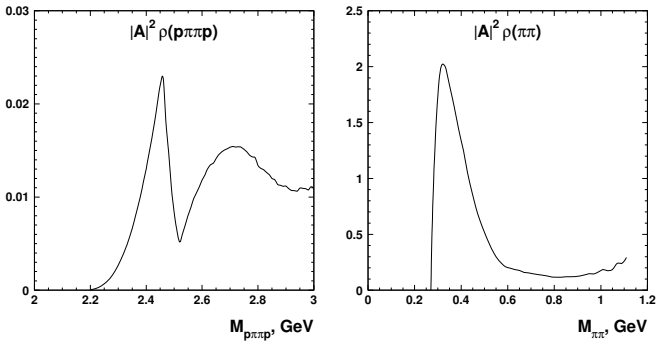

Fig. 2: The contributions of the box diagram to the intensity of the reaction $pp \to p\pi\pi p$ (left panel) and to the intensity in $\pi\pi$ channel (right panel).

As one can see, the box diagram provides a resonant-like contribution to the $pp \to p\pi\pi p$ reaction in the energy region just below twice the mass of the intermediate $\Delta(1232)$ resonance. This intensity which is equal to the production of amplitude squared and $p\pi\pi p$ phase space is shown in the left panel of Fig. 2. Moreover the box diagram has the resonant-like behavior in $\pi\pi$ spectrum near $\pi\pi$ threshold (see right panel of Fig. 2). Such effects can play an important role in the analysis of the data obtained by the WASA experiment and undoubtfully should be under control in forthcoming analysis of the data.

The author is very grateful to A.V. Sarantsev and E. Klempt for useful discussions.

References:

[1] A. Anisovich, E. Klempt, A. Sarantsev and U. Thoma, Eur. Phys. J. A **24** (2005) 111.
[2] V.V.Anisovich and M.N.Kobrinsky, Yad.Fiz. **13** (1971) 168.

[a] Helmholtz Institut für Strahlen- und Kernphysik, Universität Bonn, Germany
* Work performed in the framework of the COSY-FFE program

3 Accelerator Division

SPIN@COSY: Polarized deuteron and proton beam studies at COSY

V.S. Morozov[1], A.W. Chao[1], E.D. Courant[1], Ya.S. Derbenev[1], A.D. Krisch[1], M.A. Leonova[1], W. Lorenzon[1], R.S. Raymond[1], D.W. Sivers[1], V.K. Wong[1]; R. Gebel[2], A. Lehrach[2], B. Lorentz[2], R. Maier[2], D. Prasuhn[2], A. Schnase[2], H. Stockhorst[2]; D. Eversheim[3], F. Hinterberger[3], H. Rohdjeß[3], K. Ulbrich[3]; H. Huang[4]; H. Sato[5]; A.M. Kondratenko[6]; K. Yonehara[7]

Introduction

The ability to preserve and manipulate a beam's polarization is needed to study the spin dependence of nuclear and particle interactions. The SPIN@COSY collaboration investigated spin manipulation of vertically polarized protons and of simultaneously vector and tensor polarized deuterons stored near 2 GeV/c in COSY [1,2,3].

Experimental setup

The beam emerging from the polarized H^-/D^- ion source was accelerated by COSY's cyclotron to 45 MeV. The Low Energy Polarimeter monitored the beam polarization before injection into COSY. After injection the beam was first electron-cooled to reduce its size and momentum spread and then accelerated to about 2 GeV/c. We then spin-manipulated the beam using the ferrite-core rf dipole, which operated near 900 kHz with a maximum $\int B_{rms}dl$ of about 0.6 T·mm. The resulting polarization was measured using the EDDA detector as a polarimeter. The initial vector polarizations, before spin manipulation, reached about 80% for protons and 70% for deuterons.

Spin-manipulating stored polarized deuterons

We spin-manipulated stored 1.85 GeV/c vector and tensor polarized deuterons by sweeping the rf dipole's frequency through an rf-induced spin resonance. After such a sweep, the final vector and tensor polarizations, P_V and P_T, should be given by the modified Froissart-Stora equations:

$$\frac{P_V}{P_V^i} = (1+\hat{\eta})\exp\left[\frac{-(\pi\varepsilon f_c)^2}{\Delta f/\Delta t}\right] - \hat{\eta}, \qquad (1)$$

$$\frac{P_T}{P_T^i} = \frac{3}{2}\left\{(1+\hat{\eta})\exp\left[\frac{-(\pi\varepsilon f_c)^2}{\Delta f/\Delta t}\right] - \hat{\eta}\right\}^2 - \frac{1}{2}; \qquad (2)$$

P_V^i and P_T^i are the initial vector and tensor polarizations, $\hat{\eta}$ is the limiting spin-flip efficiency, ε is the resonance strength, f_c is the deuteron's circulation frequency, and Δf is the sweep's full frequency range during its ramp time Δt.

We first experimentally determined the spin resonance frequency. We then chose a frequency range Δf large enough to fully cover the resonance width and centered it at the resonance frequency. We next varied the ramp time Δt with all other parameters fixed. The measured vector and tensor polarization ratios, P_V/P_V^i and P_T/P_T^i, are plotted against Δt for the 4 spin states in Fig. 1. Note especially the interesting behavior of the tensor polarization. The vector and tensor data are well described by the solid lines, which are fits to Eqs. (1) and (2). The vector and tensor spin-flip efficiencies and resonance strengths obtained from these fits agree within their errors [3].

We also precisely determined the spin-flip efficiency η by measuring the vector polarization after n frequency sweeps; this measured vector polarization ratio P_V/P_V^i is plotted vs. n in Fig. 2. We obtained a spin-flip efficiency of $\eta = 98.5 \pm 0.3\%$ by fitting these data to

$$P_V/P_V^i = (-\eta)^n. \qquad (3)$$

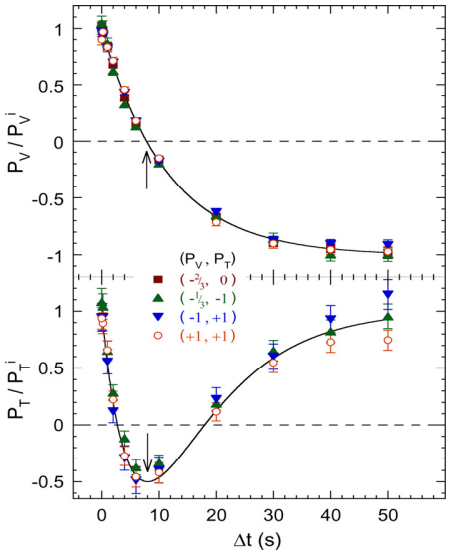

Fig. 1: The vector and tensor deuteron polarization ratios at 1850 MeV/c are plotted vs. the rf dipole's ramp time Δt; its frequency half-range $\Delta f/2$ was 100 Hz, and its $\int B_{rms}dl$ was 0.54 T·mm. The curves are fits to Eqs. (1) and (2).

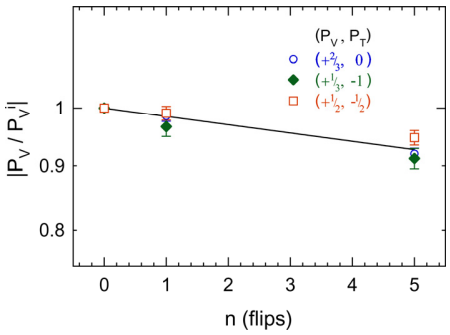

Fig. 2: The measured vector deuteron polarization ratio at 1850 MeV/c is plotted vs. the number of flips. The rf dipole's Δt was 60 s; its $\Delta f/2$ was 75 Hz, and its $\int B_{rms}dl$ was 0.60 T·mm. The line is a fit to $P_V/P_V^i = (-\eta)^n$.

Studies of rf-induced spin resonance strength

During our polarized beam studies at COSY, we found large deviations of the measured rf-magnet-induced spin resonance strength ε_{FS} from its ε_{Bdl} obtained from the dipole's $\int B_{rms}dl$. We then analyzed all available data on the spin flipping of stored polarized protons, electrons and deuterons [4] and found similar deviations. One must understand these deviations to properly design a spin flipper for very high energy rings.

Each resonance strength, ε_{FS}, was obtained by fitting to Eq. (1) its curve of P vs. Δt (see Figs. 1 and 3). It was also obtained from the rf dipole's $\int B_{rms}dl$ using

$$\varepsilon_{Bdl} = \frac{1}{\pi\sqrt{2}}\frac{e(1+G\gamma)}{p}\int B_{rms}dl; \qquad (4)$$

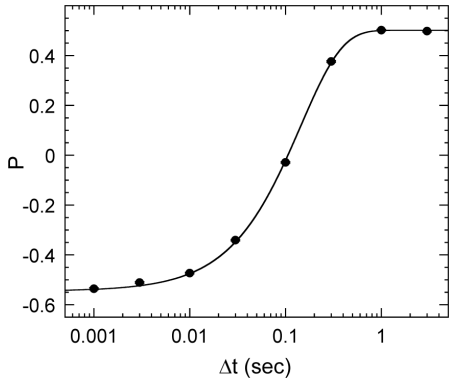

Fig. 3: The measured proton polarization at 2.1 GeV/c is plotted vs. the rf dipole's Δt; its $\Delta f / 2$ was 4 kHz, and its $\int B_{rms} dl$ was 0.025 T·mm. The curve is a fit to Eq. (1).

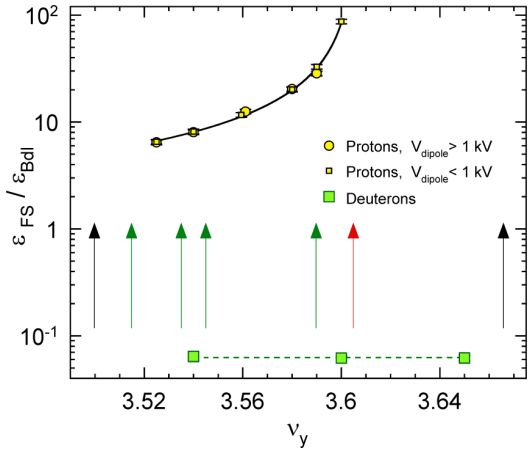

Fig. 4: The measured $\varepsilon_{FS} / \varepsilon_{Bdl}$ ratio is plotted vs. the vertical betatron tune ν_y. The proton data were fit to $\varepsilon_{FS} / \varepsilon_{Bdl} = A + B / |\nu_y - \nu_y^r|$. The black arrows show the beam loss resonances; the red and green arrows show the 1st and 3rd order proton spin resonances, respectively.

e is the particle's charge, G is its gyromagnetic anomaly, γ is its Lorentz energy factor, and p is its momentum [5]. For the data in Fig. 3, ε_{FS} is about 50.3×10^{-6} while ε_{Bdl} is about 4.4×10^{-6}. To understand such disagreements, we studied experimentally the dependence of ε_{FS} on the transverse beam size and the vertical betatron tune using polarized 1.85 GeV/c deuterons and 2.1 GeV/c protons stored in COSY. We first measured the $\varepsilon_{FS} / \varepsilon_{Bdl}$ ratio while varying the fast quadrupole current to change the beam's size, but both proton and deuteron data showed no dependence on the current. We next measured $\varepsilon_{FS} / \varepsilon_{Bdl}$ as a function of the vertical betatron tune ν_y. As shown in Fig. 4, the deuteron data show no dependence on ν_y, however, the proton's $\varepsilon_{FS} / \varepsilon_{Bdl}$ ratio grows sharply near the 1st-order intrinsic resonance $\nu_y^r = 8 - G\gamma$ shown by the red arrow. We are now preparing a paper about these large deviations of $\varepsilon_{FS} / \varepsilon_{Bdl}$ and their possible explanations [4].

Kondratenko crossing studies

We also started investigating Kondratenko's proposed new method to preserve beam polarization during a spin resonance crossing [6]. The method uses 3 rapid changes of the rf dipole's frequency near the resonance.

The Kondratenko crossing shape shown in Fig. 5 contains 5 linear segments defined by Δt_{slow}, Δf_{slow}, Δt_{fast}, Δf_{fast}, and

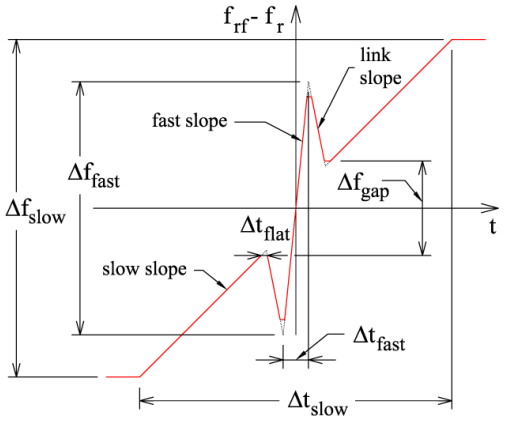

Fig. 5: Kondratenko crossing shape with its parameters.

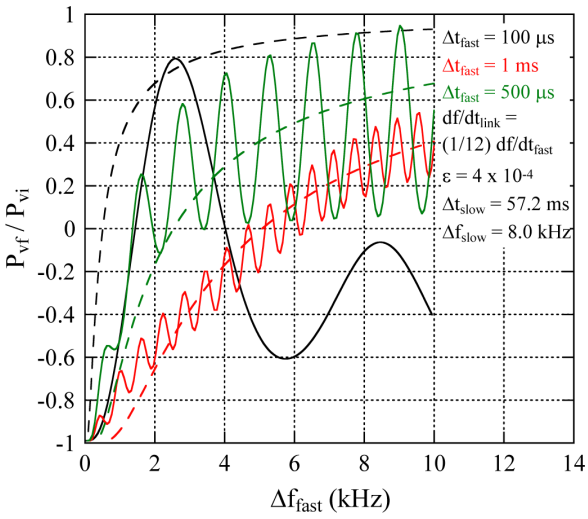

Fig. 6: The single particle predictions for Kondratenko crossing are shown by the solid lines. The dashed lines show the Froissart-Stora prediction for simple fast crossing.

the link slope $(\Delta f / \Delta t)_L$. Using the new Chao formalism [7], we calculated the final P_V for a single particle, after sweeping through a spin resonance with this shape; the solid lines in Fig. 6 show P_V vs. Δf_{fast} for three different Δt_{fast} values. The dashed lines show the Froissart-Stora prediction for a simple fast crossing of the resonance. Note that, for some crossing parameters, the Kondratenko shape may better preserve the polarization than simple fast crossing.

We tested Kondratenko's idea using 2.1 GeV/c polarized protons stored in COSY. The fast-slope / link-slope ratio was 157; this gave a Δf_{gap} (see Fig. 5) greater than the spin resonance width. We centered the crossing shape at the resonance frequency f_r and then measured the final polarization for different Δf_{fast} with all other relevant parameters fixed. These data are plotted in Fig. 7 as solid blue circles. We also measured a few points with simple fast crossing for comparison, which are shown in Fig. 7 as open red circles. Figure 7 also shows single-particle predictions for Kondratenko crossing and simple fast crossing as blue solid and red dashed lines, respectively. The data and the predictions indicate that, with our crossing parameters, the Kondratenko crossing result seems close to simple fast crossing. Thus, further tests with a better choice of the crossing parameters are needed.

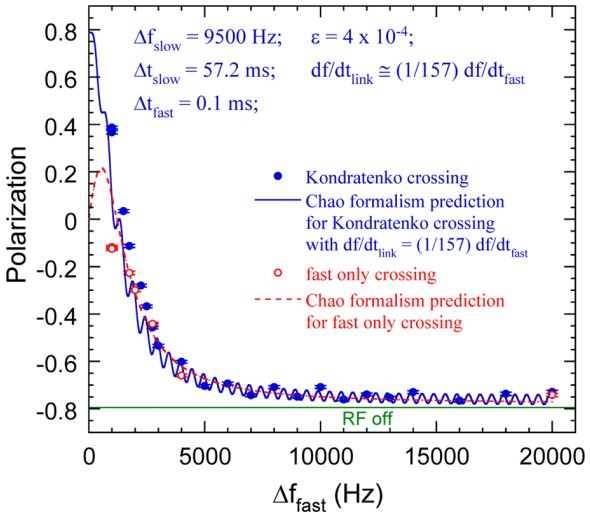

Fig. 7: The measured proton polarization at 2.1 GeV/c is plotted vs. the fast frequency range Δf_{fast}. The dashed and solid lines show single-particle predictions for simple fast crossing only and Kondratenko crossing, respectively.

Plans for Siberian snake studies

To successfully accelerate polarized protons in a very high energy ring, one must overcome many spin depolarizing resonances by using one or more Siberian snakes. A full transverse Siberian snake rotates each proton's spin by 180° around a horizontal axis, but is optically transparent for the orbital motion.

A Siberian snake can be formed in COSY by using one or two Michigan superconducting solenoids, shown in Fig. 8:

- The existing warm Cooler solenoids (0.6 T·m), plus WASA's 0.7 T·m solenoid, and one Michigan solenoid in series; these would give 2.7 T·m, enough for a full snake at 720 MeV/c;
- Two Michigan 1.4 T·m solenoids; 2.8 T·m (750 MeV/c).

A third Michigan solenoid could provide the 90° spin rotation in the injection line needed to match the injected beam's polarization to COSY's stable spin direction.

Installing a Siberian snake in COSY would allow studies of higher-order snake resonances, spin flipping with a nearly and exactly 100% Siberian snake, and snake synchrotron-sideband resonances.

Summary

SPIN@COSY has studied the spin manipulation of polarized protons and deuterons stored in COSY [1,2,3]. We confirmed the interesting behavior of the deuteron's tensor polarization during spin manipulation found earlier at IUCF [8]; we also achieved a record deuteron spin-flip efficiency of 98.5 ± 0.3% [3]. We recently studied the dependence of an rf-dipole-induced spin resonance's strength ε on the vertical betatron tune ν_y; we found that its strength was greatly enhanced by its proximity to a 1st-order intrinsic spin resonance [4]. We just started investigating Kondratenko's proposed new method for preserving the polarization during a resonance crossing [6]. We hope to soon install a Siberian snake in COSY to explore its interesting and important changes to the spin dynamics.

Fig. 8: One of the Michigan superconducting solenoids.

Acknowledgements:

We thank the COSY staff for the successful operation of COSY, its cyclotron, and its polarized ion source. This research was supported by the German BMBF Ministry.

References:

[1] V.S. Morozov et al., PRST-AB 7, 024002 (2004)
[2] M.A. Leonova et al., PRL 93, 224801 (2004)
[3] V.S. Morozov et al., PRST-AB 8, 061001 (2005)
[4] M.A. Leonova, Studying unexpected rf spin resonance strength enhancements and reductions, to be published
[5] H. Stockhorst and B. Lorentz, COSY int. rep. (2003); S.Y. Lee, *Spin Dynamics and Snakes in Synchrotrons*, World Scientific Pub. Co., Singapore (1997).
[6] A.M. Kondratenko et al., Physics of Particles and Nuclei Letters 1, No.5, 266 (2004)
[7] A.W. Chao, PRST-AB 8,104001 (2005)
[8] V.S. Morozov et al., PRL 91, 214801 (2003)

[1] Univ. of Michigan, Ann Arbor, MI 48109-1120 USA
[2] Forschungszentrum Jülich, IKP, D-52425 Jülich
[3] Helmholtz Institut, Universität Bonn, D-53115 Bonn
[4] Brookhaven National Laboratory, Upton NY 11973 USA
[5] KEK (J-PARC), Tsukuba-shi, Ibaraki-ken 305-0801 Japan
[6] OOG Zaryad, Novosibirsk, 630058 Russia
[7] Illinois Institute of Technology, Chicago, IL 60616, USA

Summary of the results of first tests of a new dissociator for the polarized Ion Sources at COSY/ Jülich

A.S. Belov, O. Felden, R. Gebel, A. Kieven, P. von Rossen, N. Rotert

Dissociator design modifications

Several changes have been made in the design of a new dissociator for the COSY polarized ion source:

- The dissociator tube array has a smaller volume due to shortening of tubes connecting the hydrogen, deuterium, oxygen and nitrogen valves with the dissociator tube. The dissociator tube itself has smaller length.
- The nozzle cooling accommodator has been changed. Its length has been increased to 50 mm and the diameter of the channel has been decreased to 5 mm. The nozzle throat diameter has been decreased to 2.3 mm.
- A two-stage cooling of the dissociator tube and nozzle has been introduced. A preliminary cooling stage has been added. In this stage the dissociator pyrex tube part with length of 50 mm has been cooled by a surrounding aluminum block to ~ 100K to ensure cooling of atomic hydrogen with its minimal recombination in this dissociator tube section.

The temperature of the nozzle was varied in the range of 35-100 K to find the optimum conditions for atomic hydrogen beam formation. The beam parameters were measured with the set-up of a beam chopper, a quadrupole mass spectrometer and a time of flight mass spectrometer described in the contribution to the last annual report [1].

Results of the first measurements

The peak intensity of molecular and atomic hydrogen beam was found to reach its maximum value at significantly smaller feeding hydrogen gas amount per pulse due to smaller dissociator tube and connecting tubes total volume. This will allow operation with higher repetition rate without loss of atomic hydrogen beam intensity due to scattering. Higher RF power for a comparable dissociation degree is necessary due to probably stronger recombination in the longer nozzle section.

Better cooling of the atomic hydrogen flux to the temperature of the surrounding nozzle wall has been achieved by the longer nozzle channel and the existence of the preliminary cooling channel section. Figure 1 shows the most probable velocities of the atomic hydrogen beam obtained with the new dissociator as well as with the dissociator of the previous design. For the previous dissociator design the most probable velocity increases with the rise of gas flux and relative RF power. For a RF power higher than 500 W a sharp increase of the most probable velocity has been observed which is connected to plasma penetration through the nozzle section. For the new dissociator design the most probable velocity remains almost constant with increase of flux and RF power even to the level of 1 kW.

A higher density of atoms in the atomic beam for a given temperature of the nozzle has been reached. Figure 2 shows the results of measurements of the density of atomic hydrogen beam vs. gas flux for the new dissociator and old one for a temperature of the dissociator nozzle of 77 K. The figure shows that a slightly higher atomic hydrogen beam density is achieved for a significantly smaller hydrogen valve pulse duration. The number of hydrogen molecules per pulse decreased sharply due to the decrease of the total volume of the dissociator tubes. A higher atomic hydrogen beam density is obtained due to higher peak hydrogen gas density in the dissociator tube and a higher level of RF discharge power used. An increase of the RF discharge power to 2-4 kW would allow to reach even a higher density of atomic hydrogen beam.

References

[1] A.S. Belov et al.; Velocity measurements of the pulsed atomic hydrogen beam of the COSY polarized ion source; IKP Annual Report 2004

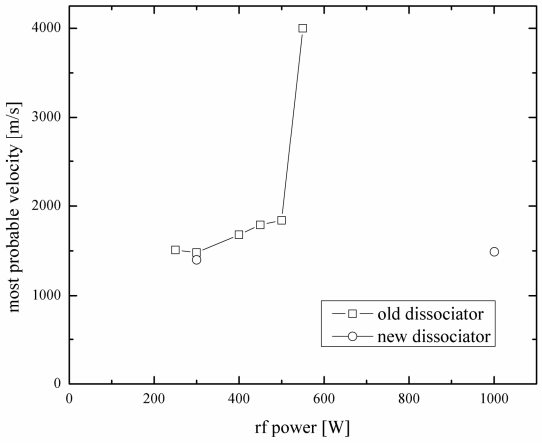

Fig. 1: Most probable hydrogen atoms velocity vs. RF discharge power for old and new dissociator design.

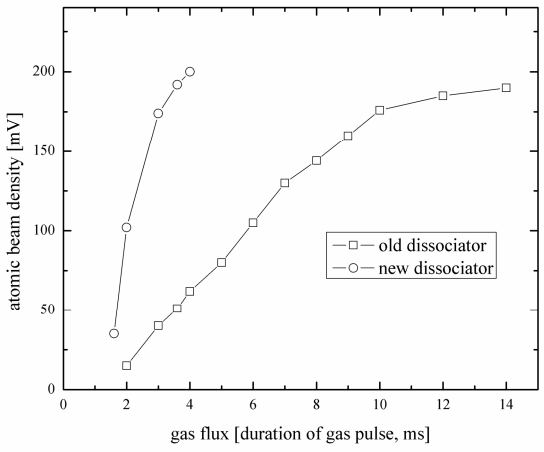

Fig. 2: Density of atomic hydrogen beam without sextupole magnets

A.S. Belov, W. Derissen, O. Felden, R. Gebel, A. Kieven, P. von Rossen, N. Rotert

The operation of the dissociator part of the well and reliable performing polarized ion source works in routine operation close to the technical limits. The peak intensity of 7.5×10^{16} atoms/s [1] is comparable to the best performing continuously working atomic beam sources and in accordance with its design. To reach the level of performance of modern pulsed atomic beam sources with peak intensities of up to 2×10^{17} atoms/s substantial changes in the design have been necessary.

Recent measurements of the atomic beam parameters have motivated the improvement of the cooling system to optimize the matching to the focusing magnet system. The uses of permanent hexapole magnets with pole tip strength of up to 1.4 T justify the efforts to achieve best matching.

The operation of the dissociator system showed up also a tendency to get leaks in the water cooling circuit when running over periods longer than 2 months. The result of the leakage is an instable discharge and an increased probability of a blocked tube and nozzle. Blocking the tube by ice routinely destroys the pyrex tube between the nozzle and the cooling tube.

The main design goals for the construction of a new dissociator module have been:

- Improved cooling capabilities of the nozzle
- An additional accommodator stage for precooling
- A reduced gas consumption
- Optional insertions of fast valves
- No water cooling of the discharge tube
- Compatibility with the existing vacuum chambers

These goals have been realized successfully. The new setup is shown in fig. 1 and 2. The cooling capability is depicted in fig. 3. After 2 hours of cooling at the nozzle a temperature of 26 K has been reached, 10 K below the minimum temperature of the old design. The quality of the rf discharge is shown in fig. 4.

The results of first measurements of beam parameters have confirmed the improvement with respect to the improved cooling capabilities [2].

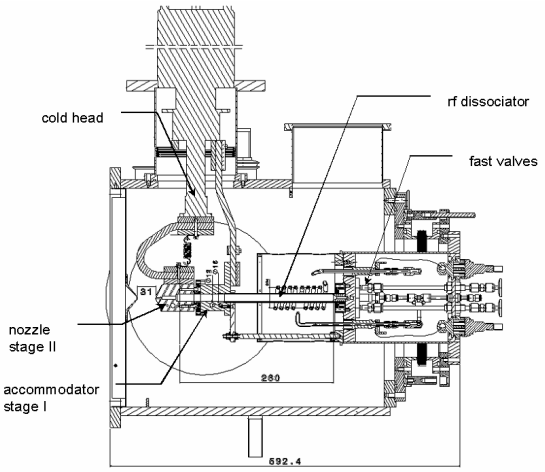

Fig. 1: Schematic view of the new dissociator assembly.

References

[1] A.S. Belov et al.; IKP Annual Report 2004
[2] A.S. Belov et al.; this IKP Annual Report

Fig. 2: The dissociator system pre-assembled on the workbench.

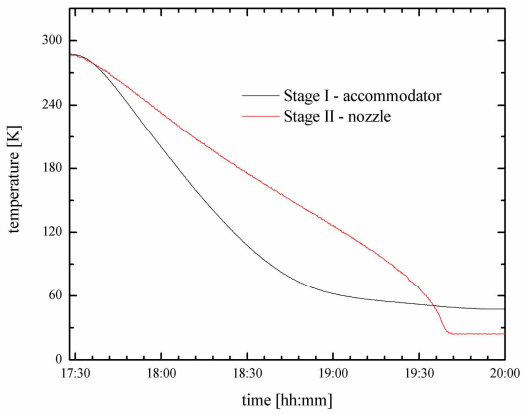

Fig. 3 : Cooling down of the nozzle and the accommodator

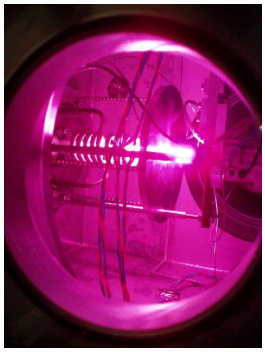

Fig 4 : The rf discharge during first measurements of atomic beam parameters.

Particle Beam Profile Measurement Based on Fluorescence

C. Böhme‡, J. Dietrich, V. Kamerdzhiev, I.N. Meshkov+, I. Mohos, A.N. Parfenov+, T. Weis‡

Interaction of an ion beam passing through a gaseous media results in atom excitation and / or ionization. De-excitation of the atom is partly possible by the emmission of visible light, which can be detected by photomultiplier techniques and therefore can be used to determine the ion beams location and distribution.

While detecting the photons to determine the beam profile the measurement is much faster compared to diagnostic techniques using the ionisation products. And the light is not disturbed, e.g. by magnetic fields. However, the cross section for light emission is much lower compared to the production of electrons / ions. This leads to a small quantity of photons being available for detection.

The photons emitted are focused with a lens onto a Hamamatsu 32 channel linear array photomultiplier (PM), in which each 4 channels were combined, resulting in 8 groups for the readout. The complete electronic setup for control and readout of the PM was developed and built at the IKP, FZ-Jülich [1]. The basic setup and first successful results concerning the determination of beam location and profile at the JESSICA beamline have been described in detail in [2] and were presented in [3] and [4].

In a second step of the ongoing program we moved the PM to the ANKE area at the COSY ring. The residual gas pressure in this area during our measurement has been at the level of 10^{-8} mbar, while using the ANKE gas target it increased to the level of 10^{-7} mbar. Due to low residual gas pressure compared to the measurements at the JESSICA extraction beam line typical maximum counting rates per channel of 200/s to 300/s have been registered at 45 MeV with typically 10^{10} protons stored inside the ring.

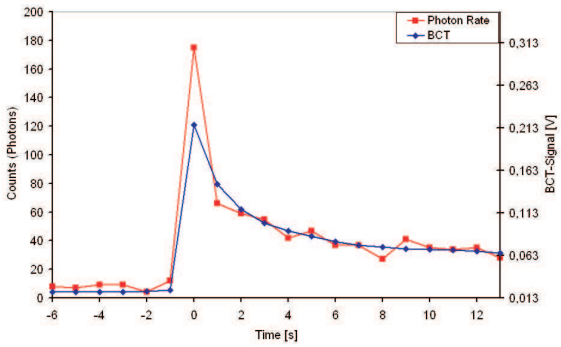

Fig. 1: Registered photons per second and BCT-signal proportional to beam current versus time. Beam injection at t=0.

By summing up these events during some time, typically about one second, reliable beam profile measurements could be performed. It was possible to register the beam profile continuously for several seconds in order to see changes in the profile. As shown in Fig. 1 the registered photons per second compared to the beam current transformer (BCT) signal allows for a quantitive determination of the beam currents, respectively the number of particles in COSY. In this figure the gradient of registered photons during some time is shown and scaled to it the BCT signal. For t=0, at injection of the protons into COSY, the number of events registered by the PMT is increased originating from high particle loss.

Measurements of the cross section for light production of protons passing through Nitrogen and Xenon have been reported in [5]. With our earlier experiments at the JESSICA extraction beam line, described in [2], we could reproduce the cross section for N_2 ($2 \cdot 10^{-20}$ cm^2 at 2.5 GeV).

During the experiments at the ANKE area measurements were taken with residual gas as well as with activated gas target. With activated gas target (mainly N_2 residual gas pressure, instead of mainly H_2 residual gas pressure with the gas target shut off) the registered number of photons increased tremendously. The increased detection rate could definitely not be explained with the increasing background pressure alone and led to the assumption that the cross section for light production of N_2 is orders of magnitude larger compared to that of H_2. This could indeed be verified by experiments with N_2 and H_2 at the JESSICA beamline at 40 MeV beam energy using our test vacuum chamber at different gas pressures. The ratio $\sigma_{H_2}/\sigma_{N_2}$ shown as a function of pressure in Fig. 2 turned out to be in the order of 1%, explaining the results obtained at ANKE in the COSY ring.

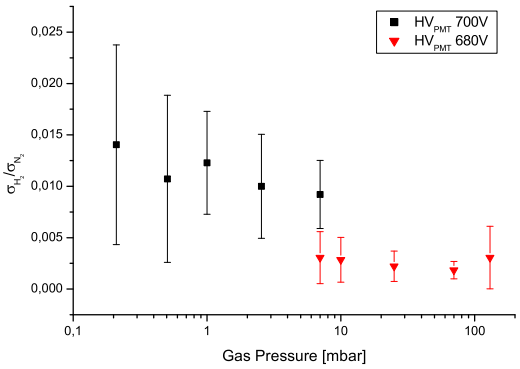

Fig. 2: Ratio of the crossection of H_2 to N_2 at different pressures with different voltages of the PM.

It can be seen in Fig. 2 the measured cross section ratio is depending on the voltage of the PM. The strong influence on the cross section with a relatively small voltage variation of 20 V is not understood and subject to further investigations.

Another subject for further investigation is the wavelength composition of the produced light, as the used PM has a wavelength dependent registration probability. Some basic measurements have been performed for N_2 by M. Plum in [5] and measurements at lower proton energy have been described in [6]. Furthermore the data analysis system have to be automated for using it in the COSY control room.

References:

[1] I. Mohos, private communication.
[2] J. Dietrich et al., IKP Annual Report 2004
[3] J.Dietrich et al., First Beam Profile Measurements Based on Light Radiation of Atoms Excited by a Particle Beam, 33rd ICFA Advanced Beam Dynamics Workshop on High Intensity and High Brightness Hadron Beams, Oct. 18. - 22., 2004, AIP Conf. Proc. Vol. 773 pp. 184-187.
[4] C.Böhme et al., Beam profile measurements by light radiation of excited gas atoms, 26. Arbeitsbericht der Arbeitsgruppe Energiereiche Atomare Stöße, edited by J. M. Rost and J. Ullrich (MPI für Physik komplexer Systeme, Dresden, 2005)
[5] M.A. Plum et al., Nucl. Instr. Meth. A492 (2002), p.74.
[6] D.A. Dahlberg et al., Phys. Rev. **164**, 1967, p.20.

+ JINR Dubna, Russia; ‡ University Dortmund, Germany

Operation of the Injector Cyclotron and Ion Sources at COSY/ Jülich

R. Brings, O. Felden, R. Gebel, A. Kieven, P. von Rossen, N. Rotert

Cyclotron operation

In 2005 the injector cyclotron did provide beams for 6212 hours for the accelerator facility COSY. In that year in December the injector passed the notable mark of 100,000 h of operation since it started delivering beams as COSY injector in 1989 after a major refurbishment. The time distribution over the years is shown in fig. 1.

The otherwise reliable operation of the cyclotron in 2005 was interrupted for around 400 hours due to a failure of the matching capacitor of the central conductor of the rf system. A water leak was quickly fixed provisionally providing operation until end of the scheduled running period.

Besides serving COSY as injector the cyclotron was crucial in providing irradiations at the internal and external target stations for external users, e.g. the Institute for Nuclear Chemistry (INC) and the Fraunhofer Gesellschaft (FHG).

Ion source operation

The operation of the ion sources showed no failures in 2005. The improved sophistication of the filament driven operation allowed operation of the filaments in excess of 1000 hours. The operational time of the filaments for the different sources is shown in figure 2.

Recent gains in polarized intensities

The intensities of polarized beams extracted from the cyclotron exceeded 1.9 µA for deuterons and 2.0 µA for protons. With intensities of this magnitude it was possible to provide 2.6×10^{10} polarized deuterons at maximum beam momentum in COSY for experiments. The time dependence of the unpolarized and polarized deuteron beam current during a cycle in the synchrotron is shown in fig. 3 and 4. The circulating beam current reaches 35,4 mA for unpolarized and 6.3 mA for polarized deuterons. The analysis of the signal from the beam current transformer demonstrates the capability to inject, to capture and to accelerate the provided beams with high efficiencies.

The development of the polarized D^- and H^- beam intensity since 2000 is shown in fig. 5.

In a very fruitful collaboration with the Institute for Nuclear Research (INR Troitsk, Russia) the optimization of ion source components resulted in an increased performance of the polarized ion source with respect to intensity and reliability. To increase the pulsed intensities for hydrogen and deuterium nuclear polarized beams an improved dissociator has been designed and constructed in 2005. The optimization studies are partly funded by the European Community under the contract acronym HP-NIS (High Performance Negative Ion Sources).

Replacement of aged cyclotron components

The cyclotron is in use since the mid 60s of the last century. Most of the systems were refurbished between 1980 and 1989. But again 20 years later wear-out of tubing, the loss of elasticity of vacuum and water seals becomes more prevalent.

The upgrade of the vacuum system has proceeded. The replacement of the two main turbo molecular pumps has been completed after the implementation of a new control system. The degree of automation of the replaced control programs will be reached after some iterations.

The reported inoperability of the water-cooled solenoid "LV1" has been successfully eliminated during the summer shutdown in 2005. Unfortunately, the damaged soldering in the water distribution to the first solenoid in the injection path to the cyclotron made it necessary to dismount the whole injection column in the center of the cyclotron, which was quite elaborate. The corresponding water connections at the subsequent solenoids were refurbished in one go to reset the time to a similar failure for all three solenoids.

For similar reasons the control and regulation circuits for the inflector and the buncher have been refurbished. The position control circuits for the inflector have been replaced successfully.

By bad chance the newly available full functionality of theses elements was offset by a rise in vacuum pressure in the cyclotron chamber. The pressure dependence of the

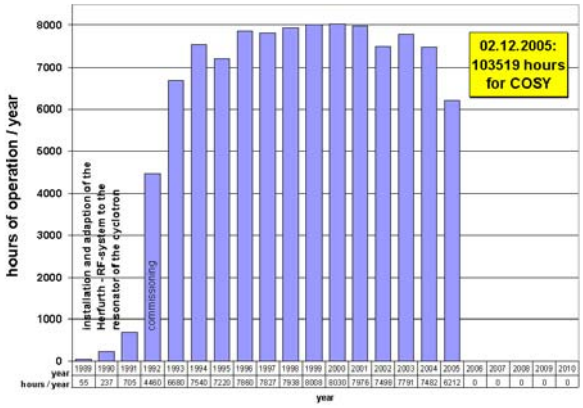

Fig. 1: Operation of the Cyclotron as the injector for COSY. At the end of 2005 the total operating time of the cyclotron rf reached 206,148 hours.

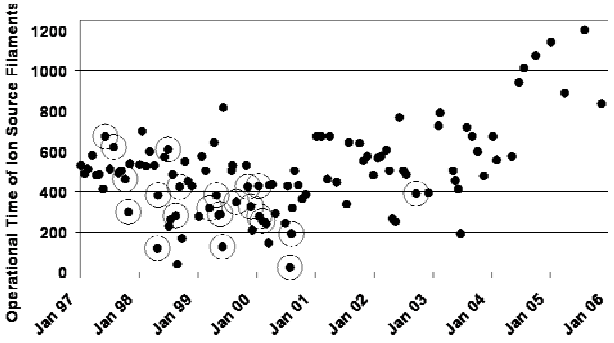

Fig. 2: Up-time of the filament driven ion sources since beginning of 1997. Circles mark an unscheduled exchange of a filament during operation.

intensity close to the extraction radius is depicted in figure 6. Without great difficulties a pressure around $2x10^{-7}$ mbar was reachable in 1998 keeping beam losses practically negligible. Beam losses reached a critical level of over 50% in November 2005 and prevented for instance the polarized beam from going beyond the 3 µA mark.

The state of the vacuum system has reduced the performance for beam delivery of the injector in an intolerable way. The ongoing increase of pressure in the main cyclotron chamber and the pressure dependence of the beam intensity in front of the extraction elements are also visible in figure 6. After setting the system in operation at the end of the summer shutdown the full pumping speed was not available and it was identified that the three installed cryogenic pumps were in need of a complete overhaul. In order not to interrupt the beam schedule for users the overhaul was postponed until the winter shutdown because it was evident that only after a time consuming replacement of worn out parts and a lengthy recovery procedure the pumps would be ready again for operation at the cyclotron chamber.

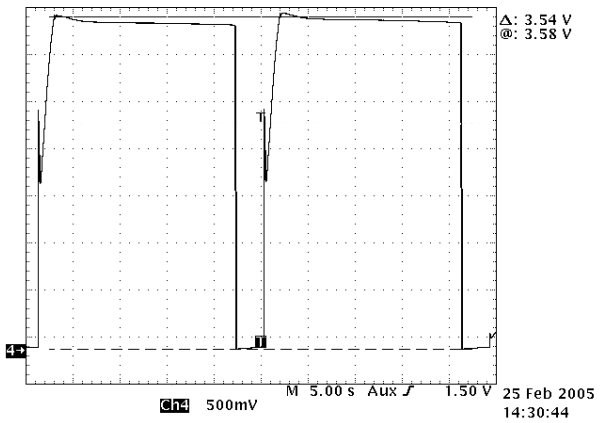

Fig. 3: Two COSY cycles of unpolarized beam deuteron current showing 35,4 mA at the maximum beam momentum.

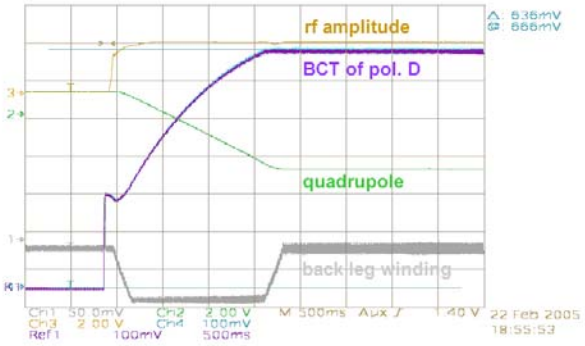

Fig. 4: 6,36 mA polarized deuteron beam current inside COSY for the GEM experiment at the start of the cycle.

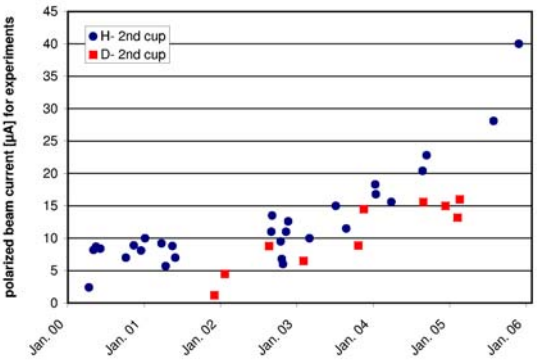

Fig. 5: Beam current development of the polarized ion source since 2000 measured at the second cup of the source beam line. The data is taken from the logbook kept during user beam times.

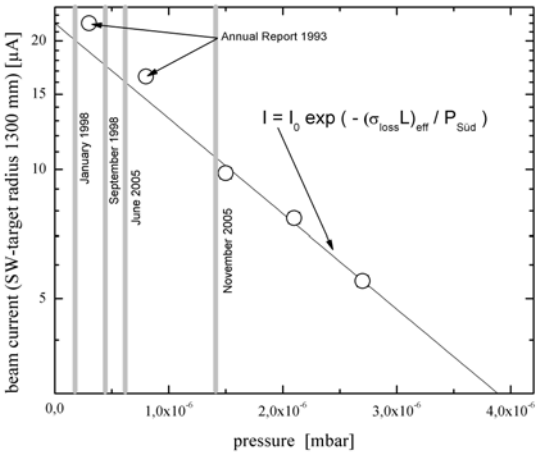

Fig. 6: A semi-log plot of the beam intensity close to the extraction radius as a function of the measured pressure. For the fit the last three points taken in November 2005 have been used.

Slot-finger Super Conducting structure with RF focusing

Yu. Senichev and N. Vasyukhin

General Concepts of Slot structure

The linear accelerator based on a superconducting structure with a high accelerating gradient accordingly has a strong RF defocusing factor. The focusing system elements are located outside the cavity and a transition between the cold and the warm systems is required. Therefore an additional drift space between cryostats is needed, which decrease real estate gradient and can cause parametric resonance in the longitudinal plane in the energy range of $3 \div 20$ MeV. We consider the novel superconducting H resonator based on the TE211 mode with a slot and RF finger, providing the high-intensity beam focusing in the large range of low energy of $3 \div 50$ MeV, and above 50 MeV we suggest using the slot structure with the external quadrupoles giving the better condition for the transverse beam stability in comparison with the spoke structure [1].

In this structure as the first step to minimize the RF defocusing factor we introduce the quadrupole component in the accelerating gaps by two stems alternatively situated in the horizontal and vertical planes from gap to gap in the H resonator (Fig. 1). Thus, instead of the drift tube, like in the spoke structure, we have vertical and horizontal slots between stems. The fundamental TE211 creates the π mode in the longitudinal plane with the accelerating period $\beta\lambda/2$ and the alternative RF quadrupole field with period $\beta\lambda$. Besides, the slot structure is simpler in comparison to the spoke resonator, since it does not require 3D brazing of the drift tubes.

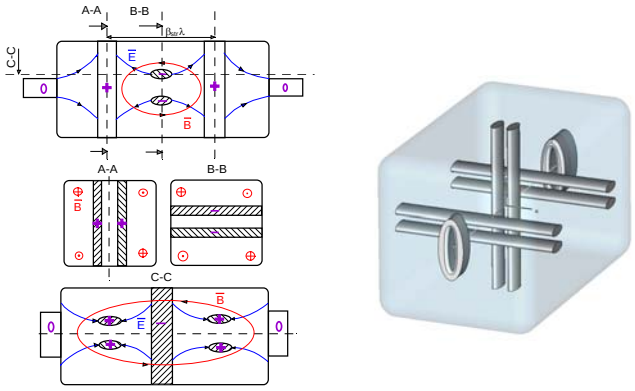

Fig. 1: *Schematic and 3d view of the slot structure*

The analytical estimation shows that for the low energy part the defocusing factor can be partly compensated. At least the transverse motion is stable without any focusing elements for the synchronous phase $|\overline{\varphi}_{qs}| \approx 5^0$.

Nevertheless, even the slot focusing and the additional sliding effect together cannot provide the appropriate RF focusing channel with a reasonable aperture for the high-intensity beam.

Slot-Finger structure

Now let us consider the structure with additional RF electrodes installed on the extreme slots and the cavity ends as shown in figure 2. To minimize the influence of finger on the neighboring mode excitation the cavity has to be symmetrical relative to the cavity center. Therefore the fingers are installed symmetrically in the extreme cells only. Such a cavity is called the slot-finger resonator.

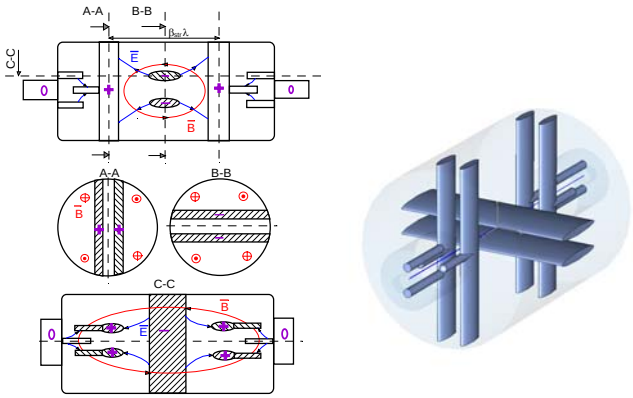

Fig. 2: *Slot-finger structure*

One of the drawbacks of the structure with additional focusing electrodes is the accelerating gain restriction by the high electric field between these electrodes. But because of the properties of H mode the electric field have cosine distribution along the cavity, which allows preventing of the accelerating gradient drop if the additional electrodes installed in the extreme cells.

Numerical simulations

The beam dynamic is simulated using the 3D PIC code [2] in the 3D electrical and magnetic fields exported from CST Microwave Studio. The beam dynamics in the accelerating channel based on the slot-finger structure with the FOODDOOF lattice was simulated. Main parameters presented in Table 1.

Initial energy	3 MeV
Final energy	21.6 MeV
Channel focusing type	FFOODDOO
Average Real Estate Gradient	1.6 MV/m
Cavity Number	40
Maximal Average Current, with allowed losses below 1W/m	40mA
Channel transverse acceptance, norm	5·π·mm·mrad

[1] Yu.Senichev and N. Vasyukhin, in Phys. Rev. ST Accel. Beams 8, 070101 (July 2005), http://prst-ab.aps.org/pdf/PRSTAB/v8/i7/e070101

[2] N.Vasyukhin, R.Maier and Yu.Senichev, in *Proceedings of the European Particle Accelerator Conference, 2004* (ISBN 92-9083-231-2, Lucerne, 2004),pp. 2002-2004, http://accelconf.web.cern.ch/accelconf/ e04/PAPERS/WEPLT067.PDF

A Test of Electron Cooling at 70 keV Electron Energy

H.J. Stein, D. Prasuhn

Electron cooling at COSY is routinely used at injection applying an electron energy of about 24.5 keV for 45 MeV protons. Originally, the COSY electron cooler had been designed for up to 100 keV electron energy. The capability to produce a 3 A, 100 keV electron beam was clearly demonstrated during the commissioning tests in 1992. In later years HV sparking occurred above 70 keV. In September 2005 we tried successfully to operate the electron cooler at 70 keV in order to study the cooling at elevated proton energies.

Fig. 1 shows the behavior of proton beam current (lower curve) and H^0 rate (upper curve) observed in cycles of 2 min duration. The electron beam with a current of 250 mA was switched on only after the proton beam was accelerated from the injection energy level of 45 MeV to 129 MeV, corresponding to 70 keV electron energy.

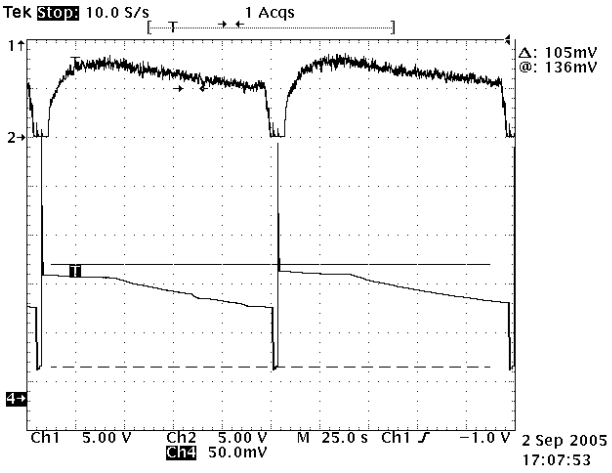

Fig.1: Electron cooling at 70 keV electron energy with 250 mA electron current. The electron beam is switched on only after the proton beam is accelerated and debunched. In contrast to cooling at injection energy, initial losses during the cooling process are negligible. However, more than 50% of the injected coasting beam is lost during bunching before acceleration. The remaining cooled beam intensity (lower curve) is 0.9 mA= $7x10^9$ circulating protons. (a 100 mV BCT signal corresponds to 1 mA proton beam current.) The corresponding H^0 rate (upper curve) is 2300 counts/s (10 V correspond to $3x10^3$ H^0 particles).

By definition, the cooling time is determined by the time when the H^0 rate reaches its maximum and the H^0 profiles reach their minimum width, see Fig. 2, was about 25 s and of course longer than the 10 s, which are typical for cooling at injection [1]. Proton beam losses occurred in the first seconds due to bunching and acceleration, but there were practically no initial losses during the cooling process, which were always present when the proton beam is directly cooled after injection [1]. The continuous decrease of the proton beam intensity starting at about 40 s is due to a horizontal coherent oscillation after the beam is fully cooled. These oscillations are seen as betatron frequencies on the transverse Schottky FFT analyzer [2]. From time to time the horizontal oscillation jumped to the vertical plane but soon back to the horizontal plane, see also Fig. 4, second cycle. The stepping down of the proton current is due to these short periods of a vertical oscillation causing increased losses because the vertical acceptance in COSY is smaller than the horizontal one.

Without applying our feedback system [3], the instability could be avoided by i) reducing the electron current down to 130 mA, Fig. 3, or ii) by slightly misaligning the electron beam horizontally by 0.35 mrad, Fig. 4. Reducing the electron current resulted in a longer cooling time of about 50 s, the misalignment yielded a larger horizontal emittance as observed by the H^0 profile monitor, Fig. 5.

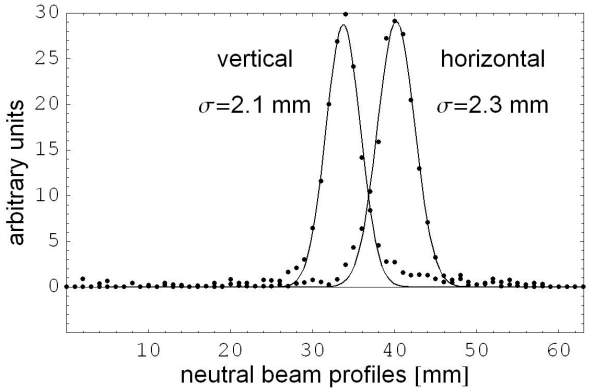

Fig.2: H^0 beam profiles corresponding to the well cooled beam in Fig.1 measured at about 30 s after injection before onset of the horizontal oscillation. Lattice model based optical functions at the position of the electron cooler (β_x = 9 m, β_y = 18 m, D= – 6 m) yield 2 σ emittances of ϵ_x = 0.28 μm and ϵ_y = 0.35 μm.

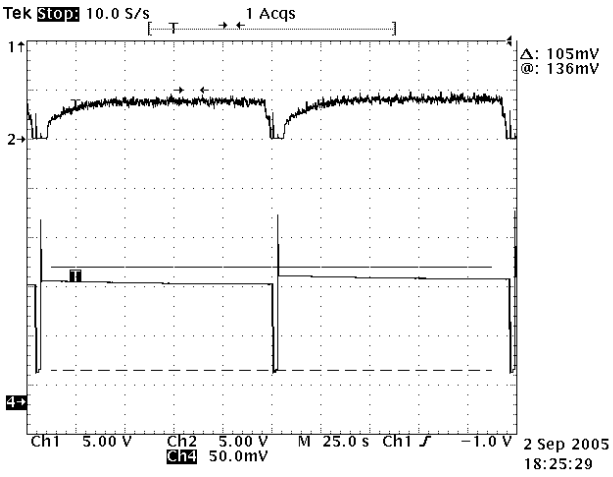

Fig.3: Electron cooling at 70 keV electron energy with 130 mA electron current. No coherent oscillations at all. The slight, exponential decrease of the proton intensity within the 2 min cycle is interpreted as single scattering beam loss due to the residual gas in the 183 m long COSY ring, which had a mean pressure of about $2x10^{-9}$ mbar.

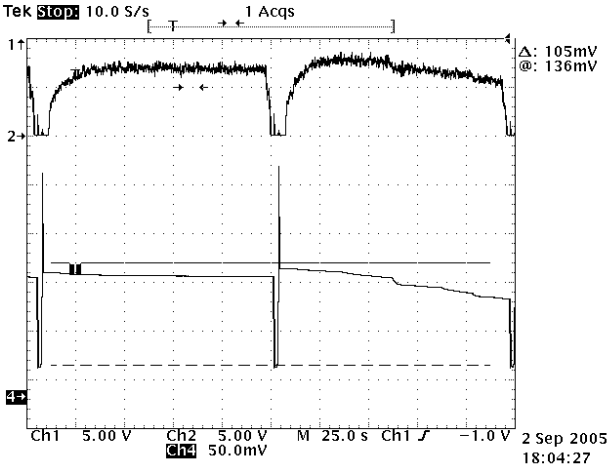

Fig.4: Electron cooling at 70 keV again with 250 mA electron current but in the first cycle with a slightly 0.35 mrad horizontally misaligned electron beam. No coherent oscillations at all. In the following cycle the misalignment was removed resulting again in coherent oscillations as observed by the betatron frequencies seen in the transverse Schottky signal.

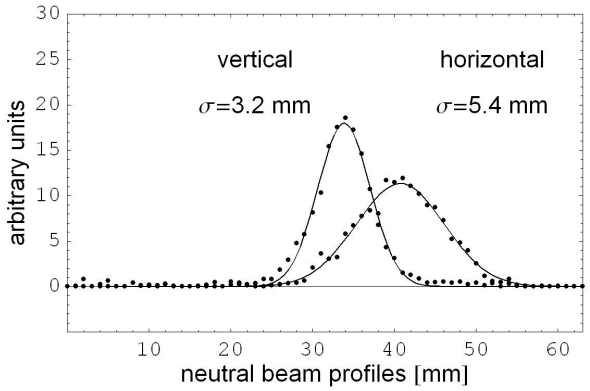

Fig.5: Horizontal and vertical H^0 profiles with a 0.35 mrad horizontally misaligned electron beam. Electron beam current 130 mA. Here, the 2 σ emittances are $\epsilon_x = 1.6$ μm and $\epsilon_y = 0.8$ μm.

Finally, Fig. 6 shows two cycles without cooling electron beam. The proton intensity after acceleration is the same. Also here one sees a slight beam decrease due to single scattering losses but they are not of exponential nature as in Fig. 3 or Fig.4. The reason is that the beam size grows due to multiple scattering with the consequence that the acceptance angle of the ring is getting smaller with increasing beam size. Obviously, the emittance growth due to multiple scattering is fully compensated by electron cooling maintaining a constant beam size.

Besides the details of the above observations we like to make an important conclusion in view of the "initial losses", cf. [1] and [4]. The fact that at 70 keV cooling no initial losses (of incoherent nature) were observed are a strong indication that right after injection the initial losses are caused by the large emittance (and large $\Delta p/p$) so that in this case the ion beam is larger than the electron beam. In the case of cooling after acceleration the ion beam has lost tails in ε and $\Delta p/p$ by the preceding bunching and shrinks during the acceleration

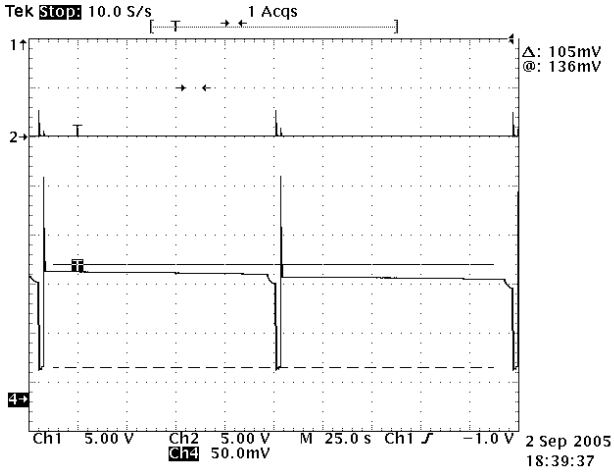

Fig.6: Two cycles without cooling electron beam, therefore, no H^0 signal. Here, the slight decrease of the proton beam intensity is no more exponential.

References:

[1] J. Dietrich et al., Characteristic Features of Electron Cooling at COSY, IKP Annual Report 2004.

[2] V. Kamerdzhiev et al., Instability Phenomena of Electron-Cooled Ion Beams at COSY, Nucl. Instrum. Methods Phys. Res. A 532 (2004) 285-290.

[3] Beam Feedback System for Cooled Ions, IKP Annual Report 2004.

[4] H.J. Stein et al., Present Performance of Electron Cooling at COSY-Juelich, Proceedings of the 18th Conference on Charged Particle Accelerators (RUPAC 2002) Obninsk, Russia, 01.-04.10.2002, editor-in-chief: I.N. Meshkov, Vol. 1 (2004) 220-226.

Design of HIPPI Triple-Spoke Cavity for 352 MHz and β=0.48

E. Zaplatin, R. Maier, M. Pap, R. Tölle

RF Aspects of Cavity Design

The basics of the electrodynamics of the spoke-type cavity are well known and have been discussed many times elsewhere [1]. The electrodynamic design of any SC RF cavity aims to optimise the cavity geometry to reach the highest accelerating efficiency, in other words to minimize values of peak electrical and magnetic fields on the cavity surface relative to the accelerating electrical field on the cavity axis (B_{pk}/E_{acc} and E_{pk}/E_{acc}). The good separation of electrical and magnetic fields in the space gives a freedom to the cavity shape design. The design of the end cell of multi-spoke cavity is defined by two factors – to reach the minimum of magnetic field on the spoke surface and the design of the cavity end cap. The first affects also the distribution of the electrical field along the multi-gap cavity but its profile can be corrected by the end gap length reduction. The end cap design mainly comes from its mechanical properties. The geometry and parameters of the cavity are shown in Fig.1 and Table 1.

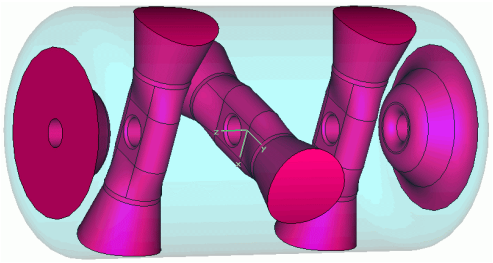

Fig.1: 4-gap H-cavity geometry.

Table1: Some Parameters of HIPPI Triple-Spoke Cavity.

Frequency	MHz	352.9
β=v/c		0.48
R aperture	cm	2.5
βλ/2	cm	20.44
Cavity radius	cm	21.7
Cavity length	cm	78
QR_s	Ohm	93
E_{pk} / E_{acc}		4.65
B_{pk} / E_{acc}	mT/MV/m	10.97
B_{pk} / E_{pk}	mT/MV/m	2.36

The role of the cone in the spoke base for electrodynamics is to increase the spoke diameter right in the region of the maximal B_{pk}. That moves B_{pk} from the outer spoke region closer to the middle of the spoke and reduces B_{pk}/E_{acc}.
The position of the coupler on the cavity and its type (electrical or magnetic) should be checked in terms of the Q_{ext} simulations. The position of the E-field coupler opposite to the mid-spoke looks attractive because of the symmetry of its position. The magnetic field in this region equals zero. This port is designed for CF56 and will fit the coupler developed by IPN Orsay. A second access or coupler port for CF100 is located on the other side (Fig.2).

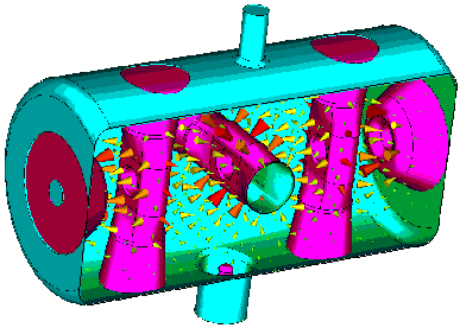

Fig.2: 4-gap H-cavity with electrical coupler and vacuum port.

Simulations with MAFIA indicate the sufficiency of the coupling. For our beam-field parameters (Table 2) the E-field coupler should be installed deep (around 40 mm) inside the coupler port.

Table 2: CW power requirements for the coupler for two accelerating field options and B_{pk}=80 mT.

L_{cav}	beam	Power	Power
m	mA	@ E_{acc}=8 MV/m	@ E_{acc}=10 MV/m
0.78	20	**108.10 kW**	**135.12 kW**

B_{pk}	**80**	mT
E_{pk}	35.34	MV/m
E_{0T}	8.96	MV/m
Voltage	7.28	MV
P_{beam}	121.07	KW
Q_{ext}	3.2E6	

Cavity mechanical stiffening analyses

The very first cavity investigation in terms of the mechanical properties is its mechanical eigen modes. We use the criterion of 200 Hz for the first mode that would be sufficient for the cavity rigidity. To improve the cavity rigidity stiffening rings on both cavity ends are used (Fig.3). The stiffening rings are 3 cm high and 2.5 cm wide. The cavity fixation in four points by every ring is arbitrary and in fact not practical but it allows investigating the modes that are related only to the cavity. The FZJ test cryostat that is planned to be used for the cavity measurements is a vertical bath cryostat. Provisionally, the cavity is to be mounted to the upper flange by means of four rods connected to the cavity walls. To show the structural cavity properties the simulations of the cavity modal analysis with the completely fixed joints, which are supposed to be used for the connection of the rods to the cavity, have been provided. The lowest cavity mechanical eigen-mode is around 261 Hz, indicating sufficient cavity rigidity.
The further strategy of such type cavity design should include integrated simulations of RF and mechanical properties. In our design we consider the installation of the tuner in the middle of the cavity and apply the tuning

pressure to the cavity walls close to the central spoke where the magnetic field is close to its maximal value. The slow cavity tuning is mainly required for the cooldown-to-cooldown difference compensation and 1 bar pressure frequency shift compensation. ANL practical experience shows that 20-50 kHz will be sufficient. Our simulations result in 75 kHz/mm tuning sensitivity for the relatively local pressure application.

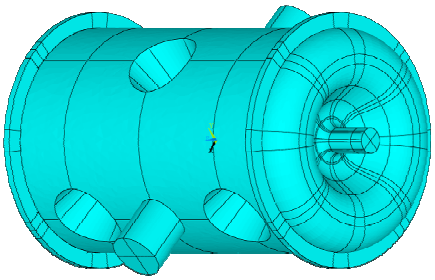

Fig.3: Triple-spoke cavity with stiffening rings.

The most flexible elements in the cavity are the end caps. Let's consider the option with additional end cap eight stiffening ribs (Fig.4).Here the rings are 4 cm high and 2.5 cm wide. The ribs are 10 degrees wide, and should follow the end cap surface increase with radius. Thus the end cap rigidity increases with radius.

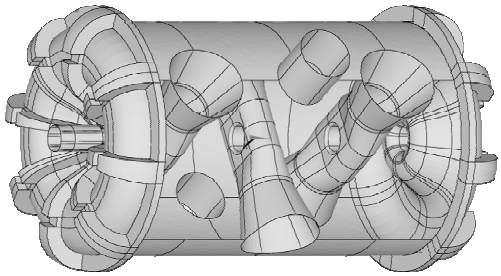

Fig.4: Triple-spoke cavity with stiffening end cap ribs.

Assuming that the end caps do not move at all, the frequency shift from 1 bar pressure would be defined mainly by the magnetic field volume change (cavity inductance reduction). The end cap displacement caused by 1 bar pressure results in the last gap's length reduction (cavity capacitance increase). It means that both effects work in opposite directions concerning the cavity frequency change. Hence, one can find end cap stiffening that would result in an end cap deformation compensating the frequency change owing to magnetic field volume change. The rib height variation shows the effect of frequency shift compensation with the frequency shift crossing the zero line (Fig.5). An uncertain factor here is the end cap wall thickness. So we investigated two different cases for end cap wall thickness (3 and 4 mm for end cap, the rest cavity including spokes is 4 mm).

The action of the Lorentz forces in the region of the magnetic field is directed outside, which is opposite to the action of the 1 bar pressure. It means that the effects of cavity wall and end cap deformations have to be added. In this case the use of the tuners (say, cavity wall fixation in these places) reduces Lorentz force cavity detuning.

For further LFD reduction one could use small ribs (1 cm x 2.5 cm) on the cavity walls in the regions of maximal deformations (Fig.6). LFD rib installations will also affect the cavity frequency shift caused by 1 bar pressure. LFD ribs should be installed as the tuner will compensate the bigger LHe pressure detuning and LFD will be lower. Let's finally note, that investigations and optimizations of all effects are within 0.1 mm, which means strong uncertainties between simulations and the final cavity geometry as the tolerances on cavity manufacturing are within 0.5 mm. Nevertheless, the final practical cavity adjustment is possible if the methods of fine-tuning are included in the mechanical cavity design beforehand. With a use of LFD ribs the dependence on the cavity wall thickness for the frequency shift is negligible.

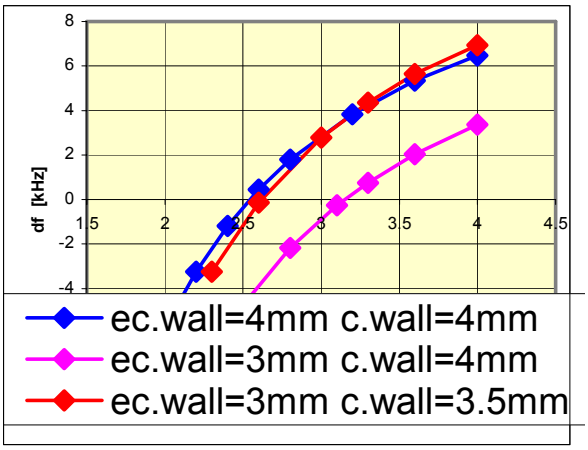

Fig.5: Cavity reaction on 1 bar external loads vs. end cap stiffening rib height.

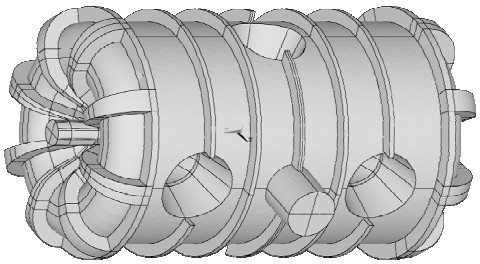

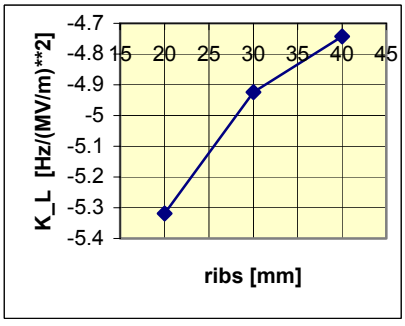

Fig.6: Triple-spoke cavity with stiffening end cap ribs, LFD ribs and cavity reaction on Lorenz forces vs. rib height.

References

[1] E. Zaplatin et al., "Low-β SC RF Cavity Investigations", *SCRF2001, Tsukuba, Japan, 2001.*

Acknowledgements

We acknowledge the support of the European Community Research Infrastructure Activity under the FP6 "Structuring the European Research Area" programme (CARE, contract number RII3-CT-2003-506395)

The WASA-Detector installation inside the COSY accelerator necessitated several changes to the infrastructure installations as well as to the building. Those modifications can only be done after a proper discussion and in accordance with the regulatory authorities to obtain their mandatory approval. One very crucial topic was the discussion about the removal of the top shielding of the ring above the WASA-Detector, because the height of the pellet target exceeded the upper clearance, as seen in fig. 1.

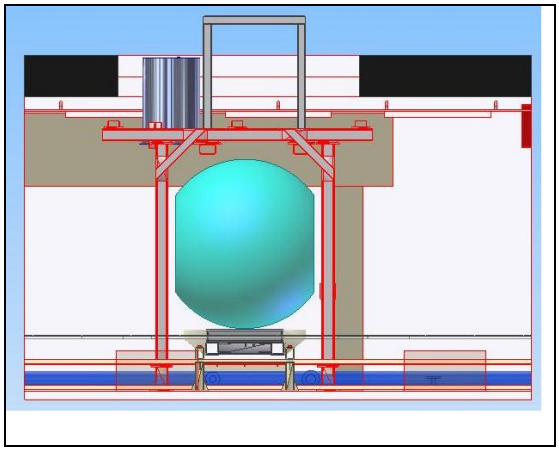

Figure 1: Schematic view of the WASA-detector installation. Depicted is the central detector and the supporting frame for the pellet target inside in the COSY tunnel. The concrete cover of the tunnel is shown in black.

Because of the geometry and materials involved of the central detector its shielding efficiency was compared to that of the top covering made from concrete.
From the Moyer-formula $\lambda = k \cdot A^{(1/3)} / \rho$

with λ = radiation length
k = constant 480 Kg/m²
A = mass number
ρ = density

a dose reduction to 0,35% is obtained in case of the detector made from 11cm iron and 35cm Cs-iodide compared to a reduction to 0,31% for 50cm concrete for neutrons [1,2,3]. This means that the shielding effect of the detector can substitute the concrete lid.
Dismounting of the detector was done by staff members from the research center, collaborating universities, and members of The Svedberg Laboratory. The applied doses to the research center staff during this work ranges up to 21µSv. No parts of the detector exhibited measurable activations except for the beam pipe around the target. There the dose rate is about 25µSv/h. This allowed to transport all part as normal goods except for the beam pipe which had to be labeled as radioactive part.

In the first quarter of 2005 like in the second half of 2004 the neutron detectors badges, which have to be worn when entering the inner hall of COSY showed partly doses up to about 2,3 mSv (cf. fig.2) while in the past the measured doses had always been around or mostly below the detection limit. In spite of checking the other personal dosimeters (film badge and pencil-dosimeter), the working modes of COSY, and the data from the 48 neutron monitors installed around COSY and inside the inner hall these findings from the MPA (Material-Prüfungsamt), which is responsible for the analysis of the badges, could not be explained. [4,5]

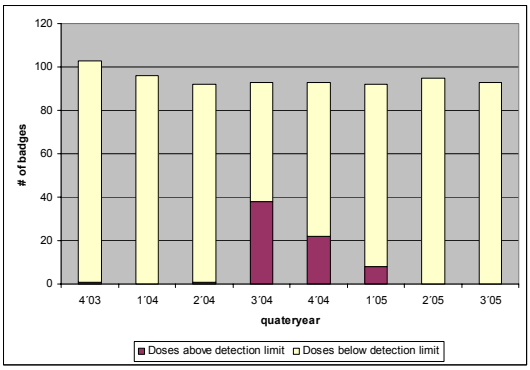

Figure 2: Number of neutron badges showing doses above and below detection limit.

After a common thorough investigation together with the MPA the neutron badges recorded again doses in accordance with the past experience and compliant with the other redundant detection systems used at IKP/COSY.
To ensure, that the neutron detectors are working properly checks are done on a permanent basis. In case of a faulty operation, the control system informs the COSY crew and the radiation protection group immediately [5,6]. Additionally, detectors are calibrated once a year with a strong radioactive source. Another "offline" test is, to look at the behavior of a group of detectors installed near each other. Fig. 3 shows a sample of three monitors installed outside and the corresponding neutron monitor inside the hall.

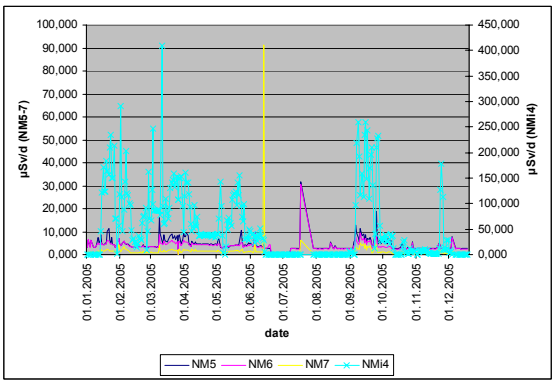

Figure 3: Comparative check of the neutron monitors installed inside and outside of the COSY hall.

W. Derissen, F. Hinterberger, K. Kruck, D. Kirillov, M. Lesiak, H. Machner, R. Maier, P. v. Rossen, R. Siudak, R. Tölle, GEM-, and HIRES collaboration

Three major runs took place at BIG KARL for GEM, ENSTAR, and HIRES. Sufficient time gaps between those runs were scheduled to allow for adequate preparation as complete new setups had to be installed and commissioned for each of the experiments.

The first experiment in January used the high granularity Germanium Wall mounted close to the target. The goal was to look for the (pol)d d→ α η to study isospin violation. For the first time an electron cooled vector and tensor polarized deuteron beam was extracted. The reduced phase space of the deuterium beam through electron cooling was an important precondition as the beam had to pass through the narrow center hole of the Germanium Wall. In addition the cooling was indispensable in reducing the background originating from beam halo to a 10^{-4} level.

After the successful test run, the ENSTAR detector was used to study the reaction p A → X η in the search for η-mesic nuclei. In a coincidence measurement ^{3}He analysed in BIG KARL and the decay products registered in the ENSTAR detector were investigated. The position of this detector in the BIG KARL system is schematically shown in fig.1.

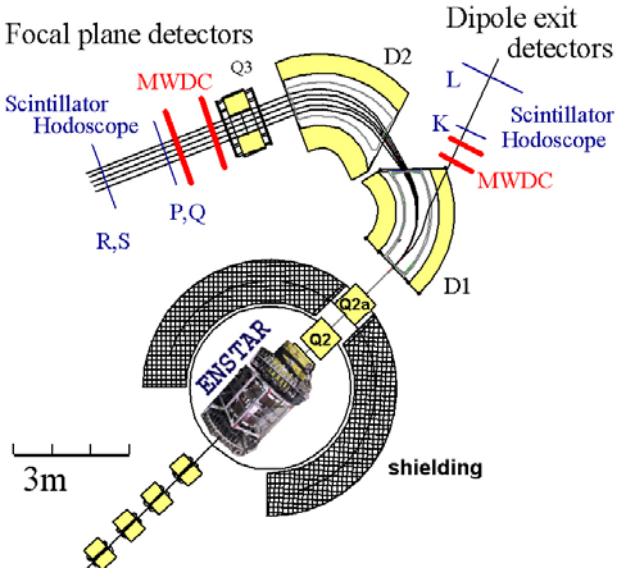

Fig. 1: BIG KARL with its detector systems at the focal plane and at the auxiliary detection position behind the side exit of dipole 1.The ENSTAR detector is mounted in front of quadrupole Q1.

Due to the horizontal extend of the ENSTAR detector the target ladder is not located at the standard position of the spectrograph but a position that is 12 cm upstream. As the first quadrupole of the spectrograph has a very small focal length such a change results in a large change of the ion optics. The standard envelope structure is depicted in figure 2 for a vertical angle acceptance of 100 mrad. The ion optics is optimized such that the ejectiles pass through the narrow gap of the dipoles.

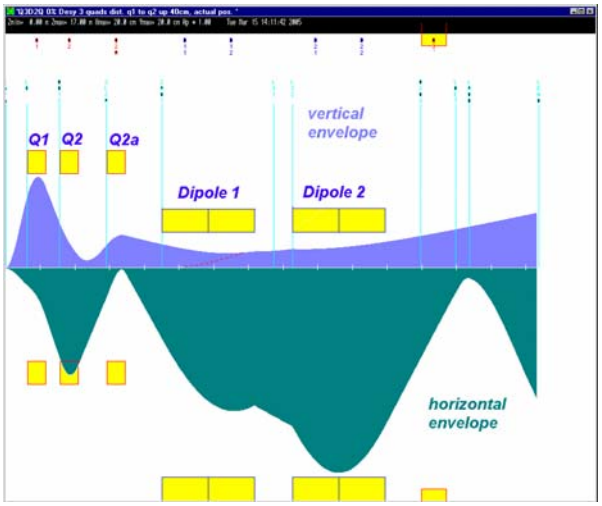

Fig. 2: Envelope structure in the spectrograph in the standard high-resolution mode

This situation changes dramatically if the target is moved upstream. If the standard setting is used one obtains an envelope structure as plotted in fig. 3. The dramatic increase in vertical size inside the dipoles leads to a strong reduction of the vertical acceptance. To alleviate this problem a new parameter set has been generated that allows for a much better transmission. The effect of this new setting is demonstrated in fig. 4. Shown are the particle tracks inside the focal plane detectors in the vertical and the horizontal position. The scale is in millimeter. The upper

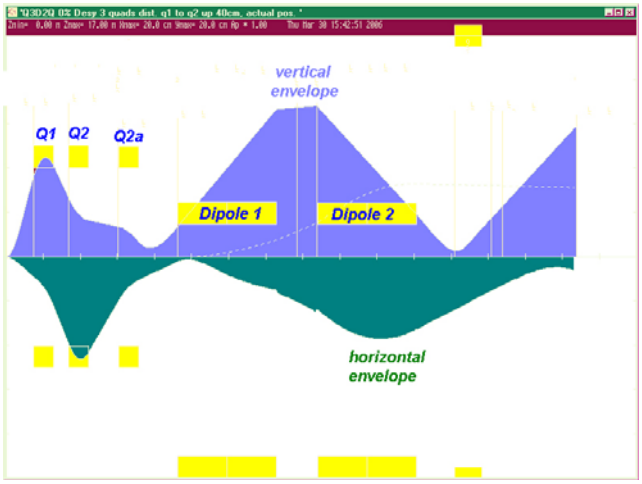

Fig. 3: Envelope structure inside the spectrograph with the standard high resolution setting if the target is moved 12 cm upstream.

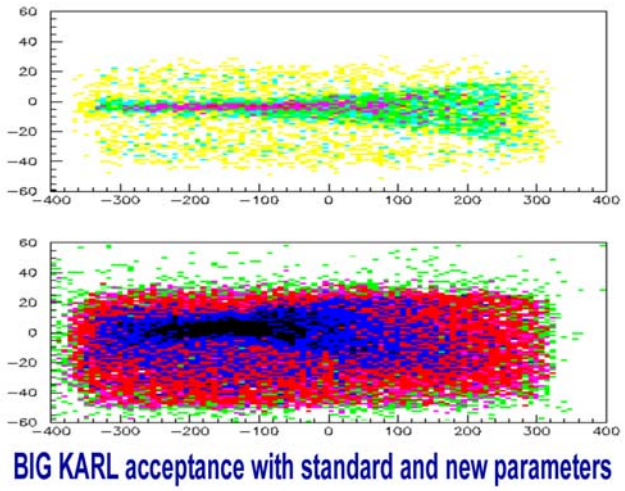

Fig. 4: The effect of the new parameter set to accommodate the different ENSTAR target position. Shown is the particle position distribution inside the focal plane. The upper part is the standard setting the lower is the result of the new mode.

part is the result of the standard setting revealing the extreme cut of the vertical acceptance. By changing the setting of the entrance quadrupoles one obtains a vastly increased acceptance. This new ion optic was an important prerequisite for the feasibility of the ENSTAR experiment.

The HIRES collaboration collected successfully data for the pp→ p K^+ Λ reaction. This was a finalizing measurement that completed the data taken in previous runs. The analysis of the data is in progress.

More information concerning the mentioned experiments are found in dedicated articles of this report.

4 Preparations for FAIR

Design Work for the High-Energy Storage Ring (HESR)*

A. Lehrach[1], S. An[1], T. Bergmark[4], O. Boine-Frankenheim[2], K. Bongardt[1], J. Dietrich[1], A. Dolinskii[2], R. Eichhorn[1], B. Gålnander[4], R.W. Hasse[2], F. Hinterberger[3], T. Johnson[4], T. Lofnes[4], B. Lorentz[1], R. Maier[1], S. Martin[1], G. Norman[4], D. Prasuhn[1], D. Reistad[4], A. Schnase[1], E. Senicheva[1], Y. Senichev[1], M. Steck[2], H. Stockhorst[1], R. Tölle[1], E. Zaplatin[1]

Abstract

The High-Energy Storage Ring (HESR) of the future International Facility for Antiproton and Ion Research (FAIR) at GSI in Darmstadt is planned as an antiproton synchrotron storage ring in the momentum range of 1.5 to 15 GeV/c. An important feature of this new facility is the combination of phase space cooled beams and dense internal targets (e.g. pellet targets), which results in demanding beam parameter requirements for two operation modes: high luminosity mode with peak luminosities of up to $2\cdot10^{32}$ cm^{-2} s^{-1}, and high resolution mode with a momentum spread down to 10^{-5}, respectively. To reach these beam parameters one needs a very powerful phase space cooling, utilizing high-energy electron cooling and high-bandwidth stochastic cooling.

Design Issues and Experimental Requirements

The HESR is dedicated to the field of antiproton physics over a broad momentum range from 1.5 to 15 GeV/c [1,2]. The lattice has a racetrack-shaped design, consisting of two 180° arc sections connected by two long straight sections (see Fig. 1). One straight section will mainly be occupied with the electron cooler. In a later stage a Siberian snake can be added to ensure a possible upgrade for polarized beams. The other straight section will host the experimental installation PANDA [3] with an internal frozen H_2 pellet jet target, injection kickers/septa and RF cavities. Two pickup tanks for stochastic cooling are located close to the ends of each straight section while the stochastic kicker tanks are placed opposite in the other straight section, diagonally connected with signal lines. Special requirements for the lattice are dispersion-free straight sections and betatron amplitudes of a few meters at the internal interaction point. Larger betatron amplitudes to get sufficient beam-target overlap are under discussion [2]. Furthermore imaginary transition energy and optimized ion optical conditions for beam cooling can be provided (e.g. matched betatron amplitudes at the pickups and kickers of the stochastic cooling system and in the electron cooler section, scaling with beam momentum for optimum beam overlap and cooling). Details of the ion optical layout and features of the lattice design are discussed in [4]. The antiproton beam is accumulated in the CR/RESR complex at 3.8 GeV/c before injected into the HESR [2]. Beam parameters at injection, experimental requirements and operation modes are summarized in Table 1.

The HESR was planned with one internal interaction point only, equipped with the PANDA detector [3]. Two other experimental groups (ASSIA [5] and PAX [6]) proposed antiproton spin physics experiments at HESR.

TABLE 1. Design beam parameters and operation modes.

Injection Parameters	
Transverse emittance	1 mm·mrad (normalized, rms) for $3.5\cdot10^{10}$ particles, scaling with number of accumulated particles: $\varepsilon_\perp \sim N^{4/5}$
Relative momentum spread	$1\cdot10^{-3}$ (normalized, rms) for $3.5\cdot10^{10}$ particles, scaling with number of accumulated particles: $\sigma_p/p \sim N^{2/5}$
Bunch length	200 m
Injection Momentum	3.8 GeV/c
Injection	Kicker injection using multi-harmonic RF cavities
Experimental Requirements	
Ion species	Antiprotons
Production rate	$2\cdot10^7$ /s ($1.2\cdot10^{10}$ per 10 min)
Momentum / Kinetic energy range	1.5 to 15 GeV/c / 0.83 to 14.1 GeV
Number of particles	10^{10} to 10^{11}
Target thickness	$4\cdot10^{15}$ atoms/cm^2
Transv. beam size at IP	Range of one millimeter
Operation Modes	
High resolution (HR)	Peak luminosity $2\cdot10^{31}$ cm^{-2} s^{-1}, 10^{10} $\bar{p}$ rms momentum spread $\sigma_p/p \sim 10^{-5}$ 1.5 to 9 GeV/c, electron cooling
High luminosity (HL)	Peak luminosity $2\cdot10^{32}$ cm^{-2} s^{-1}, 10^{11} $\bar{p}$ rms momentum spread $\sigma_p/p \sim 10^{-4}$ 1.5 to 15 GeV/c, stochastic cooling above 3.8 GeV/c

R&D work

Highest priority is assigned to the high-energy electron cooler. The main issue is the reliable operation of high-brilliance electron beams in high-voltage environment. The design work is lead by TSL in cooperation with the Budker Institute, the Fermi National Accelerator Laboratory (FNAL), and industry.

With regard to maximum field strength, magnet aperture and ramping rate RHIC-type super-conducting "cosθ"-magnets installed in the interaction regions fit the HESR requirements except for the magnet length. Short straight super-conducting magnets demands a careful R&D work. Prototypes have to be built to ensure the design choice. In addition R&D work with high priority is allotted to curved super-conducting magnets for improved sagitta in the HESR energy range.

* Work supported by European Community RESEARCH INFRASTRUCTURES ACTION under the FP6 program: DESIGN STUDY (Contract No. 515873 – DIRAC Secondary-Beams), and by INTAS-GSI grants (Ref. No. 03-54-5584).

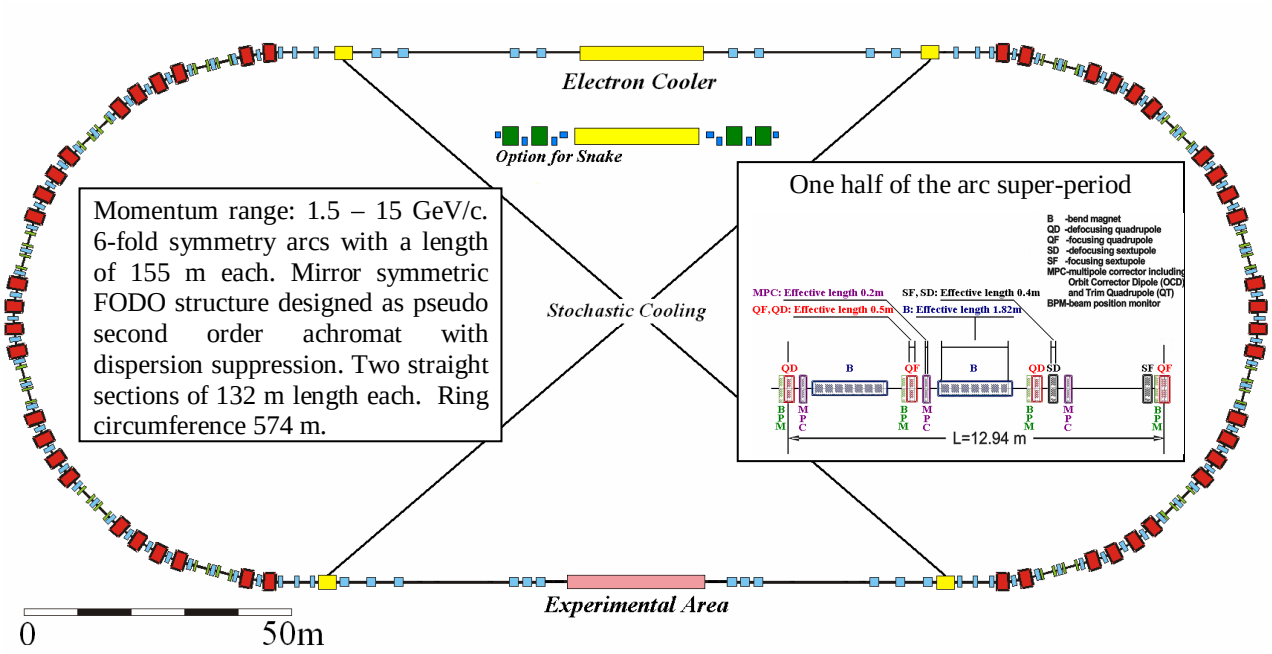

Fig. 1: Schematic view of the HESR with 6-fold symmetry lattice. Tentative positions for injection, cooling devices and experimental installations are indicated. Also shown is the arrangement of elements in the super-period

Prototyping of critical components for the stochastic cooling system has high priority. The main stochastic cooling parameters were determined for a system utilizing quarter-wave loop pickups and kickers. Stochastic cooling is presently specified above 3.8 GeV/c.

The development of low impedance kicker and septa is of great importance for an optimized injection scheme. Furthermore broad-band amplifiers for beam feedback, alignment and assembly issues for bent cryostats and super-conducting multilayer magnets combining several multipoles will be investigated.

The R&D work covers the years 2005-2008.

Conclusion

A correction scheme for the lattice is being developed to correct for field errors, misalignments and chromatic effects of magnets. Main R&D issues are feasibility demonstration for magnetized high-energy electron cooling, prototyping of super-conducting magnets and for high-bandwidth stochastic cooling. In parallel simulation codes for cooled beams interacting with internal targets are improved.

References:

[1] An International Accelerator Facility for Beams of Ions and Antiprotons, Conceptual Design Report, GSI Darmstadt, November 2001, see http://www.gsi.de/GSI-Future/cdr/.

[2] FAIR Project, Technical Report, to be published.

[3] Strong Interaction Studies with Antiprotons, Letter-of-Intent, PANDA collaboration, January 2004, see http://www.gsi.de/documents/DOC-2004-Jan-1151.pdf.

[4] Y. Senichev et al., Lattice Design Study for HESR, Proc. of the European Accelerator Conference, Lucerne, 653 (2004).

[5] A Study of Spin-dependent Interactions with Antiprotons, Letter-of-Intent, ASSIA collaboration, January 2004, see http://www.gsi.de/documents/DOC-2004-Jan-152-1.pdf.

[6] Antiproton-Proton Scattering Experiments with Polarization, Letter-of-Intent, PAX collaboration, January 2004, see http://www.gsi.de/documents/DOC-2004-Jan-1251.pdf; F. Rathmann et al., Phys. Rev. Lett. 93, 224801 (2004).

[1] Institut für Kernphysik, Forschungszentrum Jülich

[2] Gesellschaft für Schwerionenforschung Darmstadt

[3] Helmholtz-Institut für Strahlen- und Kernphysik, Universität Bonn

[4] The Svedberg Laboratory, Uppsala University

BEAM PERFORMANCE AND LUMINOSITY LIMITATIONS IN THE HIGH-ENERGY STORAGE RING (HESR) *

A. Lehrach[1], O. Boine-Frankenheim[2], F. Hinterberger[3], R. Maier[1], and D. Prasuhn[1]

An important feature of High-Energy Storage Ring [1,2] is the combination of phase space cooled beams and dense internal targets (e.g. pellet targets), which results in demanding beam parameter requirements for two operation modes: high luminosity mode with peak luminosities of up to $2 \cdot 10^{32}$ cm^{-2} s^{-1}, and high resolution mode with a momentum spread down to 10^{-5}, respectively. The effects of beam-target scattering and intra-beam interaction are investigated in order to study beam equilibria and beam losses for the two different operation modes [3].

Beam equilibrium is of a major concern for the high-resolution mode. Calculations of beam equilibrium between electron cooling, intra-beam scattering and beam-target interaction are being performed utilizing different simulation codes like BETACOOL by I.N. Meshkov et al. (JINR, Dubna), MOCAC by A.E. Bolshakov et al. (ITEP, Moscow), and PTARGET by B. Franzke at al. (GSI, Darmstadt). Results from different codes for HESR conditions are compared in [4]. Studies of beam equilibria for the HESR are also carried out by D. Reistad for electron cooled beams [2] and by H. Stockhorst for stochastically cooled beams [5] utilizing the BETACOOL code. To simulate the dynamics of the core particles, an analytic rms model was applied for the calculation presented in this paper [6]. The empirical magnetized cooling force formula by V.V Parkhomchuk was used for electron cooling [7], and an analytical description was applied for intra-beam scattering [8]. Beam heating by beam-target interaction is described by transverse and longitudinal emittance growth due to Coulomb scattering and energy straggling, respectively [9,10]. The presently available numerical models to calculate beam equilibrium parameters of cooled beams interacting with internal targets will be further improved. Important tasks covered by an INTAS research project are studies of beam equilibria, and cooled beam distributions in the presence of intra-beam scattering and internal target scattering.

The main restriction for high luminosities is beam losses, since the antiproton production rate is limited. Three dominating contributions of the beam-target interaction have been identified: Hadronic interaction, single Coulomb scattering and energy straggling of the circulating beam in the target. In addition, single intra-beam scattering due to the Touschek effect has also to be considered for beam lifetime estimations. Beam losses due to residual gas scattering can be neglected compared to beam-target interaction, if the vacuum is better than 10^{-9} mbar. For beam-target interaction, the beam lifetime is independent of the beam intensity, whereas for the Touschek effect it depends on the beam equilibria and therefore on the beam intensity.

To calculate the average luminosity, machine cycles and beam preparation times have to be specified. After injection at 3.8 GeV/c, the beam is pre-cooled to equilibrium (with target off), and then ac-/decelerated to the desired beam momentum. Beam steering and focusing in the target region is required before beam cooling and pellet beam are switched on, and the physics experiment can be performed.

CONCLUSION

The main restriction for the high-resolution mode is intra-beam scattering. To reach the specified momentum spread, the beam has to be heated transversely. This is also required to get a sufficient beam-target overlap. In addition, simulation codes have to be improved to describe the dynamics of tail particles, especially with respect to the beam-target interaction. Beam losses are of major concern for the high-luminosity mode. Hadronic interaction, single Coulomb scattering, energy loss straggling and Touschek effect due to single intra-beam scattering are main causes of the beam loss. At lower momenta, the beam losses are too large compared to the antiproton production rate. An optimized beam cooling scenario and a factor of two larger longitudinal ring acceptance is required to reach average luminosities on the order of 10^{32} cm^{-2} s^{-1}.

References:

[1] An International Accelerator Facility for Beams of Ions and Antiprotons, Conceptual Design Report, GSI Darmstadt, November 2001, see http://www.gsi.de/GSI-Future/cdr/.
[2] FAIR Project (subproject HESR), Technical Report, to be published.
[3] A. Lehrach, O. Boine-Frankenheim, F. Hinterberger, R. Maier, D. Prasuhn, Nucl. Instr. Meth. A 44704 (2006).
[4] A. Dolinskii et al., Simulation Results on Cooling Times and Equilibrium Parameters for Antiproton Beams in the HESR, Proc. of the European Accelerator Conference, Lucerne, 1969 (2004).
[5] H. Stockhorst et al., Cooling Scenario for the HESR Complex, to be published in Proc. of International Workshop on Beam Cooling and Related Topics, Galena IL, USA (2005).
[6] O. Boine-Frankenheim et al., Cooling equilibrium and beam loss with internal targets in the High-Energy Storage Ring (HESR), to be published.
[7] V.V. Parkhomchuk, Nucl. Inst. Meth. A 441, 9 (2000).
[8] A.H. Sørensen, CERN Accelerator School (edited by S. Turner) CERN 87-10, 135 (1987).
[9] F. Hinterberger, T. Mayer-Kuckuk and D. Prasuhn, Nucl. Instr. Meth. A 275, 239 (1989).
[10]F. Hinterberger, D. Prasuhn, Nucl. Instr. Meth. A 279, 413 (1989).

[1] Institut für Kernphysik, Forschungszentrum Jülich
[2] Gesellschaft für Schwerionenforschung Darmstadt
[3] Helmholtz-Institut für Strahlen- und Kernphysik, Universität Bonn

* Work supported by INTAS-GSI grants (Ref. No. 03-54-5584).

HESR closed-orbit correction

D.M. Welsch[1], A. Lehrach[1], B. Lorentz[1], R. Maier[1], S. Martin[1], and R. Tölle[1]

The High-Energy Storage Ring (HESR) of the future GSI Facility for Antiproton and Ion Research (FAIR) is designed as a synchrotron storage ring for antiproton physics with high quality beams over a broad momentum range from 1.5 to 15GeV/c [1]. In this paper a closed-orbit correction scheme is discussed.

Since it is not possible to align all elements e.g. magnets perfectly one has to deal with several problems, like closed-orbit deviation. The angular and spatial positioning errors of magnets have different effects on the beam. For example a beam with an ideal orbit will see a kick in quadrupoles only because of its misalignment. The magnet cannot be built perfectly either. Therefore all particles in the beam are influenced by higher order field errors. The main contribution for the closed orbit deviations are angular and spatial positioning error of magnets. The positioning errors are assumed to be smaller than 1 mm and the angular smaller than 0.55 mrad respectively. All those errors are chosen to be normal distributed up to the maximal values. Field errors for the bending dipoles in the arcs and the quadrupoles are also taken into account. Descriptions of RHIC magnets are used for dipole and quadrupole field errors: RHIC D0 dipole and RHIC insertion quadrupole [2]. A sample of 10 orbits in x direction were calculated using the MAD-X code for different seeds generated by a random number generator (see Fig. 1).

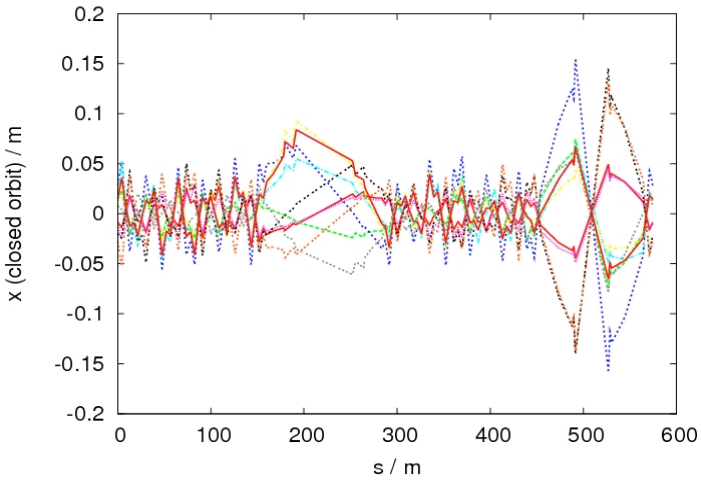

Fig. 1: Horizontal closed orbits for different distributed errors vs. longitudinal position in the ring.

Large closed orbit deviations of more than 150 mm at a longitudinal position in the ring of 500 m were found in the straight section close to the target, where the betatron amplitude exceeds 400 m. The closed orbit with the largest deviation of maximum 156.5 mm was picked to prove whether those closed orbits can be corrected with realistic corrector strengths to less than 5 mm. The kick strength of each corrector should not exceed 1 mrad. 120 beam position monitors and 108 orbit correctors are placed within the lattice of the storage ring. All locations chosen are as close to the quadrupoles as possible and reasonable.

For correction MAD-X with the MICADO algorithm is used. Due to local minima it is not possible to run the code with all correctors switched on simultaneously. Therefore one has to choose a small number of correctors to start with. Then one has to find those correctors in the HESR lattice providing the most efficient closed-orbit correction. Afterwards the number of utilized correctors has to be increased step by step and only the locations of the additional orbit correctors will be cycled through all remaining and not used correction dipoles. Thus it is possible to improve the orbit correction successively. The number of additional orbit correctors per step should be small, too. Otherwise the amount of arising possible combinations explodes and the whole task begins to be very time consuming. That is why we have chosen to use only two additional correctors per step.

With 10 orbit correctors at certain positions it is possible to reduce the maximal orbit deviation down to 4.7 mm. The uncorrected and corrected orbits are plotted in Fig. 2.

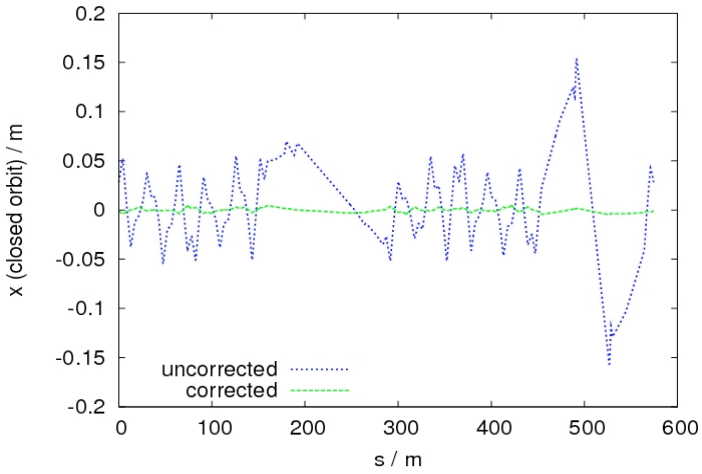

Fig. 2: Corrected and uncorrected horizontal closed orbits vs. longitudinal position in the ring.

Eight of the correction dipoles are located in the arcs and two in the straights. The rms value was reduced from roughly 38 mm down to less than 2 mm. Corrector strengths of less than 0.8 mrad are required as maximal kick angle in the arcs, and 0.55 mrad in the straights respectively.

Applying the assumed angular and spatial positioning error of magnets the closed-orbit can be corrected to less than 5 mm. Closed-orbit bumps at various positions (e.g. injection point, interaction point, position of beam cooling devices) have to be investigated to complete the steering concept for the HESR.

References:

[1] FAIR Project (subproject HESR), Technical Report, to be published.
[2] M. Anerella et al., Nucl. Inst. Meth. A 499, 280 (2003).

[1] Forschungszentrum Jülich, 52425 Jülich, Germany

Injection, Refill and Acceleration in the HESR Synchrotron

S.An[1], K.Bongardt, J.Tang[2], R.Maier

Abstract

The HESR synchrotron [1], part of the GSI FAIR project, has to provide anti-protons from 1.5GeV/c to 15GeV/c. Accumulated and cooled anti-protons at 3GeV with about 200m bunch length are injected from the RESR ring. Momentum spread depends on particle intensity. HESR users asked for two dedicated modes: high resolution (HR) mode with about 10^{10} particles up to 8GeV and high luminosity (HL) mode with less than 10^{11} particles for the whole HESR energy range. The change in energy of 200eV/turn is determined by the dipole ramping rate of 25mT/s. To minimise particle losses caused by the HESR momentum acceptance limit of about $\pm 10^{-3}$, RF manipulation is required at different stages in the cycle. Since beam parameter and refilling schemes are different for the two operation modes, RF manipulation has to be adapted accordingly.

RF manipulations for 10^{10} particles

A 200m long pulse is injected from RESR with $N=10^{10}$ particles and an initial rms momentum spread of $\sigma_p/p = 1.43\cdot10^{-4}$ (rms energy spread of 0.53 MeV). Phase dilution by a factor of two leads to a bunch length of 400m, but a reduced rms momentum spread of $\sigma_p/p = 7.2\cdot10^{-5}$ (0.27 MeV). Phase dilution by bunch rotation is achieved after about $1.8\cdot10^4$ turns or 36 ms, in dual harmonic RF system with RF amplitudes of: V_1=90V and $V_2=-0.31\cdot V_1$= -28 V.

After further reduction of energy spread by beam cooling, the cooled HR bunch has to be matched to and captured in an accelerating bucket. For a DC beam with 10^{10} particles at 3GeV, intrabeam scattering limits the achievable rms momentum spread to $4\cdot10^{-5}$ (0.15 MeV) [1]. After phase compression by a factor of 4, this short and cooled HR bunch with rms momentum spread of $16\cdot10^{-5}$ or rms energy spread of 0.6MeV is captured for acceleration with a single harmonic RF system with 20° synchronous phase and RF amplitude of 700V. RF amplitude values are kept unchanged during acceleration, leading to adiabatic change in phase and energy spread without changing longitudinal emittance.

At experiment energy phase dilution leads to a DC beam with almost unchanged rms energy spread of 0.15MeV. Before turning on the pellet target, final cooling reduces momentum spread further. A clearing gap of 10% of the machine circumference is required to improve lifetime limited by trapped particles. This will be achieved with either barrier buckets or dual harmonic ones. At the end of the machine cycle remaining particles are dumped.

RF manipulations for 10^{11} particles

Refilling is necessary to accumulate 10^{11} particles. In order to reach the specified average luminosity, the remaining particles at the end of the machine cycle are kept in the HESR and transferred to the injection energy of 3GeV, before newly injected particles are added. In this procedure the bunch length of remaining particles has first to be shortened to about 200m, done by bunch rotation with a dual harmonic RF system. By single turn injection, a new 200m long RESR pulse is placed into the empty dual harmonic bucket. Both bunches are well separated in time, but differ in energy spread. Synthetic RF waveform with 5 harmonics increases energy spread of one bunch due to bunch rotation, whereas the other bunch is kept matched. More details are given in [3]. Tracking results from 1d–ORBIT [2] simulations are shown in figure 1 at 3 GeV injection energy, by using these voltages: V_1=0.057kV, V_2=1.42kV, V_3=-0.017 kV, V_4=0.044kV, V_5=-0.018kV. Initial energy spread differs by a factor of 3, but being identical after 3300 turns. At 3GeV HESR energy acceptance is about ±5MeV.

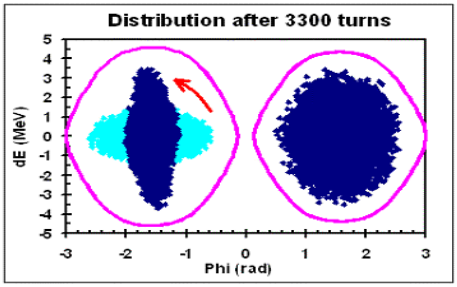

Fig. 1: Bunch rotation for RESR bunch, matched for remaining particles

After bunch rotation RF voltages are turned off, leading to an almost uniform line density without changing the momentum distribution. For 10^{11} particles cooling reduces rms momentum spread to 10^{-4} (0.37MeV). After phase compression by a factor of two, this long HL bunch with rms momentum spread of $2\cdot10^{-4}$ (0.75MeV) is captured in the accelerating bucket by a dual harmonic RF system with 30° and 40° synchronous phases and RF amplitude of V_1= 700V and $V_2=-0.31\cdot V_1$=-217V. Figure 2 shows the RF potential (relative to bunch centre). Accelerating up to 10^{11} particles leads to phase damping and increase of energy spread like in a single RF system, as particles see a harmonic focusing potential. For energies above 8 GeV phase and amplitude values must be adjusted to stay within the HESR momentum acceptance. After reaching the desired energy, phase dilution by bunch rotation leads to a DC beam again. Resulting energy spread is almost unchanged, whereas momentum spread is reduced.

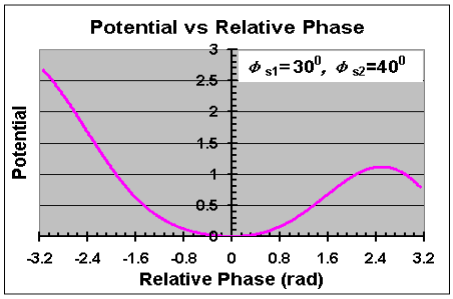

Fig. 2: RF Potential for dual harmonic RF system: Phase (for h=1) is relative to bunch centre

References:

[1] HESR Baseline Technical Report, to be published
[2] ORBIT User Manual, SNS-ORNL-AP TN0011, 1999. J.A.Holmes et al. EPAC 2004,Lucerne, p. 1530
[3] S.An et al, to be presented at EPAC 2006.

[1] on leave from IMP Lanzhou, China
[2] IHEP Beijing, China

Tracking Results for a Cooled HESR Bunch at 8 GeV

S.An[1], K.Bongardt, J.Tang[2], R.Maier

Abstract

The HESR synchrotron [1] has to provide anti-protons from 1.5GeV/c to 15GeV/c. At user energy cooling reduces momentum spread before switching on the pellet target. For the circulating antiproton beam at the experimental beam energy a clearing gap of 10% of the machine circumference is required to improve lifetime, achievable either with barrier or dual harmonic (d=-0.31) buckets. After about 10 synchrotron oscillation periods reflections from potential wall changes Gaussian input to uniform one for high harmonics only. Voltage ripple between potential walls caused either by less harmonics or amplitude and phase errors hinders change of line density. Impedances are modifying the distribution but do not lead to instability as even cooled HESR bunches are emittance, but not space charge dominated.

Sinusoidal Barrier buckets for bunch length Bl = 0.8

In figure 1, resulting RF waveforms are shown, starting from a "perfect" sinusoidal one with half width of 0.2π, up to a half width of π. Depending on the number of harmonics, voltage ripple occurs between potential walls. An extended bucket width leads to less ripple for some harmonics. A square bucket instead of a sinusoidal one enlarges voltage ripple.

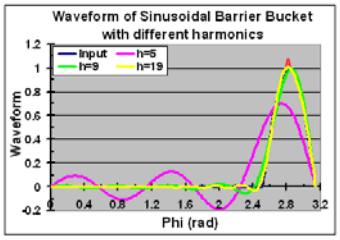

Fig. 1: sinusoidal bucket: input and reconstructions

Tracking results for cooled HESR bunch at 8 GeV

For the HESR high resolution (HR) mode with 10^{10} particles at 8GeV, intrabeam scattering limits the achievable rms momentum spread to about $2 \cdot 10^{-5}$ (rms energy spread 0.19 MeV). In figure 2 tracking results from 1d–ORBIT [2] simulations are shown for cooled Gaussian HESR bunch with bunching factor 0.8 (maximum phase extent ±2.4rad), rms energy spread of 0.19MeV together with phase space boundary and barrier bucket waveform. Amplitude of 16.2V limits energy acceptance to about ±0.7MeV. Required RF amplitudes are: V_1=1.30V, V_2= -3.56V, V_3=4.54V, V_4=-4.70V, V_5=4.05V.

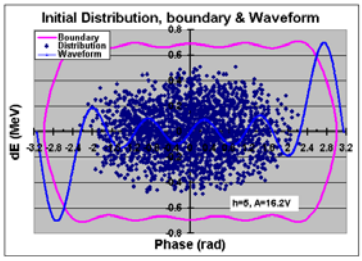

Fig. 2: Initial Gaussian distribution, waveform and boundary.

Resulting phase space distribution after 10^6 turns, about 1.5 synchrotron oscillation periods for outermost particles, is shown in figure 3, leading to a clearing gap of about 10% of the machine circumference. Voltage ripple causes "islands of stability" for innermost particles, but energy oscillations for outermost particles [3]. Phase space distribution in a "perfect" sinusoidal bucket after 0.5 synchrotron oscillation shows debunching for innermost, but wall reflections for outermost particles [3,4]. Even for a "perfect" barrier bucket without voltage ripple, requiring a quite high number of harmonics, energy loss cannot be compensated. Resulting dipole oscillation is damped after 0.5 synchrotron oscillations. Using instead a "flattened" bucket, obtained by dual harmonic RF waveform with voltage ratio 0.3 between 1st and 2nd harmonic, allows to compensate energy loss by RF steering.

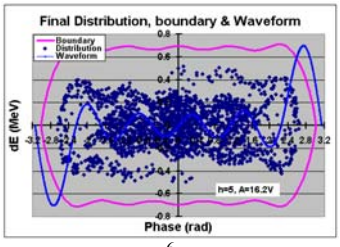

Fig. 3: Distribution after 10^6 turns, waveform and boundary

Line densities after long times

In figure 4, line densities after 10 synchrotron oscillation periods are shown for the same Gaussian input beam distribution, but different harmonics, leading to uniform line density only for high harmonics. Asymptotic distributions are independent of initial mismatch [3]. Resulting edges depend on details of potential wall as for self-consistent distributions [5]. Amplitude and phase errors lead to voltage ripple, maybe compensated by sophisticated RF control systems [6]. For emittance dominated cooled HESR bunches, impedances modify the change of distribution, but cause no instability [3].

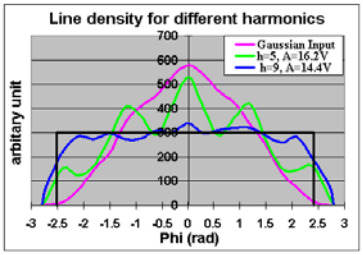

Fig. 4: initial and final (10^7 turns) line densities

Impedances are also modifying the beam distribution, but do not lead to instability, as even cooled HESR bunches are dominated by emittance, rather than by space charge.

References:

[1] HESR Baseline Technical Report, to be published.
[2] ORBIT User Manual, SNS-ORNL-AP TN0011, 1999, J.A.Holmes et al. EPAC 2004, Lucerne, p. 1530
[3] S.An et al. to be presented at EPAC 2006.
[4] S.Y.Lee, K.Y.Ng, Phys Rev E 55, p.5993, 1997
[5] O.Boine-Frankenheim, I.Hofmann, PRStAB5, p.034207
[6] M.Fuijeda et al, PRSTAB 2, p.122001, 1999

[1] on leave from IMP Lanzhou, China
[2] IHEP Beijing, China

A Polarized Ion Source Concept for the FAIR Project

A.S. Belov, R. Gebel, and P. von Rossen

Introduction

Although polarized beams had not been a prime issue of the Facility for Antiproton and Ion Research (FAIR) at GSI during its inception their relevance has increased substantially over time when people began to realize the potential to address questions that otherwise would be inaccessible. This prompted an investigation to look into technical concepts and specifications of established sources and their potential for further development and application at FAIR.

Performance of atomic beam-type ion sources

An atomic beam-type polarized hydrogen ion source with a resonant charge-exchange ionizer might be a good candidate for the FAIR project. The source had been developed at Institute of Nuclear Research of Russian Academy of Sciences. It can produce positive or negative polarized hydrogen ions using a resonant charge-exchange reaction for direct conversion of polarized thermal hydrogen atoms into polarized positive or negative ions in a deuterium plasma:

$$H^{\circ}\uparrow + D^{+} \rightarrow H^{+}\uparrow + D^{\circ} \qquad (1)$$
$$H^{\circ}\uparrow + D^{-} \rightarrow H^{-}\uparrow + D^{\circ} \qquad (2)$$

Deuterium ions are used for charge exchange to eliminate any reduction in polarization of the beam by unpolarized ions. The use of deuterium makes the reaction not exactly resonant due to isotopic shift of energy levels of deuterium atoms in comparison with hydrogen. But this shift does not change cross-sections of the reactions even for small energies of the colliding particles. For a collision energy of ~10 eV the cross-section for reaction (1) is $5 \cdot 10^{-15}$ cm^2 and for the reaction (2) is 10^{-14} cm^2. Low colliding energies are achieved by using a deuterium plasma for the production and transport to the collision area of the deuterium ions. The large cross sections make it possible achieving high efficiencies for the conversion of thermal polarized hydrogen atoms into polarized protons or negative hydrogen ions. As it is not foreseen to use stripping injection with negative hydrogen ions as in the case of COSY a polarized proton source will be required.

To illustrate the state of the art in this field some of the data of the polarized proton source at INR, Moscow are given. It has produced pulsed polarized proton beams with peak currents up to 6-10 mA, a polarization of 80-90%, a normalized emittance of 1.7 π mm mrad, a repetition rate up to 10 Hz and pulse duration of ~ 100 μs [1,2]. The highest peak intensity of 10 mA was obtained with a deuterium plasma ion current density in the charge-exchange region of 200 mA/cm^2. At this deuterium ion density the conversion efficiency of polarized hydrogen atoms into polarized protons in the plasma ionizer is estimated to be 70%.

A schematic diagram of this source is shown in fig. 1. Atomic hydrogen is produced in the source with a hydrogen dissociator using a pulsed RF-power up to 4 kW and with a pulsed molecular hydrogen supply. Atomic hydrogen leaves the dissociator into vacuum through a channel whose walls are cooled by liquid nitrogen. Two electromagnetic sextupoles are used for the spin selection of hydrogen atoms. The magnetic field at pole tips of these magnets is up to 9 kG. The atomic beam apparatus produced pulsed polarized atomic hydrogen beams with peak intensities of $2 \cdot 10^{17}$ atoms per sec into the ionizer. The atomic hydrogen beam is injected into the ionization region inside the ionizer solenoid through a three-electrode extraction system.

The deuterium plasma is produced by an arc-discharge

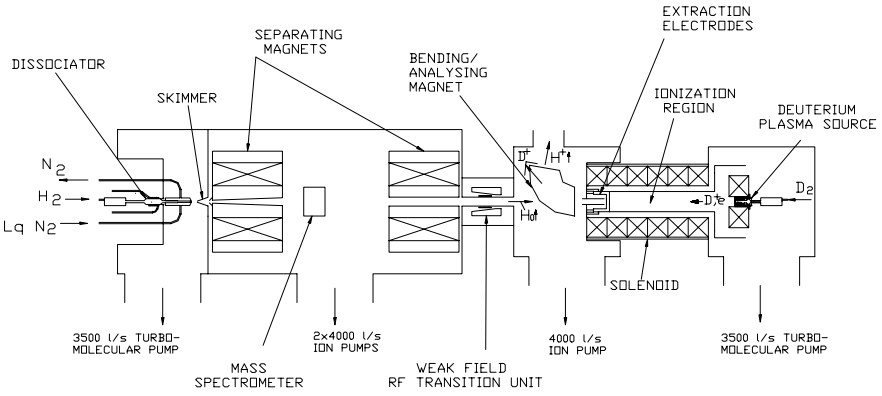

Fig.1. Schematic layout of the Polarized Proton Source with Resonant Charge-Exchange Plasma Ionizer

plasma source. The plasma source has a pulsed discharge with a duration of 200 μs and a matching pulsed gas supply. The plasma is injected into the charge-exchange region along the axis of the ionizer solenoid having a magnetic field on the axis of about 1.3 kG.

Polarized protons are formed in charge-exchange collisions between polarized hydrogen atoms and unpolarized deuterium ions in plasma. The polarized protons are confined in the radial direction by the magnetic solenoid field and move to the extraction electrode system under the influence of weak ambipolar electric field in the plasma. Inside the extraction electrode system the polarized protons are accelerated to 25 keV together with unpolarized deuterium ions. Polarized and unpolarized ion beams are in a later stage separated with a bending magnet.

Outlook

A newly designed polarized proton source for FAIR should incorporate techniques and components that have a proven record and have been tested under the demanding routine operation of COSY. For instance the cooling technique of the dissociator nozzle by a cryogenic generator, permanent sextupole magnets with magnetic field of ~1.5 T for focusing the electron-spin polarized H^o, and strong field RF-transition units for fast reversal of polarization are established components.

The number of polarized protons from such a source for one pulse with a peak current of 10 mA and a 100 μs duration is $6 \cdot 10^{12}$ which would satisfies the present requirements for the FAIR-project.

Higher polarized beam intensities with smaller beam emittance could be obtained with the same source type by using a storage cell installed in the charge-exchange region of the plasma ionizer [3, 4] but such a design would require additional R&D work.

Work in part supported by the EU under the HP-NIS-Project Contract No: HPRI-CT-2001-50021.

References

Belov A.S., Esin S.K., Kubalov S.A., Kuzik V.E., Stepanov A.A., and Yakushev V.P., Nucl. Instr. and Meth. In Phys. Research, **A255,** 442-459 (1987).

Belov A.S., Esin S.K., Kubalov S.A., Kuzik V.E., Yakushev V.P, "Intense polarized proton source with charge-exchange at Moscow INR", in Proc. of International Workshop on Polarized Ion Sources and Polarized Gas Jets, ed. Y.Mori, KEK, Tsukuba, Japan, 1990, KEK report 90-15, 1990, p.p. 69-80.

Belov A.S., Esin S. K., Netchaeva L.P., Klenov V. S., Turbabin A. V., and Vasil'ev G. A., "Polarized ions from a storage cell", in Proc. of Seventh International Workshop on Polarized Gas Targets and Polarized Beams", Urbana, IL, 1997, eds. Roy J. Holt and M.A. Miller, AIP Conf. Proc., **421**, 362 (1998).

Belov A.S., Esin S. K., Netchaeva L.P., Turbabin A. V., and Vasil'ev G. A, " Polarized Ion Source with Resonant Charge-Exchange Plasma Ionizer", in Proc. of 13th International Symposium on High Energy Spin Physics, Protvino, Russia, 9-12 September, 1998, eds. N.E. Tyurin et.al., World Scientific, 1999, p.p. 622-624.

A.S. Belov, R. Gebel, P. von Rossen, Atomic Beam Intensity Measurements at the COSY Polarized Ion Source, IKP Annual Report 2003, Jül 4107 Jan 2004 ISSN 0944-2952

A.S. Belov, O. Felden, R. Gebel and P. von Rossen, Velocity measurements of the pulsed atomic hydrogen beam of the COSY polarized ion source, IKP Annual Report 2004, Jül 4107 März 2005 ISSN 0944-2952

Design Status of the Antiproton Polarizer Ring

A. Garishvili[a,b], A. Lehrach[a], B. Lorentz[a], S. Martin[a], and F. Rathmann[a]

At the core of the PAX proposal [1] is to polarize antiprotons by spin filtering of stored antiproton beam via multiple passage through an internal polarized storage cell hydrogen target. A storage ring is ideal to efficiently achieve a high degree of beam polarization. Therefore, PAX collaboration aims to build a dedicated Antiproton Polarizer Ring (APR).
In this report the preliminary result on the lattice design study for such type of ring is presented. In fig. 1 a floor plan of the suggested APR is shown, for preparation of which the computer code WinAgile [2] has been used. Following the known requests [1], 4 straight sections are required for the insertions: (a) injection and extraction of the antiproton beam, (b) a low β–section for the gas target, (c) the opposite section reserved for the Siberian snake (to longitudinally align the antiproton spin), and (d) electron cooling in the straight section opposite to the injection. Various ion optical conditions have to be met in the four straight sections: (*i*) in the target, e–cooler, and Siberian snake sections the beam cross section has to be circular and the beams phase space ellipse has to be upright, (*ii*) in all straight sections the dispersion should be zero, (*iii*) the antiproton beam in the e–cooling should be parallel and variable in order to match the size of the electron beam, (*iv*) and the radius of the beam spot at the target should be around 10 mm.
As a first exploration, the following main parameters has been choosen: beam energy - 250 MeV, beam emittance - 250 π mm mrad, and magnetic rigidity - 2.4 Tm. The quadrupole arrangements in the straight sections enable tuning of the beam within a wide choice of optical conditions. Total circumference of the APR is 86.5 m, with each of the four straight sections of about 12 m long. In addition, APR contains two symmetrical arcs and length of each arc is about 19 m. In the current design of the APR, 46 quadrupole magnets has been used with length of 30 cm and 4 bending magnets with the length of 25 cm.
In the target straight section, a free space of 1 m is provided, for design of which the three and five quadrupoles cases was compared. Distribution for beta function ($\beta_{x,y}$) was calculated by equation (1) and beam radius ($R_{x,y}$) with equation (2):

$$\beta_{x,y}(s) = \beta_{x,y}(0)\left(1+\frac{s^2_{x,y}}{\beta^2_{x,y}(0)}\right) \quad (1)$$

$$R_{x,y}(s) = \sqrt{\varepsilon_{x,y}\times\beta_{x,y}(s)} \quad (2)$$

The minimum beta function for three quadrupoles case is 21 m and beam radius is 7.25 mm in the center. However, in this case we have very high spikes for beta function along the quadrupole section (dashed line in fig. 2).
For the five quadrupoles case, the beta function behavior is much flat (solid line) in the target cell region, than for three quadrupoles case. The minimum beta function is 0.31 m and beam radius is 8.8 mm in the center (fig. 2). This numbers is still acceptable for APR optics. This was a reason to choose design with five quadrupoles.
Since the antiprotons should be also longitudinally polarized [1], the ring has to contain a Siberian snake, which is located in the opposite side of the target (see fig. 1).

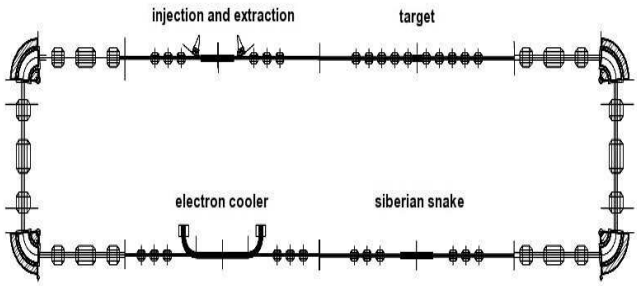

Fig. 1: Floor plan of the APR lattice.

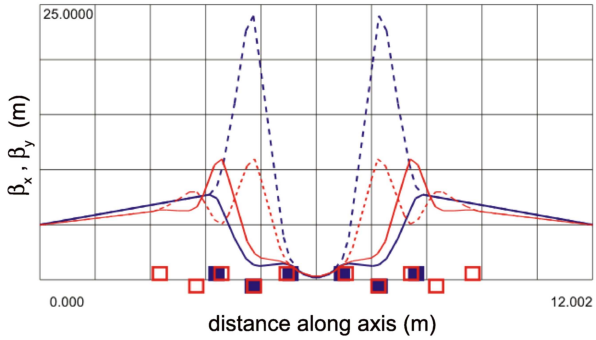

Fig. 2: Beta functions of APR (β_x - solid, β_y - dashed) along the target section. Blue and red colors corresponds to 3 and 5 quadrupole cases, respectively.

To provide longitudinally polarized beam at the position of the storage cell, integrated field strength should be roughly 2.74 Tm. This can be done with 1.1 T solenoid of 2.5 m length. The space between quadrupole triplets in this straight section is 4.1 m and it is enough for this solution. To calculate solenoid field Thomas BMT equation [4] has been used: $\chi = (1+G)/B\rho \cdot \int B dL$, where χ is the precession angle in solenoid, G is the anomalous magnetic moment $G = (g-2)/2$, while g is the gyromagnetic ratio.
The beam degradation, the geomatrical blow–up and the subsequent smearing of the beam energy needs to be corrected by phase–space cooling, preferably by electron cooling. For the electron cooling (located next to the Snake straight section), a free space of 6.2 m is reserved. The antiproton beam in the electron cooling section should be parallel and it's cross section should be variable in order to match the size of the electron beam.
Efficient system for injection and extraction of the antiproton beam has to be provided in the ring as well. For the injection and extraction of antiproton beam (located in the opposite side to the electron cooling section), the free space of 4.1 m is foreseen. In this straight section two septums and one kicker are placed.
Finally in the APR we have two symmetrical arcs. In each arc two bending magnet and triplet of quadrupole magnets has been used. Triplets was choosen because of: less aberrational errors, large acceptance ring requires multipole correctors, and dispersion in such design is zero by symmetry.
In more detail the other characteristics of this ring can be found in the talk [3].

References:

[1] Proposal for *Antiproton-Proton Scattering Experiments with Polarization*, **PAX Collaboration**, arXiv:hep-ex/0505054 (2005).
[2] P.J. Bryant, AC Division, CERN.
[3] A. Garishvili and S. Martin, CANU meeting, 2005, available from *http://www.fz-juelich.de/ikp/pax.*
[4] V. Bargmann et al., PRL, 435 (1959).

[a] IKP FZJ, Jülich, Germany
[b] HEPI TSU, Tbilisi, Georgia

Event Rate Estimates for the Spin Filtering Experiment at the AD–ring of CERN*

M. Tabidze[a], J. Haidenbauer, A. Kacharava[b], P. Lenisa[c], and F. Rathmann

The PAX collaboration [1] suggests to study the polarization buildup in an antiproton beam at the AD–ring (CERN) in the energy range of 50–200 MeV [2]. The experimental basis for predicting the polarization buildup in a stored antiproton beam is practically non–existent. The polarization buildup, by spin filtering of stored antiprotons by multiple passage through a polarized internal hydrogen gas target, gives a direct access to the spin dependence of the antiproton–proton total cross section. Once the experimental data base will be made available by the AD experiments, the final design of a dedicated Antiproton Polarizer Ring (APR) [3] can be targeted.

In this report we present results of the event rate estimates for $\bar{p}p$ elastic scattering process in the energy range of 20–250 MeV. For the analysis, a model for the nucleon–antinucleon interaction [4] based on the meson–baryon dynamics, has been used. The model enables a simultaneous description of nucleon–antinucleon scattering and annihilation phenomena with fair quality. We decided to use the calculated results of the differential cross section $d\sigma/d\Omega$ and of the analysing power $A_y(\theta)$ from this model in the following analysis.

For each fixed beam energy, the Figure of Merit ($FoM(\theta) = A_y^2(\theta) \cdot d\sigma/\Omega$) *vs* antiproton polar angle (θ) was calculated and the value of the maximum FoM was determined. In Fig.1 the angular dependence of the differential cross section (upper row), analyzing power (middle), and FoM (lower row) at three different antiproton beam energies (T_{Pbar}), are shown.

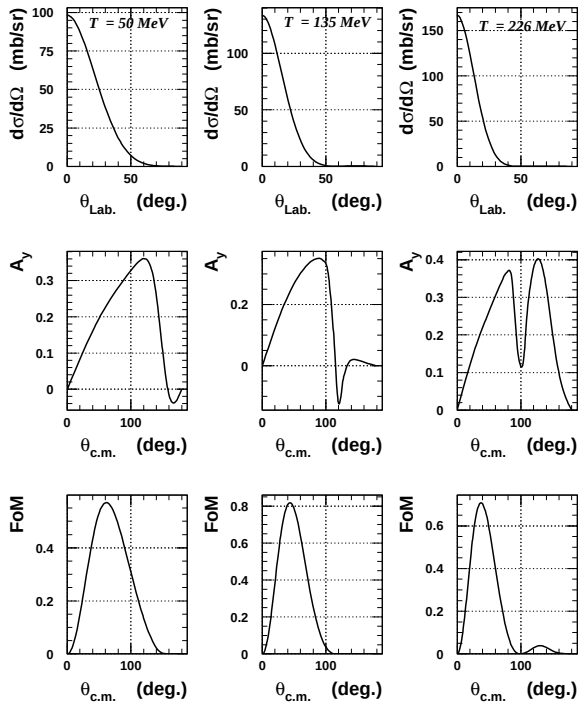

Fig. 1: The angular dependence of the differential cross section (upper row), analyzing power (middle), and FoM (lower row).

The maximum of FoM moves towards smaller forward angles with increasing beam energy, where the differential cross section is dominant.

To estimate of the $\bar{p}p \to \bar{p}p$ elastic count rates, we have considered a scenario with detection of both particles. To detect recoil protons we suppose to use a similar detector system as it is presently used at ANKE, a so–called Silicon Tracking Telescope (STT) [5]. Recoil protons can be identified via the $\Delta E/E$ method over an energy range from 2.5 MeV to 30 MeV with the resolution of 150–250 keV. In this kinematics, the forwarde antiproton is the fast particle and by using the STT, it is possible to determine the flight direction, which is sufficient, in combination with the recoil proton, to reconstruct the vertex position in the storage cell of the Polarised Internal Target [6].

Based on the features shown in Fig.1, we assumed that for each beam energy the *forward* telescope system will cover laboratory polar angles $\theta = 15^\circ - 30^\circ$, which is possible with the present STT detector design.

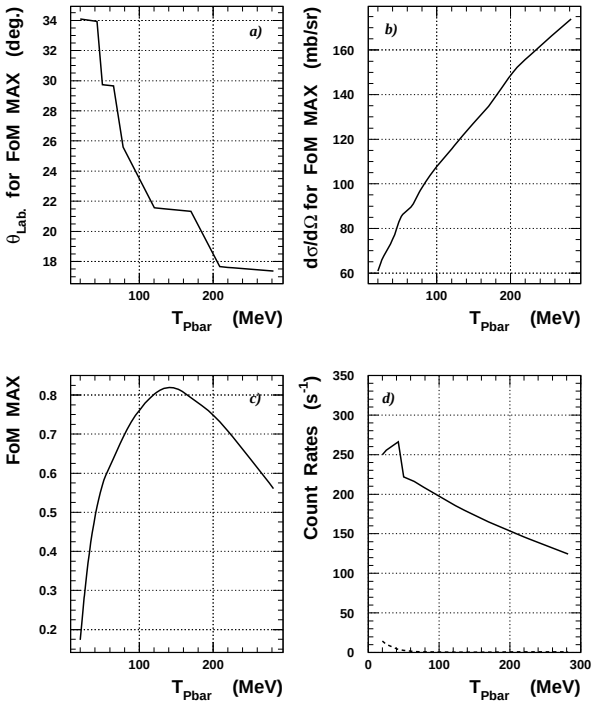

Fig. 2: The energy dependence of: a) the antiproton polar angle θ corresponding to the maximum FoM, b) the differencial cross section corresponding to the maximum FoM, c) maximum FoM, and d) the count rates. Dashed line on the fig.1.d corresponds to the background due to misidentification of antiprotons.

In these estimates, a luminosity of $L = 10^{27}\text{cm}^{-2}\text{s}^{-1}$ has been used, which is based on the following assumptions: The AD provides about 3×10^7 stored antiprotons. Through stacking, one may be able to increase the number of stored antiprotons by about a factor of five, wherefrom also the

other experiments at the AD would benefit. With a beam current corresponding to about 10^8 stored antiprotons, a luminosity of $L = N_{\bar{p}} \cdot f \cdot d_t = 10^8 \cdot 10^6\,\mathrm{s}^{-1} \cdot 10^{14}\,\mathrm{atoms/cm}^2 = 10^{28}\ \mathrm{cm}^{-2}\mathrm{s}^{-1}$ may be achievable. To provide a larger number of stored antiprotons in the AD in the first place is important, because after spin filtering for a few beam lifetimes one wants to be left with a substantial beam intensity to carry out the beam polarization measurements. In our calculations, a detection efficiency of 100 % was assumed, and dead–time correction factor of 1. Under these conditions, the estimated antiproton–proton elastic rates are about 120–250 s^{-1} (see Fig. 2.d).

Based on these rough estimations, we plan to do more precise calculations with Monte Carlo simulation, using the GEANT4 program developed for ANKE. This will include the real sizes of the ANKE target chamber, disposition of two STT systems around the long (40 cm) storage cell target, and the density distribution of the PIT target. It will then be possible to address the other issues concerning the experimental conditions, like resolution and backgound estimates made more accurately.

References:

[1] Technical Proposal for *Antiproton–Proton Experiments with Polarization*,
PAX Collaboration, arXiv:hep-ex/0505054 (2005).

[2] Letter–of–Intent for *Measurement of the Spin–Dependence of the $\bar{p}p$ Interaction at the AD–Ring*, November 2005 (available from http://www.fz-juelich.de/ikp/pax).

[3] A. Garishvili and S. Martin, see contribution to this Ann. Rep.

[4] V. Mull and K. Holinde, Phys. Rev. **C 51** (1995) 2360; J. Haidenbauer, K. Holinde and A .W. Thomas, Phys. Rev. **C 45** (1992) 952; T. Hippchen, J. Haidenbauer, K. Holinde and V. Mull, Phys. Rev. **C 44** (1991) 1323.

[5] A. Mussgiller, Ph.D. thesis, University of Cologne (2006), (available from http://www.fz-juelich.de/ikp/anke/theses.shtml)

[6] A. Kacharava, F. Rathmann, and C. Wilkin for the ANKE Collaboration, COSY Proposal #152, *Spin Physics from COSY to FAIR*, arXiv:nucl-ex:0511028.

[a] HEPI Tbilisi State Univerisity, Georgia
[b] Erlangen University, Germany
[c] Ferrara University, Italy

* supported by the DAAD program

5 Technical Developments

Laboratory for Semiconductor Detectors

D. Protić, G. Fiori, F. J. Hackemüller, T. Krings, H. Metz, K. Schwill

Research and development of large-volume Si(Li) detectors with position-sensitive structures on both contacts have been the main activities of the laboratory during the last years. In the course of the work on large-diameter diodes a serious problem concerning the Li-driftability of the p-type silicon has become more and more apparent. As was feared [1], even relatively thin (4-5 mm) slices of the 5-inch p-type silicon could not be completely compensated even for 4 times longer drifting time. Unfortunately, also some of the 4-inch slices (purchased as Li-driftable p-type silicon) needed prolonged drifting time, especially in their central parts. Now, we are preparing a gettering procedure to eliminate defects inside the starting material that prevent the Li-drift process.

Each position-sensitive structure on our Si(Li) detectors are generally surrounded by an about 5 mm wide guard-ring which prevents the influence of usually high surface leakage current generated on the surface of the Li-compensated region between the detector contacts. Therefore, the area of a guard-ring is practically dead area of a contact surface. Normally, the detector user would like to have the guard-rings as narrow as possible. Concerning only the surface leakage, 1-2 mm wide guard-rings would be a possible solution. But an additional problem has been known since long time: "Surface states" on the Li-compensated region between the contacts distort the normally parallel electric field lines inside a Si(Li) detector. As a result, position and energy information for interactions several mm apart from the edge of the detector contacts could not be correct. Extensive investigations have been undertaken, applying three different methods, to explore the influence of the surface states on the detector response as function of bias voltage, temperature, shaping time constant and the time since the last surface treatment. This investigations were performed within the scope of EURON JRA EXL-working group. The first results were presented in [2].

Both above described topics are definitely important concerning the Si(Li)-detectors for the ANKE-experiments. Additionally to 5 mm thick detectors, several 7 mm thick Si(Li)-diodes are under preparation. One of the 10 mm thick diodes, just in the Li-drift process, is also foreseen for the prototype detector which will be combined with the MATE readout chip (developed at SACLAY). As in the past, the ANKE vertex group was supported in preparation of the chip-based readout electronics. A second-hand pull tester was refurbished and put into operation. Using the device extensive tests were performed to find the best parameters for high quality bond connections on detectors, chips, PCB and flexible printed foils. Firm connections with 25 μm Al-wire that sustain up to 10 gr. forces were achieved. Such firm connections are of great importance for operating the detectors or chips near strong magnetic fields, as in ANKE-experiments, where also vibrations could destroy relatively weak bonds.

During the last GEM-experiment (November 2004) two accidental events caused serious damage on the fully equipped detector system "Germanium Wall" (Quirl-detector followed by three 17 mm thick ΔE-detectors). Firstly, about 1000 V – far beyond the breakdown voltage – were applied on the Quirl-detector, normally operated at 70 V. The resulting breakdown current destroyed the bonded Al-wires (25 μm in diameter) that connect the position-sensitive structure with the printed Kapton foil. In addition, a vacuum breakdown occurred, while the detectors operated at LN_2-temperature under full bias voltage. The thick ΔE-detectors could be recuperated by several heating sequences under good vacuum. The Quirl-detector could not be repaired so that a new one has to be installed and thoroughly tested. As two GEM-experiments are foreseen during 2006, two Quirl-detectors and several thick ΔE-detectors are under preparation to be ready for exchange of eventually radiation damaged or destroyed detectors.

Within the scope of the effort to develop a Compact Si+Ge Compton Camera at LLNL additional large-volume Si(Li) diodes (about 10 mm thick and 102 mm in diameter) were manufactured. One of them was structured on the same way as the first one delivered in July 2004 [3]: 32 strips on each contact, with a pitch of 2 mm. The results achieved with this detector at LLNL were presented at IEEE-Conference 2005 in Puerto Rico, USA [4, 5]. The firstly delivered detector was accidentally damaged in April 2005 through a not expected warming-up process. A lot of work was invested to repair the detector. The third detector is still in the preparation and will be delivered to LLNL at the beginning of 2006.

In addition to already described investigations concerning the EXL-working group extensive activities in connection with GSI future projects have been undertaken. For the SPARC collaboration the two-dimensional germanium microstrip detector was repaired after an accident caused by lack of liquid nitrogen. Stimulated through excellent results achieved with this detector, especially its capability to reveal the polarization grade of incoming photons, we are still constructing a Si(Li)-polarimeter [6]. This polarimeter will clearly outperform the two-dimensional germanium microstrip detector in the photon energy range 50-150 keV [6]. Two 7 mm thick transmission Si(Li) detectors, with 8 pads on the boron-implanted contact are under preparation for tests under UHV conditions at GSI-Darmstadt, within the scope of the EXL-project. A Si(Li) stack consisting of a transmission Si(Li) detector and a E-detector has been delivered to the DESPEC working group.

Several 5 mm thick transmission Si(Li) detectors with pad structure on the implanted p^+-contact are under preparation for MUST II collaboration (Saclay, Orsay, GANIL). Two of them are now mounted in a test holder. Substantial tests have been performed to characterize the behaviour of each pad (leakage current, resistance to the neighbours and

energy resolution for α-particles at room temperature and 273 K). In the planned collaboration with the IKP an important aspect will be to investigate the operating characteristics of Si(Li) pad detectors with the chip readout. Saclay has been developing the MATE-chip, one of the most promising chips for this purpose.

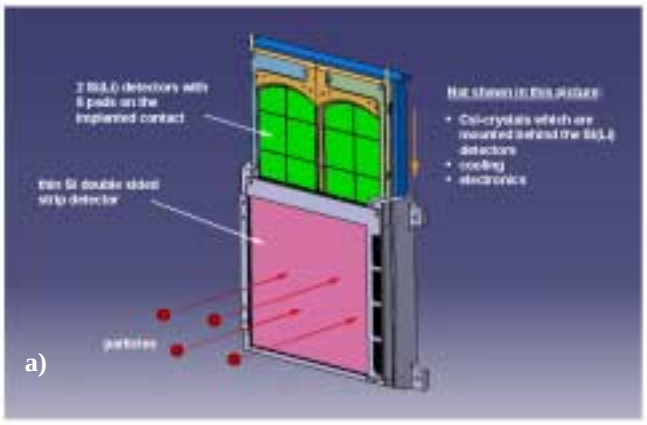

Fig. 1: a) First two detector layers of a MUST II telescope for recoil particles (the sketch was made by the MUST II collaboration). Two Si(Li) pad detectors are mounted in a frame which can be inserted into the telescope holder. b) One of the transmission Si(Li) detectors, about 5 mm thick, with 8 pads on the implanted p^+-contact.

A proposal CompCam – Electronically Collimated Gamma Camera for Cancer Diagnosis and Treatment Monitoring, in which our large-volume Si(Li) strip detectors play a decisive role, is submitted by Prof. Walenta to EU (FP6-2005-LIFESCIHEALTH-7). Several stacks of about 10 mm thick Si(Li) strip detectors, as scatter part of the Compton Camera, should be combined with an Anger Camera (as absorber) for photons of higher energies. But for lower photon energies (100-200 keV) only the Si(Li) stacks will be sufficient enough.

References:

[1] Annual report IKP 2004

[2] D. Protić and T. Krings, "Detection Characteristics Near Edges of Large-Volume Si(Li) Detectors", 10th European Symposium on Semiconductor Detectors, Wildbad Kreuth, 2005.

[3] Annual report IKP 2004

[4] M. F. Cunningham, M. Burks, C. E. Cork, L. Fabris, D. J. Lange, T. Krings, E. L. Hull, L. Mihailescu, K. Nelson, T. R. Niedermayr, D. Protić, J. D. Valentine, K. Vetter, D. Wright, "First Generation Hybrid Compact Compton Imager", presented at the IEEE Nucl. Sci. Symp., Puerto Rico, USA, 2005.

[5] L. Mihailescu, M. Burks, D. H. Chivers, C. E. Cork, M. F. Cunningham, L. Fabris, D. L. Gunther, E. L. Hull, D. J. Lange, K. E. Nelson, T. R. Niedermayr, D. Protić, J. D. Valentine, K. Vetter, D. Wright, "Methods for Increasing the Efficiency of Compton Imagers", presented at the IEEE Nucl. Sci. Symp., Puerto Rico, USA, 2005.

[6] Annual report IKP 2005

Performance Test of a 2D µ-Strip Ge(i) Detector at the Sychnrotron Facility ESRF

U. Spillmann, Th. Stöhlker , H.F. Beyer, S. Hess, C. Kozhuharov, R. Reuschl, S. Tashenov, S. Trotsenko
GSI-Darmstadt, Germany and IKF, University of Frankfurt, Germany

T. Krings and D. Protic
IKP, FZ-Jülich, Germany

D. Banas
Swietokrzyska Academy, Kielce, Poland

J.Cl . Dousse, M. Kavcic, J. Szlachetko
University of Fribourg, Switzerland

The x-ray spectroscopy program of the SPARC collaboration strongly relies on the availability of two-dimensional, energy dispersive strip detectors with their inherent advantages concerning spectroscopy and imaging capabilities as well as polarization sensitivity. Here we report on a performance test of a first prototype 2D µ-strip germanium detector developed at IKP Jülich. This germanium diode has on the front contact 128 strips on an area of 32 mm x 56 mm (pitch of 250 µm) and on the rear contact 48 strips (pitch of 1167 µm), respectively (for details compare [1]). For an accurate determination of the response characteristics of this detector (accuracy in position determination and polarization sensitivity) in-beam test measurements were performed at the European Synchrotron Radiation Facility (ESRF) in Grenoble. At the ESRF, the high energy beam line ID15A has been chosen where 98% linearly polarized synchrotron radiation at energies of 60 keV and 210 keV was provided for the experiment. The beam size on the detector was close to 50 µm x 50 µm, ideally suited for this test purpose. For the experiment, each detector segment was connected to a separate electronic readout. This allowed us to register simultaneously for every segment the energy deposition and the hit probability as a function of the beam position on the detector. For the latter purpose, the photon beam was scanned over the active detector area in steps of 50 µm. From this scanning technique detailed information on the effects of electronic cross talk and in particular of charge splitting for the different photon energies used is obtained. A further important aspect of this study was to utilize the detector as a Compton polarimeter and to investigate its polarization sensitivity. Sample 2D images for Compton scattering of 210 keV photons are depicted in Fig. 1 as observed for different energies of the Compton scattered photons. Utilizing the kinematical relation between Compton scattering angle θ and the energy of the scattered photons, the various images displayed refer to the spatial intensity distributions related to different scattering angles (from almost 0 deg up to 180 deg). In the figure, an almost dipolar intensity pattern is observed close to scattering angles of 90 deg (cluster plot in the middle). This finding visualizes that for our initial energy of 210 keV, Compton scattering is most sensitive to the linear polarization at scattering angles close to 90 deg. To illustrate the excellent performance in more detail, we display in Fig. 2 the intensity distribution for 90 deg scattering along an arbitrarily chosen radius vector of 5 mm around the center of the image (position of the beam spot on the detector). The solid line displayed gives the result of the Klein-Nishina formula [3] for 100% linearly polarized light and a scattering angle of 90 deg. An excellent agreement between the data and the calculation must be stated.

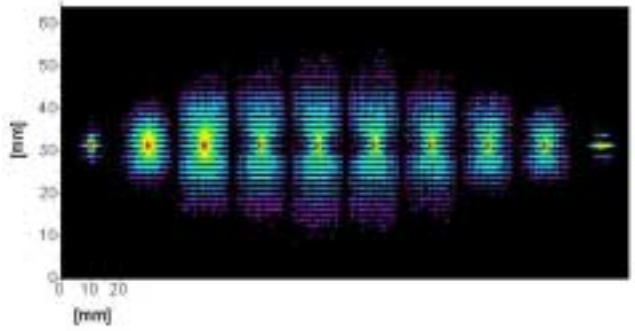

Figure 1: Preliminary 2D images for Compton scattering of 210 keV photons (for details compare text).

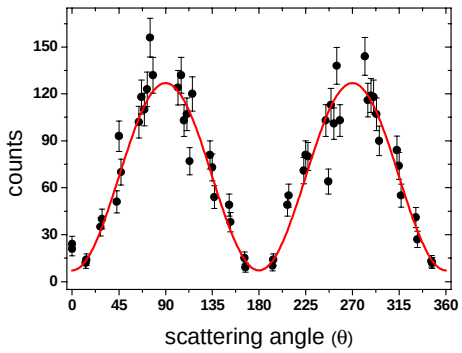

Figure 2: Intensity distribution for Compton scattering of 210 keV photons at 90 deg (for details compare text) .

[1] Technical Report of the SPARC collaboration
http://www.gsi.de/fair/experiments/sparc/index_e.html
[2] D. Protić, Th. Stöhlker, T. Krings, I. Mohos, U. Spillmann, IEEE (2006) in print
[3] K. Siegbahn Alpha-, Beta- and Gamma-Ray Spectroscopy, Vol. 2, North-Holland, 1968

Acknowledgment: The authors would like to thank the staff of the ESRF beamline ID15A and especially Dr. Th. d'Almeida for the excellent support during the experiment.

Electronics Laboratory

C.Berchem, N.Dolfus, W.Ernst, R.Nellen, J.Sarkadi, H.Schiffer, T.Sefzick

The activities of the IKP Electronics Laboratory can be assigned to mainly the following three topics:

Electronics and Data Acquisition for experiments

For the straw chamber project at TOF the ongoing development of pre–amplifiers and signal conversion circuitry has been continued. Several investigations took place to choose the cable type which matches the experiments requirements best. Adapter boards and system crates for the ASD8 bases readout system were developed and prototypes were produced.

For the TOF experiment continuous support has been given for the ongoing development of the liquid hydrogen target system and the SIMATIC S7 and WinCC based vacuum control system. The control system of the liquid hydrogen target was improved. Moreover, continuous support was necessary to ensure the operation of the liquid hydrogen target at TOF.

For the spectator detector at ANKE extensive support was given to the ADC development at ZEL. Additional low–voltage, high–current ($\pm$5V, 2A) power supplies working at high voltage offsets without showing significant leakage currents were ordered and will be finally inspected upon delivery. Cable tests to select coaxial measuring lines were carried out.

For the ANKE multi-wire proportional chambers which are under development printed circuit boards for a test–chamber needed to contact the individual wires were designed and ordered for production.

The atomic beam source (ABS) setup was moved to the so–called LKW–Schleuse in the COSY hall and tested. At this occasion some gauges and instruments were replaced. The whole system was then rebuilt within the ANKE experiment and tested again. Signal distributor boxes for the Lamb shift polarimeter were designed and built. The S7–300 PLC based target positioning system for movement of a double xy-table was extended with position encoders for more precise positioning. It was tested in a beamtime with success.

The interlock system needed to protect detectors at ANKE and in laboratory setups against damage in case of vacuum leakage was put into operation. In case of increasing pressure in the target chamber the high voltage supplies of the detectors will be ramped down with a defined rate.

In the ATRAP-II experiment a scintillating fiber hodoscope, consisting of appr. 1800 channels read out by 16-fold multianode photomultipliers followed by pre–amplifiers, will be used. Time measurement of the signals is based on a RAL111 system. Components for readout modules needed for four additional photomultipliers were purchased and the production of these modules is under way.

For the WASA experiment which is currently installed at COSY several support has been given on several fields: Together with the ZEL the disassembly of data acquisition and signal cables was planned and supported. The cable installation at the new location at COSY is currently under development. For the data acquisition system which is developed and build mainly at ZEL the needed materials and electronic components were purchased. Passive splitter boxes with summing amplifiers and partly with preamplifiers are actually under development, prototypes are build and test measurements concerning crosstalk and impedance matching are going on.

At the pionic hydrogen experiment at PSI the crystal spectrometer was built up and taken into operation, which includes operation of the control electronics for angle and temperature measurement and stepper motor control system. The hydrogen fluoride target control system was calibrated.

The new crystal spectrometer for the pionic hydrogen experiment at PSI has been set–up in the so–called south hall of the cyclotrone building. Here, several temperature detectors were calibrated, the system for angle measurement was adjusted, and the control software was adapted to the new system.

COSY diagnostics

For the emittance measurement electronics and for a programmable current generator Labview 7.1 based control software was written. Calibration measurements using the new current generator were carried out. This included a part time supervision of a diploma student.

Maintenance was provided for the multi–wire chambers for beam diagnostics in the extraction beamlines und for the viewer cameras.

Computer network

After planning and measurements the installation of wireless LAN access points in the institute, COSY, and cyclotron buildings still awaits completion. The installation in building 09.6 (COSY office building with accommodation facility) was completed. Frequent support was granted to ensure continuous operation of the existing networks.

Miscellaneous

On the occasion of the Einstein year an experimental setup for demonstrating the function of a magnetic trap using a fine beam tube together with Helmholtz coils was developed as a prototype. The final exhibit shown on the Einstein ship was produced by an external company.

Like every year substantial support was given with regard to short term maintenance and repair or replacement of electronics. In some cases the urgent demand didn't allow a time-consuming outside repair procedure, in other cases the manufacturer doesn't even exists anymore, but the electronics can not be replaced easily, or the manufacturer was unable to perform the repair.

Prototypes and small series of cables or electronics, for which an outside production would not have been reasonable, were delegated to infrastructure facilities or done here, mainly by trainees and student auxiliary workers.

The standard data acquisition systems at several COSY experiments were taken care of to assure stable operation during several beamtimes.

In addition, some members of our laboratory supported experiments by taking over shifts at beamtimes, mainly at COSY-11 and at the pionic hydrogen experiment at PSI.

Regarding S7 systems continuous support was given to the radiation safety division and to the cyclotron group.

ZAT Scientific Report – Central Department of Technology

The ZAT is part of the FZJ infrastructure and strongly supports the IKP in its efforts to conduct cutting edge experiments. The following topics have been covered in 2005:

- *Frozen Spin target Polarized Solid Material for TOF*
- *WASA-Detector – Wide Angle Shower Apparatus*
- *Niobium Super conducting Resonator*
- *ATRAP – Trapped Anti- Hydrogen*
- *HESR - High Energy Storage Ring at FAIR*

In close collaboration with the spokes persons of the various experiments and projects the best procedures are worked out to meet the challenge. The longstanding expertise of the ZAT makes it often possible to offer solutions that have already a proven record. But if necessary research is conducted breaking new ground in technology to meet the goals of the experiments.

Details to those topics are given in German

---

1. Frozen Spin Target

Das Flugzeitspektrometer TOF (Time of Flight), eine externe Experimentiereinrichtung an der Beschleunigeranlage COSY, soll unter Mitwirkung der ZAT im Sommer 2006 mit einem speziellen Targetsystem einschließlich neu konzipierter und gefertigter Detektorkomponenten ausgerüstet werden.

Vorgesehen ist der Aufbau eines transversal polarisierten Festkörpertargets in vertikaler Anordnung, das von der Universität Bonn entwickelt und gebaut wurde. Der Einsatz der in Bonn existenten und mehrfach bewährten Targetapparatur an COSY stellt aufgrund der beengten Platzverhältnisse am Experiment eine besondere Herausforderung dar. Betrieben werden soll das Polarisierte Target im “frozen spin mode“, das heißt, der Eigendrehimpuls der Nukleonen ist gleichgerichtet und in dieser Orientierung eingefroren. Ein Solenoid mit hoher magnetischer Flussdichte (ca. 2,5 T) übernimmt zunächst die Ausrichtung der Hüllenelektronen bevor in einem zweiten Schritt ein Mikrowellengenerator durch Einstrahlung von Mikrowellen mit abgestimmter Frequenz die Polarisation auf die Kerne überträgt. Eine kryotechnische Anlage kühlt das Targetmaterial auf niedrige Temperatur (ca. 100 mK) und verlangsamt damit stark die Relaxation. Die Relaxationszeit des Spins kann unter Anwendung eines magnetischen Haltefeldes (ca. 0,4 T) zwei bis vier Tage betragen. Besondere Anforderungen ergeben sich für die zum Teil neuartigen, in Targetnähe platzierten Detektoren. Komplett auf einer Trägerplatte montiert, müssen die Haltestrukturen der Detektoren so ausgearbeitet werden, dass sie eine separate Justage bzw. Fixierung der einzelnen Detektorebenen transversal und longitudinal zum Strahl erlauben und so eine bestmögliche Ausrichtung zur optischen Achse ermöglichen.

Damit der Solenoid aus seiner Ruhestellung senkrecht unter das Target positioniert werden kann, ist es unumgänglich das Targetumfeld frei zu räumen. Zu diesem Zweck muss ein Support die Detektorplattform absenken. Im Anschluss daran wird der Solenoid auf seinem horizontal gelagerten Schlitten manuell in die Betriebsposition gefahren und über eine Spindelhubeinheit motorisch soweit angehoben, dass er das Targetrohr vollständig umhüllt, Bild 1.1.

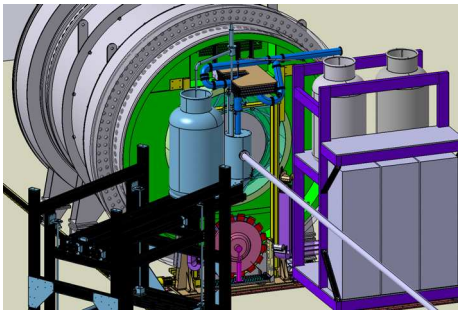

Bild 1.1: Solenonid in Betriebsposition

Die Auf- und Abwärtsbewegung der Detektorplattform soll gleichfalls automatisiert erfolgen und mittels Wegaufnehmer und einstellbarer Anschläge begrenzt werden, Bild 1.2. Zur abschließenden Kontrolle, dass alle nicht ortsfesten Detektoren mit ihren empfindlichen Messflächen in der definierten Sollposition stehen, wird zusätzlich deren Standpunkt relativ zum TOF-Tank optisch überprüft. Damit wird garantiert, dass der auf die theoretische Tankachse gelenkte COSY-Strahl die freien Detektoröffnungen möglichst zentrisch passiert und Beschädigungen ausbleiben. Ebenso ist die genaue und reproduzierbare Lage sowie Ausrichtung des Frozen Spin Targets und des Magneten sicherzustellen. Um eine höhere Auflösung bei der Spurrekonstruktion der Reaktionsprodukte zu erreichen, sollen außerdem Straw -Driftkammern über einen Trägerring an den TOF-Tank angebunden werden.

Die vorgesehene Aufhängung muss eine radiale Positionierung des Detektors zulassen. Der Wunsch, den Straw-Detektor auch mit unterschiedlich vielen Doppellagen (Straw-Rahmen) zu betreiben, bzw. defekte Ebenen austauschen zu können, erfordert den freien Zugang mit vertretbarem Zeitaufwand. Gewährleistet wird dies durch die Möglichkeit, den Detektorsupport und die Versorgungsplattform getrennt voneinander von Hand auf radial zum TOF-Tank verlegten Schienen nach rechts außen zu versetzen. Zum Schutz der innenliegenden Szintillatoren vor einfallenden Lichtquanten muss der Vakuumtank mit einer lichtdichten Abdeckung verschlossen werden.

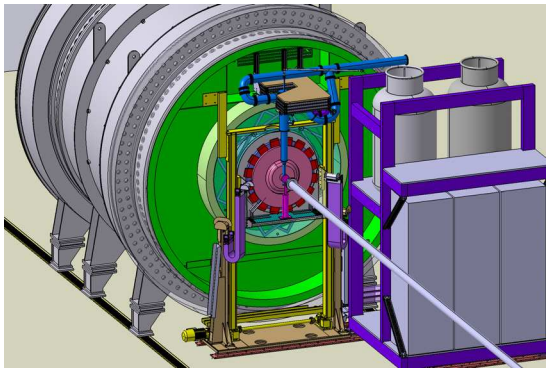

Bild 1.2: Detektorplattform in Messposition

Die evakuierte Strahlführung im Spektrometer erfolgt durch ein nichtmetallisches, divergentes Strahlrohr, das an der Vorderseite mit einem extrem dünnen Strahleintrittsfenster belegt ist. Die Auswahl geeigneter Werkstoffe mit kleiner Kernladungszahl schafft zusammen mit anderen spezifischen Maßnahmen die Voraussetzung dafür, störende Wechselwirkungen mit dem Strahl weitestgehend zu vermeiden.

Im Einzelnen hat die ZAT folgende Arbeitspakete, unter Berücksichtigung der vorgegebenen Anforderungen und der vor Ort bestehenden Randbedingungen, zur Bearbeitung übernommen:

- Extraktionsbeamline bestehend aus Vakuumkomponenten und Unterbauten
- Austauschbares Strahlaustrittsfenster aus Kapton mit kleiner Apertur (Ø 50 mm) und geringer Folienstärke (ca. 50 µm)
- Detektorsupport einschließlich Plattform mit getrennter Aufnahme bzw. Zustellung der einzelnen Detektorebenen sowie automatisierter Bewegung der gesamten Einheit in vertikaler Richtung (Reproduzierbarkeit: ± 0,1 mm)
- Sichere Kabelmitnahme von ca. 1000 Signal- und Leistungskabeln durch Energieketten
- Versorgungsplattform für Dewar-Kannen und Elektronikschränke, die auch als begehbare Bühne für Montagearbeiten dient
- Schienensystem für den Detektorsupport und die Versorgungsplattform mit minimierter Bauhöhe
- Steuerung einschließlich Verriegelungsschaltung für die Stellantriebe
- Optische Sicherheitseinrichtung, aufgebaut aus Leuchtdiode mit vorgesetzter Blende und lichtempfindlichem Transistor (evtl. auch CCD-Kamera)
- Aufhängung inklusive Trägerring für die Straw-Driftkammern mit radialer Ausrichtung auf die Strahlachse (Positionsgenauigkeit: ± 0,2 mm)
- Lichtdichte Abdeckung für den TOF-Tank aus nichtmetallischer (PE), dünnwandiger (ca. 500 µm) und reißfester Folie im sensitiven Bereich des Straw-Detektors (aktiver Durchmesser: ca. 1.000 mm)
- Evakuierte Strahlführung unter Hochvakuum-Bedingungen durch das Spektrometer mit zweigeteiltem, elastomer abgedichtetem Strahlrohr

  1. Teilabschnitt: nichtmetallisch (GFK), dünnwandig (ca. 500 µm) und konisch ($Ø_{Ein}$ ca. 18 mm; $Ø_{Aus}$ ca. 70 mm; LTeil1 ≤ 2.500 mm)
  2. Teilabschnitt: metallisch (VA), zylinderförmig mit Absatz ($Ø_{Ein}$ ca. 70 mm; $Ø_{Aus}$ ca. 130 mm; LTeil2 > 3.000 mm)

- Auswechselbares Strahleintrittsfenster aus Hostaphan (PETP) mit kleiner Apertur (Ø 15 mm), minimierter Folienstärke (ca. 5 µm) und möglichst geringer Materialanhäufung im Bereich der Anbindung zum Strahlrohr
- Montagevorrichtung für den Straw-Detektor
- Platzverwaltung mit Kollisionsüberprüfungen und Zugänglichkeitsbetrachtungen
- Montageablaufplan und Dokumentation

Das Spektrum der auszuführenden Arbeiten umfasste in der ersten Phase die Projektierung des Gesamtaufbaues, die Erstellung von Kontruktionsentwürfen und die Ableitung erster fertigungsgerechter Detailzeichnungen. Zum vereinbarten Leistungsumfang gehören im Anschluss daran die mechanische Fertigung der Bauteile und Komponenten, die technische Betreuung interner bzw. externer Fertigungsabläufe einschließlich durchgängiger Qualitätskontrollen, sowie die Test- und Endmontage der funktionsfähigen Baugruppen am Experiment.

2. WASA-Detektor

WASA (Wide Angle Shower Apparatus) ist ein existierendes komplexes Detektorsystem der Universität Uppsala, die im COSY-Ring eingebaut wird. Mit WASA (4 Pi Detektor) können Reaktionsprodukte nachgewiesen werden, die in beliebige Richtungen emittiert werden. WASA besteht aus mehreren Untersystemen, Bild 2.1: dazu gehören das Pellet-Target, die Zentral- und Vorwärts-Detektoren, das He-Kühlsystem, die Supporte zur Aufnahme der beiden Detektorhalbkugeln, der Unterbau mit Schienen und das Ständerwerk.

Um WASA in den COSY-Ring aufnehmen zu können, sind eine Reihe von Umbau- und Anpassungsmaßnahmen notwendig. Von ZAT werden für die Integration von WASA im COSY-Ring Konstruktions- und Fertigungsarbeiten durchgeführt. Für den bereits erfolgten Abbau in Uppsala und den Tranport nach Jülich wurden für die zwei über 5 t schweren Detektorhabkugeln und für den Vorwärtskonus spezielle Transportgestelle angefertigt. Um die Supporte modifizieren zu können, werden die Detektorhalbkugeln mit einer neugefertigten Hebevorrichtung vorübergehend auf Absetzgestelle umgesetzt. In Bild 2.2 sind die Ergebnisse der FEM-Auslegungsberech-nung für die Hebevorrichtung dargestellt.

Für die COSY-Winterabschaltung 2005/2006 sind das Schienensystem 1 und der Pellettarget-Versuchsstand für den Ein- bzw. Aufbau fertiggestellt worden. Die Schienen werden auf die WASA-Position im COSY eingemessen und montiert. Auf dem Schienensystem 1 werden in der Endmontage die Zentraldetektorhalbkugeln mit den Supporten in den COSY-Tunnel gefahren und dort auf das Achskreuz Pelletrohr/Strahlrohr eingemessen und positioniert. Im Pellettargetversuchsstand soll in Vorversuchen die Funktionsfähigkeit des gesamten Pellettargets erprobt und nachgewiesen werden.

Das Schienensystem 2 ist als Kran-Lastaufnahmevorrichtung konstruiert und ausgelegt und dient als Zubringersystem. Der auf dem Schienensystem 2 montierte Zentraldetektor wird in der Endmontage mit dem Hallenkran an das Schienensystem 1 angedockt. Bis zur Endmontage sind u.a. das Schienensystem 2, die Montage- und die Positioniervorrichtung für den Vorwärtskonus zu konstruieren und zu fertigen. Mit der Montage- und Positioniervorrichtung (Bild 2.3) wird der Vorwärtskonus in Position gefahren und hochgenau (≤ 0,1 mm) einjustiert. Die notwendige Reproduzierbarkeit wird mit einem präzisen Arretiermechanismus erreicht.

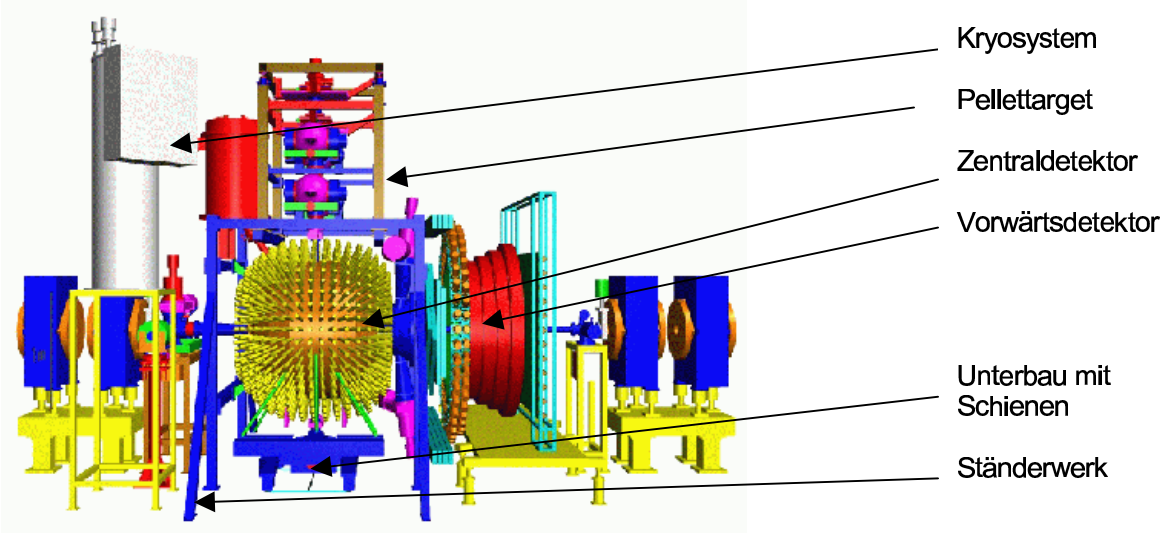

Bild 2.1: WASA-Detektor

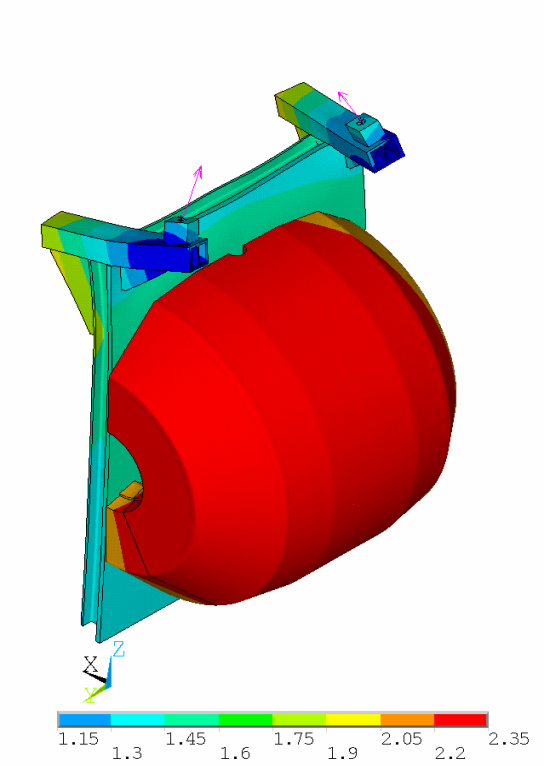

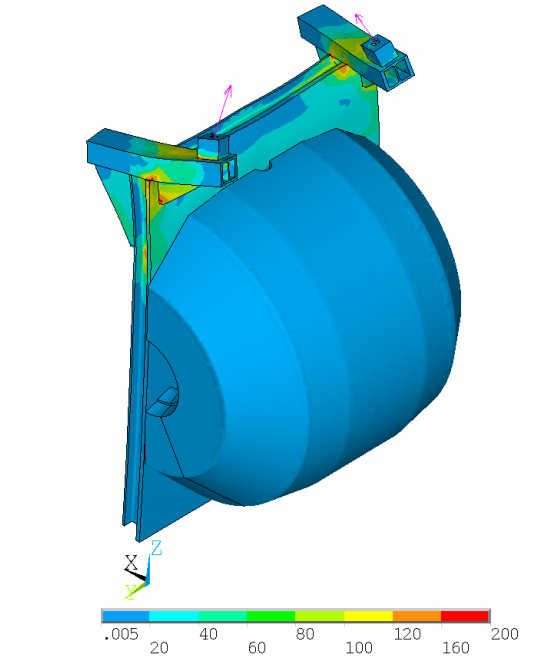

Bild 2.2:
FEM-Auslegungsberechnung der Hebevorrichtung
Oben die Verschiebungen [mm]
Unten die Vergleichsspannungen [N/mm²]
(die Verformungen in den Abbildungen sind 100fach überhöht dargestellt)

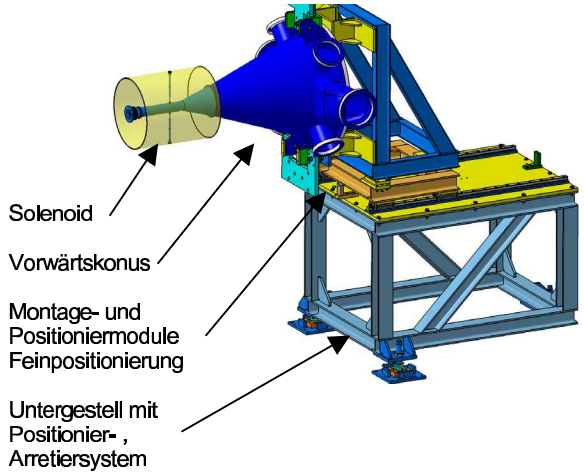

Bild 2.3:
Einbau- u. Positioniervorrichtung für den Vorwärtskonus

Für das Pellettarget werden identische Glasdüsen zur Herstellung der Wasserstoffpellets wiederholt benötigt. Diese Glasteile wurden bisher im Labor in Uppsala hergestellt und sollen in Zukunft durch die Glastechnik der ZAT im FJZ bereitgestellt werden. Das Ziel der Eigenfertigung ist es, eine geringe Ausschussrate bei gleich bleibend hoher Präzision sicher zu stellen.

Die Düse wird durch Ausziehen des erwärmten Glasrohres erzeugt. Die ausgezogene Spitze wird an der Stelle eingeritzt und abgetrennt, an der der gewünschte Innendurchmesser vorliegt. Dieser Trennvorgang wird unter einem Messmikroskop kontrolliert durchgeführt. Zum genauen Ausmessen des erreichten Innendurchmessers wird die stirnseitige Öffnung unter einem Inversmikroskop analysiert. Das Glasrohr selbst, mit einem Innendurchmesser von 1,7 mm, muss in seiner Düsenspitze, die einen Durchmesser von typisch 0,006 bis 0,012 mm haben soll, absolut rotationssymmetrisch sein, um den austretenden Flüssigkeitsstrahl nicht abzulenken.

Die besonderen Schwierigkeiten in der Herstellung der Düse bestehen in dem Einschmelzen eines gesinterten Filterelementes aus rostfreiem Stahl, das bei dem Einschmelzvorgang genau positioniert sein muss und zu dem umgebenden Glasrohr dicht abschließen soll. Der Filter - Porenweite 2 µm - darf bei der Fertigung nicht verschmutzt werden. Das gesamte Bauteil muss extrem sauber sein, da jeder Fremdkörper den tiefkalten Wasserstoffstrahl bereits im Rohr zum Gefrieren bringt. Der Düse ist eine Injektionskapillare nachgeschaltet. Sie hat einen Innendurchmesser von 0,9 mm und verjüngt sich an ihrer Spitze in einer vorgegebenen Form auf 0,58 mm, Bild 2.4. Die Präzision dieser Kapillare und die Geometrie ihrer Spitzen sind entscheidend für die Qualität der entstehenden Pellets.

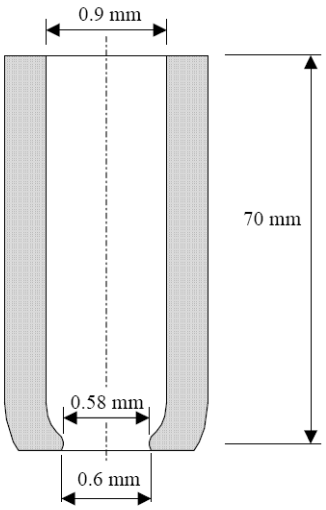

Bild 2.4: Injektionskapillare

Die Spitze der Injektionskapillare wird durch gezieltes Anschmelzen der Randzone des gerade abgeschnittenen Glasröhrchens und anschließendes Planschleifen der Austrittsebene geformt. Durch einen stabilen, mechanisch geführten Prozess soll ein reproduzierbarer Innendurchmesser der entstehenden Verjüngung von 0,58 mm erreicht werden. Der Durchmesser der Austrittsebene wird durch die Tiefe des Planschliffes eingestellt. Wie bei der Düsen-Fertigung wird das Ergebnis der Verjüngung und des Planschliffes unter den oben beschriebenen Mikroskopen beurteilt.

3. Fertigstellung eines supraleitenden Resonators aus Niob

Der im Vorjahr gefertigte 760-MHz-Resonator wurde im Frühjahr 2005 im Forschungszentrum CEA Saclay, Frankreich, einer Reinigungs- und Abtragsbeizbehandlung unterzogen. Durch kontrolliertes Füllen des Resonators mit aggressiver Säure wurden 104 µm der inneren Resonatoroberfläche abgetragen, um sowohl eine minimale Rauhigkeit zu erreichen als auch etwaige Verunreinigungen zu entfernen, Bild 3.1. Als Säure wurde eine Mischung aus Flusssäure, Salpetersäure und Phosphorsäure im Mischungsverhältnis 1:1:2 verwendet. Die Abtragsrate betrug durchschnittlich 0,8 µm/min.

Bild 3.1: Füllen des Resonators mit Säure

Die laufende Kontrolle des absoluten Abtrags erfolgte zwischen den einzelnen Füllungen durch Gewichtsmessung des Resonators. Im unmittelbar darauf folgenden Arbeitsgang wurde der Resonator zunächst außen und innen mit drucklosem deionisiertem Wasser gereinigt, um Säurereste zügig zu entfernen. Anschließend erfolgte die Hochdruckreinigung der Resonatorinnenfläche auf einer speziell hierfür entwickelten Hochdruckspüleinrichtung im Reinraum mit deionisiertem Wasser, um letzte Säurereste und Staubpartikel von der inneren Oberfläche zu entfernen, Bild 3.2. Hierbei fährt eine Spüllanze von unten in den sich drehenden Resonator. Um das beste Reinigungsergebnis zu erzielen, wurde die Lanze nacheinander in jeden der 4 Resonatorstutzen eingeführt.

Bild 3.2: Resonator in Hochdruckspüleinrichtung montiert.

Nach dem Hochdruckspülen erfolgte die Trocknung des Resonators im Reinraum unter einer Laminar-Flow-Box-Strömung und die anschließende Montage von Antenne, Koppler, Blindflanschen und Ventilen. Mit dieser ersten Antennen- und Kopplerkombination und einer bei 500 W limitierten Kopplerleistung wurden die elektrophysikalische Eigenschaften in einem vertikalen Helium-Badkryostat durch das IKP bei 4,2 K gemessen. Die Messungen zeigen eine gute Übereinstimmung der Messwerte mit den berechneten Parametern. Um die Charakteristik des Resonators noch eindeutiger zu bestimmen, werden weitere Messungen bis Anfang 2006 durch das IKP durchgeführt, wie beispielsweise die Reduzierung der Heliumbadtemperatur von 4 auf 2 K oder die Messungen bei fixierten Strahlstutzen. Schon heute kann festgestellt werden, dass die ZAT in der Lage ist, supraleitende Speichenresonatoren zu fertigen, die einerseits von hoher Qualität und Güte sind, und andererseits eine gute Übereinstimmung von Messwerten zu berechneten Parametern zeigen.

4. ATRAP

Das am CERN laufende ATRAP - Experiment, eine Kollaboration von Wissenschaftlern aus Jülich, Harvard, York, München und Mainz erzeugt aus Antiprotonen und Positronen Antiwasserstoffatome, die in geeigneten „Teilchenfallen“ gespeichert und spektroskopisch untersucht werden. Dies geschieht unter extremen Vakuumbedingungen bei Flüssigheliumtemperatur (4K). In der ZAT wurden dazu im vergangenen Jahr verschiedene Arbeiten zur Entwicklung und zum Bau eines Fallenbehälters, der supraleitenden Quadrupol-Spulen und Solenoide sowie der optischen Laserports durchgeführt. Der Fallenbehälter nimmt die supraleitenden Spulen auf und dient zur Kühlung und zur Gewährleistung der mechanischen Stabilität. Die Bilder 4.1 und 4.2 zeigen das Design und die Fertigung des Prototypbehälters in der ZAT. Ziel der Herstellung des Prototypen war in erster Linie die Klärung fertigungstechnischer – und hier insbesondere schweißtechnischer – Fragestellungen bzgl. Machbarkeit und Toleranzen.

Bild 4.1: Prototypbehälter aus Titan für ATRAP II.

Bild 4.2:
Fertigung des Drehkreuzes für die Aufnahmen der Spulen.

Die optischen Fenster trennen das Experimentiervakuum und das Isolationsvakuum voneinander und dienen der Durchführung des Strahls zur Laserspektroskopie. Diese Trennung ist notwendig, um ein extrem hohes Vakuum von 10^{-15} mbar im Experimentierbereich zu gewährleisten; andererseits muss jedoch der Aufenthaltsort der Antiwasserstoffatome für laserspektroskopische Untersuchungen zugänglich sein. Dazu ist ein Titanflansch mit CF-Geometrie und einem Magnesiumdifluorid-Fenster entwickelt worden, der sowohl mögliche Druckunterschiede beherrscht als auch den Einsatz im Tieftemperaturbereich bei 4K ermöglicht. Magnesiumdifluorid (MgF_2) wurde ausgewählt, weil es eines der wenigen Materialien ist, das bei der Spektroskopiewellenlänge von 121nm (Lyman-α) transparent ist. Eine Eigenentwicklung war notwendig, da kein Hersteller den Einsatz bei Heliumtemperaturen garantieren konnte. Bild 4.3 zeigt den entwickelten Titanflansch mit dem dazugehörigen MgF_2-Fenster.

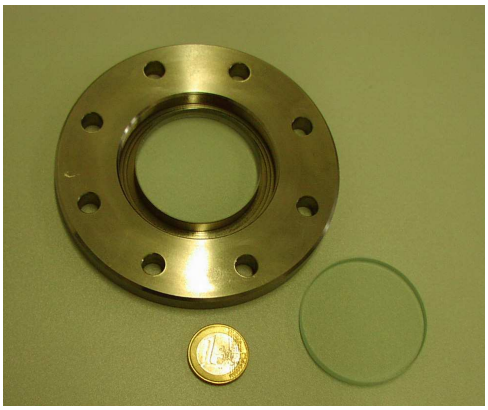

Bild 4.3:
Optisches Fenster bestehend aus Titanflansch und MgF_2-Fenster.

Die Kombination der beiden Materialien MgF_2 und Titan ist aus kryotechnischer Sicht günstig, weil beide bei Raumtemperatur einen sehr ähnlichen thermischen Ausdehnungskoeffizienten von 8,5 bzw. 8,9 x 10^{-6} K^{-1} aufweisen. Trotzdem wurde in dem Titanflansch eine nur etwa 250µm breite Lamelle ausgedreht, um auch die geringe unterschiedliche Ausdehnung des daran eingeklebten MgF_2-Fensters mit dem Titanflansch auszugleichen.

Es wurden Versuche unternommen MgF_2-Scheiben in Titandeckel einzukleben. Als Kleber wurden ein Epoxy-Kleber bzw. Stycast verwendet. Die Leckraten nach Beendigung der Tests waren besser als 10^{-6} mbar l s^{-1}. Erste Abkühlversuche mit eingeklebtem Borofloatglas, welches ein ähnliches Ausdehnungsverhalten besitzt, zeigten, dass diese Verbindung stabil ist und auch mehrmaliges Zyklieren zwischen 77K und Raumtemperatur übersteht. Für diese Abkühlversuche wurde das optische Fenster in den Vakuumraum zwischen zwei CF Flansche thermisch abgekoppelt eingebracht und diese Anordnung in ein Bad mit flüssigem Stickstoff gelegt. Auf diese Weise konnten Abkühlzeiten von etwa 3 Stunden realisiert werden, die den realen Verhältnissen beim späteren Experimentierbetrieb nahe kommen, Bild 4.4.

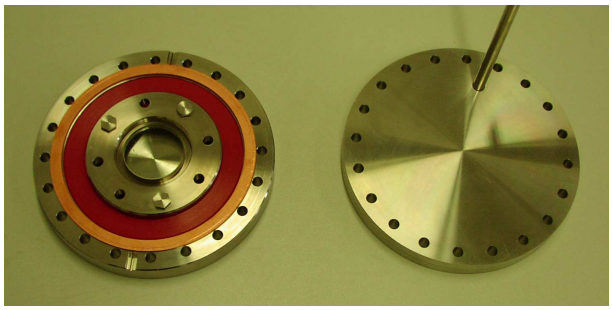

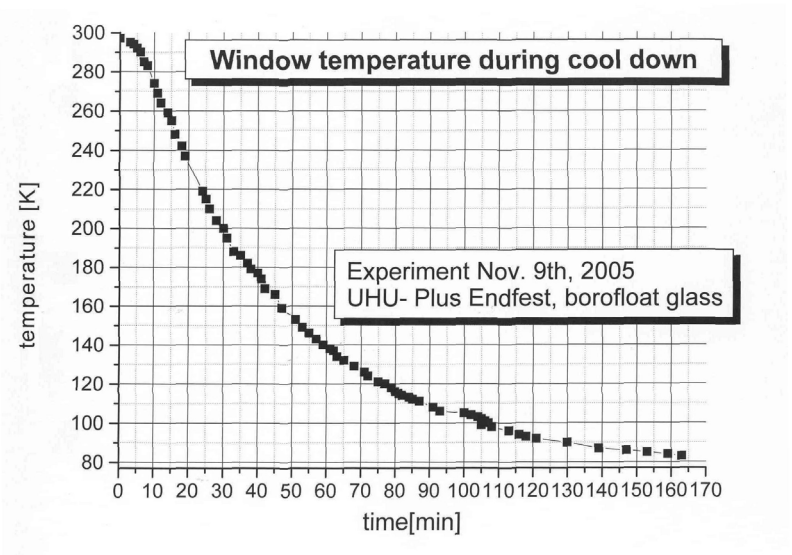

Bild 4.4:
Abkühlversuch des optischen Fensters (siehe Bild 4.2) mit Abkühlkurve.

Im Jahr 2006 werden Tests mit eingeklebten MgF_2-Scheiben folgen, wobei auch die optischen Eigenschaften bei tiefen Temperaturen an der Universität Mainz untersucht werden sollen. Neue Erkenntnisse insbesondere hinsichtlich der erforderlichen Festigkeit des Strukturmaterials führten zu einem neuen, wesentlich massiveren Behälterdesign, der auch höheren Ansprüchen genügt. Dieses Design (Bild 4.5) reduziert die Vergleichsspannungen nach Mises unter Annahmen einer senkrecht nach innen gerichteten Spulenkraft von 200 kN um den Faktor 10 (Bild 4.6 und Bild 4.7). Die Kräfte werden hier von einem massiven Titankörper im Zentrum des Behälters abgefangen.

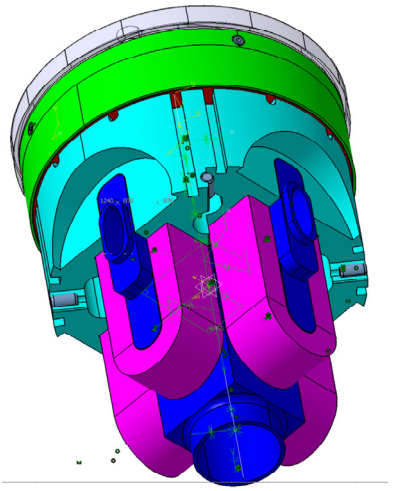

Bild 4.5:
Aufbau des neuen Fallenbehälters für ATRAP II (blau: Ti-Körper, violett: Quadrupol-Spulen, türkis: Al-Körper, grün: Solenoid).

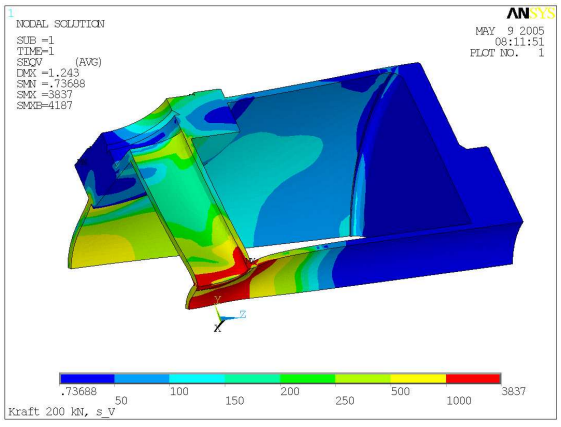

Bild 4.6:
Mechanische Auslegungsrechnung der resultierenden Vergleichsspannungen im Prototypbehälter unter Annahme einer Spulenkraft von 200kN.

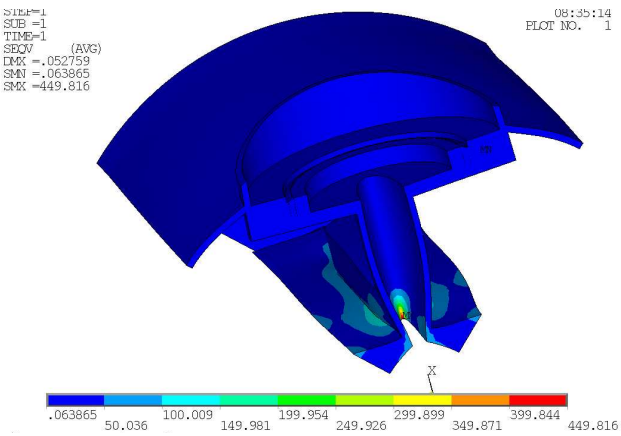

Bild 4.7:
Mechanische Auslegungsrechnung der resultierenden Vergleichsspannungen für das neue Design des Fallenbehälters unter Annahme einer Spulenkraft von 200 kN.

Zur genaueren Ermittlung der resultierenden Spulenkräfte wurden zudem magnetische Berechnungen mit dem BEM (Boundary Element Methode) Programm der Firma IES durchgeführt. Bild 4.8 zeigt die 4 Quadrupol-Spulen und die 2 Solenoid-Spulen mit den dazugehörigen Kraftdichten in diesem Modell. Im Bereich der Rundungen der Quadrupol-Spulen treten die maximalen Flussdichten auf, die die Stromdichten innerhalb der Spulen auf etwa 300 A mm^{-2} begrenzen. Die Pfeile geben die Stromrichtung in den Spulen an.
Bild 4.9 zeigt ein mit diesem Modell berechnetes Potential, in welchem die neutralen Antiwasserstoffatome gefangen werden, wenn sie eine kleinere Energie aufweisen als einer der Temperatur von etwa 400 mK entsprechenden.

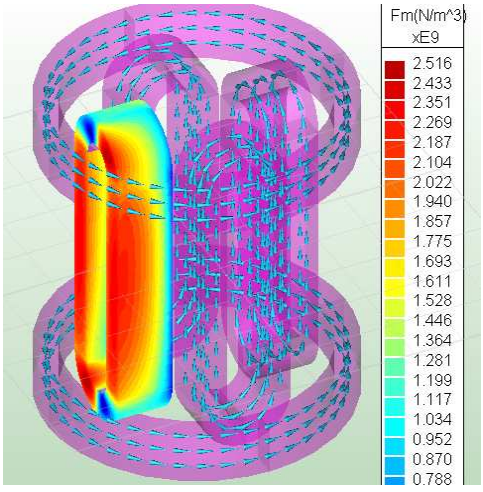

Bild 4.8:
Berechnung der Kraftdichten für die Spulenanordnung im Fallenbehälter für ATRAP II.

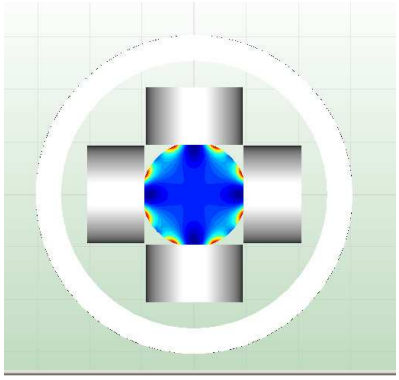

Bild 4.9:
Berechnung der Magnetfelder innerhalb der Spulenanordnung im Fallenbehälter für ATRAP II.

Grundprinzip des neuen Behälterdesigns ist das Vergießen der Spulen mit einem zweigeteilten Aluminiumkörper, der der Vorspannung der Spulen dient, Bild 4.3. Durch den größeren thermischen Ausdehnungskoeffizienten des Aluminiums von 24,2 x 10^{-6} K^{-1} gegenüber 8,9 x 10^{-6} K^{-1} von Titan wird beim Abkühlen eine Vorspannung der Spulen erreicht. Die Quadrupol-Spulen werden direkt auf den Titankörper gewickelt, der aus einem massiven Halbzeug gefertigt wird. Die Solenoide erhalten einen eigenen Wickelkörper, der auf den Aluminiumkörper aufgeschoben und verstiftet wird. Die Kühlung der Quadrupol-Spulen erfolgt im Wesentlichen durch Kühlbohrungen im Aluminium, die der Solenoide über die Oberfläche des Wickelkörpers aus Titan. Die supraleitenden Drähte werden sowohl im Titan als auch im Aluminium in Nuten geführt und oberhalb des Aluminiumkörpers verbunden. Das Wickeln der Spulen erfolgt bei einer externen Firma, während die Fertigung aller Komponenten und Bauteile in der ZAT erfolgt, insbesondere die Ummantelung der Spulen mit dem Titanbehälter (analog Prototypbehälter in Bild 4.1).

5. Vorarbeiten für HESR (High Energy Storage Ring)

Das IKP ist federführend bei der Entwicklung und Auslegung des neuen Speicherrings HESR tätig. Dies ist ein Teil des 2. Stufenplans im Projekt FAIR (Facility for Antiproton and Ion Research) an der GSI, Darmstadt. Die ZAT ist in diesem Projekt an mehreren Stellen eingebunden. In einem ersten Schritt wurde mit der Erarbeitung des Designs für die Beamline und die Planung des Gesamtaufbaus des HESR-Rings in einem Aufstellungsplan begonnen. Neben der Integration des Großexperimentes PANDA ist in einem späteren Ausbau auch der Aufbau von COSY innerhalb des Rings vorgesehen. Bild 5.2 gibt einen Überblick, wobei der COSY-Ring im Innern angedeutet ist.

Eng verbunden mit dem Aufstellungsplan ist eine grobe Vordimensionierung des Behälters für die Aufnahme der supraleitenden Dipole, Quadrupole und Sextupole. Insgesamt enthält der HESR-Ring je 48 Dipol- und Sextupol-magnete sowie 112 Quadrupolmagnete. Bild 5.1 zeigt eine Dipol- und Quadrupoleinheit, die aus dem RHIC-Design in Brookhaven abgeleitet ist.

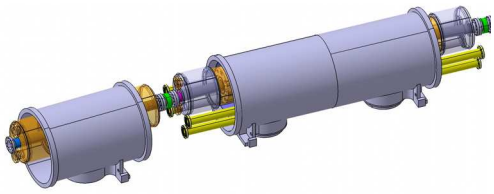

Bild 5.1: Quadrupol- und Dipoleinheit für den HESR-Ring.

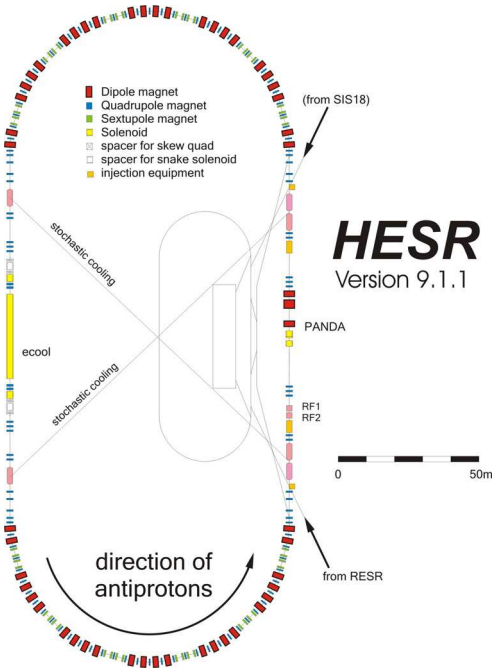

Bild 5.2:
Layout des HESR-Rings mit dem Aufbau von COSY (Stand 13.09.2005).

Mit der groben Vordimensionierung des Rings und einer ersten Auswahl hinsichtlich Wandstärken und Material für die Hauptkomponenten wie Kryostatbehälter, thermisches Schild oder Heliumgasleitungen ist begonnen worden. Ein wichtiges Augenmerk liegt dabei auf die Auslegung der Kalt-Warm-Übergänge, da nicht der gesamte Ring supraleitend ausgeführt wird, sondern einzelne Sektionen normalleitend sind. In Bild 5.3 sind jeweils die kalten und warmen Sektionen des HESR-Rings farbig markiert.

Weitere Arbeitspakete sind u.a. die kryotechnische Grobdimensionierung des Heliumsystems für den HESR-Ring und hier insbesondere die der Heliumleitungen, da diese einen direkten Einfluss auf die magnetische Auslegung der Magnete haben. Ein weiterer Schwerpunkt der Untersuchungen liegt in der Ausführung der Dipol-Spulen. Im Rahmen einer Studie in Zusammenarbeit mit der Industrie soll die Herstellung gebogener Dipol-Magnete untersucht werden, da dies für die Strahldynamik des Rings wesentliche Vorteile mit sich bringt. Nach einer detaillierten kryotechnischen Auslegung des Gesamtsystems liegen weitere Aufgaben in der mechanischen Auslegung und der Konstruktion der Kryostate für die verschiedenen Magnete und weiteren Einbauten des HESR-Rings.

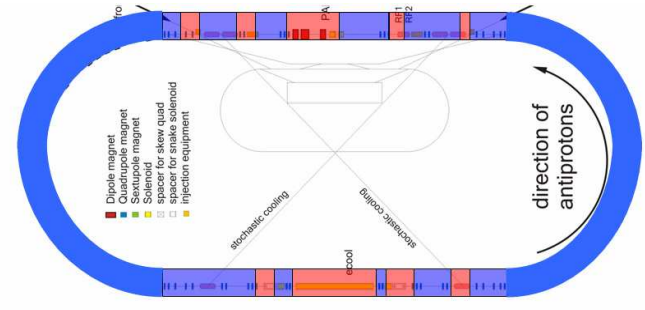

Bild 5.3: Kalte und warme Sektionen des HESR-Rings.

6 Miscellaneous

Cooperation with Japanese Scientists since more than 40 Years — A Brief History of Networking among Physicists

O.W. Schult

Promotion of Science is optimally accomplished in international cooperation and this is fundamental for a successful globalization. Cooperation in a given field requires that the cooperating partners accept and respect each other and join forces. The better their coherence, the greater will be the success of their work. Cooperation is at least between two persons. It can be between scientists from different countries. The support of the cooperation by the countries is essential. Regarding global fairness collaboration should not be restricted: true multilateral collaboration serves the advancement of science in the best possible way.

It is not essential to ask whether the merchants or the scientists play the more important role to promote agreement between nations and guarantee peace. It is crucial, however, that states and politicians do not hinder but rather strongly support international cooperation. In this regard the Japan Society for the Promotion of Science (JSPS) has been an excellent example.

I will write about experiences of interaction with Japanese scientists. Cooperation with them has lasted for more than 40 years now. It has been a major part of my life and I am indebted to all of my Japanese friends and colleagues, also to those, whose names are not explicitly mentioned in my text.

1962 I came to Denmark, where two young colleagues of mine, Ulf Gruber and Bernd Maier and I wanted to carry out high-resolution spectroscopy of neutron-capture γ rays at the DR-3 reactor of the Research Establishment of the Danish Atomic Energy Commission (AEK) at Risoe near Roskilde. This work was initiated through a letter which Prof. Dr. O. Kofoed-Hansen, the director of the physics department at Risoe had written to Prof. Heinz Maier-Leibnitz, director of the Institut für Technische Physik at the Technische Hochschule München. In that letter, Kofoed-Hansen informed us about the neutron fluxes in the beam holes of the DR-3 reactor. Maier-Leibnitz gave me the letter. I immediately realized that this reactor with a neutron flux at the target position being 60-times that of the FRM reactor near Garching was ideal for our work. Maier-Leibnitz said: "go to Kofoed-Hansen and discuss details with him". Kofoed-Hansen gave us full support. The board of management of the AEK mentioned that there would be a significant annual charge for using the DR-3 beam tube. A little later I was told, that Niels Bohr, who was the director of the AEK, had come across one of my letters, in which I had asked for data on the neutron fluxes in regions of the beam holes, where we had to design shielding plugs. Niels Bohr was so happy about the fact that the DR-3 reactor should be used for research - this reactor had originally been built for material testing - that he decided, that we could use the beam tube free of charge for two years. It finally became 10 years. In those years, the DR-3 reactor was the world's best research reactor, and we were permitted to use it! We always had the full assistance and encouragement of the Danish scientists, all persons at the DR-3, all people in the whole Research Establishment, and also the scientists at the Niels Bohr Institute in Copenhagen, especially Ben Mottelson and Aage Bohr. All Danish people met us in a most friendly way and helped us much more than we had ever expected. All of us had a very good time in Denmark, a place where international collaboration had a long tradition and where we experienced this in a most wonderful manner. "Across the road" of Risoe was the tandem accelerator of the Niels Bohr Institute. Elbek, Herskind and Olesen studied, together with a Japanese scientist, Dr. Yasukazu Yoshizawa, the γ-vibrational bands of rare earth nuclei through Coulomb excitation. We met in the cafeteria at Risoe and Dr. Yoshizawa discussed with me in a very open minded, friendly and cooperative atmosphere the advantages and limitations of their approach. They could only study the lowest level, the band head, but measure the absolute transition probability. I told him that through our neutron-capture γ-ray spectroscopy we could see numerous transitions within the γ-vibrational band and transitions depopulating these levels. But we could only measure relative transition probabilities. The results of Dr. Yoshizawa permitted us to obtain absolute transition strengths which were of interest for the theorists in the Niels Bohr Institute. Our relationship with Dr. Yoshizawa, a very modest and fine person and excellent scientist, developed into a cordial life-long friendship.

In the Niels Bohr Institute I met Raymond Sheline who studied (d, p)-reactions at the tandem of the Florida State University in Tallahassee. His approach was complementary to our spectroscopy. Sheline invited me and I joined him as research associate late in 1965. Originally a chemist, Ray developed very broad interest. One of his co-workers was a nuclear theorist, Dr. Takeshi Udagawa, with whom I shared the room. Our desks were opposite to each other so that we looked into our faces which both of us liked. We had lots of discussions and when I had a problem, Takeshi, a very capable but personally very modest and most pleasant scientist, said: "let me help you! I have the most advanced code and it takes me only a few minutes to calculate the level energies. I could benefit a lot from him. Our families were connected through a very friendly and cordial relationship.

Ray had another Japanese co-worker: Yoshi Shida. Yoshi worked with us to carry out the (d, p) reaction studies. He was a very skilled experimenter, had an extremely solid basis and solved almost all problems. He was never frustrated. It was fun to work with him. Shortly before I left Tallahassee, I had to participate in a conference in Santa Fe. I mentioned to Ray's new co-worker, a US citizen, that he could already move at my desk, but that I left in the shelves a few documents which I would like to pick up when I was back from Santa Fe. After my return I went into my old room. Everything that I had left on the shelves had been thrown away and could not even

be recovered from the dumping site. The desks had been separated and two cabinets for computer cards had been moved between them so that the persons could no longer see their faces. I was infinitely sad. People are different and some like to build up walls instead of tearing them down.

After my return to the Technische Hochschule München in 1967, the Institut für Technische Physik had developed into a Physik-Department at Garching, where Dr. Haruhiko Morinaga, the father of in-beam γ-ray spectroscopy, had become full professor. He asked me whether I could help him. I said "yes" and have never regretted that. Morinaga gave me full freedom regarding my research and I helped him to find a practicable way through the jungle of German bureaucracy. Prof. Morinaga built up a team of co-workers who did research with great skill and efficiency. Soon Yoshi Shida, my old friend joined Morinaga's institute. It was great to see him again and to continue our cooperation. Morinaga had also visits from other Japanese guests like Dr. Toshimitsu Yamazaki, Dr. Hirojasu Ejiri and Prof. Akito Arima, all scientists with outstanding international reputation. A young Japanese student, Jun Imazato, came to work with Morinaga for his doctoral thesis. As he had arrived without official visa, hoping that this could be easily settled after his entry into Germany, I was contacted by the Bavarian office for aliens. Several times I succeeded to convince — in Bavarian tongue, of course — the lady on the other end of the telephone to give us a prolongation of a couple of months. Finally, it was in the month of December, I was called again. The lady said that now Mr. Imazato definitely had to return. I knocked at the ladies heart with the argument of helping young guys, humanity and understanding. As that could not melt the ice I asked what was the real problem. She told me that German workers whose visa had run out because of a delay in their work had got into difficulties in Japan and that it is "diplomatic habit" to treat everybody equally. I informed Morinaga and he said: "that is no problem. Jun has been with us now for quite some time and it is good for him to visit his family during the time of the new year which is important in Japan". When Jun came back he had got his visa in Tokyo without any difficulty. He finished his thesis work excellently under Morinaga's guidance.

In December 1972 I moved to Jülich as professor at the University of Köln and director at the Institut für Kernphysik of the Kernforschungsanlage Jülich. Dr. Peter Kleinheinz, a very careful and experienced nuclear physicist joined my group and we succeeded to convince the Alexander von Humboldt Foundation to support Dr. Masao Ogawa from the TIT at Yokohama as Alexander von Humboldt fellow. Around 1976 he came with his wife Hiroko and their children for about two years. Masao, a hard working and most cooperative scientist did a perfect job in Peter Kleinheinz' team. As Kleinheinz was scientifically cooperating with persons from different countries, Finland, Poland, Italy, Spain, the US, and even Latvia, Argentina and Turkey in those years and later on, I used one of my guest-scientist positions to support Yasuki Nagai. He also came with his wife Kiyoko and their children from 1978 to 1980. Nagai was also a very powerful co-worker in the team of Peter Kleinheinz . I had integrated the JOSEF (Jülich Online Separator for Fission products) group into my institute under the guidance of Dr. Kornel Sistemich. Also Sistemich's team enjoyed collaboration with Japanese scientists. Dr. Kiyoshi Kawade from the University of Nagoya came with his wife Masako and worked with Sistemich from 1978 – 80. Kiyoshi was highly experienced in fast coincidences and significantly helped to improve our data. A little later Dr. Kiyoshi Shizuma joined Sistemich's group from 1980 – 83. He had come from the University of Hiroshima, from my old friend, Y. Yoshizawa, who had become full professor and director of the nuclear physics institute in the mean while. From 1983 – 84, Dr. Takeshi Seo, a very capable, courteous and cooperative scientist from the University of Kyoto, worked with Kornel Sistemich. All these people worked together very well both scientifically and also regarding their personal relationships. Their work was clearly mutually beneficial. Masao Ogawa returned to us in order to continue his work together with Peter Kleinheinz in 1984 and 1985 for shorter periods. Peter Kleinheinz went to Japan in 1996 and worked there together with Masao on extremely interesting problems.

As I was responsible for our large magnetic spectrograph BIG KARL, it was most natural that a strong interaction and cooperation was established with Prof. Hidetsugu Ikegami, who was one of the most experienced scientists in that field, worldwide. To my knowledge, all nuclear physics laboratories in Japan, where magnetic spectrographs or cyclotrons were built, have benefited a lot from Prof. Ikegami's advice and help. And so did we. In 1977 I attended the International Conference on Nuclear Structure in Tokyo, visited the INS and the TIT and went to the RCNP, Osaka, to participate in a symposium. This strengthened very much our ties between the RCNP and our nuclear physics institute in Jülich. Hidetsugu had visited us in 1980 and he sent one of his brightest co-workers, Dr. Ichiro Katayama, to us. Ichiro joined our BIG Karl team in July 1980 and worked with us in the most constructive and efficient way. Ichiro had come with his wife Mitsuko and their two sons. They integrated themselves to German life in a really excellent manner. Ichiro carried out extremely interesting research in the field where nuclear reactions and atomic physics merge. I was even considering to offer him a permanent contract, But I always felt that one should refrain from brain drain, and it would certainly not have been fair against Hidetsugu. Ichiro and his family returned to the RCNP after having been with us for two years.

At a later visit of TIT I met Yasuo Tokunaga. He told me that he would like to work for his doctoral degree under my supervision. I accepted him immediately. Only the brightest and most engaged and hard working young students undergo the trouble to continue their education under the difficult conditions to learn other languages and adjust themselves to the other, foreign boundary conditions. Yasuo came to Jülich, passed all tests demanded by the physics department of the University of Köln and all German language examinations that were required for him to be accepted as graduate student.

He had been studying hard indeed. It turned out to be even more difficult: For his thesis work, the neutron-capture γ-ray spectroscopy of selenium isotopes, he had to go to Grenoble, France, to make use of the very high-resolution curved-crystal spectrometers built by my co-workers, Rüdiger Koch and Hans Börner. Thus Yasuo had to learn French and intensify his knowledge of English in addition. He carried out all of his work in a spotless manner. Our faculty accepted, of course, that his thesis work was written in English. On May 15th 1982 he passed all examinations with best grades. He was indeed one of my best students.

Hidetsugu Ikegami had become director of the RCNP. He developed plans to significantly extend the research possibilities of the institute. He intended to set up a sector cyclotron that permitted acceleration of protons to about 400 MeV, to develop a storage ring and Grand Raiden, the worlds best high-resolution spectrometer. Early in 1983 he had asked the JSPS to support my visit to Japan and stay at his institute. He perfectly organized our visit to the University of Tokyo, the TIT, the INS, the RIKEN, the JAERI, the Cyclotron and Radioisotope Centre of the Tohoku University, and the University of Osaka. There, Prof. Hiroyasu Ejiri, director of the Nuclear Physics Institute, informed me about his very interesting research activities. I also visited the University of Hiroshima, where I met again my old friends Yasukazu Yoshizawa and Kiyoshi Shizuma, and the University of Kyushu at Fukuoka, where I could discuss with Prof. Matoba the possibility to cooperate on a COSY experiment. At these other research institutions I gave various reports on our work, also at the March Meeting of the Japanese Physical Society. I spoke about contributions of nuclear physicists to applied sciences at the Department of Nuclear Engineering of the University of Nagoya. The RCNP was my home base. When Hidetsugu asked me, whether I would like to stay in a western style room or in a Japanese room, I asked him in which country I was living. In Japan, I certainly preferred to live the Japanese way. He permitted me to use, in the RCNP guesthouse, the large and beautiful Japanese style room with a wonderful tatami floor and a nice flat table under which I could stretch my legs when working. Hidetsugu had found a position for my student and friend Yasuo Tokunaga in the RCNP. Yasuo helped me a lot and showed me even how to prepare "bamboo babies". My friend Ichiro was back at the RCNP and gave me full support. It was great to meet his family again at Kobe. I took part in the Kikuchi Summer School in Kyoto and gave a talk about nuclear studies at a high current spallation source. On the occasion of the conference in Tokyo I had the pleasure to meet again Prof. Dr. Eiichi Arai and his wife. Prof. Arai has always been one of the most engaged promoters of Japanese - German cooperation. Prof. Hiroshi Ogata, Hidetsugu Ikegami, Michiya Kondo, Hiroyasu Ejiri, Ichiro Katayama and others had organized a very large and most successful International Symposium in Osaka, in which I also participated. We discussed a lot. I took part in an experiment at the RCNP, where we used the AVF cyclotron with 85 MeV protons, twice the energy we could get at Jülich, to search together with Prof. Muhsin Harakeh from Groningen and other Japanese colleagues for special nuclear excitations. Hidetsugu Ikegami, Prof. Hiromichi Kamitsubo from RIKEN, Prof. Juri Oganesian from Dubna and I also visited Sumitomo Heavy Industries in Niihama. This visit was most impressive and it showed how Japanese scientists and companies cooperate most successfully. We enjoyed the cherry blossom in early spring and later the wonderful azaleas in full bloom. In the midst of my friends and colleagues, also Prof. Dr. Hiroyasu Ejiri and Dr. Yoshitaka Fujita from the Osaka University, Prof. Dr. Shumpei Morinobu, now at the Kyushu University at Hakata, and Prof. Mamoru Fujiwara from RCNP, I never felt like being in a foreign country. Most enjoyable was the close and open minded collaboration and atmosphere and the unsurpassable hospitality of our Japanese hosts. The support by the JSPS was in any respect very generous and exemplary for other organizations who wish to support international cooperation.

The following years were important for both, the RCNP and our institute at Jülich. Hidetsugu and his wife Noriko visited us in Fall 1983. He gave a series of lectures, the last on Josef Haydn, Hidetsugu's favourite composer. We also hiked together in the Schwarzwald in the south-west of Germany. In our institute we had concentrated on possibilities to exploit the spallation source facility: isotope separation with the later option to add radioactive beam acceleration and COSY, a cooler synchrotron. My colleague, Prof. Dr. Claus Mayer-Böricke retired late in 1983. One of his research associates was Dr. Gono, who worked in the spectroscopy group and later went to RIKEN. In July 1985 Minister Riesenhuber stopped the spallation neutron source (SNQ) project. The chairman of the board of executive directors in our Kernforschungsanlage (KFA) in Jülich, Prof. Dr. Wolf Häfele recommended us to concentrate on COSY now, which he had wisely considered a good back-up solution for the SNQ. For our institute this was the best solution. We began to enter the field of medium-energy nuclear physics, which was not trivial for people coming from nuclear spectroscopy. I kept the door to my room usually open. One day somebody knocked on it. It was Takeshi Udagawa, who had become full professor for theoretical nuclear physics at the University of Texas in Austin in the mean time. Takeshi worked together with Dr. Franz Osterfeld from our institute for theoretical nuclear physics and he came back every year for his sabbatical until Franz Osterfeld sadly passed away. Actually, the former director of that institute, Prof. Dr. Amand Faessler, had also Japanese scientists working with him, among others Prof. Dr. Hiroshi Toki, now at the RCNP. Dr. Yasuo Tokunaga had joined a Japanese company which sent him to their laboratory in Bavaria. Yasuo went there together with his wife Kiriko. Both liked that very much. While we were preparing ourselves for COSY, Hidetsugu started, in 1989, to set up the RCNP ring cyclotron with 6 sectors for acceleration of light ions and protons up to 400 MeV, a very interesting energy, with the AVF cyclotron serving as injector. The first beam was delivered in November 1991, a time when I had gone to the RCNP again. Hidetsugu also succeeded to build the storage ring and Grand Raiden. In 1993 we had the inauguration of COSY. We wanted to measure the lifetime of very heavy hypernuclei with targets

in the circulating COSY beam (COSY-13) and planned various experiments at our in-beam small forward angle magnetic spectrometer ANKE, where we also needed a polarized source. For COSY-13 we formed an international collaboration including scientists from Poland and Japan: Dr. Yusuke Uozumi and Prof. M. Matoba from Fukuoka. Yasuke stayed with us in 1995 and Prof. Matoba in August 1997. For building a good polarized source it is the best to get the advice of experts: Prof. W. Haeberli from Madison, Wisconsin, Prof. E. Steffens from Erlangen and Prof. Kichiji Hatanaka from the RCNP. Kichiji supported us also in our institute. During my visits of the RCNP in December 1995 and in May 1997 I could admire his excellent polarized ion sources which produced beams for axial injection into the AVF cyclotron.

Hidetsugu was very hard working on new ideas. He examined a new particle beam cooling scheme, "cyclotron maser cooling" successfully. He received the Dr. honoris cause from the University of Uppsala and continued his research about interesting aspects of "cold fusion". For my retirement, end of March 1998, Hiro Ejiri had come and gave a brilliant talk. I continued analysing our COSY-13 data and reported about the results during the International Symposium on Nuclear Electro-Weak Spectroscopy that was held near the RCNP from March 9 – 12, 1999, on the occasion of Hiro's retirement. My successor, Prof. Hans Ströher, continued the cooperation with Japanese scientists. Dr. Genichiro Wakabayashi from the Kyushu University was with us from 2002 to 2003, worked with the ANKE people and helped to ensure that the wire chambers functioned well. Now, Dr. Yoshikazu Maeda from the RCNP has been working with us since almost 4 years. Also his wife lives with him in Jülich, and their son was borne here.

Our international cooperation with the scientists from Japan is now more than 40 years old. But it remains young, guarantees optimal progress of science, serves mutual understanding and builds up friendship between people from different parts of the world. We all are grateful to the persons who have supported us: in Japan especially the JSPS, Japanese officials and many scientists. In Germany our ministry, the Alexander von Humboldt Foundation, our board of management and many of our German colleagues gave us support.

In addition to international collaboration, interdisciplinary cooperation must be emphasized. It is fundamental to innovation. Only persons well routed in their differing scientific fields, knowing each other for one or another reason and willing to cooperate, know about the unexpected benefit of interdisciplinary cooperation.

Soon after I had come to Jülich, I visited directors of other institutes in order to find out, whether we, the nuclear physicists could help them. Prof. G. Stöcklin, director of the Institute for Nuclear Chemistry told me that he produced 123I bombarding isotopically separated Te with alpha beams. I asked him, whether he would not like to use the I(d, $6n$) reaction to produce ^{123}Xe, which is ideal to produce clean ^{123}I. Stöcklin did not know that the cross section was high and he was not aware of the fact that he could use a thick and inexpensive target. He tried and the result was a very high yield. Discussion with Prof. F. Führ, director of the Institute for Radio-Agronomy had the result that we provided his group with ^{28}Mg, an isotope necessary for the study of the grape-pedicel necrosis. Another example was, that a colleague from the University of Köln, Prof. J. Willenbrink, director of the Institute of Botanics, had a problem with the application of ^{11}C to plants. I proposed that his people should come to us and use one of our laboratories, where we had permission to work with open radioactivity. The advantage was, in addition, that he could avoid long transportation and thus make better use of the produced radioactivity. His work was very successful.

The application of ^{11}C on plants was also established in Prof. Führ's institute. It turned out that also these activities resulted in a very close cooperation with scientists from Japan. It started with a report about the allocation of photosynthates within living plants written by Fritz Führ and his co-worker Dr. Gerhand Roeb. The pamphlet was written in German and illustrated with numerous pictures. This was in 1987. This report was taken to Japan by a visitor, who passed it on to scientists of the Japan Atomic Energy Research Institute. At this time, scientists from the Department of Radiation Research for Environment and Resources were looking for new programs. They were fascinated by the idea of using short-lived isotopes to look into living plants. The leaflet with the less familiar language was translated into Japanese and seeded the idea for a large new investment within JAERI. It took some time before people in Jülich noticed this activity. In 1996 Dr. Schneewei from the Medical Institute of our Research Centre informed Dr. Tomoko Nakanishi from the Agricultural University of Tokyo, when she visited him here in Jülich. He introduced Gerhard Roeb to her and Gerhard showed her the equipment he was using to apply short lived isotopes to plants. At the end of a most interesting discussion Mrs. Nakanishi asked Gerhard about his interest in a cooperation with Japanese scientists and if he could imagine spending some time in Japan. With his reply "Yes", Gerhard did not envisage that this would be the starting point for an invitation to Japan. It was organized by the Japanese Foreign Researcher Inviting Program of JAERI. Only prepared with an audio-visual CD, illustrating life in Japan, Gerhard arrived in Takasaki in October 1996. At the Department of Radiation Research for Environment and Resources he found Dr. Kume and his post-doc S. Matsuhashi most helpful. Gerhard found it most enjoyable to work with them. Together they did some pioneer work on visualizing the carbon flow from shoot to the root within plants. During this time, Gerhard became familiar with the Positron Emitting Tracer Imaging System called PETIS, which was one of the most sophisticated imaging systems used in plant research, manufactured by Hamamatsu Photonics. Thanks to the cooperation between JAERI and scientists from the Agricultural University of Tokyo, Gerhard was invited to give a talk at the Tokyo University, where he met Tomoko Nakanishi again, the most friendly woman who had lined up his invitation. At the end of his two-months stay it was clear hat the scientific work should continue. Gerhard could inspire Norbert

Keutgen, also a former student of Prof. Führ, to go to JAERI. Norbert spent a very successful period of over a year there, which contributed to his post-doctoral qualification (Habilitation). Tamikazu Kume became leader of the Department of Ion-Beam applied Biology and Shinpei Matsuhashi the group leader of the Research group for Biological Function. The concept of PETIS remains to be implemented in Germany, but a more up to date version is currently being built in the new Institute of Photosphere with technical development by the Institute of Electronics of our Research Centre. The new approach, which is called "PlanTIS", will produce 3-dimensional pictures of the carbon flow within living plants.

Besides the success of his scientific work, Gerhard was deeply impressed by the kindness of the people in Japan, their curiosity and the way how gently they deal with visitors and with all things they get in contact with.

Initiated through the Atoms for Peace idea, scientific exchange and international cooperation developed between scientists, in particular between Japan and Germany, at first in the field of nuclear physics. Soon interdisciplinary activities emerged and led to successful international cooperation between Japan and Germany in the field of life sciences as well.

A Councils

A.1 Scientific Council

Prof. J.P. Blaizot	CEA Saclay, FR	
Prof. P. Braun-Munzinger	GSI Darmstadt, DE	Chairperson
Prof. D.F. Geesaman	Argonne National Laboratory, U.S.A.	
Prof. H. Halling	ZEL, FZ-Jülich, DE	
Prof. M. Harakeh	KVI Groningen, NL (Chairman PAC)	
Prof. D. von Harrach	Universität Mainz, DE	
Prof. E. Hilger	Universität Bonn, DE	
Prof. Y. Nagai	RCNP Osaka, JP	
Prof. A.W. Thomas	Thomas Jefferson National Lab, U.S.A.	
Dr. D. Trines	DESY Hamburg, DE	

A.2 Program Advisory Committee

Prof. H. Freiesleben	TU Dresden, DE	
Prof. B. Friman	GSI Darmstadt, DE	
Prof. M. Garçon	CEA Saclay, FR	
Prof. M.N. Harakeh	KVI Groningen, NL	Chairperson
Prof. T. Johansson	Uppsala Universitet, SE	
Prof. R. Landua	CERN, CH	
Prof. V. Metag	Universität Gießen, DE	
Prof. W. Meyer	Universität Bochum, DE	
Prof. W.T.H. van Oers	University of Manitoba, CA	
Prof. E. Oset	Universitat de Valencia, ES	
Prof. E. Radermacher	CERN, CH	
Prof. C. Schaerf	INFN Roma II, IT	

B Personnel

B.1 Scientific Staff

Msc. M.-M. Abdel-Bary (E1)

Dr. Abdel Samad (E1) (until 31 August, 2005)

DP S. An (GG)

Prof. Dr. G. Baur (TH) (a.o. Prof. Univ. Basel)

Dr. U. Bechstedt (GG)

Dr. K. Bongardt (GG)

DI N. Bongers (GG)

DI W. Borgs (E2)

DI W. Bräutigam (GG) (until 30 April, 2005)

DI R. Brings (GG)

Dr. habil. M. Büscher (E2) (PD Univ. Köln)

Dr. R. Castelijns (E1) (since 1 October, 2005)

DP A. Chechenin (GG) (since 24 October, 2005)

DP D. Chiladze (E2)

DP R. Czyzykiewicz (E1) (until 7 October, 2005)

Dr. habil. J. Dietrich (GG) (PD Univ. Dortmund)

Dr. A. Djalois (E1)

DP A. Dzyuba (E2)

Dr. R Eichhorn (GG)

Dr. R. Engels (E2)

DI F.-J. Etzkorn (GG)

M. Evers (TH) (since 1 March, 2005)

Dr. P. Fedorets (E2)

Dr. O. Felden (Rs)

D. Gamermann (TH) (until 31 March, 2005)

Dr. W. Gast (E1)

Dr. R. Gebel (GG)

Dr. habil. A. Gillitzer (E1) (PD Univ. Bonn)

Dr. habil. F.Goldenbaum (E1) (PD Univ. Wuppertal)

Dr. habil.D. Gotta (E2) (PD Univ. Köln)

Dr. F. Grümmer (TH)

Dr. D. Grzonka (E1)

DI W. Günther (GG) (since 15 September, 2005)

Dr. habil. J. Haidenbauer (TH) (PD Univ. Graz)

Dr. habil. C. Hanhart (TH) (PD Univ. Bonn)

Dr. M. Hartmann (E2)

Dr. V. Hejny (E2)

DI K. Henn (GG)

Dr. F. Hügging (E1) (since 1 September, 2005)

M. Janusz (E2) (since 1 December, 2005)

B. Jany (E2) (since 15 November, 2005)

Dr. V. Kamerdjiev (GG)

DP I. Keshelashvili (E2)

DP D. Kirillov (GG)

Prof. Dr. S. Krewald (TH) (apl. Prof. Univ. Bonn)

Th. Krings (Dt)

DI K. Kruck (GG)

Dr. A. Lehrach (GG)

DP V. Lensky (TH)

DP V. Leontyev (E2)

DP M. Lesiak (E1)

Dr. B. Lorentz (GG)

Prof. Dr. H. Machner (E1) (Prof. Univ. Duisburg-Essen)

Dr. Y. Maeda (E2)

Prof. Dr. R. Maier (GG) (Prof. Univ. Bonn)

Dr. S. Martin (GG)

DP E. Matveev (GG) (until 5 September, 2005)

Prof. Dr. U.-G. Meißner (TH) (Prof. Univ. Bonn)

DI I. Mohos (GG)

Dr. H.-P. Morsch (E1)

DP A. Mussgiller (E2) (until 30 November, 2005)

Dr. M. Nekipelov (E2)

Prof. Dr. N.N. Nikolaev (TH) (Prof. Moscow State Univ.)

Dr. A. Nogga (TH)

Dr. K. Nünighoff (E1) (until 14 September, 2005)

Prof. Dr. W. Oelert (E1) (apl. Prof. Univ Bochum)

Dr. H. Ohm (E2)

DI N. Paul (E1)

DP F. Pavlov (TH)

DP B. Piskor-Ignatowicz (E1)

DP L. Platter (TH) (until 30 April, 2005)

DP P. Podkopal (E2) (since 1 October 2005)

Dr. H. Polinder (TH)

Dr. D. Prasuhn (GG)

DP D. Protic (Dt)

Dr. habil. F. Rathmann (E2) (PD Univ. Erlangen)

Ch.F. Redmer (E1) (since 1 December, 2005)

DI A. Richert (GG)

Prof. Dr. J. Ritman (E1) (Prof. Univ. Bochum)

Dr. E. Roderburg (E1)

Dr. P. v. Rossen (GG)

DP T. Rozek (E1) (until 31 December, 2005)

DI J. Sarkadi (Ec)

DP P. Saviankou (TH)

Dr. H. Schaal (E1)

Dr. habil. S. Schadmand (E1)

Dr. R. Schleichert (E2)

Dr.-Ing. A. Schnase (GG)

DI H. Schneider (GG)

DI G. Schug (GG)

Dr. Th. Sefzick (Ec)

DI E. Senicheva (GG)

Dr. Y. Senichev (GG)

DI M. Simon (GG)

DP A. Sokolov (E1)

Dr. R. Stassen (GG)

Dr. H.-J. Stein (E2) (until 31 October, 2005)

Dr. H. Stockhorst (GG)

Dr. T. Stockmanns (E1)

DP Th. Strauch (E2) (until 14 October, 2005)

Prof. Dr. H. Ströher (E2) (Prof. Univ. Köln)

Dr. R. Tölle (GG)

M. Träger (E1) (from 15 March to 14 September, 2005)

DP A. Ucar (E1) (until 14 September, 2005)

DP Y. Valdau (E2)

DI T. Vashegyi (GG)

DP N. Vasiukhin (GG)

DP P. Vlasov (E1)

Dr. K.-H. Watzlawik (E2) (until 30 June, 2005)

D. Welsch (GG) (since 1 October, 2005)

DP P. Winter (E1) (until 30 September, 2005)

Dr. P. Wintz (E1)

Dr. habil. A. Wirzba (TH) (PD Univ. Bonn)

DI J.-D. Witt (GG)

Dr. M. Wolke (E2) (since 1 October, 2005)

L. Yurev (E2) (since 10 October, 2005)

Dr. E. Zaplatin (GG)

DP D. Z. Zhang (E1)

B.2 Technical and Administrative Staff

C. Berchem (Ec)

P. Birx (GG)

M. Böhnke (GG)

J. Borsch (Rs)

P. Brittner (GG)

J. But (Ws)

M. Comuth (Ad)

B. Dahmen (GG)

C. Deliege (GG)

W. Derissen (Cd)

N. Dolfus (Ec)

G. D'Orsaneo (E2)

R. Dosdall (E1)

R. Enge (GG)

B. Erkes (GG)

W. Ernst (Ec)

K. Esser (Ad)

H.-P. Faber (GG)

G. Fiori (Dt)

H.-W. Firmenich (Ws)

N. Gad (GG)

D. Gehsing (GG) († 16 November, 2005)

J. Göbbels (Rs)

H. Hadamek (Ws)

R. Hecker (GG)

E. Heßler (Cd)

M. Holona (Ws)

H.-M. Jäger (E1)

H. J. Jansen (Ws)

M. Karnadi (E2)

A. Kieven (GG)

M. Klöcker (GG) (from 1 March to 30 November, 2005)

K. Krafft (Rs)

Ch. Krahe (Ws)

M. Kremer (Ws)

G. Krol (GG)

M. Küven (Ws)

K.-G. Langenberg (GG)

G. Lürken (Ec) (until 28 February, 2005)

H. Metz (Dt)

S. Müller (Ad)

T. Naali (GG) (until 31 March, 2005)

R. Nellen (Ec)

St. Nießen (Dt) (since 1 November, 2005)

H. Pütz (GG)

G. Roes (Ad)

N. Rotert (GG)

D. Ruhrig (GG)

T. Sagefka (GG)

R. Schäfer (Cd) (until 31 December, 2005)

F. Scheiba (GG)

H. Schiffer (Ec)

J. Schmitz (GG)

F. Schultheiß (Ws)

K. Schwill (Dt)

H. Singer (GG)

D. Spölgen (E2)

G. Sterzenbach (E1)

J. Strehl (Ws)

R. Stumm (E1) (since 28 February, 2005)

J. Uehlemann (E1)

P. Wieder (E2)

Th. Willems (E2) (since 24 February, 2005)

J. Wimmer (E1)

H. Zens (GG)

Ad = Administraion
Cd = Construction
Dt = Detectors
E1 = IKP-1
E2 = IKP-2
Ec = Electronics
GG = Accelerator Division
Rs = Radiation Safety
TH = Theory
Ws = Workshop

C Research visitors

Research Visitors
(for one week to six months):

Dr. A. Avdeenkov (TH)
from 18 September to 17 December 2005
(IPPE Obinsk, Russia)

Dr. V. Balanutsa (E2)
from 14 March to 10 April 2005
from 24 October 4 December 2005
(ITEP, Moscow, Russia)

Dr. S. Barsov (E2)
from 7 January to 2 March 2005
from 15 May to 29 June 2005
from 18 September to 2 November 2005
from 23 November to 21 December 2005
(PNPI, Gatchina, Russia)

Dr. V. Baru (TH)
from 20 March to 16 May 2005
from 1 September to 30 November 2005
(ITEP, Moscow, Russia)

Dr. T. Batsch (E1)
from 16 April to 21 April 2005
(Soltan Inst., Otwock/Swierk, Polen)

A. Belov (GG)
from 10 October to 4 November 2005
(INR, Moskau)

Dr. K. Borasoy (TH)
from 1 May to 31 July 2006
(University of Bonn, Germany)

Dr. A. Boukharov (E2)
from 21 March to 10 April 2005
from 31 October to 4 December 2005
(MPEI, Moscow, Russia)

Dr. A. Chatterjee (E1)
from 14 April to 31 May 2005
(BARC, Mumbai, India)

Dr. V. Chernetsky (E2)
from 17 January to 13 February 2005
(ITEP, Moscow, Russia)

Dr. N. Chernov
from 13 April to 4 May 2005
(PNPI, Gatchina, Russia)

I. Ciepal (E1)
from 25 Januaray to 8 February 2005
(Jagellonian University, Cracow, Poland)

E. Czerwinski (E1)
from 21 October to 5 November 2005
(Jagellonian University, Cracow, Poland)

Dr. P. N. Deepak (TH)
from 1 October 2003 to 30 April 2005
(Mangalore University, Karnataka, India)
(scholarship holder of Alexander v. Humboldt Stiftung)

A. Demekhin (E2)
from 24 October to 4 December 2005
(ITEP, Moscow, Russia)

Dr. G. Devidze (TH)
from 28 October to 11 November 2005
(HEPITU, Tbilisi, Georgia)

A. Dudarev (E2)
from 24 January to 21 February 2005
(JINR, Dubna, Moscow, Russia)

Prof. Dr. J.W. Durso (TH)
from 1 August to 31 October 2005
(Mount Holyoke College, Hadley, MA, USA)

S. Dymov (E2)
from 20 May to 20 July 2005
from 10 November to 23 December 2005
(JINR, Dubna, Moscow, Russia)

Dr. Aida Galoyan (E1)
from 14 November to 13 December 2005
(JINR, Dubna, Russia)

A. Garishvili
from 1 June to 31 August 2005
(HEPITU, Tbilisi, Georgia)

Dr. A. Gasparian (TH)
from 1 November to 30 November 2005
(ITEP, Moscow, Russia)

Dr. A. Gerasimov (E2)
from 24 October to 4 December 2005
(ITEP, Moscow, Russia)

D. Gil (E1)
from 01 October to 8 October 2005
from 20 October to 29 October 2005
(Jagellonian University, Cracow, Poland)

Prof. V. Glagolev (E2)
from 14 to 21 February 2005
(JINR, Dubna, Moscow, Russia)

K. Grigoriev (E2)
from 1 January to 31 December 2005
(PNPI, Gatchina, Russia)

Dr. V. Goryachev (E2)
from 7 November to 4 December 2005
(ITEP, Moscow, Russia)

Dr. V. Grishina (E2)
from 19 July to 9 August 2005
from 19 September to 10 December 2005
(ITEP, Moscow, Russia)

D. Gusev (E2)
from 24 January to 21 February 2005
from 10 November to 8 December 2005
(JINR, Dubna, Moscow, Russia)

Dr. L. Gusev (E2)
from 17 January to 13 February 2005
from 31 October to 4 December 2005
(ITEP, Moscow, Russia)

Dr. P. Hawranek (E1)
from 25 January to 8 February 2005
from 3 May to 17 May 2005
from 15 September to 27 September 2005
(Jagellonian University, Cracow, Poland)

T. Htay (TH)
since 11 September 2005
(University of Mandalay, Myanmar)
(scholarship holder of Gottlieb Daimler- and Karl-Benz-Stiftung)

M. Janusz (E1)
from 27 January to 13 February 2005
from 21 April to 2 May 2005
from 14 July to 13 August 2005
from 27 September to 9 October 2005
from 21 October to 6 November 2005
from 6 November to 13 November 2005
(Jagellonian University, Cracow, Poland)

B. Jany (E2)
from 4 to 26 August 2005
(Jagellonian University, Cracow, Poland)

Prof. L. Jarczyk (E1)
from 14 April to 24 April 2005
(Jagellonian University, Cracow, Poland)

V. Jha (E1)
from 14 April to 31 May 2005
(BARC, Mumbai, India)

Y.-S. Kalashnikova (TH)
from 3 October to 11 November 2005
(ITEP, Moscow, Russia)

Prof. S. Kamerdzhiev (TH)
from 10 September to 9 December 2005
(IPPE, Obninsk, Russia)

Dr. A Katcharava (E2)
from 1 January to 31 December 2005
(JINR, Dubna, Moscow, Russia)

Dr. K. Khemchandani (E1)
from 1 July to 31 July 2005
(BARC, Mumbai, India)

Dr. D. Kirillov (E1)
from 3 May to 25 May 2005
from 5 September to 27 September 2005
(JINR, Dubna, Moscow, Russia)

Dr. Y. Kiselev (E2)
from 1 to 31 July 2005
from 1 to 8 October 2005
(ITEP, Moscow, Russia)

Dr. M. Kistryn (E1)
from 16 May to 13 June 2005
(Polish Academy of Sciences, Cracow, Poland)

P. Klaja (E1)
from 27 January to 13 February 2005
from 1 April to 3 May 2005
from 2 August to 30 August 2005
from 27 September to 9 October 2005
from 6 November to 13 November 2005
(Jagellonian University, Cracow, Poland)

Dr. St. Kliczewski (E1)
from 18 January to 10 February 2005
from 23 April to 24 May 2005
from 23 August to 30 September 2005
from 1 November to 23 December 2005
(University of Cracow, Poland)

Dr. L. Kochenda (E2)
from 6 to 20 February 2005
from 24 April to 15 May 2005
from 17 to 31 August 2005
(PNPI, Gatchina, Russia)

Prof. V. Komarov (E2)
from 12 to 27 March 2005
from 11 May to 12 June 2005
from 1 to 31 July 2005
from 21 November to 18 December 2005
(JINR, Dubna, Moscow, Russia)

Prof. L. Kondratyuk (E2+TH)
from 22 May to 11 June 2005
from 19 September to 10 December 2005
from 30 November to 21 December 2005
(ITEP, Moscow, Russia)

Prof. V. Koptev (E2)
from 2 March to 3 April 2005
from 5 June to 6 July 2005
from 18 September to 19 October 2005
(PNPI, Gatchina, Russia)

V. Kozlov (E1)
from 1 May to 13 May 2005
from 4 October to 16 December 2005
(Moscow State University, Russia)

Dr. M. Kravcikova (E1)
from 24 January to 8 February 2005
from 5 May to 23 May 2005
from 6 September to 20 September 2005
(TU Kosice, Slowakia)

Dr. P. Kravtsov
from 26 January to 2 March 2005
from 6 April to 11 May 2005
from 17 August to 5 September 2005
(PNPI, Gatchina, Russia)

Prof. G. Krein (TH)
from 30 November to 21 December 2005
(Universidade Estadual Paulista, Sao Paulo, Brasilia)

Prof. Dr. A. Kudryavtsev (TH)
from 1 September to 30 November 2005
(ITEP, Moscow, Russia)

Dr. P. Kulessa (E1)
from 19 April to 30 April 2005
from 22 September to 1 October 2005
(Jagellonian University, Cracow, Poland)

Dr. A. Kulikov (E2)
from 24 January to 21 February 2005
from 17 May to 7 June 2005
from 23 November to 7 December 2005
(JINR., Dubna, Moscow, Russia)

Dr. K. Kumar (TH)
from 10 May to 9 July 2005
(Mangalore University, Karnataka, India)

Dr. V. Kurbatov (E2)
from 17 March to 7 April 2005
from 10 November to 7 December 2005
(JINR, Dubna, Moscow, Russia)

Prof. D. Lee (TH)
from 20 June to 9 July 2005
(North Carolina State University, USA)

Prof. R. Lemmer (TH)
from 21 January to 12 February 2005
(Universität Witwatersrand, Johannesburg, South Africa)

Dr. R. Lewis (TH)
from 1 August to 31 August 2005
(University of Regina, Canada)

Prof. A. Liparteliani (TH)
from 15 July to 14 October 2005
(HEPITU, Tbilisi, Georgia)

Dr. N. Lyutorovich (TH)
from 11 September to 10 December 2005
(Petersburg State University, Russia)

Prof. Z. Ma (TH)
from 9 November to 8 December 2005
(China Instiute of Atomic Energy, Beijing, China)

Dr. G. Macharashvili (E2)
from 7 January to 27 February 2005
from 11 May to 12 June 2005
from 8 July to 7 August 2005
(JINR, Dubna, Moscow, Russia)

Dr. A. Magiera (E1+E2)
from 25 January to 6 February 2005
from 3 to 13 March 2005
from 5 May to 17 May 2005
(Jagellonian University, Cracow, Poland)

N. Maity (E1)
from 3 May to 15 July 2005
(Indian Inst. of Technology, Kharagpor, India)

Prof. G. Martinska (E1)
from 24 January to 8 February 2005
from 5 May to 23 May 2005
(University of Kosice, Slowakia)

Dr. S. Merzliakov (E2)
from 1 January to 31 December 2005
(JINR, Dubna, Moscow, Russia)

I. Meshkov (GG)
from 8 May to 16 May 2005
from 17 August to 31 August 2005
(JINR, Dubna, Moscow, Russia)

Dr. M. Mikirtytchiants (E2)
from 24 January to 6 March 2005
(PNPI, Gatchina, Russia)

Dr. S. Mikirtytchiants (E2)
from 7 January to 6 April 2005
(PNPI, Gatchina, Russia)

S. Mineev (E2)
from 14 March to 10 April 2005
(ITEP, Moscow, Russia)

Prof. P. Moskal (E1)
from 28 January to 27 February 2005
from 1 April to 30 April 2005
from 1 July to 31 August 2005
from 27 September to 10 October 2005
(Jagellonian University, Cracow, Poland)

Prof. Dr. K. Nakayama (TH)
from 17 May to 16 August 2005
(University of Georgia, Athens, USA)

Prof. H. Nann (E1)
from 24 January to 31 January 2005
(IUCF Bloomington, USA)

Dr. A. Nefediev (TH)
from 1 October to 15 November 2005
(ITEP, Moscow, Russia)

Prof. M. Nioradze (E2)
from 1 January to 24 January 2005
from 20 May to 2 June 2005
(HEPITU, Tbilisi, Georgia)

Dr. Y. Oh (TH)
from 18 July to 25 July 2005
(University of Georgia, Athens, USA)

S. Orfanitskiy (E1)
from 4 April to 15 June 2005
from 4 October to 16 December 2005
(Moscow State University, Russia)

A. Parfenov (GG)
from May 12 to May 19 2005
from August 17 to September 3 2005
(JINR, Dubna, Moscow, Russia)

T. Pietrzak (E1)
from 25 January to 8 February 2005
(Jagellonian University, Cracow, Poland)

DP C. Piskor-Ignatowicz (E1)
from 10 November to 30 November 2005
(Jagellonian University, Cracow, Poland)

Dr. N. Piskunov (E1)
from 24 January to 14 February 2005
from 2 May to 25 May 2005
from 5 September to 27 September 2005
(JINR, Dubna, Moscow, Russia)

Dr. S. Podchasky (E2)
from 14 March to 10 April 2005
from 24 October to 4 December 2005
(ITEP, Moscow, Russia)

DP J. Przerwa (E1)
from 1 April to 2 May 2005
from 27 September to 9 October 2005
from 26 October to 13 November 2005
(Jagellonian University, Cracow, Poland)

Dr. M. Puchala (E1)
from 24 May to 7 June 2005
(Jagellonian University, Cracow, Poland)

Dr. K. Pysz (E1+E2)
from 1 to 11 February 2005
from 17 May to 13 June 2005
(Jagellonian University, Cracow, Poland)

Dr. A. Rakhimov (TH)
from 30 November to 31 December 2005
(University of Tashkent, Uzbekistan)

Prof. K. Rashid (E2)
from 24 to 27 January 2005
from 5 to 12 July 2005
(Quaid-I-Azam University, Islamabad, Pakistan)

V. Reva (GG)
from 13 June to 2 July 2005
(BINP, Novosibirsk)

A. Rouba (E2)
from 15 March to 11 April 2005
from 12 to 17 December 2005
(Research Institute of Nuclear Problems, Minsk, Belarus)

N.Ya. Roukhlyada (GG)
from 20 June to 26 June 2005
(Obninsk Institute)

Dr. B. Roy (E1)
from 14 April to 31 May 2005
from 1 November to 10 November 2005
(BARC Mumbai, India)

R. Salmin (E1)
from 30 June to 24 July 2005
(JINR, Dubna, Moscow, Russia)

Dr. A. Semenov (E2)
from 21 March to 10 April 2005
from 31 October to 4 December 2005
(MPEI, Moscow, Russia)

Dr. V. Serdyuk (E2)
from 13 April to 31 December 2005
(JINR, Dubna, Moscow, Russia)

Y. Shatunov (GG)
from 21 May to 24 June 2005
(BINP, Novosibirsk)

A. Sidorin (GG)
from 28 March to 16 April 2005
from 17 August to 31 August 2005
(JINR, Dubna, Moscow, Russia)

M. Siemaszko (E1)
from 9 April to 21 April 2005
from 30 October to 6 November 2005
(University of Katowice, Poland)

A. Simon (E2)
from 4 to 19 August 2005
(Jagellonian University, Cracow, Poland)

Dr. I. Sitnik (E1)
from 27 January to 14 February 2005
from 3 May to 25 May 2005
from 8 September to 23 September 2005
(JINR, Dubna, Moscow, Russia)

A. Smirnov (GG)
from 31 January to 23 February 2005
from 17 August to 31 August 2005
(JINR, Dubna, Moscow, Russia)

Dr. J. Smyrski (E1)
from 24 April to 1 May 2005
from 3 July to 22 July 2005
from 7 September to 28 September 2005
(Jagellonian University, Cracow, Poland)

Dr. M. Tabidze (E2)
from 21 May to 2 June 2005
from 28 October to 27 December 2005
(HEPITU, Tbilisi, Georgia)

Dr. G. Tertychny (TH)
from 18 September to 17 December 2005
(IPPE, Obninsk, Russia)

Dr. V. Trofimov (E2)
from 26 January to 2 March 2005
from 6 April to 11 May 2005
from 31 July to 31 August 2005
(PNPI, Gatchina, Russia)

Dr. S. Trusov (E2)
from 1 January to 31 December 2005
(Moscow State University, Russia)

Dr. V. Tselyaev (TH)
from 18 September to 17 December 2005
(IPPE, Obninsk, Russia)

Dr. M. Ulicny (E1)
from 6 September to 27 September 2005
(University of Kosice, Slowakia)

Dr. J. Urban (E1)
from 23 January to 8 February 2005
from 5 May to 23 May 2005
from 6 September to 27 September 2005
(University of Kosice, Slowakia)

Dr. A. Usmani (TH)
from 1 December to 31 December 2005
(Aligarh Muslim University, Aligarh, India)

Dr. Y. Uzikov (E2)
from 26 January to 25 February 2005
from 23 August to 21 September 2005
from 24 December to 13 December 2005
(JINR, Dubna, Moscow, Russia)

Dr. A. Vassiliev (E2)
from 24 January to 6 March 2005
from 18 September t 4 October 2005
(PNPI, Gatchina, Russia)

M. Vedenev (GG)
from 13 June to 2 July 2005
(BINP, Novosibirsk)

Prof. M. Voloshin (TH)
from 1 May to 31 August 2005
(University of Minnesota, USA)
(scholarship holder of Alexander v. Humboldt Stiftung)

Prof. C. Wilkin (E2)
from 31 January to 9 February 2005
from 4 to 9 March 2005
from 11 to 18 June 2005
from 10 to 16 July 2005
from 28 September to 8 October 2005
from 8 to 15 December 2005
(University College London, U. K.)

Dr. M. Wojciechowski (E1)
from 21 May to 14 June 2005
(Jagellonian University, Cracow, Poland)

L. Yurev (E2)
from 17 to 31 May 2005
(JINR, Dubna, Moscow, Russia)

Dr. B. Zakharov (TH)
from 1 January to 2 March 2005
from 31 October to 31 December 2005
(Landau Inst. for Theor. Phys., Moscow, Russia)

Dr. W. Zipper (E1)
from 30 October to 6 November 2005
(University of Katowice, Poland)

Dr. V. R. Zoller (TH)
from 12 November to 31 December 2005
(ITEP, Moscow, Russia)

Dr. I. Zychor (E2)
from 10 to 30 April 2005
from 18 September to 10 December 2005
(The Andrzej Soltan Inst. for Nucl. Studies, Swierk-Otwock, Poland)

ITEP =	Institute for Theoretical and Experimental Physics, Moscow, Russia
PNPI =	St. Petersburg Nuclear Physics Institute, Gatchina, Russia
MPEI =	Moscow Power Engineering Institute, Moscow, Russia
HEPITU =	High Energy Physics Institute, Tbilisi State University, Tbilisi, Georgia
JINR =	Joint Inst. for Nuclear Research, Dubna, Moscow, Russia

D Publications 2005

1. Experiment

1. Abdel-Bary, M.; Budzanowski, A.; Chatterjee, A.; Ernst, J.; Hawranek, P.; Hinterberger, F.; Jha, V.; Kilian, K.; Kliczewski, S.; Kirillov, D.; Kolev, D.; Kravcikova, M.; Kutsarova, T.; Lesiak, M.; Lieb, J.; Machner, H.; Magiera, A.; Maier, R.; Martinska, G.; Nedev, S.; Niskanen, J.; Piskunov, N.; Prasuhn, D.; Protic, D.; von Rossen, P.; Roy, B. J.; Sitnik, I.; Siudak, R.; Smiechowicz, M.; Tsenov, R.; Ulicny, M.; Urban, J.; Vankova, G.; Wilkin, C.
Detailed comparison of the $pp \to \pi^+ pn$ and $pp \to \pi^+ d$ reactions at 951 MeV
Physics Letters B, **610** (2005), 31

2. Abdel-Bary, M.; Budzanowski, A.; Chatterjee, A.; Ernst, J.; Hawranek, P.; Jahn, R.; Jha, V.; Kilian, K.; Kliczewski, S.; Kirillow, D.; Kolev, D.; Kravcikova, M.; Kutsarova, T.; Lesiak, M.; Lieb, J.; Machner, H.; Magiera, A.; Maier, R.; Martinska, G.; Nedev, S.; Piskunov, N.; Prasuhn, D.; Protic, D.; von Rossen, P.; Roy, B. J.; Sitnik, I.; Siudak, R.; Smiechowicz, M.; Stein, H. J.; Tsenov, R.; Ulicny, M.; Urban, J.; Vankova, G.; Wilkin, C.
A precision determination of the mass of the η meson
Physics Letters B, **619** (2005), 281 – 287

3. Abdel-Bary, M.; Abdel-Samad, S.; Kilian, K.
2m heat pipe-cryogenic targets for COSY-TOF experiment
Nuclear Instruments and Methods in Physics Research Section A, **551** (2005), 236 – 244

4. Abdel-Bary, M.; Abdel-Samad, S.; Kilian, K.
A very light and thin liquid hydrogen/deuterium heat pipe target for COSY experiments
Cryogenics, **45** (2005), 489 – 495

5. Abdel-Bary, M.; Abdel-Samad, S.; Kilian, K.
Automatic control system for the COSY-TOF vacuum system
Nuclear Instruments and Methods in Physics Research Section A, **539** (2005), 93 – 99

6. Abdel-Bary, M.; Abdel-Samad, S.; Dolfus, N.; Kilian, K.; Sefzick, T.
Implosion monitor for vaccum systems
Nuclear Instruments and Methods in Physics Research Section A, **538** (2005), 154 – 158

7. Abdel-Samad, S.; Abdel-Bary, M.; Kilian, K.
Residual gas analysis in the TOF vacuum system
Vacuum, **78** (2005), 83 – 89

8. Abdel-Samad, S.; Abdel-Bary, M.; Kilian, K.; Ritman, J.
Deuterium heat pipes-crogenic targets for COSY experiments
Nuclear Instruments and Methods in Physics Research Section A, **550** (2005), 61 – 69

9. Adam, H. H.; Khoukaz, A.; Lang, N.; Lister, T.; Santo, R.; Steltenkamp, S.; Czyzykiewicz, R.; Janusz, M.; Jarczyk, L.; Kamys, B.; Moskal, P.; Piskor-Igantowicz, C.; Przerwa, J.; Smyrski, J.; Grzonka, D.; Kilian, K.; Oelert, W.; Sefzick, T.; Winter, P.; Wolke, M.; Wüstner, P.; Budzanowski, A.; Rozek, T.; Siemaszko, M.; Zipper, W.
New results on $pd \to {}^3\mathrm{He}\eta$ production from threshold up to $Q = 40$ MeV
International Journal of Modern Physics A, **20** (2005), 643

10. Ahrens, J.; Alexeev, V. M.; Annand, J. R. M.; Arends, H. J.; Beck, R.; Caselotti, G.; Cherepnya, S.N.; Drechsel, D.; Filkov, L.V.; Föhl, K.; Giller, I.; Grabmayr, P.; Hehl, T.; Hornidge, D.; Kashevarov, V.L.; Kotulla, M.; Krambrich, D.; Krusche, B.; Lang, M.; MacGeorge, J. C.; MacGregor, I. J. D.; Metag, V.; Moinester, M.; Novotny, R.; Pfeiffer, M.; Rost, M.; Schadmand, S.; Scherer, S.; Thomas, A.; Unkmeir, C.; Walcher, Th.
Measurement of the π^+ meson polarizabilities via the $\gamma p \to \gamma\pi^+ n$ reaction
European Physical Journal A, **23** (2005), 113

11. Altmeier, M.; Bauer, F.; Bisplinghoff, J.; Büßer, K.; Busch, M.; Colberg, T.; Demirörs, L.; Engelhardt, H. P.; Eversheim, P. D.; Eyser, K. O.; Felden, O.; Gebel, R.; Glende, M.; Greiff, J.; Hinterberger, F.; Jonas, E.; Krause, H.; Lindemann, T.; Lindlein, J.; Lorentz, B.; Maier, R.; Maschuw, R.; Meinerzhagen, A.; Prasuhn, D.; Rohdjeß, H.; Rosendaal, D.; von Rossen, P.; Schirm, N.; Schwarz, V.; Scobel, W.; Trelle, H. J.; Ulbrich, K.; Weise, E.; Wellinghausen, A.; Ziegler, R.
Excitation functions of the analyzing power in elastic proton-proton scattering from 0.45 to 2.5 GeV
European Physical Journal A, **23** (2005), 2, 351 – 364

12. Anagnostopoulos, D. F.; Biri, S.; Gotta, D.; Gruber, A.; Indelicato, P.; Leoni, B.; Fuhrmann, H.; Simons, L. M.; Stingelin, L.; Wasser, A.; Zmeskal, J.
On the characterization of a Bragg spectrometer with X-rays from an ECR source
Nuclear Instruments and Methods in Physics Research Section A, **545** (2005), 217

13. Bartholomy, O.; Crede, V.; Anisovich, A.; Anton, G.; Bantes, R.; Beloglazov, Y.A.; Bogendoerfer, R.; Ehmanns, A.; Ernst, J.; Fabry, I.; Flemming, H.; Fosel, A.; Freiesleben, H.; Fuchs, M.; Funke, C.; Gothe, R.; Gridnev, A.B.; Gutz, E.; Hoeffgen, S.; Horn, I.; Hossl, J.; Joosten, R.; Junkersfeld, J.; Kalinowsky, H.; Klein, F.; Klempt, E.; Koch, H.; Konrad, M.; Kopf, B.; Krusche, B.; Langheinrich, J.; Loehner, H.; Lopatin, I.V.; Lotz, J.; Matthay, G. G.; Menze, D.; Messchendorp, J. G.; Morales, C.; Novinski, D.; Ostrick, M.; van Pee, H.; Radkov, J. O.; Reinnarth, J.; Sarantsev, A.; Schadmand, S.; Schmidt, C.; Schmieden, H.; Schoch, B.; Suft, G.; Sumachev, V.V.; Szczepanek, T.; Thoma, U.; Walther, D.; Weinheimer, Ch.
Neutral-pion photoproduction off protons in the energy range 0.3 GeV $< E_\gamma <$ 3 GeV
Physical Review Letters, **94** (2005), 012003

14. Bauer, F.; Bisplinghoff, J.; Büsser, K.; Busch, M.; Colberg, T.; Dahl, C.; Demirörs, L.; Eversheim, P. D.; Eyser, K. O.; Felden, O.; Gebel, R.; Greiff, J.; Hinterberger, F.; Jonas, E.; Krause, H.; Lehmann, C.; Lindlein, J.; Maier, R.; Meinerzhagen, A.; Pauly, C.; Prasuhn, D.; Rohdjess, H.; Rosendaal, D.; Rossen, P.; Schirm, N; Scobel, W.; Ulbrich, K.; Weise, E.; Wolf, T.; Ziegler, R.
Excitation functions of spin correlation parameters ANN, ASS, and ASL in elastic $\vec{p}\vec{p}$ scattering between 0.45 and 2.5 GeV
Physical Review C, **71** (2005), 054002

15. Brinkmann, K.; Abdel-Bary, M.; Abdel-Samad, S.; Clement, H.; Doroshkevich, E.; Dshemuchadse, S.; Dutz, H.; Ehrhardt, K.; Erhardt, A.; Eyrich, W.; Filippi, A.; Freiesleben, H.; Fritsch, M.; Georgi, J.; Gillitzer, C. G.; Gonser, M. A.; Jäkel, R.; Karsch, L.; Kilian, K.; Koch, H.; Kreß, J.; Kuhlmann, E.; Marcello, S.; Meyer, W.; Michel, P.; Morsch, H. P.; Möller, K.; Mörtel, H.; Naumann, L.; Pinna, L.; Pizzolotto, L.; Roderburg, E.; Schamlott, A.; Schönmeier, P.; Schröder, W.; Schulter-Wissermann, M.; Sefzick, T.; Steinke, M.; Stinzing, F.; Sun, G. Y.; Ucar, A.; Ullrich, W.; Wagner, G. J.; Wagner, M.; Wilms, A.; Wintz, P.; Wirth, S.; Wüstner, P.; Zupranski, P.
Vector Meson Production in Collisions of Nucleons
International Journal of Modern Physics A, **20** (2005), 427

16. Büscher, M.
Strangeness Production at COSY
Nuclear Physics A, **754** (2005) , 231c – 242c

17. Crede, V.; Bartholomy, O.; Anisovich, A.; Anton, G.; Bantes, R.; Beloglazov, Y.A.; Bogendoerfer, R.; Ehmanns, A.; Ernst, J.; Fabry, I.; Flemming, H.; Fosel, A.; Freiesleben, H.; Fuchs, M.; Funke, C.; Gothe, R.; Gridnev, A.B.; Gutz, E.; Hoeffgen, S.; Horn, I.; Hossl, J.; Joosten, R.; Junkersfeld, J.; Kalinowsky, H.; Klein, F.; Klempt, E.; Koch, H.; Konrad, M.; Kopf, B.; Krusche, B.; Langheinrich, J.; Loehner, H.; Lopatin, I.V.; Lotz, J.; Matthay, G. G.; Menze, D.; Messchendorp, J. G.; Morales, C.; Novinski, D.; Ostrick, M.; van Pee, H.; Radkov, J. O.; Reinnarth, J.; Sarantsev, A.; Schadmand, S.; Schmidt, C.; Schmieden, H.; Schoch, B.; Suft, G.; Sumachev, V.V.; Szczepanek, T.; Thoma, U.; Walther, D.; Weinheimer, Ch.
Photoproduction of η mesons off protons for 0.75 GeV $< E_\gamma <$ 3 GeV
Physical Review Letters, **94** (2005), 012004

18. Czyzykiewicz, R.; Adam, H. H.; Budzanowski, A.; Grzonka, D.; Janusz, M.; Jarczyk, L.; Kamys, B.; Khoukaz, A.; Kilian, K.; Klaja, P.; Kowina, P.; Moskal, P.; Oelert, W.; Piskor-Igantowicz, C.; Przerwa, J.; Rozek, T.; Santo, R.; Sefzick, T.; Siemaszko, M.; Smyrski, J.; Täschner, A.; Winter, P.; Wolke, M.; Wüstner, P.; Zipper, W.
Production of η meson in proton-proton collisions
International Journal of Modern Physics A, **20** (2005), 708

19. Engels, R.; Emmerich, R.; Grigoryev, K.; Paetz gen. Schieck, H.; Ley, J.; Mikirtytchiants, M.; Rathmann, F.; Sarkadi, J.; Seyfarth, H.; Tenckhoff, G.; Vasilyev, A. Background reduction by a getter pump around the ionization volume of a
Lamb-shift polarimeter and possible improvements of polarized ion sources
Review of Scientific Instruments, **76** (2005), 053305

20. Engels, R.; Emmerich, R.; Ley, J.; Paetz gen. Schieck, H.; Mikirtytchiants, M.; Rathmann, F.; Sarkadi, J.; Seyfarth, H.; Ullrich, T.; Vassiliev, A.
Nuclear Polarization Measurement of H/D Atoms Extracted from a Storage Cell with a Lamb-shift Polarimeter
Nuclear Instruments and Methods in Physics Research Section A, **536** (2005), 3, 334 – 337

21. Eyrich, W.; Brinkmann, K.; Abdel-Bary, M.; Abdel-Samad, S.; Clement, H.; Doroshkevich, E.; Dshemuchadse, S.; Dutz, H.; Ehrhardt, K.; Erhardt, A.; Filippi, A.; Freiesleben, H.; Fritsch, M.; Georgi, J.; Gillitzer, C. G.; Gonser, M. A.; Jäkel, R.; Karsch, L.; Kilian, K.; Koch, H.; Kreß, J.; Kuhlmann, E.; Marcello, S.; Meyer, W.; Michel, P.; Morsch, H. P.; Möller, K.; Mörtel, H.; Naumann, L.; Pinna, L.; Pizzolotto, L.; Roderburg, E.; Schamlott, A.; Schönmeier, P.; Schröder, W.; Schulter-Wissermann, M.; Sefzick, T.; Steinke, M.; Stinzing, F.; Sun, G. Y.; Ucar, A.; Ullrich, W.; Wagner, G. J.; Wagner, M.; Wilms, A.; Wintz, P.; Wirth, S.; Wüstner, P.; Zupranski, P.
COSY-TOF Research on Θ^+
Acta Physica Polonica B, **36** (2005), 2189

22. Gillitzer, C. G.; Grzonka, D.
Strangeness Physics with the WASA Detector at COSY
International Journal of Modern Physics A, **20** (2005), 539

23. Hartmann, M.; Maeda, Y.; Keshelashvilli, I.; Koch, H. R.; Mikirtichyants, S.; Barsov, S.; Borgs, W.; Büscher, M.; Hejny, V.; Kleber, V.; Koptev, V.; Kulessa, P.; Mersmann, T.; Mussgiller, A.; Ohm, H.; Pysz, K.; Schleichert, R.; Stein, H. J.; Ströher, H.; Watzlawik, K.-H.; Wüstner, P.
ϕ-meson production in pp collisions close to threshold
Nuclear Physics A, **755** (2005), 459 – 462

24. Hinterberger, F.; Nedev, S.N.; Siudak, R.
The final state interaction in the reactions $pp \to K(\Lambda p)$ and $pp \to \pi(np)$
International Journal of Modern Physics A, **20** (2005), 291

25. Machner, H.
Physics at COSY
International Journal of Modern Physics A, **20** (2005), 1582

26. Morsch, H. P.; Zupranski, P.
Structure of the breathing mode of the nucleon from high-energy p-p scattering
Physical Review C, **71** (2005), 065203

27. Moskal, P.; Adam, H. H.; Budzanowski, A.; Czyzykiewicz, R.; Grzonka, D.; Janusz, M.; Jarczyk, L.; Kamys, B.; Khoukaz, A.; Kilian, K.; Klaja, P.; Majewski, J.; Oelert, W.; Piskor-Igantowicz, C.; Przerwa, J.; Rozek, T.; Sefzick, T.; Siemaszko, M.; Smyrski, J.; Täschner, A.; Winter, P.; Wolke, M.; Wüstner, P.; Zipper, W.
Hadronic interaction on the η meson with two nucleons
International Journal of Modern Physics A, **20** (2005), 1880

28. Oelert, W.
Observation of Cold Antihydrogen
Nuclear Physics A, **752** (2005), 77c – 86c

29. Przerwa, J.; Adam, H. H.; Budzanowski, A.; Czyzykiewicz, R.; Grzonka, D.; Janusz, M.; Jarczyk, L.; Kamys, B.; Khoukaz, A.; Kilian, K.; Klaja, P.; Lang, N.; Moskal, P.; Oelert, W.; Piskor-Ignatowicz, C.; Rozek, T.; Santo, R.; Sefzick, T.; Siemaszko, M.; Smyrsik, J.; Täschner, A.; Winter, P.; Wolke, M.; Wüstner, P.; Zipper, W.
Search for bremsstrahlung radiation in quasi-free $np \to np\gamma$ reaction
International Journal of Modern Physics A, **20** (2005), 625

30. Rathmann, F.; Lenisa, P.; Steffens, E.; Contalbrigo, M.; Dalpiaz, P. F.; Kacharava, A.; Lehrach, A.; Lorentz, B.; Maier, R.; Prasuhn, D.; Ströher, H.
A Method to Polarize Stored Antiprotons to a High Degree
Physical Review Letters, **94** (2005), 1, 014801

31. Ritman, J.
The PANDA detector at the GSI-FAIR project
International Journal of Modern Physics A, **20** (2005), 567 – 569

32. Ritman, J.
Experiments with the WASA detector at COSY
International Journal of Modern Physics A, **20** (2005), 525 – 531

33. Rozek, T.; Grzonka, D.; Kilian, K.; Kowina, P.; Oelert, W.; Sefzick, T.; Winter, P.; Wolke, M.; Wüstner, P.; Siemaszko, M.; Zipper, W.; Czyzykiewicz, R.; Janusz, M.; Jarczyk, L.; Kamys, B.; Klaja, P.; Moskal, P.; Piskor-Igantowicz, C.; Przerwa, J.; Smyrski, J.; Adam, H. H.; Budzanowski, A.; Khoukaz, A.; Santo, R.; Siemaszko, M.; Täschner, A.
Threshold hyperon production at COSY-11
International Journal of Modern Physics A, **20** (2005), 680

34. Schadmand, S.
Experimental review of baryons in the nuclear medium
Nuclear Physics A, **755** (2005), 188c

35. Smyrski, J.; Kolf, Ch.; Adam, H.-H.; Budzanowski, A.; Czyzcykiewicz, R.; Grzonka, D.; Heczko, A.; Janusz, M.; Jarcyk, L.; Kamys, B.; Khoukaz, A.; Kilian, K.; Kowina, P.; Misiak, A.; Moskal, P.; Oelert, W.; Piskor-Ignatowicz, C.; Przerwa, J.; Quentmeier, C.; Rozek, T.; Santo, R.; Schepers, G.; Sefzick, T.; Siemaszko, M.; Täschner, A.; Winter, P.; Wolke, M.; Wüstner, P.; Zipper, W.
Drift chamber with a c-shaped frame
Nuclear Instruments and Methods in Physics Research Section A, **541** (2005), 3, 574 – 582

36. Tishchenko, V.; Herbach, C. M.; Hilscher, D.; Jahnke, U.; Galin, J.; Goldenbaum, F.; Letourneau, A.; Schröder, U.
Fast decision in favor of the slow fission process
Physical Review Letters, **95** (2005), 162701

37. Trnka, D.; Anton, G.; Bacelar, J. C. S.; Bartholomy, O.; Bayadilov, D.; Beloglazov, Y.A.; Bogendoerfer, R.; Castelijns, R.; Crede, V.; Dutz, H.; Ehmanns, A.; Elsner, D.; Ewald, R.; Fabry, I.; Fuchs, M.; Essig, K.; Funke, R. J.; Gothe, R.; Gregor, R.; Gridnev, A.B.; Gutz, E.; Hoeffgen, S.; Hoffmeister, P.; Horn, I.; Hoessl, J.; Jaegle, I.; Junkersfeld, J.; Kalinowsky, H.; Klein, F.; Klein, F.; Klempt, E.; Konrad, M.; Kopf, B.; Kotulla, M.; Krusche, B.; Langheinrich, J.; Loehner, H.; Lopatin, I.V.; Lotz, J.; Lugert, S.; Menze, D.; Messchendorp, J. G.; Mertens, T.; Metag, V.; Morales, C.; Nanova, M.; Novotny, R.; Ostrick, M.; Pant, L.M.; van Pee, H.; Pfeiffer, M.; Roy, A.; Radkov, J. O.; Schadmand, S.; Schmidt, Ch.; Schmieden, H.; Schoch, B.; Shende, S.; Suft, G.; Sumachev, V.V.; Szczepanek, T.; Suele, A.; Thoma, U.; Varma, R.; Walther, D.; Weinheimer, Ch.; Wendel, Ch.
Observation of In-Medium Modifications of the ω Meson
Physical Review Letters, **94** (2005), 192303

38. Wronska, A.; et al.
Near threshold η meson production in the $dd \rightarrow {}^4\mathrm{He}\eta$ reaction near threshold
European Physics Journal A, **26** (2005) 421

39. Wronska, A.; Hejny, V.
Near threshold η-meson production in $dd \rightarrow {}^4\mathrm{He}\eta$
International Journal of Modern Physics A, **20** (2005), 2/3, 640 – 642

40. Yahlalia, N.; Diaz, J.; Aphecetche, L.; d'Enterria, D.G.; van Goethem, M. J.; Hoefman, M.; Kugler, A.; Loehner, H.; Martinez, G.; Ostendorf, R. W.; Schadmand, S.; Schutz, Y.; Turrisi, R.; Wagner, W.; Wilschut, H. W.
Deep subthreshold π^0 production in ^{36}Ar + ^{197}Au collisions
Nuclear Physics A, **749** (2005), 190

41. Yahlalia, N.; Daz, J.; Aphecetche, L.; d'Enterria, D.G.; van Goethem, M. J.; Hoefman, M.; Kugler, A.; Loehner, H.; Martnez, G.; Ostendorf, R. W.; Schadmand, S.; Schutz, Y.; Turrisi, R.; Wagner, W.; Wilschut, H. W.
Transverse momentum distributions of neutral pions produced at deep subthreshold energies
International Journal of Modern Physics A, **20** (2005), 609

42. Yaschenko, S.; Dymov, S.; Kacharava, A.; Komarov, V.; Macharashvili, G.; Rathmann, F.; Barsov, S.; Gebel, R.; Hartmann, M.; Khoukaz, A.; Kulessa, P.; Kulikov, A.; Kurbatov, V.; Lang, N.; Lehmann, I.; Lorentz, B.; Mersmann, T.; Merzliakov, S.; Mikirtytchiants, S.; Mussgiller, A.; Nioradze, M.; Ohm, H.; Prasuhn, D.; Schleichert, R.; Seyfarth, H.; Steffens, E.; Stein, H. J.; Ströher, H.; Uzikov, Yu.; Zalikhanov, B.; Zhuravlev, N.
Measurement of the Analyzing Power in Polarised $pd \to (pp)n$ with a Fast Forward Diproton
Physical Review Letters, **94** (2005), 072304

43. Zychor, I.; Koptev, V.; Büscher, M.; Dzyuba, A.; Keshelashvilic, I.; Kleber, V.; Koch, R.; Krewald, S.; Maeda, Y.; Mikirtichyants, S.; Nekipelov, M.; Ströher, H.; Wilkin, C.
Indication of an excited hyperon state in pp collisions with ANKE at COSY-Jülich
Nuclear Physics A, **755** (2005), 403

2. Theory

44. Achenbach, P.; Baumann, D.; Böhm, R.; Boillat, B.; Bosnar, D.; Carasco, C.; Ding, M.; Distler, M. O.; Friedrich, J.; Glöckle, W.; Golak, J.; Goussev, Y.; Grabmayr, P.; Heil, W.; Hügli, A.; Jennewein, P.; Jover Manas, J. L.; Jourdan, P. O.; Kamada, H.; Klechneva, T.; Krusche, B.; Krygier, K. W.; Llongo, J.G.; Lloyd, M.; Makek, M.; Merkel, H.; Micheli, C.; Müller, U.; Nogga, A.; Neuhausen, R.; Normand, Ch.; Nungesser, L.; Ott, A.; Otten, E.; Parpan, F.; Perez Benito, R.; Potokar, O. P.; Rohe, D.; Rudersdorf, D.; Schmiedeskamp, J.; Seimetz, M.; Sick, I.; Sirca, S.; Skibinski, R.; Stave, S.; Testa, G.; Trojer, R.; Walcher, Th.; Weis, M.; Witala, H.; Wöhrle, H.
Measurement of the asymmetries in ^{3}H$e(e,e'p)d$ and ^{3}H$e(e,ep)np$
European Physical Journal A, **25** (2005), 177

Bartos, E.; Gevorkyan, S. R.; Kuraev, E. A.; Nikolaev, N. N.
Multiple exchanges in lepton pair production in high-energy heavy ion collisions
Journal of Experimental and Theoretical Physics, **100** (2005), 645

45. Baru, V.; Haidenbauer, J.; Hanhart, C.; Kudryavtsev, A.; Meißner, U. G.
Flatté-like distributions and the $a_0(980)/f_0(980)$ mesons
European Physical Journal A, **23** (2005), 523 – 533

46. Bernard, V.; Hemmert, T. R.; Meißner, U. G.
Chiral extrapolations and the covariant small scale expansion
Physics Letters B, **622** (2005), 141 – 150

47. Bernard, V.; Kubis, B.; Meißner, U. G.
The Fubini-Furlan-Rosetti sum rule and related aspects in light of covariant baryon chiral perturbation theory
European Physical Journal A, **25** (2005), 419 – 425

48. Bogner, S.K.; Schwenk, A.; Furnstahl, R.J.; Nogga, A.
Is nuclear matter perturbative with low-momentum interactions?
Nuclear Physics A, **763** (2005), 59

49. Borasoy, B.; Bruns, P.C.; Meißner, U. G.; Nißler, R.
Gauge invariance in two-particle scattering
Physical Review C, **72** (2005), 065201

50. Bruns, P.C.; Meißner, U. G.
Infrared regularization for spin-1 fields
European Physical Journal C, **40** (2005), 97 – 119

51. Bulgac, A.; Magierski, P.; Wirzba, A.
Fermionic Casimir Effect in Case of Andreev Reflection
Europhysics Letters, **72** (2005), 3, 327 – 333

52. Deepak, P.N.; Haidenbauer, J.; Hanhart, C.
Partial-wave analysis of $pp \to pp\pi^0$ data
Physical Review C, **72** (2005), 024004

53. Deepak, P.N.; Hanhart, C.; Ramachandran, G.; Vidya, M.S.
Spin-dependence of meson production in NN collisions
International Journal of Modern Physics A, **20** (2005), 599 – 601

54. Epelbaum, E.; Glöckle, W.; Meißner, U. G.
The two-nucleon system at next-to-next-to-next-to-leading order
Nuclear Physics A, **747** (2005), 362 – 424

55. Epelbaum, E.; Meißner, U. G.
Isospin-violating nucleon-nucleon forces using the method of unitary transformation
Physical Review C, **72** (2005), 044001

56. Epelbaum, E.; Meißner, U. G.; Palomar, J. E.
Isospin dependence of the three-nucleon force
Physical Review C, **71** (2005), 024001

57. Frink, M.; Meißner, U. G.; Scheller, I.
Baryon masses, chiral extrapolations, and all that
European Physical Journal A, **24** (2005), 395 – 409

58. Gasparyan, A.; Haidenbauer, J.; Hanhart, C.
Extraction of scattering lengths from final-state interactions
Physical Review C, **72** (2005), 034006

59. Golak, J.; Skibinski, R.; Wita la, H.; Glöckle, W.; Nogga, A.; Kamada, H.
Electron and photon scattering on three-nucleon bound states
Physics Reports, **415** (2005), 89

60. Golak, J.; Skibinski, R.; Witala, H.; Glöckle, W.; Nogga, A.; Kamada, H.
Proton polarizations in polarized ^{3}H*e* studied with the ^{3}H$e(e,e'p)d$ and ^{3}H$e(e,e\prime p)pn$ processes
Physical Review C, **72** (2005), 054005

61. Grishina, V. Yu.; Kondratyuk, L. A.; Sibirtsev, A.; Büscher, M.; Krewald, S.; Meißner, U.-G.; Sassen, F. P.
The K^- scattering length and the reaction $dd \to \alpha K^- K^+$
European Physical Journal A, **25** (2005), 159 – 164

62. Haidenbauer, J.; Meißner, U. G.
Jülich hyperon nucleon model revisited
Physical Review C, **72** (2005), 044005

63. Hanhart, C.; Haidenbauer, J.; Nakayama, K.; Meißner, U. G.
On the determination of the parity of the Θ^+
Physics Letters B, **606** (2005), 67 – 76

64. Hanhart, C.
Isospin breaking in hadronic reactions
International Journal of Modern Physics A, **20** (2005), 543 – 545

65. Hyun, C.H.; Lee, S.J.; Haidenbauer, J.; Hong, S.W.
Parity-nonconserving observables in thermal neutron capture on a proton
European Physical Journal A, **24** (2005), 129 – 135

66. Kalashnikova, Yu.S.; Kudryavtsev, A. E.; Nefediev, A.V.; Hanhart, C.; Haidenbauer, J.
The radiative decays $\phi \to \gamma a_0/f_0$ in the molecular model for the scalar mesons
European Physical Journal A, **24** (2005), 437 – 443

67. Kistryn, St.; Stephan, E.; Biegun, A.; Bodek, K.; Deltuva, A.; Epelbaum, E.; Ermisch, K.; Glöckle, W.; Golak, J.; Kalantar-Nayestanaki, N.; Kamada, H.; Kis, M.; Klos, B.; Kozela, A.; Kuros-Zolnierczuk, J.; Mahjour-Shafiei, M.; Meißner, U. G.; Micherdzinska, A.; Nogga, A.; Sauer, P.U.; Skibinski, R.; Sworst, R.; Witala, H.; Zejma, J.; Zipper, W.
Systematic study of three-nucleon force effects in the cross section of the deuteron-proton breakup at 130 MeV
Physical Review C, **72** (2005), 044006

68. Krebs, H.; Bernard, V.; Meißner, U. G.
Orthonormalization procedure for chiral effective nuclear field theory
Annals of Physics, **316** (2005), 160 – 186

69. Krewald, S.; Schneider, S.; Meißner, U. G.
Two-pion production in the pion-nucleon reaction
International Journal of Modern Physics A, **20** (2005), 590 – 592

70. Krewald, S.; Schneider, S.; Sibirtsev, A.; Haidenbauer, J.; Meißner, U.-G.
Decay of baryon resonances
International Journal of Modern Physics A, **20** (2005), 1662 – 1667

71. Lensky, V.; Baru, V.; Haidenbauer, J.; Hanhart, C.; Kudryavtsev, A. E.; Meißner, U. G.
Precision calculation of $\gamma d \to \pi nn$ within chiral perturbation theory
European Physical Journal A, **26** (2005), 107 – 123

72. Meißner, U. G.; Raha, U.; Rusetsky, A.
The pion-nucleon scattering lengths from pionic deuterium
European Physical Journal C, **41** (2005), 213 – 232

73. Meißner, U. G.
Challenges in hadron physics
International Journal of Modern Physics A, **20** (2005), 514 – 524

74. Nikolaev, N. N.; Schäfer, W.
Breaking of K^+ factorization for single jet production off nuclei
Physical Review D, **71** (2005), 014023

75. Nikolaev, N. N.; Schäfer, W.; Zakharov, B. G.
Nonuniversality aspects of nonlinear $k(T)$-factorization for hard dijets
Physical Review Letters, **95** (2005), 221803

76. Nikolaev, N. N.; Schäfer, W.; Zakharov, B. G.; Zoller, V. R.
Why breakup of photons and pions into forward dijets is so different: Predictions from nonlinear nuclear $k(T)$-factorization
Physics of Atomic Nuclei, **68** (2005), 661

77. Nikolaev, N. N.; Schäfer, W.; Zakharov, B. G.; Zoller, V. R.
Nonlinear $k(T)$-factorization: A new paradigm for hard QCD processes in a nuclear environment
JETP Letters, **82** (2005), 364

78. Niskanen, J. A.; Sibirtsev, A.; Haidenbauer, J.; Hanhart, C.
η-nuclear scattering parameters
International Journal of Modern Physics A, **20** (2005), 634 – 636

79. Nogga, A.; Timmermans, R.G.E.; van Kolck, U.
Renormalization of One-Pion Exchange and Power Counting
Physical Review C, **72** (2005), 054006

80. Platter, L.; Hammer, H. W.; Meißner, U. G.
On the correlation between the binding energies of the triton and the α-particle
Physics Letters B, **607** (2005), 254 – 258

81. Polinder, H.; Rijken, Th.
Soft-core meson-baryon interactions. I. One-hadron-exchange potentials
Physical Review C, **72** (2005), 065210

82. Polinder, H.; Rijken, Th.
Soft-core meson-baryon interactions. II. πN and K^+N scattering
Physical Review C, **72** (2005), 065211

83. Sassen, F.; Krewald, S.
An Investigation of the $D_s^+\pi^0 - -DK - D_s^+\eta$ coupled channel dynamics
International Journal of Modern Physics A, **20** (2005), 705 – 707

84. Sekiguchi, K.; Sakai, H.; Witala, H.; Glöckle, W.; Golak, J.; Hatanaka, K.; Hatano, M.; Itoh, K.; Kamada, H.; Kuboki, H.; Maeda, Y.; Nogga, A.; Okamura, H.; Saito, T.; Sakamoto, N.; Sakemi, Y.; Sasano, M.; Shimizu, Y.; Suda, K.; Tamii, A.; Uesaka, T.; Wakasa, T.; Yako, K.
Resolving the Discrepancy of 135 MeV pd Elastic Scattering Cross Sections and Relativistic Effects
Physical Review Letters, **95** (2005), 162301

85. Sibirtsev, A.; Haidenbauer, J.; Krewald, S.; Meißner, U. G.
Analysis of Θ^+ production in K^+Xe collisions
European Physical Journal A, **23** (2005), 491 – 499

86. Sibirtsev, A.; Haidenbauer, J.; Krewald, S.; Meißner, U. G.; Thomas, A. W.
Near threshold enhancement of the $p\bar{p}$ mass spectrum in J/Ψ decay
Physical Review D, **71** (2005), 054010

87. Sibirtsev, A.; Meißner, U. G.; Thomas, A. W.
Okubo-Zweig-Iizuka rule violation in photoproduction
Physical Review D, **71** (2005), 094011

88. Skibinski, R.; Golak, J.; Witala, H.; Glöckle, W.; Nogga, A.
Different formulations of ^{3}He and ^{3}H photodisintegration
European Physical Journal A, **24** (2005), 31

89. Skibinski, R.; Golak, J.; Witala, H.; Glöckle, W.; Nogga, A.; Kamada, H.
Polarization observables in the semi-exclusive photoinduced three-body breakup of ^{3}He
Physical Review C, **72** (2005), 044002

90. Typel, S.; Baur, G.
Electromagnetic strength of neutron and proton single-particle nuclei
Nuclear Physics A, **759** (2005), 247 – 308

91. Vary, J.P.; Atramentov, O. V.; Barrett, B.R.; Hasan, M.; Hayes, A.C.; Lloyd, R.; Mazur, A.I.; Navratil, P.; Negoita, A.G.; Nogga, A.; Ormand, W.E.; Popescu, S.; Shehadeh, B.; Shirokov, A.M.; Spence, J.R.; Stetcu, I.; Stoica, S.; Weber, T.A.; Zaytsev, S.A.
Ab initio No-Core Shell Model — Recent results and future prospects
European Physical Journal A, **25** (2005), Suppl. 1, 475 – 480

92. Wirzba, A.; Sondergaard, N.; Cvitanovic, P
Wave Chaos in Elastodynamic Cavity Scattering
Europhysics Letters, **72** (2005), 4, 534 – 540

93. Yakhshiev, U. T.; Meißner, U. G.; Wirzba, A.; Rakhimov, A. M.; Musakhanov, M. M.
Nucleon-Nucleon Potential in Finite Nuclei
Physical Review C, **71** (2005), 034007

3. Accelerator

94. Lehrach, A.
Polarized Beam Acceleration in COSY and Future Options for Polarization at HESR
ICFA Beam Dynamics Newsletters, **37** (2005), S. 80 – 88

95. Morozov, V. S.; Krisch, A. D.; Leonova, M. A.; Raymond, R. S.; Sivers, D. W.; Wong, V. K.; Gebel, R.; Lehrach, A.; Lorentz, B.; Maier, R.; Prasuhn, D.; Schnase, A.; Stockhorst, H.; Eversheim, D.; Hinterberger, F.; Rohdjes, H.; Ulbrich, K.; Yonehara, K.
Spin manipulating stored 1.85 GeV/c vector and tensor polarized spin-1 bosons
Physical Review Special Topics, Accelerators and Beams, **8** (2005), 061001

96. Schnase, A.; Nomura, M.; Tamura, F.; Yamamoto, M.; Anami, S.; Ezura, E.; Hara, K.; Ohmori, C.; Takagi, A.; Yoshii, M.
Cascaded integrator comb filters with smoothly varying coefficients for reduced delay in synchrotron feedback loops
Physical Review Special Topics, Accelerators and Beams, **8** (2005), 122001

97. Senichev, Y.; Vasyukhin, N. E.
Slot-finger superconducting structure with rf focusing
Physical Review Special Topics, Accelerators and Beams, **8** (2005), 070101

4. Others

98. Protić, D.; Stöhlker, Th.; Krings, T.; Mohos, I.; Spillmann, U.
Two-Dimensional Microstrip Germanium Detector for X-Ray Spectroscopy of Highly-Charged Heavy Ions
IEEE Transactions on Nuclear Science, vol. **52**, December 2005

99. Protić, D.; Hull, E.L.; Krings, T.; Vetter, K.
Large-Volume Si(Li) Orthogonal-Strip Detectors for Compton-Effect-Based Instruments
IEEE Transactions on Nuclear Science, vol. **52**, December 2005

100. Bartolozzi, M.; Drozdz, S.; Leinweber, D.B.; Speth, J.; Thomas, A. W.
Self-Similar Log-Periodic Structures in Western Stock Markets from 2000
International Journal of Modern Physics C, **16** (2005), 9, 1347 – 1361

101. Schult, O. W. B.
Europäische Union — quo vadis?
Die neue Ordnung, 60. Jahrgang, Heft 1, Februar 2006

5. Textbooks

Dietrich, J.
Strahlfokussierung (geladene Teilchen)
Effekte der Physik und ihre Anwendungen / ed.: M. von Ardenne — Frankfurt, Harri-Deutsch, 2005 — 3. überarb., neu strukturierte, wesentlich erw. Auflage. — 3-8171-1682-9.— S. 132

Dietrich, J.
Strahlkühlung
Effekte der Physik und ihre Anwendungen / ed.: M. von Ardenne — Frankfurt, Harri-Deutsch, 2005 — 3. überarb., neu strukturierte, wesentlich erw. Auflage. — 3-8171-1682-9. — S. 139

Dietrich, J.
Teilchenbeschleunigung
Effekte der Physik und ihre Anwendungen / ed.: M. von Ardenne — Frankfurt, Harri-Deutsch, 2005 — 3. überarb., neu strukturierte, wesentlich erw. Auflage. — 3-8171-1682-9. — S. 154

Machner, H.; Krewald, S.
Giant Resonances
Encyclopedia in Physics / ed.: R. G. Lerner, G. L. Trigg. — Weinheim, Wiley-VCH, 2005 — 3-527-40554-2. — S. 2291

Machner, H.
Einführung in die Kern- und Elementarteilchenphysik
Weinheim, Wiley-VCH, 2005 — ISBN: 3-527-40528-3

E Teaching Positions

Institute	Name	University
IKP-1	Dr. habil. A. Gillitzer	Bonn
	Dr. habil. F Goldenbaum	Wuppertal
	Prof. Dr. H. Machner	Essen
	Prof. Dr. W. Oelert	Bochum
	Prof. Dr. J. Ritman	Bochum
IKP-2	Dr. habil. M. Büscher	Köln
	Dr. habil.D. Gotta	Köln
	Dr. habil. F. Rathmann	Erlangen-Nürnberg
	Prof. Dr. H. Ströher	Köln
Theory	Prof. Dr. G. Baur	Basel
	Dr. habil. J. Haidenbauer	Graz
	Dr. habil. C. Hanhart	Bonn
	Prof. Dr. S. Krewald	Bonn
	Prof. Dr. U.-G. Meißner	Bonn
	Prof. Dr. N.N. Nikolaev	Moscow
	Dr. habil. A. Wirzba	Bonn
GG	Dr. habil. J. Dietrich	Dortmund
	Dr. A. Lehrach	Bonn
	Prof. Dr. R. Maier	Bonn

F Beam Time at COSY 2005

Date	Experiment	Duration	Reaction
14.01.–24.01.	ANKE	1 week	$dp \to {}^3\mathrm{He}\eta$
28.01.–09.02.	GEM	2 weeks	$\vec{d}d \to {}^4\mathrm{He}\eta$
11.02.–21.02.	ANKE	1 week	$\vec{d}p \to (pp)n$
21.02.–24.02.	ANKE	1 week	cell tests
25.02.–14.03.	ANKE	2 weeks	$dd \to {}^3AN\pi$
14.03.–04.04.	ANKE	3 weeks	$pp \to ppK^+K^-$
08.04.–02.05.	COSY-11	3 weeks	$dp \to {}^3\mathrm{H}\pi^+/{}^3\mathrm{He}\pi^0$
06.05.–23.05.	GEM	2 weeks	$pA \to X$
27.05.–13.06.	PISA	2 weeks	$pA \to$ spallation
09.09.–26.09.	HIRES	2 weeks	$pp \to pK^+\Lambda$
30.09.–10.10.	COSY-11	1 week	$pp \to ppK^+K^-$
21.10.–07.11.	COSY-11	2 weeks	$\vec{p}p \to pK^+\Lambda$
11.11.–21.11.	SPIN@COSY	1 week	spin manipulation
21.11.–05.12.	ANKE	2 weeks	cell tests
Total '05		25 weeks	

G List of Authors